uOttawa

L'Université canadienne
Canada's university

FACULTÉ DES ÉTUDES SUPÉRIEURES ET POSTOCTORALES

uOttawa

L'Université canadienne
Canada's university

FACULTY OF GRADUATE AND POSDOCTORAL STUDIES

Vinay Mulgundmath
AUTEUR DE LA THÈSE / AUTHOR OF THESIS

Ph.D. (Chemical Engineering)
GRADE / DEGREE

Department of Chemical Engineering
FACULTÉ, ÉCOLE, DÉPARTEMENT / FACULTY, SCHOOL, DEPARTMENT

Thermal Pressure Swing Adsorption (TPSA) System for the Removal of Carbon Dioxide

TITRE DE LA THÈSE / TITLE OF THESIS

Handan Tezel
DIRECTEUR (DIRECTRICE) DE LA THÈSE / THESIS SUPERVISOR

CO-DIRECTEUR (CO-DIRECTRICE) DE LA THÈSE / THESIS CO-SUPERVISOR

EXAMINATEURS (EXAMINATRICES) DE LA THÈSE / THESIS EXAMINERS

Xudong Cao

Dhananjai Shah

Marc Dubé

Jason Zhang

Gary W. Slater
Le Doyen de la Faculté des études supérieures et postdoctorales / Dean of the Faculty of Graduate and Postdoctoral Studies

THERMAL PRESSURE SWING ADSORPTION (TPSA) SYSTEM FOR THE REMOVAL OF CARBON DIOXIDE

VINAY MULGUNDMATH

Thesis submitted to the Faculty of Graduate and Postdoctoral Studies

In partial fulfillment of the requirements for the degree of

DOCTOR OF PHILOSOPHY

In Chemical Engineering

Department of Chemical & Biological Engineering

Faculty of Engineering

University of Ottawa

Your file Votre référence
ISBN: 978-0-494-51802-1
Our file Notre référence
ISBN: 978-0-494-51802-1

TABLE OF CONTENTS

CHAPTER III

CHAPTER IV

CHAPTER V

CHAPTER VII

APPENDICES

LIST OF FIGURES

CHAPTER I

CHAPTER II

CHAPTER III

CHAPTER IV

CHAPTER V

CHAPTER VI

LIST OF TABLES

CHAPTER II

CHAPTER III

CHAPTER IV

CHAPTER V

CHAPTER VI

CONTRIBUTIONS OF COLLABORATORS AND/OR CO-AUTHORS

I hereby declare that I am the first author of this thesis project which was undertaken with the guidance of my supervisor, Dr. F. Handan Tezel. I supervised three undergraduate students who contributed to my thesis by performing experiments and have been listed as third authors. Ms. Melissa Kunkel performed the experimental runs to determine the Henry's law constants for Alcan Actiguard 600 PC/650PC adsorbents. Ms. Feifei Hou performed the binary CH_4-N_2 experiments for Alcan activated Alumina AA- 320AP at 40 °C and 100 °C, while Mr. Tolga Saatcioglu performed the binary CO_2 -N_2 experiments for Ceca 13X at 40 °C and 100 °C. Each of these undergraduate students performed the above experiments only while I analysed their experimental data. I performed the remaining experimental runs to determine the Henry's law constants, single component and binary mixture behaviour. The dynamic adsorption analysis system and the control software were designed by me and were built by the team of Mr. Louis Tremblay, Mr. Franco Ziroldo and Mr. Gerard Nina. I troubleshooted the system and performed breakthrough as well as parametric study experiments. Modelling the adsorption breakthrough concentration and temperature behaviour in Visual FORTRAN 6.0 was done in collaboration with Dr. Jules Thibault and Mr. Rudy Jones. The remaining authors listed in the papers are our industrial collaborators who provided financial support and guidance to the direction of the project.

ABSTRACT

Adsorption behaviour of various gases have been studied in this work for air pre-purification, landfill gas, coal gas, natural gas and flue gas applications.

This study included physical adsorption of commonly found impurities in air like carbon dioxide, methane, ethylene, acetylene, nitrous oxide, acetonitrile, methyl tert-butyl ether, methyl sulfoxide, dimethyl sulfoxide and methanol which constitute a safety hazard in the cryogenic air separation plant when present even in small quantities. Henry's law constants and heat of adsorption values were determined using the concentration pulse chromatographic technique for pure and composite adsorbents. It was found that latter performed better for these separations.

Single component and binary mixture adsorption isotherms were obtained using constant volume and concentration pulse chromatographic techniques for three gas separation applications: CH_4 - N_2, CO_2 - CH_4 and CO_2 - N_2. Experimental x-y diagrams and equilibrium separation factors determined showed that Ceca 13X is a promising adsorbent to preferably adsorb CO_2 from N_2 and CO_2 from CH_4.

A novel, lab scale two bed advanced dynamic adsorption analysis system was designed and built in-house. Ceca 13X was used in this system to study the temperature and concentration profiles in the column, for a composition of 10 % CO_2 (by vol) in N_2 which represented dry flue gas. Column breakthrough experiments were performed to compare the Pressure Swing Adsorption (PSA) process with Thermal Pressure Swing Adsorption (TPSA) process for CO_2 recovery. A novel and yet a simple approach was used to model

the non-isothermal adsorption in the fixed bed which exhibited significant heat effects for this system. Also, effects of various operating parameters on the TPSA performance such as purge/feed flow ratio, purge temperature, purge time and column pressure were investigated to optimise the CO_2 recovery.

Results indicated that better regeneration conditions used in a TPSA cycle was essential over a PSA cycle for recovering the maximum adsorption capacity of the used 13X. The developed model indicated to be an adequate representation of the experimental data. It was also observed that purge time had the most significant effect on CO_2 recovery.

RESUME

Dans cette recherche, les phénomènes d'adsorption de plusieurs gaz ont été étudiés pour diverses applications : la purification de l'air, les gaz émanant des sites d'enfouissement, les gaz provenant du charbon, le gaz naturel et les gaz de combustion.

Cette étude inclus l'adsorption physique des impuretés trouvées dans l'air telles le dioxyde de carbone, le méthane, l'éthylène, l'acétylène, l'oxyde nitreux, l'acétonitrile, le méthyl-tert-butyl-éther, le sulfoxyde de méthyle, le diméthylsulfoxyde et le méthanol qui constituent un danger dans la séparation de l'air par cryogénie quand ils sont présents en grandes quantités. Les constantes d'Henry et de la chaleur d'adsorption des adsorbants purs et des composés d'adsorbants ont été déterminées à l'aide de la technique chromatographique d'une impulsion en concentration. Le deuxième était plus efficace pour les séparations.

Les isothermes d'adsorption pour les composants pures et mélanges binaires ont été obtenues pour trois applications de séparation des gaz : CH_4-N_2, CO_2-CH_4 et CO_2-N_2 en utilisant des techniques chromatographiques à volume constant et à impulsion de concentration. Les diagrammes x-y d'adsorption expérimentaux et les facteurs de séparation à l'équilibre montrent que le Ceca-13X est un adsorbant qui adsorbe préférentiellement le CO_2 d'un mélange N_2-CO_2 et CO_2 d'un mélange CH_4-CO_2.

Un système novateur de deux lits d'adsorption a été conçu et construit en laboratoire pour étudier la dynamique d'adsorption. Le Ceca-13X a été utilisé dans ce système pour

étudier la progression à travers le lit des profils de température et de concentration pour un mélange de 10% de CO_2 (en volume) dans N_2 qui se rapproche des gaz de combustion. Des expériences ont été réalisées pour déterminer la progression des profils de concentration dans la colonne d'adsorption afin de comparer les procédés d'adsorption par variation de pression (PSA) et d'adsorption par variation de température (TPSA) pour la récupération du CO_2. Une approche nouvelle et relativement simple a été utilisée pour modéliser les phénomènes d'adsorption dans un lit fixe où les effets thermiques sont importants. De plus, les effets de quelque paramètres (le ratio des débits purge/alimentation, la température de la purge, le temps de purge et la pression de la colonne) sur la performance du TPSA ont été étudiés pour optimiser la récupération de CO_2.

Les résultats obtenus indiquent que pour récupérer la capacité d'adsorption maximale de l'adsorbant Ceca-13X, les conditions de régénération utilisées dans un cycle de TPSA comparées à celles du PSA sont supérieures. Le modèle développé dans cette étude représente adéquatement les données expérimentales. Il a été aussi observé que le temps de purge a eu l'effet le plus significatif sur la récupération de CO_2.

ACKNOWLEDGEMENTS

I wish to express my sincere gratitude to my thesis supervisor, Dr. Handan Tezel for her guidance & encouragement throughout the course of this study. Her knowledge and expertise in adsorption domain provided me with a good foundation to build my research skills.

I want to thank Dr. Jules Thibault for providing me with valuable suggestions for modelling in Visual FORTRAN 6.0. I would also like to thank my colleagues for offering me their friendship, support and knowledge. I would take this opportunity to thank all the faculty members, staff, technicians and students at the department of Chemical and Biological engineering for their support.

Several sources of financial support contributed to the completion of my thesis. University of Ottawa provided me with a full admission scholarship while the Ontario Centres of Excellence contributed by awarding the prestigious W.A. Miller Ph. D. scholarship. Ontario Graduate Scholarship in Science and Technology (OGSST) from the government of Ontario and financial contributions from our industrial collaborators, Air Products and Chemicals Inc., and RioTinto Alcan are also acknowledged.

I dedicate this thesis to my parents, Prabhu and Vishala Mulgundmath and family members. Most importantly, I would like to thank my wife Chaitra for her boundless patience, encouragement, love and support throughout this period.

CHAPTER I

INTRODUCTION

RESEARCH OBJECTIVES

THESIS STRUCTURE

REFERENCES

INTRODUCTION

Global warming which is attributed to the accumulation of greenhouse gases in the atmosphere is a hotly debated topic of the 21st century. The increasing concentration of carbon dioxide, methane, and other impurities emitted from process industries contribute to this problem. Separation of gas mixtures is considered to be a major operation in the process industry for the purification of the effluent streams in order to meet the strict regulatory standards.

According to the International Energy Agency Working Party on Fossil Fuels [1], combustion of fossil fuels account for 25 billion tons per year of carbon dioxide being released into the atmosphere. Carbon capture and sequestration from power plant flue gas, automobile, and landfill gas (LFG) emissions has received enormous global attention to reduce the carbon footprint and combat global warming. Along with the environmental concerns, industries have potential applications for the removal of CO_2 from gas streams. Examples include the cryogenic separation of air for the production of oxygen, nitrogen and argon, landfill gas and natural gas purification, food refrigeration industry, beverage carbonation, metals fabrication, fire extinguishers, enhanced oil recovery and emergency life support systems for hazardous environments, to name a few.

Several initiatives have been taken to increase the efficiency and to reduce the cost of CO_2 separation processes for the last 15 years [2, 3]. Adsorption processes are increasingly being used in the intermediate to the high process capacity gas separation applications as an alternative to the conventional separation techniques as they tend to utilise less resources and energy and are highly efficient.

Separations of CH_4 - N_2, CO_2 - CH_4, and CO_2 - N_2 gas pairs could play a vital role in alleviating the environmental concerns as well as finding potential industrial applications. More recently, research is focussed on the development of new adsorption cycles (Pressure Swing Adsorption (PSA), Vacuum Swing Adsorption (VSA), Thermal Swing Adsorption (TSA), and Thermal Pressure Swing Adsorption (TPSA)), and novel adsorbents for the adsorption process to operate effectively under different operating conditions.

The significant features of these adsorption cycles are:

In a PSA process, adsorption is performed at a high pressure and the adsorbent is regenerated at atmospheric pressure, at constant temperature.

In a VSA process, adsorption is performed at a high pressure and regeneration is achieved at pressures below atmospheric levels (at vacuum) at constant temperature.

In a TSA process, adsorption is performed at a low temperature and regeneration is achieved at high temperatures at constant pressure.

In a TPSA process, adsorption is performed at a high pressure and a low temperature (favourable for adsorption) while regeneration is achieved at atmospheric pressure and a higher temperature.

Figure I-1 demonstrates the various classifications of adsorption cycles used for gas separation applications according to various operating temperatures, To, T_1, T_2, T_3 & pressures P_1 and P_2 (P_2 < 1atm).

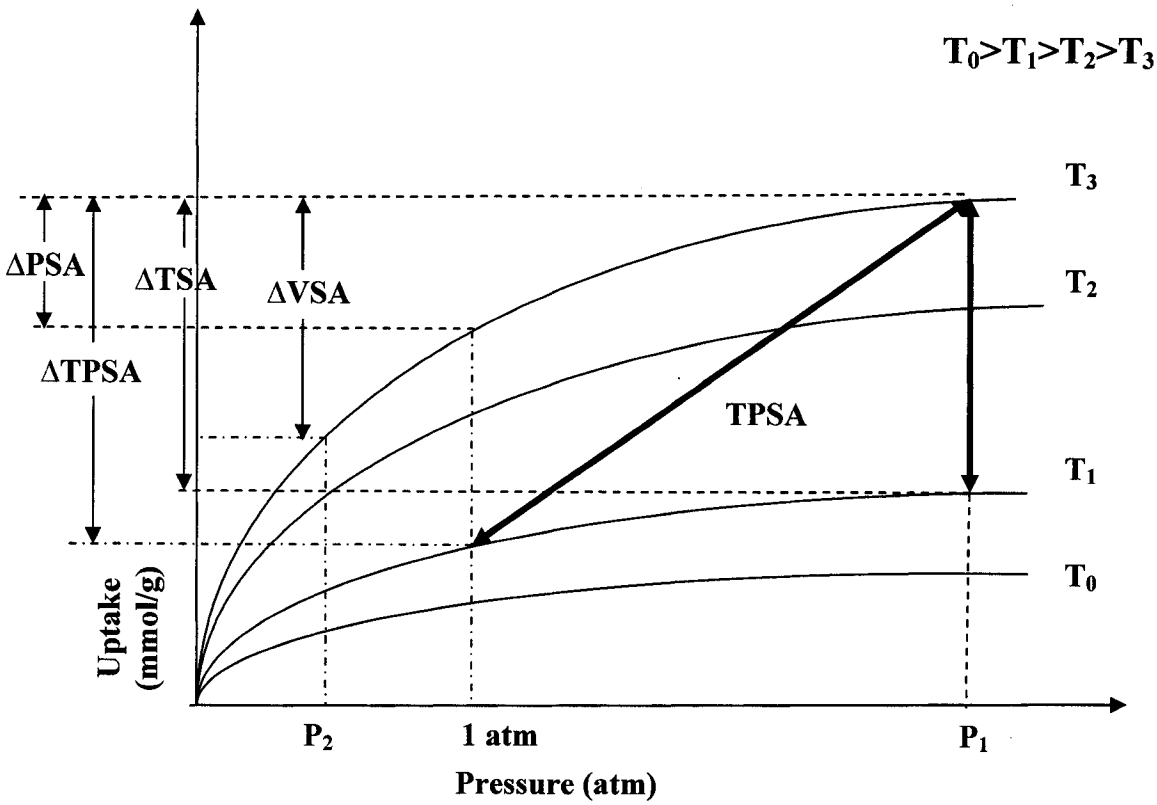

Figure I- 1. Classifications of various adsorptive separation processes.
Source: Class notes, Tezel [4].

The four isotherm plots represent adsorption equilibrium uptake curves at different pressures. PSA cycles are characterised by shorter cycle times and smaller beds while TSA cycles require longer cycle durations and larger beds. As seen from Figure 1, the effective working capacity (the difference in amount adsorbed) in a TPSA cycle is much higher than that of TSA and PSA cycles. TPSA cycle also has the advantage to minimise the regeneration energy and increase the life of an adsorbent when compared to a TSA cycle.

In this study, single component and binary adsorption separations of CH_4 - N_2, CO_2 - CH_4, and CO_2 - N_2 gas pairs have been studied by the volumetric and concentration pulse

chromatographic methods, respectively, for their potential in industrial applications. The chosen adsorbent has been explored for the separation of flue gas (composition 10 % CO_2 by volume in N_2) by the TPSA cycle in the novel lab scale set up which was designed and built in-house.

RESEARCH OBJECTIVES

This project had the following objectives:

1. To design and build a two bed laboratory scale dynamic adsorption analysis system for the separation of gas mixtures. The key challenge was to coordinate the construction of this novel unit in-house, commission and troubleshoot it.

2. To study the physical adsorption of various trace impurities present in air using pure and composite adsorbents. The hypothesis of this study was that composite adsorbents were better than pure adsorbents for certain separations.

3. To study the single component and binary adsorption behaviours of CH_4, N_2 and CO_2 gases which find separation applications in the upgrading of methane from coal bed gas, natural gas, landfill gas, and separation of CO_2 from flue gas.

4. To study and model the concentration and temperature breakthrough behaviour for a flue gas composition of 10% CO_2 in 90% N_2 (by volume) within the laboratory scale TPSA setup. The developed non-isothermal model should

incorporate both mass and heat transfer in the bulk feed gas flowing within the bed, as well as the transport within the porous solid adsorbent pellets. The model should have the capability to predict concentration and temperature profiles simultaneously at all locations within the packed column and agree with the experimental data.

5. To optimise the carbon dioxide recovery in a TPSA cycle for the flue gas composition of 10% CO_2 in 90% N_2 (by volume) within the laboratory scale setup. The effect of interaction parameters namely adsorption column pressure, Purge/Feed flow ratio, purge temperature, and purge time were to be studied for the optimal recovery of CO_2 in the lab scale set-up.

THESIS STRUCTURE

This thesis is presented in paper format and comprises of seven chapters. Chapter 1 (Introduction) includes the introduction of the thesis topic and the research objectives for the entire study. Each of Chapters 2 through 6 is a scientific publication submitted (or to be submitted) to a refereed scientific journal. Chapter 7 includes general conclusions, contributions and recommendations for the entire study.

Chapter 2 – Mulgundmath, V.P., Kunkel, M., Tezel, F.H., Golden T.C., Mogan, J., Morin, B. Adsorption equilibrium parameters of trace impurities (Separation Science and Technology, (2009), 44:4, 874 — 893)

This study gives basic guidelines on adsorbents that can be used to target specific impurities present in air. Prior to the cryogenic distillation of air to produce oxygen, nitrogen and argon, trace impurities have to be removed since many of these compounds constitute a safety hazard in the plant. The adsorption behaviour of various trace impurities present in atmospheric air like ethylene, acetylene, nitrous oxide, acetonitrile, methyl tert-butyl ether, methyl sulfoxide, dimethyl sulfoxide, and methanol were studied in the Henry's Law low concentration region with several different adsorbents. Adsorption equilibrium parameters were determined with samples of Alcan alumina AA 300, Alcan alumina/13X composites Actiguard 600PC and Actiguard 650PC, Ceca13X, CABSORB Chabazite and Clinoptilolite by using concentration pulse chromatographic technique. Heat of adsorption values and van't Hoff plots suggested that composite adsorbents performed better than pure adsorbents for the adsorption of ethylene. Based on K_p and heat of adsorption values, Chabazite had the highest capacity and interaction with ethylene and Clinoptilolite had the highest capacity and interaction for nitrous oxide. Alcan AA-300 alumina had the lowest K_p values and heat of adsorption for nitrous oxide and ethylene. For acetylene as the adsorbate, the heat of adsorption was the highest for the composite Alcan Actiguard 650PC, and the lowest for the Alcan AA-300 alumina. All tested adsorbents find applications in the trace impurity removal from air.

Chapter 3 – Mulgundmath, V.P., Tezel, F.H., Hou, F., Mogan, J., Golden, T.C., Morin, B. Binary adsorption behaviour of methane and nitrogen gases (submitted to Journal of Porous Materials)

In this study, adsorption separation of methane and nitrogen gases were studied with Ceca 13X and Alcan activated alumina AA-320 AP adsorbents for their potential in the upgrading of Landfill gas (LFG), natural gas, and coal bed gas in order to have a commercial heating value for methane. From an environmental point of view, methane is a greenhouse gas with a Global Warming Potential (GWP) that is 25 times greater than CO_2 and its capture is critical. Adsorption could be a beneficial process to capture low purity methane and convert this to high purity commercial methane. Single component and mixture adsorption isotherms were determined at 40°C and 100°C for these adsorbents by constant volume method and concentration pulse chromatographic technique, respectively. VV - CPM (Van der Vlist and Van der Meijden Concentration Pulse Method) was used for mixture adsorption isotherms. The application of the theoretical extended Langmuir model for this binary system was also discussed and compared to the experimental results. Results of binary isotherms, equilibrium phase diagrams and separation factors indicated that zeolite Ceca 13X has a potential in the bulk separation application of methane from nitrogen when y_{CH4}>0.4, especially in LFG, coal bed gas and natural gas.

Chapter 4 – Mulgundmath, V.P., Tezel, F.H., Saatcioglu T., Golden, T.C., Mogan, J. Adsorption behaviour of CO_2/N_2 and CO_2/CH_4 by 13X zeolite (to be submitted to Canadian Journal of Chemical Engineering)

In this work, adsorption separations of CO_2 -N_2 and CO_2-CH_4 pairs were studied on Ceca 13X zeolite adsorbent for its potential in the removal of CO_2 from flue gas and upgrading of Landfill gas (LFG), respectively. Single component gas and binary mixture behaviour were studied using constant volume method and concentration pulse chromatographic technique at 40°C and 100°C. Binary adsorption isotherms were determined by the more versatile HT - CPM (Harlick Tezel Concentration Pulse Method) and compared with the predicted binary behaviour by the extended Langmuir model. The integral thermodynamic consistency tests between single component and binary adsorption isotherms for this system showed an excellent fit at both temperatures of 40°C and 100°C. Equilibrium phase diagrams obtained from the experimental binary isotherms indicated that Ceca 13X was a promising adsorbent that could be used in the flue gas separation of CO_2 from dry air and in landfill gas applications.

Chapter 5 – Mulgundmath, V.P., Jones, R., Tezel, F.H., Thibault, J. Fixed bed adsorption for the removal of carbon dioxide: breakthrough behaviour and modelling (submitted to Separation and Purification Technology journal)

The scope of this study was the experimental determination of adsorption breakthrough behaviour and heat effects in a CO_2-N_2 gas mixture (10 % CO_2 by volume in N_2) using the chosen Ceca 13X adsorbent in the laboratory scale dynamic adsorption analysis system. The effects of parameters like the initial bed temperature, feed flow rate, and

external cooling during the adsorption step were investigated. Concentration and temperature breakthrough profiles were determined to understand the adsorbent behaviour. A novel approach describing two different populations of the adsorbent pellets was used to develop a simple model for the simulation of non-isothermal adsorption in a fixed bed. Results indicated that feed flow rate and external cooling during the adsorption step significantly affected the breakthrough behaviour while the initial bed temperature was less significant for Ceca 13X. Another significant finding was the possibility of using thermocouples in a column to predict the concentration breakthrough for bulk CO_2-N_2 mixtures as in a flue gas separation application. The developed simple model was an adequate representation of the experimental data.

Chapter 6 – Mulgundmath, V.P., and Tezel, F.H. Parametric study of CO_2 recovery from flue gas in a TPSA system (submitted to Adsorption journal)

Most of the research in the CO_2 flue gas capture from power stations and industrial processes has focussed on the Vacuum Swing Adsorption (VSA) system. In this study, the application of Pressure Swing Adsorption (PSA) process has been compared with Thermal Pressure Swing Adsorption (TPSA) process for the CO_2 recovery from a flue gas composition of 10 % CO_2 (by volume) in N_2 using the chosen Ceca 13X adsorbent. Thermal Pressure Swing Adsorption (TPSA) system could be a viable option if waste heat, which is readily available in power stations, could be used to regenerate the adsorbents at atmospheric pressure. A TPSA system does not require a vacuum pump for regenerating the adsorbent (as in a VSA process) and thus, would reduce the power consumption. A factorial design set of experiments was performed to optimise the carbon

dioxide recovery and study the effects and interaction of four parameters namely: purge/feed flow ratio, purge time, heat input to purge gas, and adsorption column pressure. Results indicated that better regeneration conditions used in a TPSA cycle was essential over a PSA cycle for recovering the capacity of the used Ceca 13X adsorbent. It was found that purge time had a significant effect on the CO_2 recovery followed by column pressure, purge/feed flow ratio and purge temperature. A Minitab® statistical software was used to analyse this data and fit it to a model. The fitted model proved to be an adequate representation of the experimental data. The results showed that to maximise the CO_2 recovery, highest values of the control parameters have to be used.

REFERENCES

1. International Energy Agency Working Party on Fossil Fuels, "Solutions for the 21st century: Zero emissions technologies for fossil fuels", OECD/IEA, Paris, FR, 1-50, (2002).
2. Kikkinides, E. S. and R. T. Yang, "Concentration and Recovery of CO_2 from Flue Gas by Pressure Swing Adsorption", Industrial and Engineering Chemistry Research 32, 2714-2720 (1993).
3. Zhang, J., Webley, P.A., and Xiao, P., "Effect of Process Parameters on Power Requirements of Vacuum Swing Adsorption Technology for CO_2 Capture from Flue Gas", Energy conversion and management, 49, 346-356 (2008).
4. Tezel, F. H., Graduate course notes on "Adsorption Separation Processes", Fall 2004, University of Ottawa.

CHAPTER II

ADSORPTION EQUILIBRIUM PARAMETERS OF TRACE IMPURITIES

Mulgundmath, V.P [a], Kunkel, M [a,d], Tezel, F.H [a], Golden T.C [b], Mogan, J [c], Morin, B [c].

a Department of Chemical and Biological Engineering, University of Ottawa, 161, Louis Pasteur, Ottawa. K1N 6N5. Canada

b Air Products and Chemicals, Inc., 7201, Hamilton Blvd., Allentown, PA 18195-1501, USA.

c RioTinto Alcan, 4000 Development Drive, P O Box 250, Brockville. ON K6V 5V5. Canada.

d) Now at Iogen Corporation, 300 Hunt Club Rd. East, Ottawa. ON K1V 1C1. Canada

Published in Separation Science and Technology, (2009) 44:4, 874 — 893

Presented at 56th CSChE (Canadian Society for Chemical Engineering) Canadian Chemical Engineering Conference, Sherbrooke, Quebec, October 15-18, 2006.

ABSTRACT

Atmospheric air contains various trace impurities which include oxides of nitrogen, carbon, sulphur and light hydrocarbons. Prior to cryogenic distillation of air to produce oxygen, nitrogen and argon, these trace impurities have to be removed since many of these compounds constitute a safety hazard in the plant. In this study, adsorption has been considered for their removal. Adsorption behaviour of ethylene, acetylene, nitrous oxide, acetonitrile, methyl tert-butyl ether, methyl sulfoxide, dimethyl sulfoxide and methanol have been studied in the Henry's Law low concentration region with several different adsorbents. Adsorption equilibrium parameters have been determined with samples of Alcan pure alumina, Alcan alumina/13X composites (Actiguard 600/650PC), CABSORB Chabazite, Ceca13X and Clinoptilolite by using concentration pulse chromatographic technique. Heats of adsorption values and van't Hoff plots have been presented.

INTRODUCTION

The use of adsorption for separation processes is a growing trend in industry. Determination of equilibrium parameters and fluid solid adsorption equilibria is a crucial step in designing gas separation units. One key aspect for adsorption research is the development of new adsorbents. There has been a remarkable growth in the development of new adsorbents, especially synthetic zeolites in the late 90's for trace impurity removal applications from air [1]. Research on new and improved adsorbents has attracted considerable attention [2, 3]. In the early 90's, layered beds consisting of activated alumina and zeolites had been the norm in air pre-purification adsorption applications to tackle moisture and trace impurities [4]. For the first time, Golden et al. [4] mention the advantage of developing alumina/zeolite composites over layered beds for the removal of trace impurities from air. Tezel et al. [5] observed that composite alumina adsorbents performed better for the separation of hydrocarbons like acetylene and ethylene from olefin containing streams. In this study, various adsorbents like activated alumina and zeolites were tested for a wide range of adsorbates. In addition, composite adsorbents that consist of a mixture of zeolites and alumina were also tested. Activated alumina does not possess an ordered crystal structure and consequently, the pores are non uniform. Zeolites, on the other hand, are crystalline aluminosilicates that consist of well defined uniform intra-crystalline pore structures in the crystal and macropores in the binder system of the formed particle [6].

The study included adsorption of commonly found impurities in the atmospheric air, feed streams for carbon dioxide purification and cracked gas streams in refineries. Most of the

problem components in the cryogenic air separation process (carbon dioxide, nitrous oxide, acetylene, ethylene etc.) boil at temperatures above oxygen. Therefore, these concentrate in the oxygen product at the bottom of the low pressure column. The trace contaminants in the oxygen cause problems ranging from operability issues (fouling, plugging and contamination) to equipment damage and safety incidents, caused by the reaction of hydrocarbon compounds with high purity oxygen. For these reasons, care must be taken in both the design and operation of an air separation unit to prevent the accumulation of trace components [7, 8]. The adsorbates are examined for Henry's Law constants since they are separated at very low concentrations. Activated alumina/zeolite composites were characterised for acetylene, ethylene, carbon dioxide and nitrous oxide adsorption. The composite adsorbents were further characterised for the adsorption of acetonitrile, methyl tert-butyl ether, methyl sulfoxide, dimethyl sulfoxide and methanol as adsorbates. These tests were conducted to evaluate the efficacy of composite adsorbents for application in oxygenated species removal from various gas streams (e.g. carbon dioxide).

THEORY

A dynamic method of analysis was used to characterise and study the adsorbents based on adsorption equilibria. The concentration pulse chromatographic technique is an attractive adsorbent screening method since it is relatively fast and requires an inexpensive set up. This method was used in the present study to determine the Henry's Law constants and heats of adsorption of the systems studied. It is less cumbersome than

other unsteady state techniques commonly used, namely gravimetric and volumetric methods [9-21].

Equilibrium parameters are derived by matching the first moment of the response peak of the column packed with the adsorbent to an impulse change in concentration, at the inlet of the column. To ensure the validity of these calculations, the process has to be governed by physical adsorption (i.e. no chemisorption); else the column containing the adsorbent cannot be considered for concentration pulse chromatography technique. Under these circumstances, the signal of the detector is proportional to the adsorbate concentration which is recorded against time at the exit of the column. From this response peak, the first moment of the chromatogram μ, is determined experimentally using the Simpson's approximation [10]. The first moment is directly related to the Henry's Law constant and determined knowing the experimental set up values. Dimensionless Henry's Law constants can be calculated from the corrected first moments of the response peaks (corrected with respect to the dead time of the system, μ_D) as shown in Equation 1[14, 19]:

$$\mu = \frac{\int_0^\infty c(t-\mu_D)dt}{\int_0^\infty cdt} = \frac{L}{v}\left[1+\frac{(1-\varepsilon)K}{\varepsilon}\right] \quad \text{.....(1)}$$

where t is the time, c is the adsorbate concentration measured at the outlet of the column, L is the column length, ε is the bed porosity, v is the interstitial fluid velocity, K is the dimensionless Henry's Law adsorption equilibrium constant, and μ_D is the system dead time.

The dimensionless Henry's Law constant, K can be converted to a dimensional constant, K_p using Equation 2:

$$K_p(Dimensional) = \frac{K(Dimensionless)}{RT\rho} \quad \text{.....(2)}$$

where T is the absolute temperature, ρ is the density of the pellet (without internal pores) and K_p is the dimensional Henry's Law adsorption equilibrium constant. By determining K_p values at different temperatures, a van't Hoff plot can be constructed and the heat of adsorption, ΔH can be determined based on equation 3:

$$\ln K_p = \ln K_o - \frac{\Delta H}{RT} \quad \text{.....(3)}$$

The heat of adsorption values for these systems can be used as a pre-screening tool. For bulk separation applications using pressure swing adsorption, adsorbents that exhibit high heat of adsorption are less suitable. The bulk gas separation has significant heat effects associated with the exothermic physical adsorption due to large amount of the feed being adsorbed, which could lead to significant rise in temperature within the PSA column. Since the adsorption capacity of an adsorbent decreases with the rise in temperature for a physical adsorption process, this temperature rise decreases the efficiency of the overall process. However, for trace removal applications, since the percentage of the feed that is adsorbed is very low, heat effects are minimal even with high heat of adsorption systems. Also, if a temperature swing adsorption (TSA) process is used, regeneration can be complete even for systems with high heat of adsorption,

EXPERIMENTAL METHOD AND MATERIALS

A schematic diagram of the experimental apparatus is given in Figure II-1. Measurements were made in a Varian 1400 series Chromatograph equipped with a thermal conductivity detector and a sample injection valve. The experimental details are outlined in Table II-1.

The dead volumes between the sample injection valve, column and detector were minimised by using stainless steel piping of minimum volume (1/16"). The dead time, μ_D between the sample injection valve and detector was calculated at room temperature under fixed carrier gas flow rate by measuring the mean of the response peak produced when a gas sample pulse was passed through the column containing glass beads of the same size as the adsorbent. All experimental means of the response curves were corrected by subtracting the corresponding system dead time.

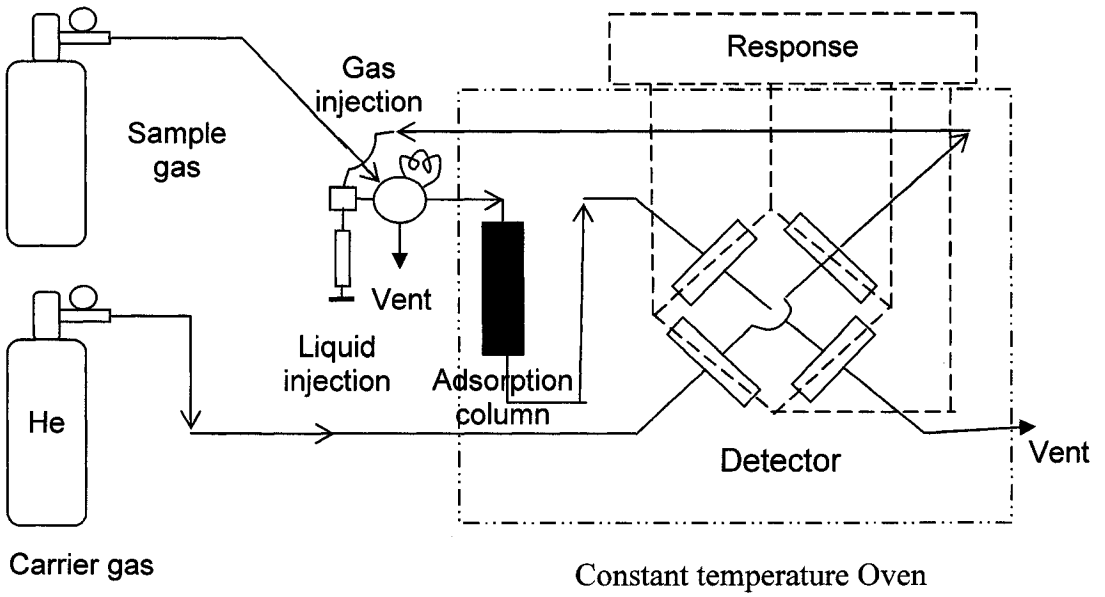

Figure II- 1. Apparatus used in the study of adsorption of single component gases

A sample pulse at atmospheric pressure was injected into the helium carrier gas stream and sent to the adsorption column packed with the adsorbent. The column was fully contained in the chromatographic oven for accurate temperature control. Two injection ports were used, one for gas injection and the second for liquid injection. The column temperature was maintained at a constant temperature higher than the liquid adsorbate

boiling temperature in order to ensure gas phase adsorption and isothermal operation. Henry's Law constants and heat of adsorption values were determined using Equations 1-3. Gas sampling, monitoring and analysis of response peaks were carried out through LABVIEW data acquisition system which ensured accurate detection of the sample introduction time. Carrier gas velocities were controlled with an MKS digital mass flow controller followed by verification with bubble meter measurements at the column exit. The bed porosity was determined using a constant volume system, by measuring the volume of a packed chromatographic column of glass beads of same size with helium gas.

Table II- 1. Experimental specifications used with concentration pulse method

Carrier gas:	Helium
Column length:	13.19 cm
Column inner diameter:	0.45 cm
Carrier gas flow rate:	8-75 cm^3/min
Regeneration temperature:	548-573 K (275-300 °C)
Regeneration time with He purge:	24 Hours
Column temperature	323-573 K (50-300 °C)
Detector temperature	Column temperature + 40 °C
Particle size:	20–60 mesh (0.0246-0.0833 cm)
Bed porosity:	0.35
Total pressure	1 atm
Thermal conductivity bridge power	100 mA

Before starting the experiments, the packed column was regenerated under helium purge for 24 hours. This ensured that any impurities or moisture adsorbed from air did not

hinder the adsorption capacity of the adsorbent. With the same reasoning, a carrier gas of helium flowed continuously through the system for purging between experimental runs. Table II-2 gives details on adsorbents used in this study while carrier and sample gases are listed in Table II-3. Henry's Law constants were determined for acetylene, ethylene, carbon dioxide and nitrous oxide with all the adsorbents studied. Alcan Actiguard 600 PC and Alcan Actiguard 650 PC adsorbents were further characterised with acetonitrile, methanol, methyl tert-butyl ether, dimethyl sulfoxide and methyl sulfoxide.

Table II- 2. Adsorbent Specifications

Commercial Name	Commercial Number	Shape	Size	Supplier
Alcan activated Alumina	AA-300	Spherical	20x60 mesh	RioTinto Alcan, Brockville, Canada
Alcan activated Alumina Composites	Actiguard 600 PC (x% 13X and y*% activated alumina) x<y	Spherical	20x60 mesh	RioTinto Alcan, Brockville, Canada
	Actiguard 650 PC (x % 13X and y % activated alumina) x<y*	Spherical	20x60 mesh	RioTinto Alcan, Brockville, Canada
Zeolite X (Si/Al=1.25)	Ceca G5-13 X	Spherical	20x60 mesh	CECA, Honfleur, France
Chabazite (Si/Al=0.15)	CABSORB	Spherical	20x60 mesh	GSA Resources Inc., Cortaro, Arizona, USA
Clinoptilolite (Si/Al=0.2)	Ash Meadows Clinoptilolite	Spherical	20x60 mesh	American Resource Corp, Amargosa Valley, Nevada, USA

* More 13X when compared to Actiguard 600 PC (i.e. y*<y)

RESULTS AND DISCUSSIONS

Equilibrium data

Henry's Law constants were calculated based on equations 1 and 2 using the first moment of the response peaks for all adsorbents studied at various temperatures. These results are summarised in Figures II-2a, II-2b and II-2c as van't Hoff plots. From the slope of these plots the heats of adsorption values were calculated using the van't Hoff equation (Equation 3).

Table II- 3. Carrier and Sample Gas Specifications [22]

Name	Purity	Dipole Moment (Debye)	Polarizability x 10^{24} cm^3	Quadrupole moment (cm^2)	Supplier
Helium (Carrier)	99.999%	0	0.20	-	Praxair Inc., Ottawa, Canada
Carbon dioxide	99.9%	0	2.91	-14.9×10^{-40}	Praxair Inc., Ottawa, Canada
Acetylene	99.9%	0	3.93	4.87×10^{-40}	Praxair Inc., Ottawa, Canada
Ethylene	99.97%	0	4.25	4.37×10^{-40}	Praxair Inc., Ottawa, Canada
Nitrous oxide	99.9%	0.16	3.03	1.6×10^{-34}	Praxair Inc., Ottawa, Canada
Methyl sulfoxide	99.9%	-	-	-	Fisher Scientific Company, Ottawa, Canada
Acetonitrile	99.8%	3.92	4.40	-	Sigma Aldrich Canada Ltd., Oakville, Canada
Dimethyl sulfoxide	99.3%	3.96	-	-	Fisher Scientific Company, Ottawa, Canada
Methyl tert-Butyl Ether	99.0%	-	10.68	-	Commercial alcohols Inc., Toronto, Canada
Methanol	99.8%	1.70	3.29	-	Fisher Scientific Company, Ottawa, Canada

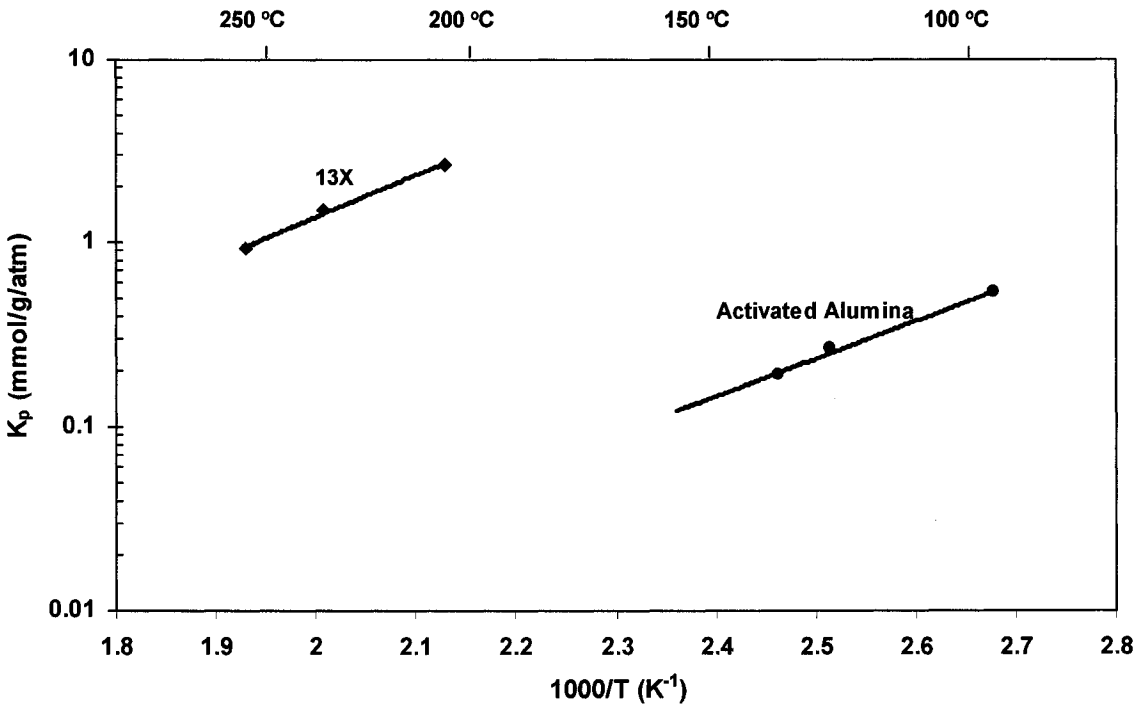

Figure II- 2a. Henry's Law constants as van't Hoff plots for Acetylene with Alcan AA-300 activated alumina and Ceca G5-13X adsorbents

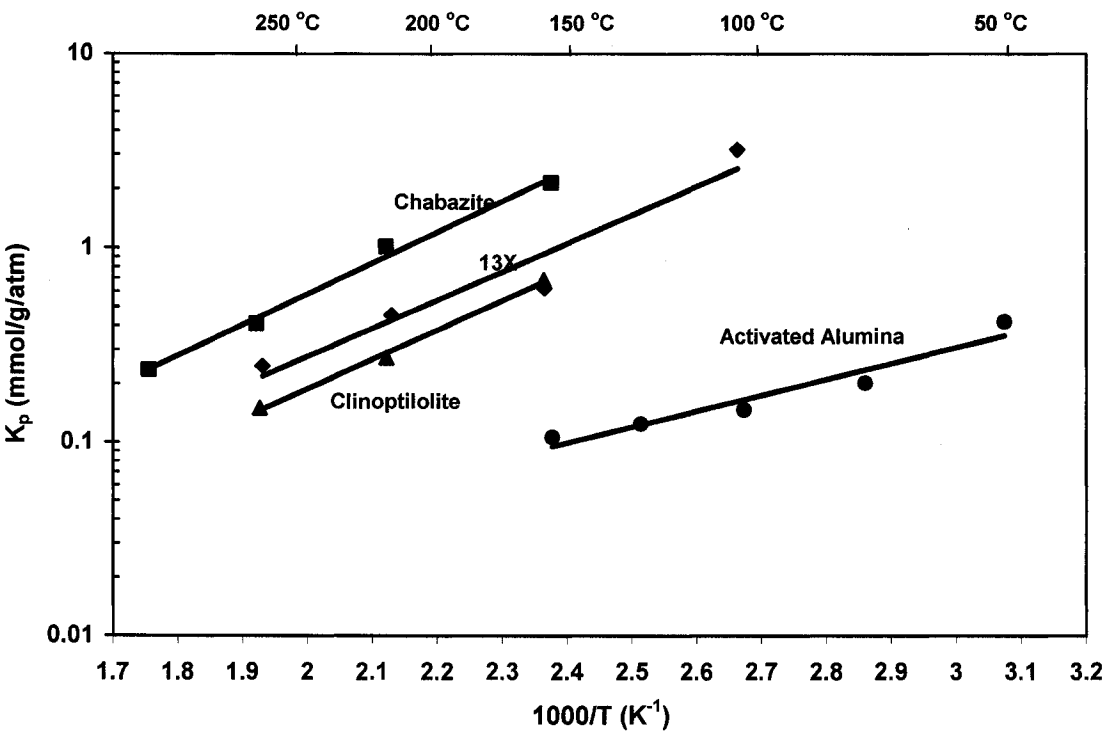

Figure II-2b. Henry's Law constants as van't Hoff plots for Ethylene with Alcan AA-300 activated alumina, CABSORB Chabazite, Ceca G5-13X and Ash Meadows Clinoptilolite adsorbents.

.

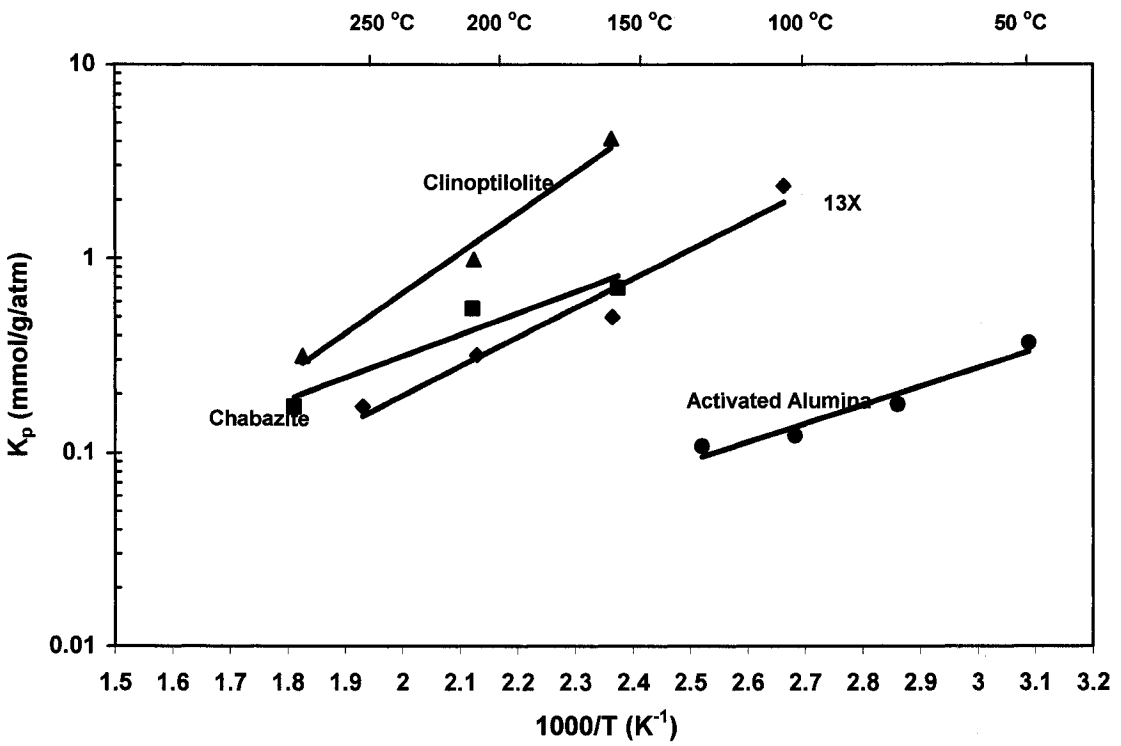

Figure II- 2c. Henry's Law constants as van't Hoff plots for Nitrous oxide with Alcan AA-300 activated alumina, CABSORB Chabazite, Ceca G5-13X and Ash Meadows Clinoptilolite adsorbents.

Alcan AA-300 activated Alumina adsorbent

This adsorbent is the base activated alumina obtained from RioTinto Alcan. The Henry's Law constants obtained for acetylene, ethylene and nitrous oxide for Alcan AA-300 alumina adsorbent in the temperature range of 50-150 °C (323-423 K) are plotted against inverse temperature in Figures II-2a, II-2b and II-2c respectively. Results showed that as the temperature of the column increased, the first moment and the Henry's Law constant decreased as expected, since physical adsorption is an exothermic process. Acetylene was much more strongly adsorbed compared to ethylene and nitrous oxide which was due to the highly active triple bond structure of the acetylene molecule. Acetylene is an air

impurity that must be removed prior to cryogenic distillation owing to its low solubility in liquid oxygen. When present in sufficient quantities, it can plug the equipment and pipes. Also, acetylene is a flammable component and its presence in oxygen constitutes a safety hazard within the cryogenic plant. Acetylene results were not plotted in Figure II-2a at the low temperatures of 50 °C and 75 °C (323K and 348K) since the peaks obtained were too wide to have an accurate first moment determination. The heat of adsorption values, van't Hoff parameters and corresponding R^2 values for Alcan AA-300 activated Alumina are given in Table II-4 for acetylene, ethylene and nitrous oxide. The heat of adsorption value for acetylene was much higher than that of double bonded ethylene followed by nitrous oxide. This is due to the dual effect of a triple bond and a quadrupole moment that acetylene has, which causes it to be much more interactive with the adsorbents.

A carbon dioxide peak was not present for any of the temperatures tested. This comes from the fact that carbon dioxide is very strongly adsorbed in pure activated alumina [23, 24]. Since the peak widens as adsorption capacity increases for the concentration pulse chromatographic technique, it was impossible to quantify the carbon dioxide peaks.

Table II- 4. Heat of adsorption, van't Hoff parameter and sum of squares data for all adsorbents

Adsorbent	Adsorbate	ΔH (cal/mol)	K_o (mol/g/atm)	R^2
Alcan AA-300	Acetylene	7846	18.14	0.9518
	Ethylene	5180	15.86	0.9650
	Nitrous Oxide	4322	14.74	0.9416
CABSORB Chabazite	Ethylene	7236	14.73	0.9929
	Nitrous Oxide	5050	13.15	0.9152
Ceca G5-13X	Acetylene	10600	17.29	1
	Ethylene	7203	15.47	0.9202
	Nitrous Oxide	6880	15.46	0.9565
Alcan Actiguard 600PC	Acetylene	10666	18.7	1
	Ethylene	5838	14.86	0.9997
	Nitrous Oxide	4721	13.98	0.9894
	Methyl Sulfoxide	9325	15.68	0.9259
	Dimethyl Sulfoxide	7783	13.82	0.8209
	Methanol	9679	14.43	0.9901
	Methyl t-Butyl	5558	11.14	0.9706
	Acetonitrile	9657	14.16	0.9513
Alcan Actiguard 650PC	Acetylene	12353	19.61	1
	Ethylene	6501	15.06	0.9996
	Nitrous Oxide	5902	14.69	0.9541
	Methyl t-Butyl	18194	22.87	1
Ash Meadows Clinoptilolite	Ethylene	6930	15.55	0.9961
	Nitrous Oxide	9471	16.85	0.9833

CABSORB Chabazite Adsorbent

This adsorbent was obtained from GSA Resources Inc. and was tested with acetylene, nitrous oxide, and ethylene in the temperature range 150 to 300°C (423-573K). The corresponding van't Hoff plots and parameters for ethylene and nitrous oxide for CABSORB Chabazite are shown in Figures II-2b, II-2c and Table II-4.

As can be seen from these results, the heat of adsorption values and Henry's Law constants for this adsorbent are much higher than those for Alcan AA-300. The experiments had to be carried out at higher temperatures compared to the AA-300 Alcan activated Alumina adsorbent to get accurate values of the Henry's Law constants. When the adsorption capacity is very high, (i.e. when the adsorbate is very strongly adsorbed), especially at low temperatures for the adsorbates studied), the first moment of the peak, μ, becomes very large (see equation 1) and the peak widens quite a bit, making it impossible to accurately identify the peak separately from the baseline. Acetylene peaks were not observed even at these high temperatures and was likely very strongly adsorbed. Ethylene had a higher K_p value at all temperatures tested and a higher ΔH value than nitrous oxide with this adsorbent due to its double bond structure which showed more interaction with the adsorbent.

CECA G5-13X Adsorbent

This is the base 13X zeolite adsorbent obtained from CECA. The Henry's Law constant values obtained for this adsorbent with acetylene, ethylene and nitrous oxide in the temperature range of 100 to 250 °C (373-523 K) are plotted as a function of inverse absolute temperature in Figures II-2a, II-2b and II-2c respectively. The corresponding

van't Hoff parameters are given in Table II-4. Acetylene peaks were only included at temperatures greater than 200 °C (473 K), due to much stronger adsorption at lower temperatures. Acetylene had the highest Henry's Law constants and the heat of adsorption values among the adsorbates studied for this adsorbent, due to the dual effect of its triple bond and its quadrupole moment. Due to the more interactive nature of the 13X adsorbent, the K_p values for acetylene, ethylene and nitrous oxide were higher when compared to Alcan activated alumina. The Heat of adsorption values, van't Hoff plot parameters and the R^2 values for each of the adsorbates are given in Table II-4. Ethylene had a slightly higher heat of adsorption value when compared to nitrous oxide due to the presence of double bond in its structure.

Ash Meadows Clinoptilolite

This is the base adsorbent obtained from American Resource Corp. The Henry's Law constant plots for Ash Meadows Clinoptilolite with ethylene and nitrous oxide are shown in Figures II-2b and II-2c for the temperature range of 150 - 250 °C (423-523 K). Results indicated that as the temperature of the column increased, Henry's Law constants decreased, which is consistent with exothermic physical adsorption. Carbon dioxide and acetylene peaks were not observed at the temperatures tested for reasons of very strong adsorption. When the results for nitrous oxide and ethylene are compared with this adsorbent, it was observed that Henry's Law constants as well as the heat of adsorption values for ethylene were much smaller than those for nitrous oxide for all the temperatures tested. ICP analysis on the Ash Meadows Clinoptilolite, showed that a large number of divalent Ca^{++} ions were present within the structure. When the zeolite has

divalent cations in its structure, rather than monovalent cations, its surface becomes more heterogeneous, since the positive and negative ion pockets on the surface are less frequent and are more concentrated. This heterogeneity of the surface makes it more attractive to polar molecules. Since nitrous oxide has a much higher quadrupole moment compared to ethylene, as well as a dipole moment, it is not surprising to see higher K_p and heat of adsorption values for this adsorbate. Higher K_p values for nitrous oxide at low temperatures make Ash Meadows Clinoptilolite a possibly useful adsorbent for nitrous oxide trace impurity removal from ambient air. The heat of adsorption for ethylene with Ash Meadows Clinoptilolite was not very different than that for other adsorbents as can be seen in Table II-4.

Alcan Actiguard 600PC Adsorbent

This is a composite of Alcan activated alumina and Ceca 13X adsorbent obtained from Rio Tinto Alcan. For all temperatures tested, a carbon dioxide peak was not observed at all, since this adsorbent contained some activated alumina in which carbon dioxide is known to be chemisorbed. The results for Alcan Actiguard 600PC with all the other adsorbates studied for temperature range of 150-300 °C (423-573 K) are shown as van't Hoff plots in Figure II-3. Corresponding heat of adsorption data are given in Table II-4. Henry's Law constants could not be obtained at low temperatures studied, since some of the adsorbates were very strongly adsorbed. This caused an unusual widening of the response peak at lower temperatures, decreasing the precision of the calculations to unacceptable levels.

Acetonitrile had the largest K_p values among the adsorbates studied, owing to its triple bond structure and a higher dipole moment of 3.92 Debye. Methanol being a polar molecule (dipole moment of 1.7 Debye) had greater attraction to the heterogeneous polar composites followed by the double bonded methyl tert-butyl ether, dimethyl sulfoxide and methyl sulfoxide. The Henry's Law constant values were inversely proportional to the column temperatures as observed earlier for other adsorbents. Acetylene was more strongly adsorbed than ethylene and nitrous oxide by Alcan Actiguard 600PC and CECA G5-13X adsorbents.

Based on the results from Table II-4, acetylene had the highest and nitrous oxide had the lowest heat of adsorption values for Alcan Actiguard 600 PC. Methanol, acetonitrile and methyl sulfoxide had similar ΔH values in the range of 9300-9600 cal/mol, followed by lower ΔH values for dimethyl sulfoxide, ethylene and methyl tert-butyl ether in decreasing order.

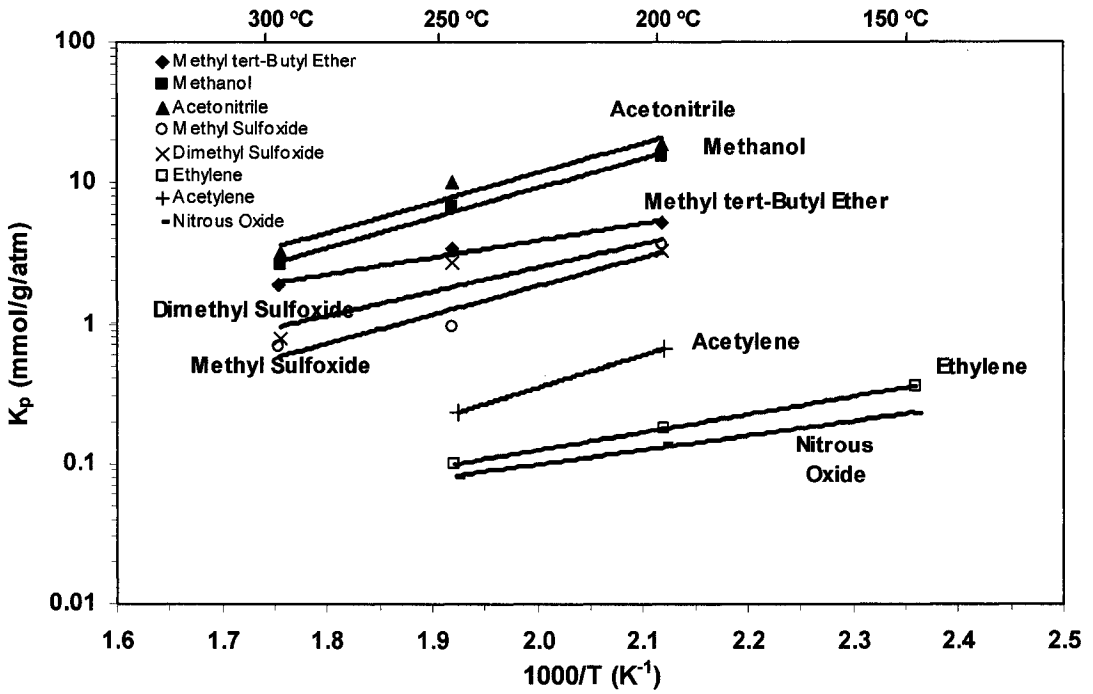

Figure II- 3. Henry's Law constants for acetonitrile, methanol, methyl tert-butyl ether, methyl sulfoxide, dimethyl sulfoxide, acetylene, ethylene and nitrous oxide impurities for Alcan Actiguard 600PC adsorbent.

Alcan Actiguard 650PC Adsorbent

This is a composite adsorbent obtained from Rio Tinto Alcan which contains a higher composition of Ceca 13X within the Alcan activated alumina adsorbent compared to Alcan Actiguard 600PC. Carbon dioxide peaks for this adsorbent were not observed at the temperatures tested for the same reasons mentioned with the discussion of the Alcan Actiguard 600PC adsorbent. The corresponding van't Hoff plots and their parameters in the temperature range of 150 - 250 °C (423-523 K) are given in Figure II-4 and Table II-4, respectively. Alcan Actiguard 650PC was a much better adsorbent compared to Alcan Actiguard 600PC, as well as Alcan AA-300 with much higher Henry's Law constants for all the adsorbates studied. This is expected, since Alcan Actiguard 650PC contains more 13X than Alcan Actiguard 600PC. As listed in Table II-2, both of the Actiguard

adsorbents contain 13X zeolite as well as regular activated alumina. Since 13X showed higher Henry's Law constant values compared to Alcan AA-300 alumina, the higher the composition of 13X in the structure of the adsorbent, the higher would be the Henry's Law constant. The order of the Henry's Law constants for all the adsorbates was the same as Alcan Actiguard 600PC, except for methyl tert-butyl ether which had a higher ΔH than acetylene.

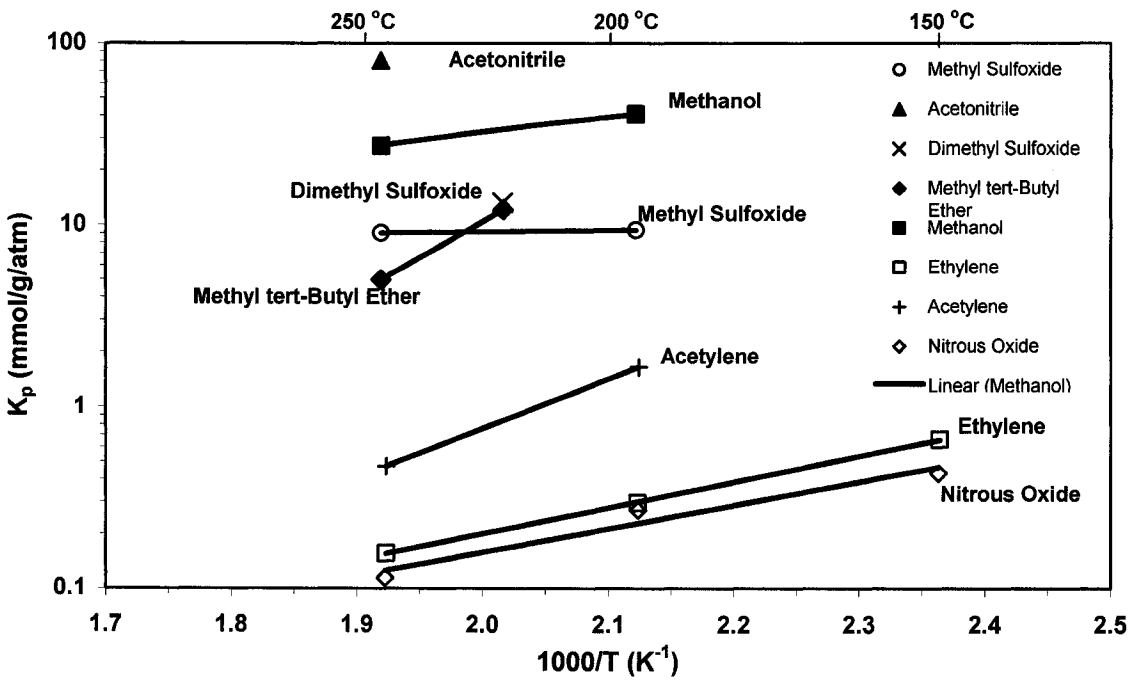

Figure II- 4. Henry's Law constant results for acetonitrile, methanol, methyl tert-butyl ether, methyl sulfoxide, dimethyl sulfoxide, acetylene, ethylene and nitrous oxide impurities for Alcan Actiguard 650PC adsorbent.

COMPARISON OF ALL ADSORBENTS TESTED

The comparison of all the six different adsorbents studied in this paper can be seen in Figure II-5. Based on their Henry's Law constant values at 423 K (150 °C), at which temperature we were able to get the most data, CABSORB Chabazite had the highest Henry's Law constant for ethylene and nitrous oxide adsorption except for Ash Meadows Clinoptilolite. The adsorbent Alcan AA-300 alumina showed the lowest Henry's Law constant values for these gases.

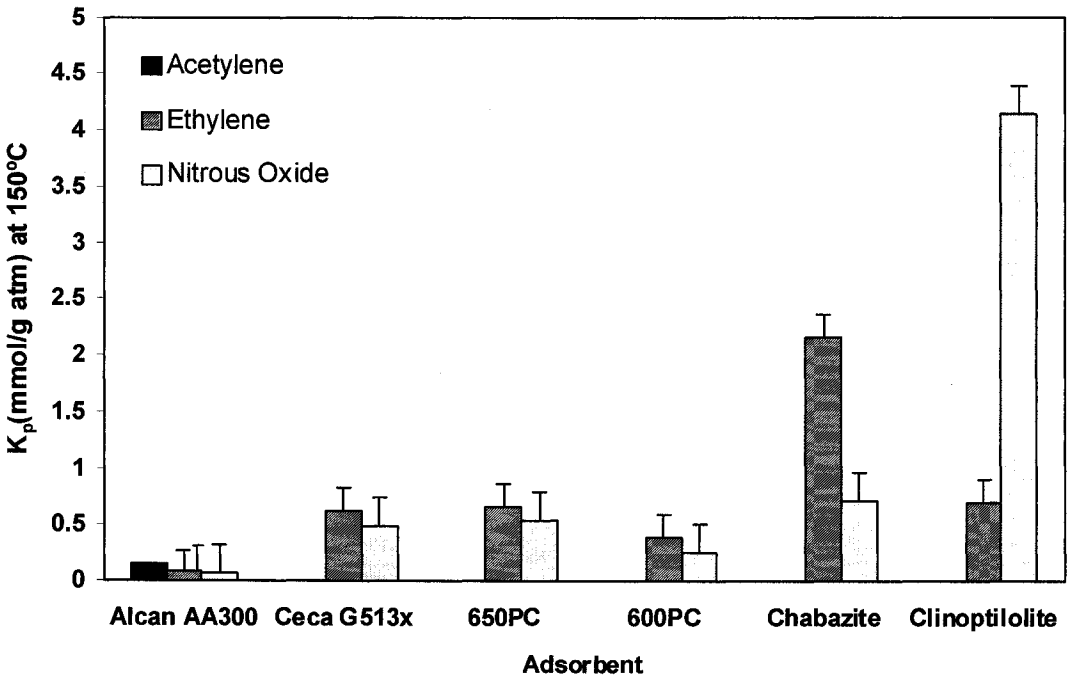

Figure II- 5. Comparison of Henry's Law constant results for acetylene, ethylene and nitrous oxide impurities at 150°C for adsorbents, Alcan AA-300, Alcan Actiguard 600PC, 650PC, Ceca G5-13X, CABSORB Chabazite and Ash Meadows Clinoptilolite.

The order of heat of adsorption for ethylene, nitrous oxide, and acetylene for tested adsorbents is shown below:

Ethylene: CABSORB Chabazite > Ceca G5-13X > Ash Meadows Clinoptilolite > Alcan Actiguard 650PC > Alcan Actiguard 600PC> Alcan AA-300 alumina

Nitrous oxide: Clinoptilolite > Ceca G5-13X > Alcan Actiguard 650PC > CABSORB Chabazite > Alcan Actiguard 600PC> Alcan AA-300 alumina

Acetylene: Alcan Actiguard 650PC > Alcan Actiguard 600PC > Ceca G5-13X > Alcan AA-300 alumina

In this study, composite adsorbents were also tested to determine the effect of the zeolite percentage in activated alumina, on the Henry's Law constants for the gas adsorbates. The results observed on Alcan Alumina, Ceca G5-13X zeolite, Alcan Actiguard 600PC and 650PC are shown in Figure II-6 at 150°C (423 K). As can be seen from this figure, the composite with a higher percentage of zeolite in its structure gave the highest Henry's Law constant values for ethylene, even compared to the pure zeolite. These results suggest that there is a linear relationship between the amount of zeolite in the composite adsorbent and the Henry's Law constant for the composites, but when the pure zeolite is taken into account, the relationship is non-linear. For nitrous oxide adsorption, this relationship is linear, even when the pure zeolite is included.

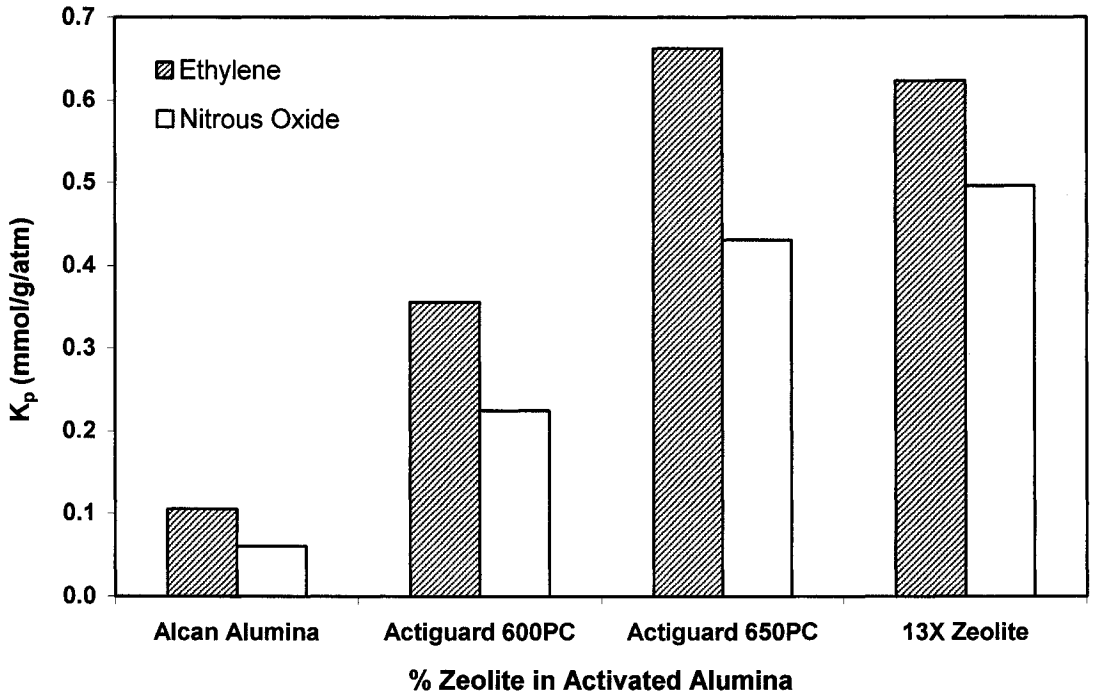

Figure II- 6. The effect of zeolite in activated alumina adsorbent for ethylene and nitrous oxide Henry's Law constants for adsorption at 150°C (423 K)

As can be seen from Figure II-6, the highest Henry's Law constant was observed with pure zeolite 13X. For the composites, the higher the zeolite percentage, the higher was the Henry's Law constant.

A comparison of Alcan Actiguard 600 PC and 650 PC adsorbents for methyl sulfoxide, acetonitrile, dimethyl sulfoxide, methyl tert-butyl ether and methanol impurities at 250 °C (523 K) are given in Figure II-7. Results suggested that Alcan Actiguard 650 PC which has a higher ratio of 13X zeolite to activated alumina in the adsorbent structure showed greater affinity for adsorption and thus higher K_p values for all these adsorbates, compared to Alcan Actiguard 600 PC. The difference between these two adsorbents was much higher for the triple bonded acetonitrile and the highly polar methanol.

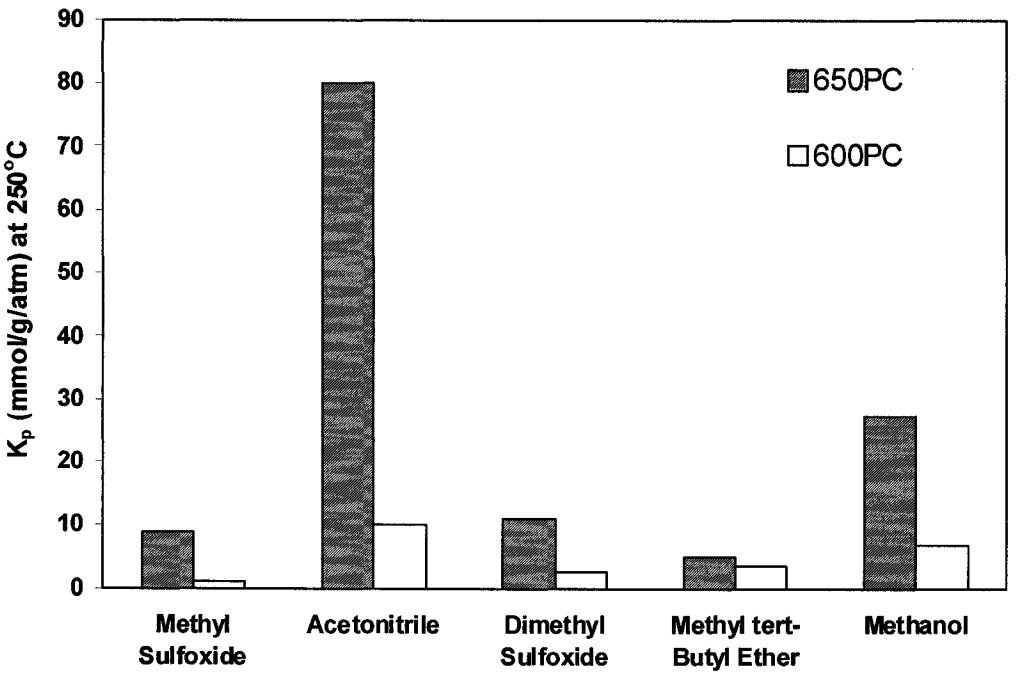

Figure II- 7. Comparison of the adsorption Henry's Law constants at 250°C for Alcan Actiguard 650PC and 600PC for five trace impurities studied.

CONCLUSIONS

This study showed the order of Henry's Law constants and heats of adsorption for six different adsorbents and for various impurity gases. The adsorbents screened included Alcan AA-300 activated alumina, activated alumina/13X zeolite composites (Alcan Actiguard 600 PC and 650 PC), CABSORB Chabazite, 13X zeolite (CECA G5-13X) and Ash Meadows Clinoptilolite adsorbent. Henry's Law constants measured were inversely proportional to the absolute temperature of the system, which validated the application of the van't Hoff equation. Based on K_p and heat of adsorption values, Chabazite had the highest capacity and interaction with ethylene and Ash Meadows Clinoptilolite had the highest capacity and interaction with for nitrous oxide. Alcan AA-300 alumina had the

lowest K_p values and heat of adsorption for nitrous oxide and ethylene. For acetylene adsorbate, the value of heat of adsorption was the highest for the composite Alcan Actiguard 650PC, and the lowest for the Alcan AA-300 alumina. All these tested adsorbents find applications in the trace impurity removal from air. The present work gives basic guidelines on adsorbents that can be used to target specific impurities present in air.

The study on the effect of 13X zeolite addition into activated alumina composite adsorbent showed that a higher ratio of 13X zeolite to activated alumina present in the Alcan Actiguard 650 PC adsorbent structure gave higher K_p values for ethylene. It was also observed that a higher composition of 13X zeolite in the composite exhibits a higher adsorption capacity, compared to both pure 13X zeolite and pure activated alumina adsorbents which indicated a combined effect between these adsorbents for the adsorption of ethylene.

The results with other impurities, acetonitrile, methanol, dimethyl sulfoxide, methyl sulfoxide and methyl tert-butyl ether also showed that Alcan Actiguard 650PC was also better than Alcan Actiguard 600PC in removing them. This observation can be tied to the compositions of the hybrid adsorbents.

For Alcan AA-300 alumina, Alcan Actiguard 650PC and 600PC, carbon dioxide peaks were not observed at the temperatures tested since they contained activated alumina, which is known to chemisorb carbon dioxide.

ACKNOWLEDGEMENTS

Financial supports received from Ontario Centres of Excellence (OCE), Air Products and Chemicals Inc., and RioTinto Alcan are gratefully acknowledged.

NOMENCLATURE

c	Sorbate concentration in bulk phase (mol/cm^3)
K	Average Henry's Law adsorption equilibrium constant (dimensionless)
K_0	Pre-exponential factor (mol/g/atm)
K_p	Average Henry's Law adsorption equilibrium constant (mol/g/atm),
L	Length of the chromatographic column (cm)
R	Gas constant (cal/mol/K)
R^2	Coefficient of determination
t	Time (s)
T	Absolute temperature (K)
v	Interstitial fluid velocity (cm/s)

Greek Letters

ΔH	Heat of adsorption at low coverage (cal/mol)
ε	Porosity of the bed (dimensionless)
μ	First moment, (s)
μ_D	System dead time, (s)
ρ	Density of the adsorbent (g/ cm^3).

Abbreviations

GC Gas Chromatograph

He Helium gas

ICP Inductively Coupled Plasma spectrometry

PSA Pressure Swing Adsorption

REFERENCES

1. Zhu, H. Y., Vansant, E. F. and Lu, G. Q "Development of Composite Adsorbents of Carbon and Intercalated Clay for N_2 and O_2 Adsorption: A Preliminary Study", Journal of Colloid and Interface Science, **1999**, 210, 352.
2. Vansant, E. F., "Proceedings of the Third International Symposium on Separation Technology", **1994**, pg. 229. Elsevier, Amsterdam.
3. Glover, T.G., Dunne, K.I., Davis, R.J. and LeVan, M.D., "Carbon–silica composite adsorbent: Characterization and adsorption of light gases", Microporous and Mesoporous Materials, **2008**, 111, 1.
4. Golden, T.C; Kalbassi, M.A.; Taylor, F.W.; Allam, R.J. Use of Zeolites and Alumina in Adsorption Processes. U. S. Patent 5,779,767, 14 July 1998.
5. Tezel, F.H, Golden, T.C., Mogan, J., Morin, B., "Use of composite activated alumina adsorbents for separation of hydrocarbons from olefin containing streams", **2005**, AIChE Annual Meeting Conference Proceedings, USA.
6. Tezel, F.H; Apolonatos, G. Chromatographic study of adsorption for N_2, CO and CH_4 in molecular sieve zeolites. Gas separation and Purification. **1992,** 7(1), 11.

7. Kumar, R; Huggahalli, M.; Deng, S.; Andrecovich, M. Trace impurity removal from air. Adsorption. **2003**, *9* (3), 243.

8. Schmidt W.P; Kovak, K.W.; Licht, W.R.; Feldman, S.L. Managing Trace Contaminants in Cryogenic Air Separation. 12th Intersociety Cryogenic Symposium, AIChE Spring Meeting, Atlanta, USA, **2000**.

9. Van der Vlist, E; Van der Meijden, J. Determination of the Adsorption Isotherms of the Components of Binary Gas Mixtures by Gas Chromatography. J. Chromatography. **1973** 79, 1.

10. Shah, D.B; Ruthven, D.M. Measurement of Zeolitic Diffusivities by Chromatography. AIChE J. **1977**, *23* (6), 804.

11. Hyun, S.H; Danner, R.P. Determination of Gas Adsorption Equilibria by the Concentration-Pulse Technique. AIChE Symp. Ser. **1982**, 34(11), 1861.

12. Buffman, B.A; Mason, M.; Yadav, G.D. Retention Volumes and Retention Times in Binary Chromatography. J. Chem. Soc. Faraday Trans. **1985**, *1*(81), 161.

13. Buffman, B.A; Mason, M.; Heslop, M.J. Binary Adsorption Isotherms from Chromatographic Retention Times. Ind. Eng. Chem. Res. **1999**, *38*(3), 1114.

14. Tezel, F.H; Tezel H.O.; Ruthven, D.M. Determination of Pure and Binary Isotherms for Nitrogen and Krypton. J. Colloid Interface Science. **1992**, 149, 197.

15. Heslop, M.J; Buffman, B.A.; Mason, G. A. Test of the Polynomial-Fitting Method of determining Binary-Gas-Mixture Adsorption Equilibria. Industrial and Engineering Chemistry Research. **1996,** *35*(4), 1456.

16. Kabir, H; Grevillot, G.; Tondeur, D. Equilibria and Activity Coefficients for Non-Ideal Adsorbed Mixtures from Perturbation Chromatography. Chemical Engineering Science. **1998**, *53*(9), 1639.

17. Harlick, P.J.E; Tezel, F.H. An experimental adsorbent screening study for CO_2 removal from N_2. Microporous and Mesoporous Materials. **2004,** 76, 71.

18. Ruthven, D.M; Tezel, F.H.; Devgun, J.S. Adsorptive Separation of Kr from N_2 – Part I adsorbent screening studies. The Canadian Journal of Chemical Engineering. **1984**, 62, 526.

19. Li, P; Tezel, F.H. Adsorption separation of N_2, O_2, CO_2, and CH_4 gases by β zeolite. Microporous and Mesoporous Materials. **2007,** 98, 94.

20. Li, P; Tezel, F.H. Equilibrium and kinetic analysis of CO_2- N_2 adsorption separation by concentration pulse chromatography. Journal of Colloid and Interface Science. **2007,** 313, 12.

21. Harlick, P. J. E; Tezel, F. H. A Novel Solution Method for Interpreting Binary Adsorption Isotherms from Concentration Pulse Chromatography Data. Adsorption. **2000**, 6, 293.

22. Lide, D. CRC Handbook of Chemistry and Physics, 87 th Ed.; Taylor and Francis: Boca Raton, USA, **2006**.

23. Krupay B. W; Amenomiya, Y. Alkali-Promoted Alumina Catalysts. Chemisorption and Oxygen Exchange of Carbon Monoxide and Carbon Dioxide on Potassium-Promoted Alumina Catalysts. Journal of Catalysis. **1981**, 67, 362.

24. K.B. Lee; Beaver, M.G; Caram H.S; Sircar, S. Chemisorption of carbon dioxide on sodium oxide promoted alumina. AIChE J. **2007,** 53, 2824.

CHAPTER III

BINARY ADSORPTION BEHAVIOUR OF METHANE AND NITROGEN GASES

Mulgundmath, V.P [a] Tezel, F.H [a], Hou, F [a], Mogan, J [b], Golden, T.C [c], Morin, B [b]

[a] Department of Chemical and Biological Engineering, University of Ottawa, 161, Louis Pasteur, Ottawa. K1N 6N5. Canada

[b] RioTinto Alcan, 1000 Development Drive, P O Box 250, Brockville. ON K6V 5V5. Canada.

[c] Air Products and Chemicals, Inc., 7201, Hamilton Blvd., Allentown, PA USA 18195-1501, USA.

Submitted to Journal of Porous Materials.

Presented at the Fundamentals of Adsorption (FOA9) conference, May 20-25, 2007, Sicily-Italy

ABSTRACT

Separation of methane and nitrogen gases is critical in the upgrading of LFG (Landfill gas), natural gas and coal bed gas in order to have a commercial heating value for methane. From an environmental point of view, methane capture from landfill gas is essential to prevent greenhouse gas emissions. Adsorption could be a beneficial process to capture low purity methane from a landfill site that is nearing the end of its lifecycle and produce high purity methane. In this work, Ceca 13X zeolite and Alcan activated Alumina AA 320-AP have been studied for their potential for this separation and compared with Silicalite in literature. Single component and mixture adsorption isotherms were determined at 40 and 100 °C for these adsorbents by constant volume method and concentration pulse chromatographic technique, respectively. Mixture adsorption isotherms for the binary system of methane and nitrogen gases at 40 and 100 °C and 1 atmosphere total pressure have been determined by VV - CPM (Van der Vlist and Van der Meijden Concentration Pulse Method). The application of extended Langmuir model for this binary system have also been discussed and compared to the experimental results.

Results show that equilibrium separation factor for silicalite is larger than zeolite Ceca 13X and Alcan activated alumina AA320-AP. Both Silicalite and Ceca 13X find application in the bulk separation of methane from nitrogen when y_{CH4}>0.4, especially in LFG (Landfill gas), coal bed gas and natural gas.

INTRODUCTION

The separation of CH_4-N_2 is critical in the upgrading of natural gas, LFG (Landfill gas) and coal bed gas. Natural gas consists mainly methane, with variable amounts of C_{2+} hydrocarbons and often nitrogen and carbon dioxide as minor impurities. The use of natural gas as a fuel is convenient and efficient from an environmental point of view and has become economically viable. It is used primarily for heat, in industrial, commercial and residential settings. Its use is expected to achieve the highest growth rate among all primary energy sources [1]. From an environmental point of view, it has the greatest advantage of producing no smoke or ash on burning. More recently natural gas is being used as a vehicular fuel, since the amount of lead discharged in exhaust gases is reduced to zero. Moreover, it is cheaper than gasoline or diesel. There are specific restrictions for the amounts of nitrogen contained in natural gas in order to meet the pipeline quality for minimum heating value specifications (typically 950 BTU/ft^3 or <4% inerts for US pipeline specifications) [2].

Methane is the primary component of landfill gas (LFG) whose composition varies from one site to another which would require the removal of nitrogen along with carbon dioxide in order to have a commercial heating value for methane. In addition to contributing to green house gas emissions when released into the atmosphere, LFG (Landfill gas) can cause nuisance odours, stress on vegetation, smog, and a risk of fire, explosion and asphyxiation especially towards the end of its lifecycle when low quality methane is no longer captured. The low quality methane cannot be marketed to consumers directly since it does not meet the grade specifications. Effectively capturing

methane from landfill gas during this period can reduce the factors contributing to global warming [3, 4]. Landfill sites generate over a quarter of the methane emissions caused by human activity in Canada, sending 1.2 million tons of this potent greenhouse gas into the atmosphere each year which is the equivalent of greenhouse gas emissions from more than six million cars or about 40 per cent of all the passenger vehicles in Canada [5]. The methane produced by Canadian landfill sites contains enough energy in the range of 18-25 x 10^3 kJ/m^3 (depending on the composition) required to heat more than 600,000 homes a year [5].

Coal mines traditionally have a higher nitrogen concentration and typically the low quality natural gas has to be upgraded. Methane (CH_4) - Nitrogen (N_2) separation also applies to enhanced oil recovery where nitrogen is injected into the reservoir and recovered as a gas fraction along with other petroleum gases. Nitrogen has to be separated from these petroleum gas fractions including the main component methane. This is necessary to obtain pure petroleum products and achieve a high heating value for methane. Traditionally, the CH_4–N_2 separation is practiced by cryogenic distillation, involving expensive high pressure units and large requirements of energy [6]. Adsorption separations are used widely among other separation processes as they tend to utilise fewer resources including energy and are highly efficient [7-12].

Methane is the most important non-CO_2 greenhouse gas which has a detrimental effect on the ozone layer in the atmosphere thereby contributing to global warming of this planet. Despite the small amounts of methane released to the atmosphere, the global warming

effect of methane is 25 times greater than that of carbon dioxide [13]. Any reduction in methane emissions is very important in the short and medium term atmosphere restoration. The separation of methane from nitrogen is critical in the upgrading of LFG, coal bed gas and natural gas in order to achieve a commercially viable heating value for methane. Hence, this study has concentrated on the adsorption behaviour of methane and nitrogen gases.

The physical properties of methane and nitrogen gases are summarised in Table III-1. Methane is non polar while nitrogen has a permanent quadrupole moment.

Table III- 1. Summary of the physical properties of methane and nitrogen gases [14]

Physical Properties	CH_4	N_2
Molecular weight, g/mol	16.04	28.01
Kinetic diameter, nm	0.38	0.364
Quadrupole moment, (x 10^{-26}esu.cm^2)	0	1.52
Dipole moment, Debye	0	0
Polarizability, (10^{-24} cm^3)	2.593	1.7403
Boiling point, K	161.48	77.3
Specific gravity (air = 1) (1 atm and 288 K)	0.554	0.967
Critical temperature, K	190.6	126.2
Critical pressure, atm	46.80	34.67
Molar heat capacity (298.15K, 1 atm), Jmol^{-1}K^{-1}	35.9	29.1
Thermal conductivity (1 atm and 273.15 K) W/(mK)	0.033	0.024

A broad range of adsorbents are available for methane-nitrogen gas separation applications. Separation occurs due to the difference in molecular weight, shape, polarity, dipole and quadrupole moments which cause some molecules to be held more strongly on the adsorbent surface or because the pores are too small to admit larger molecules. Physical characterisation permits to better tailor certain desirable properties of an adsorbent characterised by high porosity, pore volume, surface area and the type of pore size distribution. Such an ideal adsorbent provides for a good adsorptive capacity and faster kinetics.

The most widely used adsorbents for CH_4–N_2 gas separations are zeolites, with 13X and silicalite being the most popular from this class [15], and activated alumina. Zeolite 13X consists of a rigid backbone composed of silicon, aluminum, and oxygen atoms. Zeolite 13X crystal has a face centered cubic structure which consists of uniform pore sizes of approximately 10 Å [16]. Silicalite is one of the most important synthetic zeolites. Its distinctive features include high thermal and hydrothermal stability, hydrophobic and organophilic adsorptive properties and an intermediate (ten-ring) pore size which leads to molecular sieve size selectivity. Its negligible aluminum content (the Si/Al ratio in the thousands) is responsible for the hydrophobic nature of its surface [11].

Cavenati et al. [17] measured the single component adsorption capacities of CH_4 and N_2 on the hydrophilic zeolite 13X and compared them to the hydrophobic carbon molecular sieve adsorbent. Single component adsorption isotherm by Li and Tezel indicated that the

adsorption capacities of both CH_4 and N_2 on the hydrophobic silicalite were slightly lower than the zeolite 13X [18].

Activated alumina belongs to the class of hydrophilic adsorbents that are increasingly being used for various adsorption applications including moisture removal [8]. The hydrophilic alumina has better resistance against moisture and the non-uniform pore distribution ranging from 20-500 Å provides large pathways to the internal surfaces of the activated alumina structure.

In this study, Ceca 13X and Alcan activated alumina AA320-AP have been studied for adsorption separation of CH_4–N_2 at 40°C and 100°C and compared to silicalite [18] in the literature. Constant volume method and concentration pulse method (CPM) have been employed to determine the single component and binary mixture adsorption behaviours. The use of CPM technique for studying mixture behaviour is very attractive since it is relatively inexpensive to setup and has a high turnover rate [20-22]. This technique offers an alternate approach to gravimetric and volumetric methods for the experimental studies of the kinetics and the equilibria of adsorption [22, 23]. These experimentally determined behaviours of binary gas mixtures can be applied to industrial adsorption separation units [23-26]. The design of an adsorption separation unit requires a suitable adsorbent with high capacity for the target gas as well as the knowledge of preferable conditions to improve the selectivity of the adsorbent for one or more components present in the gaseous mixture. For this study, Van der Vlist and Van der Meijden Concentration Pulse

Method [VV-CPM] was chosen to obtain binary adsorption isotherms from the experimental data.

THEORY

SINGLE COMPONENT ADSORPTION ISOTHERMS

The conventional constant volume adsorption apparatus is used to determine single component gas adsorption isotherms of methane and nitrogen gases. This technique involves a known volume of the single component gas to be adsorbed on an adsorbent sample placed in a closed system while monitoring the pressure changes. The single component gas is allowed to attain equilibrium and the measured pressure decrease is used to calculate the amount of gas adsorbed under the given isothermal conditions [11].

There are many models interpreting adsorption isotherms for single component gas systems. The simplest and still the most useful single component gas isotherm model is the Langmuir isotherm [27]:

$$\theta = \frac{q}{q_m} = \frac{BP}{1+BP} \quad \text{.....(1)}$$

where B is the affinity constant, θ is the fractional coverage, q is the amount adsorbed, q_m is the saturation adsorption capacity or maximum amount adsorbed, and P is the pressure. The parameters of single component isotherm fits to Langmuir model are determined by non linear regression in MS-Excel.

BINARY ADSORPTION ISOTHERMS

In concentration pulse chromatography, a pulse of the sample gas is injected into the carrier gas stream which passes through a packed adsorbent column. The response of the column at the exit, for this sample injection is measured as concentration versus time. From this response peak, a mean retention time, μ is determined experimentally. The mean retention time is related to the effective isotherm slope, K by Equation (2) [18-22]:

$$\mu = \frac{\int_0^\infty c(t-\mu_D)dt}{\int_0^\infty cdt} = \frac{L}{v}\left[1+\frac{(1-\varepsilon)K}{\varepsilon}\right] \quad \text{.....(2)}$$

where t represents time, c is the outlet adsorbate concentration, L is the adsorption column length, ε is the porosity of the column, v is the interstitial fluid velocity, K is the dimensionless Henry's law constant and μ_D is the dead time. The dimensionless Henry's law constant, K can be converted to a dimensional constant, K_p using Equation (3):

$$K_p(Dimensional) = \frac{K(Dimensionless)}{RT\rho} \quad \text{.....(3)}$$

where R is the gas constant, T is the absolute temperature and ρ is the density of pellet (without internal pores). For a binary mixture, the K_p value is a function of the slopes of the isotherms of the individual components which is given by Equation (4) [20, 28]:

$$K_p = (1-y_1)\frac{dq_1}{dP_1} + y_1\frac{dq_2}{dP_2} \quad \text{.....(4)}$$

where $\frac{dq_1}{dP_1}$ and $\frac{dq_2}{dP_2}$ are the slopes of the binary adsorption isotherms for components 1 and 2, respectively. When K_p values are determined for various concentrations of the carrier gas, this technique allows for the experimental evaluation of both single

component isotherms and binary mixture isotherms. In this study, this technique was used for the determination of binary mixture adsorption isotherms.

Van der Vlist and Van der Meijden concentration pulse method [VV-CPM] is a third degree polynomial form that describes the binary K_p data as a function of the gas composition in the carrier gas, y_1 [25].

$$K_p = G_0 + G_1 y_1 + G_2 y_1^2 + G_3 y_1^3 \quad \text{..... (5)}$$

And these "G" coefficients can be determined from the experimental K_p vs. y_1 data by a curve fit. Following this functional form, Equations (6) and (7) describe the isotherm slope functions which are defined with unknown a_i and b_i parameters:

$$\frac{dq_1}{dP_1} = a_1 + 2a_2 y_1 + 3a_3 y_1^2 \quad \text{.....(6)}$$

$$\frac{dq_2}{dP_2} = b_1 + 2b_2(1-y_1) + 3b_3(1-y_1)^2 \quad \text{.....(7)}$$

The isotherm equations are determined by the integration of Equations (6) and (7) as follows:

$$q_1 = \left(a_1 y_1 + a_2 y_1^2 + a_3 y_1^3\right)P \quad \text{.....(8)}$$

$$q_2 = b_1(1-y_1) + b_2(1-y_1)^2 + b_3(1-y_1)^3 P \quad \text{..... (9)}$$

Inserting Equations (6) and (7) into Equation (4):

$$K_p = (1-y_1)(a_1 + 2a_2 y_1 + 3a_3 y_1^2) + y_1\left[b_1 + 2b_2(1-y_1) + 3b_3(1-y_1)^2\right] \quad \text{.....(10)}$$

By comparing Equation (10) and Equation (5) and equating the coefficients of similar powers of y_1, we have:

$$G_0 = a_1 \quad \text{.....(11)}$$

$$G_1 = (-a_1 + 2a_2 + b_1 + 2b_2 + 3b_3) \quad \text{.....(12)}$$

$$G_2 = (-2a_2 + 3a_3 - 2b_2 - 6b_3) \quad \text{.....(13)}$$

$$G_3 = (-3a_3 + 3b_3) \quad \text{.....(14)}$$

The end points of single component isotherms are known which lead to:

$$(q_1)_{y1=1} = (a_1 + a_2 + a_3)P \quad \text{.....(15)}$$

$$(q_2)_{y1=0} = (b_1 + b_2 + b_3)P \quad \text{.....(16)}$$

The six unknown coefficients (a_1, a_2, a_3, b_1, b_2, b_3) can be solved by the above six linear equations. The binary isotherms are then calculated by Equations (8) and (9). This method is referred to as VV-CPM (Van der Vlist and Van der Meijden -Concentration Pulse Method).

Binary behaviour of CH_4 and N_2 are also determined by using extended Langmuir model in this study to predict the mixture isotherms:

$$q_1 = \frac{q_{m1} B_1 P_1}{1 + B_1 P_1 + B_2 P_2} \quad \text{.....(17)}$$

where subscripts 1 and 2 refer to gases 1 and 2, respectively. These predicted binary isotherms are compared to the experimental ones to see the applicability of the Extended Langmuir model to this system.

EXPERIMENTAL DETAILS

MATERIALS

Ultra high pure methane, nitrogen and helium gases supplied by Prax Air Inc., Ottawa, Canada were used in this study. Zeolite Ceca 13X was obtained from Ceca, Honfleur, France. Activated alumina, AA 320-AP (AA) was obtained from RioTinto Alcan, in Brockville, Canada.

CONSTANT VOLUME ADSORPTION SYSTEM

For measuring the single component adsorption isotherms, an AccuSorb 2100E Physical Adsorption Analyser supplied by Micromeritics Instrument Corporation and equipped with highly precise pressure transducers and thermocouples was used. Data collection was done using a National Instruments based data acquisition card and Labview 6.1 on a computer. The adsorbent samples were regenerated at 300 °C under vacuum for 12 hours before use.

CONCENTRATION PULSE CHROMATOGRAPHIC TECHNIQUE

A schematic diagram of the experimental set up for concentration pulse chromatography used for binary isotherm determination is shown in Figure III-1. The experimental and column characteristics are given in Table III-2. Before the start of each experimental run, the adsorbent packed in the column was regenerated at 1 atm and 300 °C under helium purge for 12 hours to ensure that any impurities including moisture adsorbed from air did not affect its adsorption capacity. As shown in Figure III-1, the flow rates and concentrations of the mixed gases were controlled by two MKS mass flow controllers (A). The total flow rate of the carrier gas was maintained at 15 cm^3/min. A cylindrical gas mixing chamber was installed after the mass flow controllers (MFC) to ensure a homogeneous carrier gas mixture. The carrier gas was first allowed to pass through the reference side of the TCD (Thermal Conductivity Detector) in the GC (Gas Chromatograph) and then through the sample injection valve (B). After the injection of 1 cm^3 pulse of adsorbate sample gas into the mixed carrier gas stream, the carrier and the sample gases passed through the packed adsorption column (C) and then through the sample side of TCD, where the response of the column outlet (as a voltage) to the sample injection was monitored as a function of time.

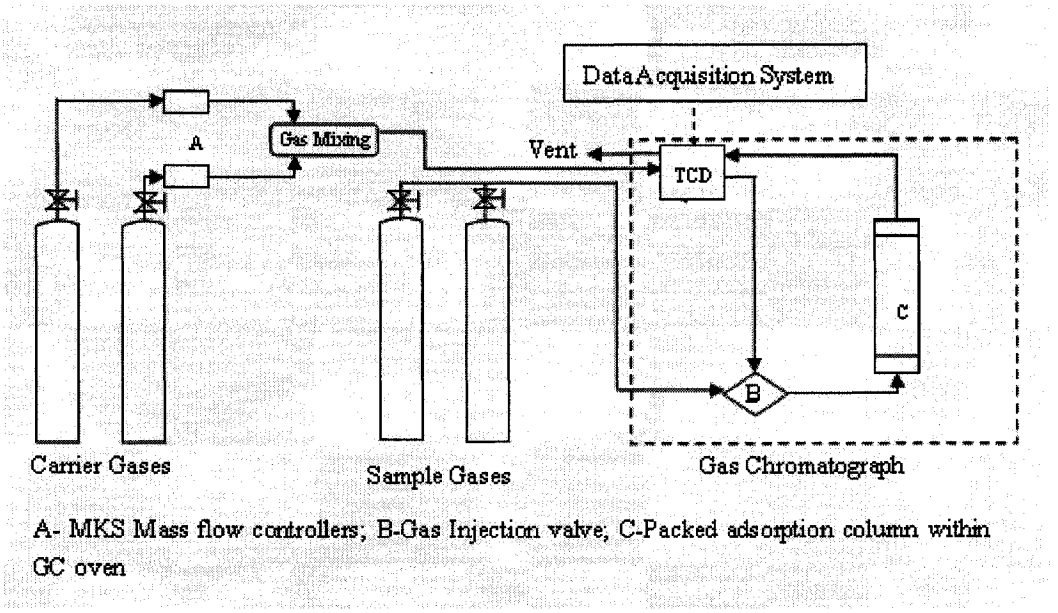

Figure III- 1. Schematic diagram of the experimental apparatus used in this study for concentration pulse chromatographic technique used for binary adsorption isotherms.

Data acquisition was performed using a National Instruments (NI) data acquisition card and Labview 6.1 on a computer. The column was packed with the adsorbent within a Varian 3300 gas chromatograph and maintained at the desired constant experimental temperature. For binary isotherm determination, mixed carrier gases of CH_4- N_2 were used with N_2 being the primary gas. Samples of each gas (both CH_4 and N_2) were injected into the column at different carrier gas concentrations (0-100%) to determine K_p. The samples were injected only after equilibrium was attained after each concentration change for various compositions of the carrier gas. Equilibrium of the carrier gas mixture with the adsorbent was confirmed by noting that the baseline of GC would be steady as equilibrium was approached.

An experimental data point represents the effective slope of the binary isotherms at a particular mixture composition. When the sample injection volume is near zero, K_p values found by both sample injections should be similar. When CH_4 is injected, the binary mixture composition increases slightly in CH_4 concentration. When N_2 is injected, the mixture composition decreases slightly in CH_4 concentration. Hence, both adsorbates were injected into the mixed carrier gas and arithmetic average retention times were taken. It was noted that the K_p values for the two adsorbates in the mixed carrier gas did not vary by more than 5% during these experimental runs.

Table III- 2. Experimental and column specifications

Ceca 13 X particle size	20 - 60 mesh
Alcan AA-320AP (AA) particle size	20 - 60 mesh
Bed porosity	0.35
Column length	10 cm
Column inner diameter	0.451 cm
Total pressure	1 atm
Regeneration temperature	300 °C
Regeneration pressure (He purge)	1 atm
Regeneration time	12 h

RESULTS AND DISCUSSION

SINGLE COMPONENT GAS ISOTHERMS

Adsorption equilibrium isotherm data for CH_4 and N_2 on Ceca 13X and Alcan activated alumina (AA) were obtained at two different temperatures (40 °C and 100 °C) for pressures up to 5 atm. which are given in Figures III-2a and III-2b as data points and compared to the literature data given as numbered curves. The curves through the data points represent the Langmuir isotherm model at the corresponding temperature. As can be seen from this figure, methane is more strongly adsorbed than nitrogen for the 2 adsorbents studied at both temperatures (40 °C and 100 °C). Since methane has no dipole or quadrupole moment, its stronger adsorption is due to a high degree of polarizability than nitrogen. The adsorption capacity increases with decreasing temperature for both of the adsorbates and both tested adsorbents, since physical adsorption is always an exothermic process.

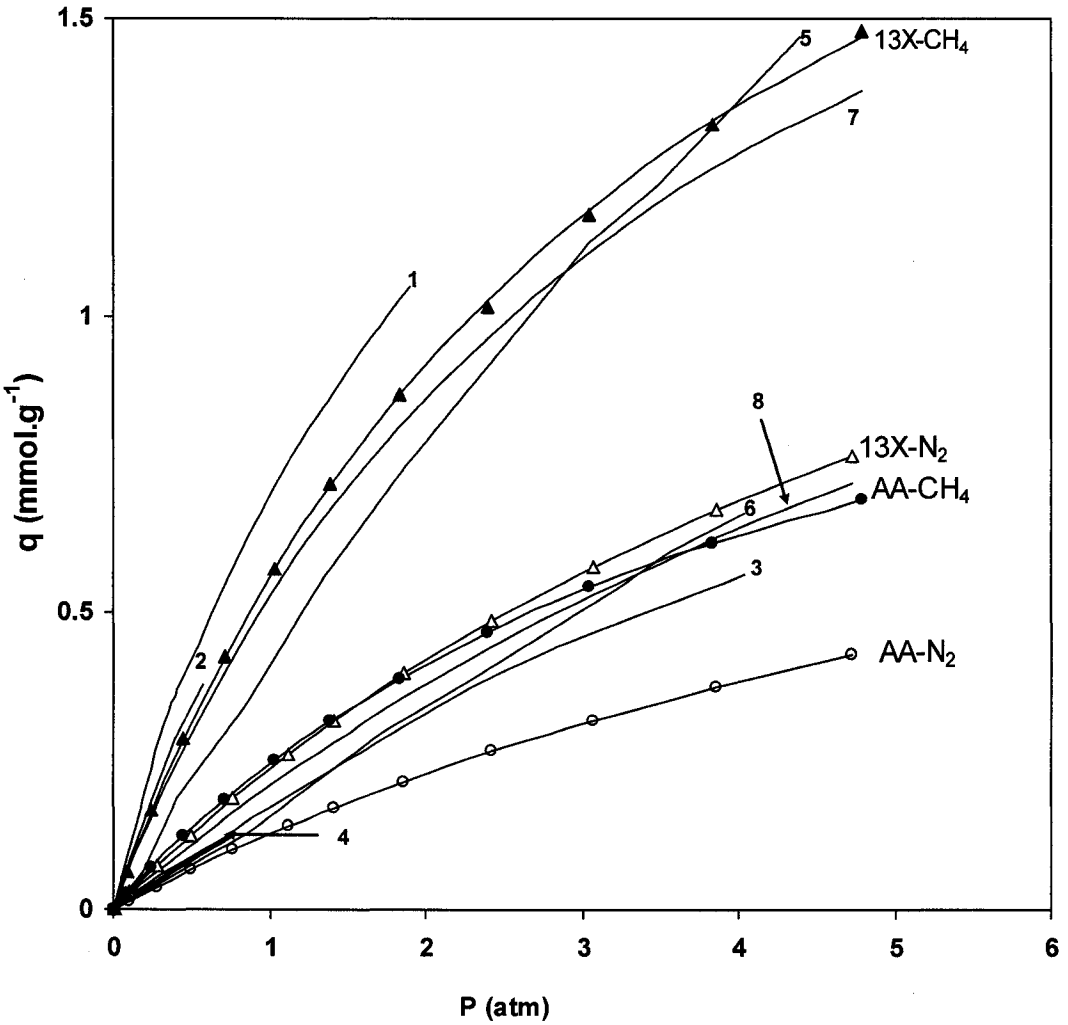

Figure III-2a. Single component adsorption isotherms for CH_4 (filled symbols) and N_2 (hollow symbols) for Ceca 13X and Alcan activated alumina (AA) at 40 °C. Numbered curves are literature comparisons:

1: CH_4 –Silicalite at 31°C (i.e., [29])

2: CH_4 – Silicalite-1 at 25°C (i.e., [30])

3: N_2 – Silicalite at 32°C (i.e., [31])

4: N_2 – Silicalite-1 at 25°C (i.e., [30])

5: CH_4 – zeolite 13X at 35°C (i.e., [17])

6: N_2 – zeolite 13X at 35°C (i.e., [17])

7: CH_4 – Silicalite at 40°C (i.e., [18])

8: N_2 – Silicalite at 40°C (i.e., [18])

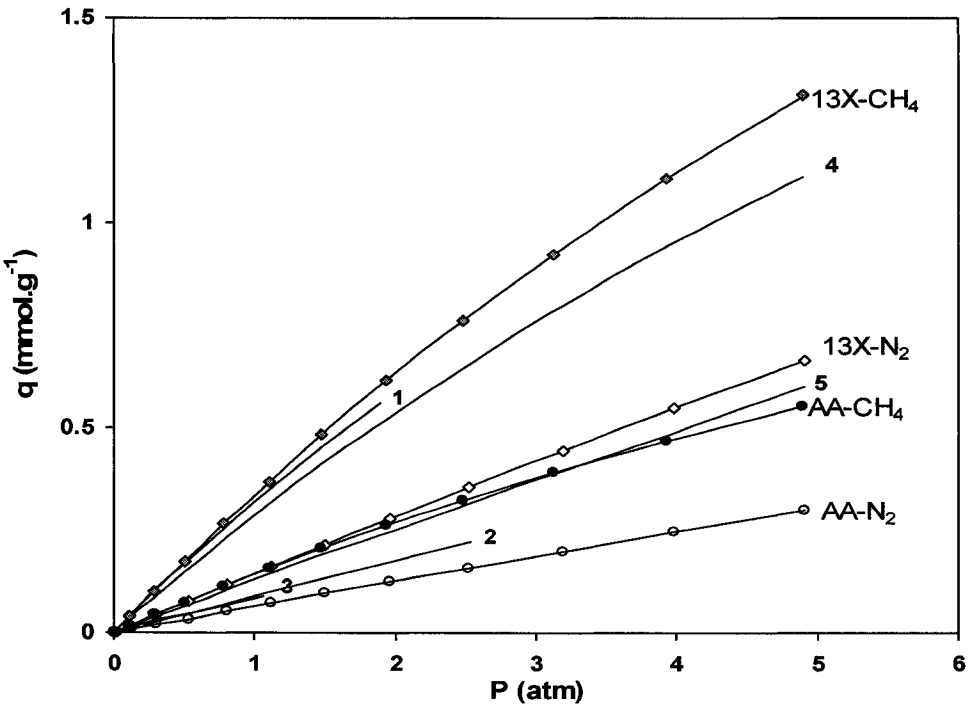

Figure III- 2b. Single component adsorption isotherms for CH_4 (filled symbols) and N_2 (hollow symbols) and N_2 for Ceca 13X and Alcan activated alumina (AA) at 100 °C. Numbered curves are literature comparisons:

1: CH_4 – Silicalite at 81°C (i.e., [29])

2: N_2 – Silicalite at 69°C (i.e., [31])

3: N_2 – Silicalite at 72°C (i.e., [33])

4: CH_4 – Silicalite at 100°C (i.e., [18])

5: N_2 – Silicalite at 100°C (i.e., [18])

When 13X adsorbent is compared to the activated alumina it was observed that 13X has higher capacities, both for CH_4 and N_2. The difference in capacities between these 2 adsorbents for CH_4 is much larger than the ones for N_2. It indicates that the cations in 13X zeolite which make the surface more heterogeneous, interacts more with the polarisable CH_4, than with N_2. When the adsorption capacities are compared for the 2 adsorbate gases, it was observed that the difference in adsorption capacities is larger for 13X at both temperatures studied.

When isotherms from the present study are compared to the ones in the literature, it can be seen that Cavenati's isotherms for 13X for both gases [17] were comparable to the ones observed in the present study, although some discrepancies were observed at low pressures. These discrepancies can easily be caused by different sample preparation, etc.

The CH_4 capacity on the silicalite as reported by Li and Tezel [18] at 40°C (curve 7 in Figure III-2a) was slightly lower than Ceca 13X at 40°C. Ceca 13X is characterised by a low Si/Al ratio (1.17) and the presence of cations in its structure renders its surface heterogeneous. This structure is responsible for its higher interaction with CH_4 when compared to the hydrophobic silicalite which has a very high Si/Al ratio (in the thousands). Among silicalites, Li and Tezel [18] observed a higher capacity for their silicalite on N_2 at 40°C (curve 8 in Figure III-2a) when compared to the observation made by Rees et al., [30] at 25 °C (curve 4 in Figure III-2a) which could be due to different silicalite samples.

It can be seen from Figure III-2b that Ceca 13X had a higher adsorption capacity for CH_4 at 100 °C followed by the observations made on silicalite at 81 °C (curve 1 in Figure III-2b by Choudhary and Mayadevi [29]), on silicalite at 100 °C (curve 4 in Figure III-2b by Li and Tezel [18]) and Alcan activated alumina (AA) at 100 °C. However, adsorption capacity of N_2 was also high for Ceca 13X compared to silicalite (curve 8 in Figure III-2a and curve 5 in Figure III-2b both obtained by Li and Tezel [18]) and Alcan activated alumina (AA) which makes it less attractive for CH_4-N_2 separation applications at both temperatures of 40 °C and 100 °C. The adsorption capacities for N_2 on silicalite (curves 2

and 3 in Figure III-2b as observed by Golden and Sircar [31] at 69 °C) and Dunne et al., [33] at 72 °C were consistent with each other but lower than silicalite data obtained by Li and Tezel [18] at 100°C which could be due to different silicalite samples.

BINARY ISOTHERMS

The K_p data obtained for CH_4-N_2 binary system along with the curve fit using VV-CPM, as a function of the gas composition at 1 atm. total pressure with Ceca 13X and Alcan activated alumina (AA) at 40 °C and 100 °C are shown in Figures III-3 and III-4, respectively. These results have been compared to silicalite [18] under the same experimental conditions. Silicalite and 13 X exhibit higher K_p values when compared to activated alumina (AA) at low gas phase concentrations of methane.

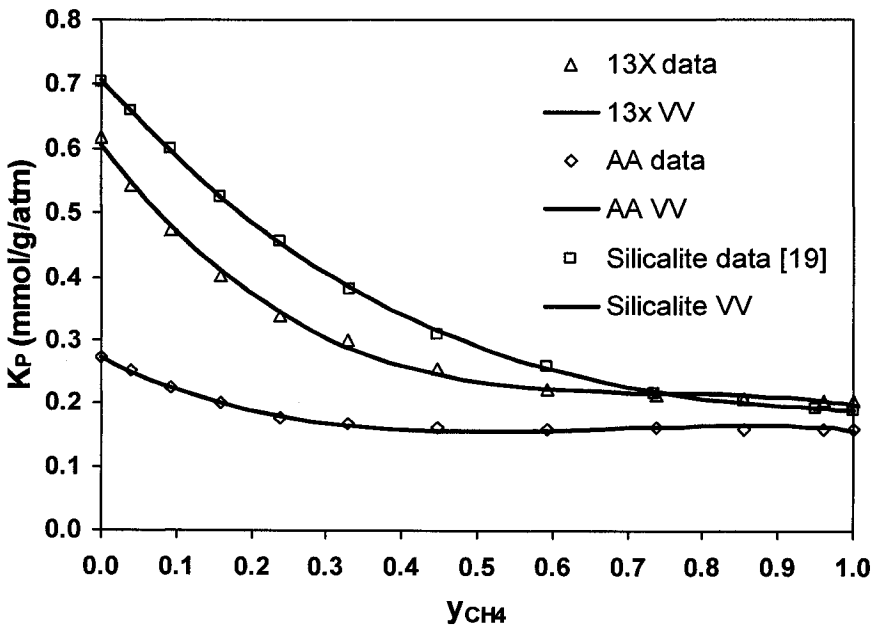

Figure III- 3. Regressions for CH_4/N_2, binary K_p data with Ceca 13X, Alcan activated Alumina (AA) and silicalite [18] by VV-CPM at 40 °C and 1 atm total pressure.

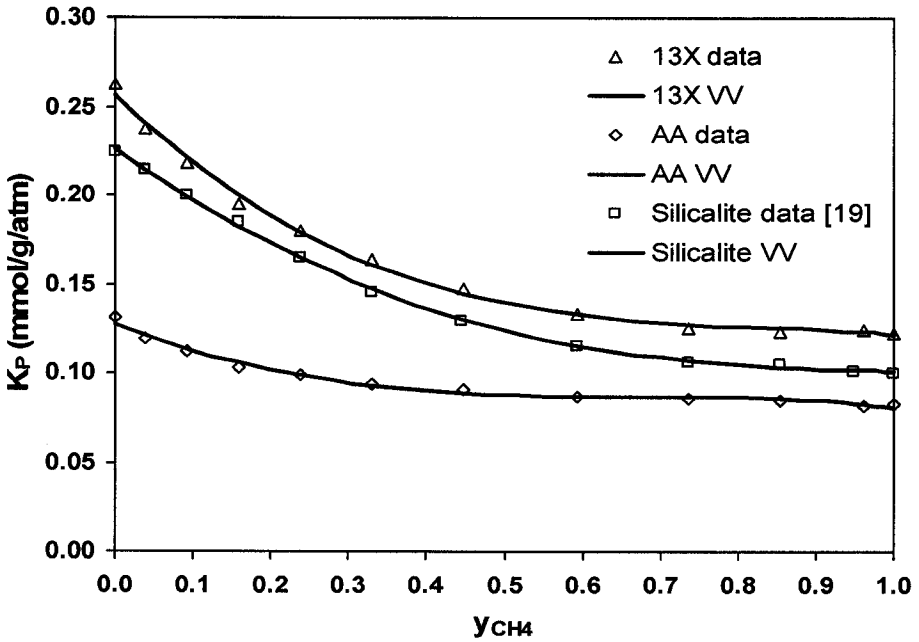

Figure III- 4. Regressions for CH_4/N_2, binary K_p data with Ceca 13X, Alcan activated alumina (AA) and silicalite [18] by VV-CPM at 100 °C and 1 atm total pressure.

By using equations (8) and (9), binary isotherms were obtained from the a_i and b_i coefficients. These experimental binary isotherms are given in Figures III-5 to III-7 for 40°C and in Figures III-8 to III-10 for 100 °C for Ceca 13X, Alcan (AA) and compared to silicalite from Li and Tezel [18]. Binary behaviour of CH_4 and N_2 mixture with these adsorbents were also predicted by extended Langmuir model. These model predictions were compared to the experimental ones in Figures III-5 to III-10, as well.

When the gas phase CH_4 composition is increased from 0 to 1, the CH_4 adsorption capacity, q_{CH4} increases and the N_2 adsorption capacity, q_{N2}, decreases as expected. Ceca 13X exhibited a higher CH_4 adsorption capacity than N_2 at $y_{CH4}>0.24$ as against Alcan AA at $y_{CH4}>0.38$ and silicalite at $y_{CH4}>0.2$. After the removal of CO_2 from landfill gas mixture, the composition of y_{CH4} and y_{N2} are around 0.88 and 0.12, respectively. At

this composition, the binary isotherms predict an effective separation of these gases. Also, when a landfill is nearing the end of its lifecycle, the production of low quality methane becomes uneconomical and it is generally flared. Results from Figures III-5 to III-10 indicate that low quality methane can be upgraded in order to achieve a better heating value of methane. Methane has to be captured during this period to prevent greenhouse gas emissions rather than burning it in an open flare where energy is not recovered. For natural gas and coal bed gas whose y_{CH4} is around 0.75-0.9, all the tested adsorbents could find applications for methane capture. It was also observed that the ideal extended Langmuir isotherms over predicted the real isotherms at all temperatures tested for methane and did not take into account the competitive adsorption. Therefore, it can only be used for a rough estimation of the binary behaviour in the absence of binary experimental data.

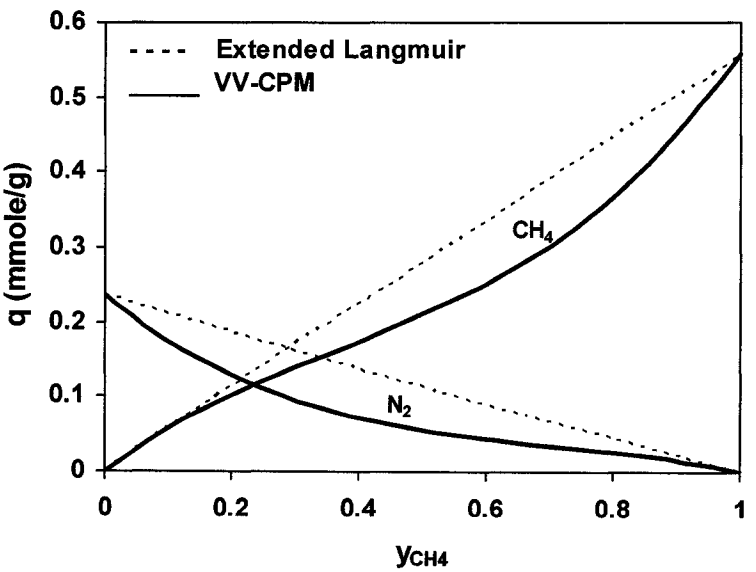

Figure III- 5. Comparison of experimental CH_4/N_2 binary isotherms for Ceca 13X with predicted ones using extended Langmuir model at 40 °C and 1 atm total pressure.

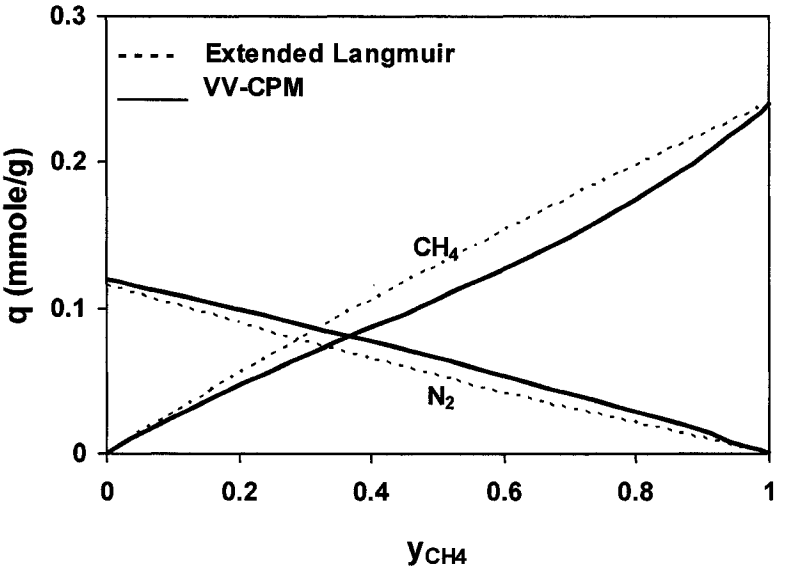

Figure III- 6. Comparison of experimental CH_4/N_2 binary isotherms for Alcan activated alumina (AA) with predicted ones using extended Langmuir model at 40 °C and 1 atm total pressure.

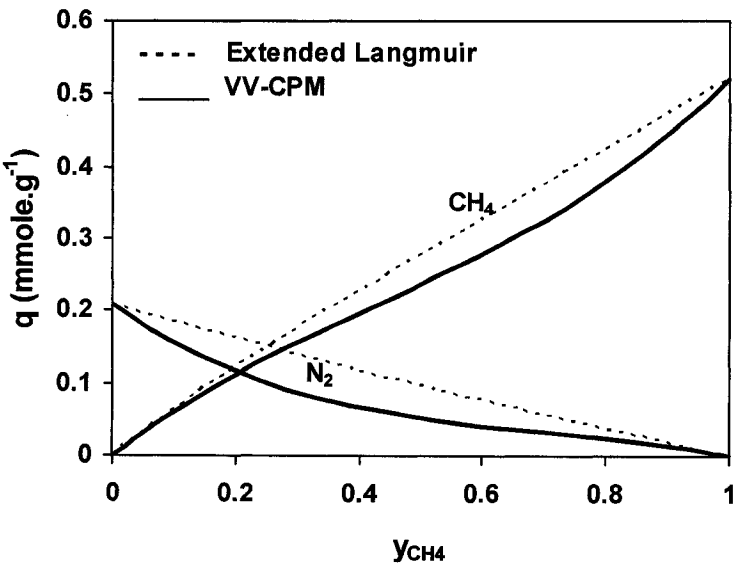

Figure III- 7. Comparison of CH_4/N_2 binary isotherms for silicalite [18] with predicted ones using extended Langmuir model at 40°C and 1atm total pressure.

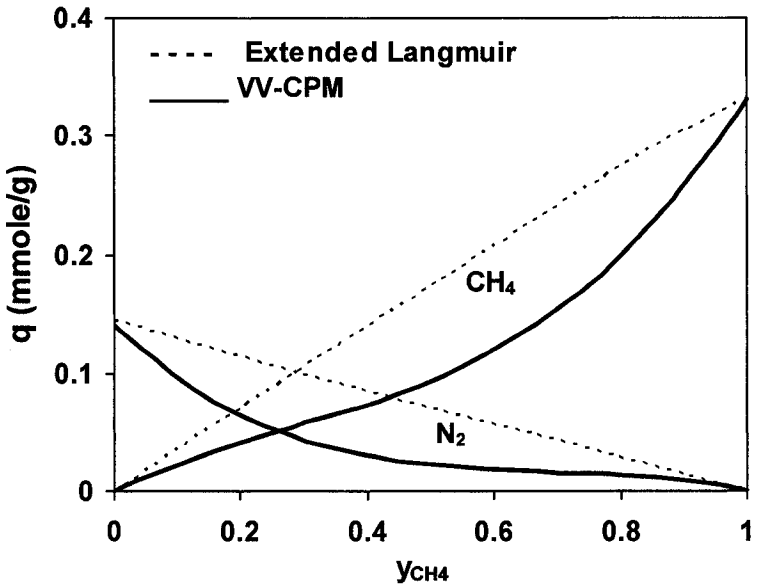

Figure III- 8. Comparison of experimental CH_4/N_2 binary isotherms for Ceca 13X with predicted ones using extended Langmuir model at 100 °C and 1 atm total pressure.

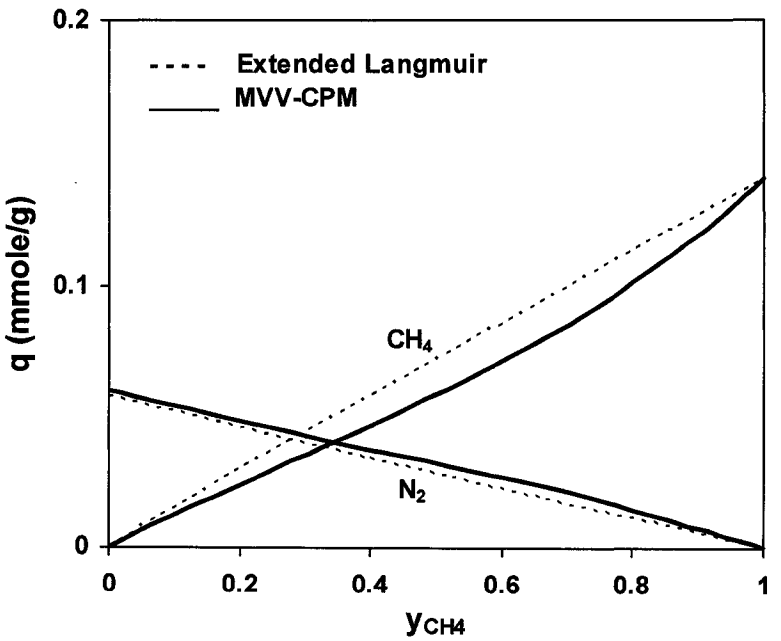

Figure III- 9. Comparison of experimental CH_4/N_2 binary isotherms for Alcan activated alumina (AA) with predicted ones using extended Langmuir model at 100 °C and 1 atm total pressure.

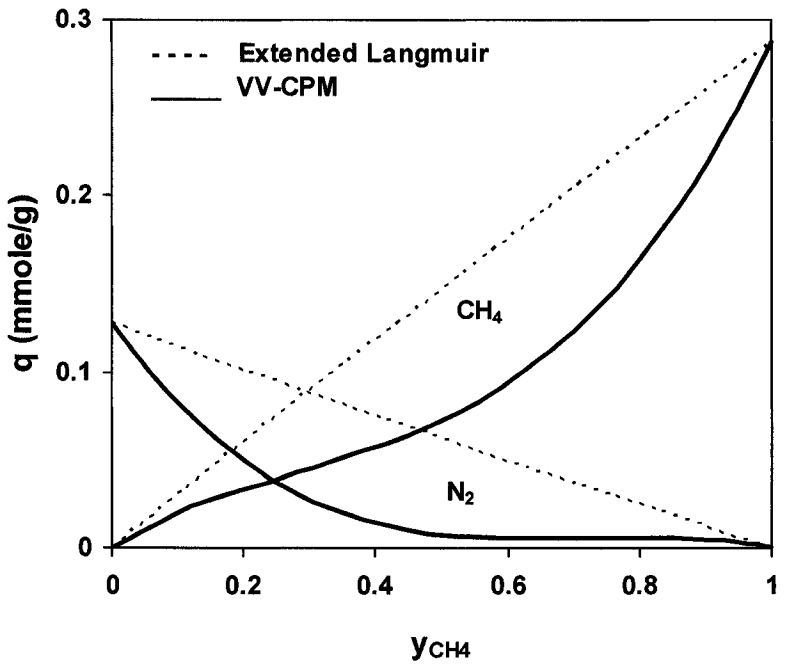

Figure III-10. Comparison of experimental CH_4/N_2 binary isotherms for silicalite [18] with predicted ones using extended Langmuir model at 100 °C and 1 atm total pressure.

The x-y phase diagrams which depict the equilibrium relationship between the compositions in the two phases of CH_4-N_2 with Ceca 13X, activated alumina (AA) and silicalite from Li and Tezel [18] at 40 °C and 100 °C are shown in Figure III-11. A better separation was achieved for silicalite as observed by Li and Tezel [18] since it was the furthest from the 45 °line followed by 13 X and activated alumina (AA).

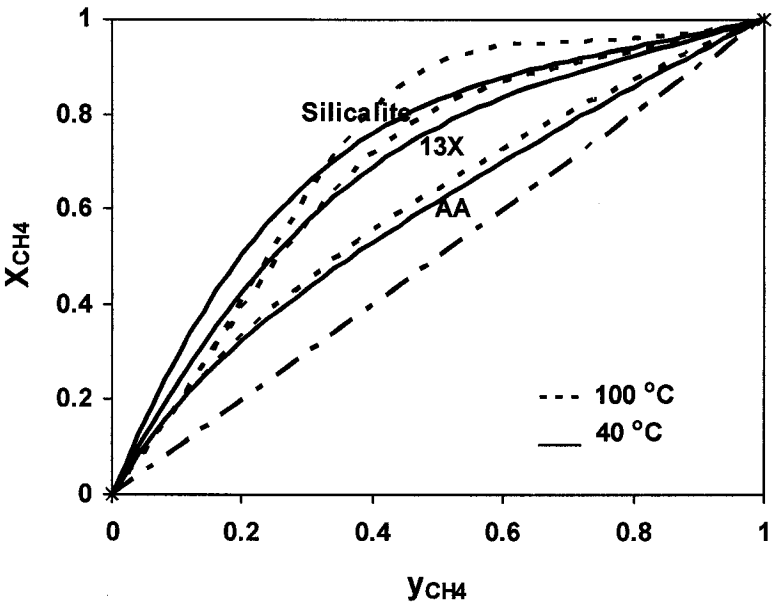

Figure III-11. The x-y diagrams for CH_4/N_2 Binary System with Ceca 13X, Alcan AA and silicalite [18] at 40 and 100°C and 1 atm total pressure.

The equilibrium separation factor defined by Equation 19 is plotted against y_{CH4} in Figure III-12.

$$\alpha_{1/2} = \frac{x_1 / x_2}{y_1 / y_2} \qquad \text{.....(19)}$$

where x_1, x_2, y_1 and y_2 are, respectively, the mole fractions of components 1 and 2 in adsorbed and fluid phases at equilibrium.

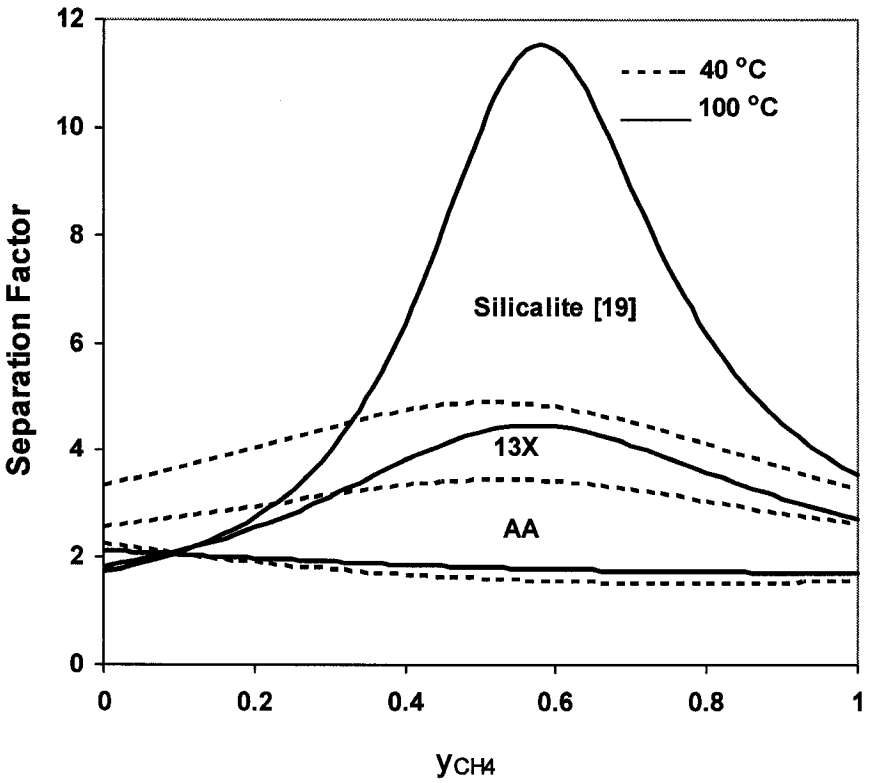

Figure III-12. Equilibrium separation factors for CH_4/N_2 binary system for Ceca 13X, silicalite [18] and activated alumina (AA) at 1 atm total pressure.

The binary CH_4-N_2 system can be separated by all of these adsorbents based on specific applications. The maximum separation factor with silicalite as observed by Li and Tezel [18] occurs in the range of y_{CH4} between 0.5 and 0.6 at 100 °C and decreases when y_{CH4}>0.6. Silicalite could be a promising adsorbent for methane capture in LFG (Landfill gas) whose y_{CH4} is around 0.88. Even for coal bed gas and natural gas whose mole fraction of methane is around 0.7-0.9, silicalite from Li and Tezel [18] had higher separation factors than Ceca 13X and Alcan AA320-AP (AA). Single component isotherm plots from Figures 2a and 2b also support this behaviour exhibited by Ceca 13 X, activated alumina and silicalite of Li and Tezel [18]. Activated alumina exhibited low capacities for both components of CH_4 and N_2 at 40 °C and 100 °C than Ceca 13X and

silicalite which explains its lower separation factors. Although the capacity of CH_4 in Ceca 13X is higher than silicalite, the capacity of N_2 too is greater for Ceca 13X than silicalite at both temperatures of 40 °C and 100 °C. Hence the equilibrium separation factors for CH_4-N_2 separation are higher for silicalite and lower for Ceca 13X. The separation factors for all the tested adsorbents at 100 °C were higher than those obtained at 40 °C which indicated that a better separation was achieved at 100 °C. This observation was similar to the behaviour exhibited by these adsorbents in the x-y phase diagram of Figure III-11.

Although individual capacities of CH_4 and N_2 for Ceca 13X were higher, the separation factors were not higher than those for silicalite, since Ceca 13X adsorbed more N_2 than silicalite.

CONCLUSIONS

1. According to the single component gas isotherm data on silicalite, Ceca 13X and Alcan activated alumina (AA), methane is adsorbed more than nitrogen. Silicalite and Ceca 13X are good candidates for CH_4 capture from N_2 in LFG (Landfill gas), natural gas and coal bed gas.
2. The binary experiments indicated higher equilibrium separation factors for CH_4-N_2 separation (y_{CH4}>0.4) at 100°C than 40 °C for all tested adsorbents.
3. Extended Langmuir is inadequate in describing the real binary system and can be used only for a rough estimation when the experimental binary data are not available.

4. Although single component CH_4 adsorption capacities were higher for Ceca 13X, equilibrium separation factors of silicalite are slightly larger than Ceca 13X and much larger than Alcan activated alumina (AA). Thus, silicalite and Ceca 13X could find application in the bulk separation of methane from nitrogen when yCH4 >0.4, especially in LFG (Landfill gas), coal bed gas and natural gas.

ACKNOWLEDGMENTS

Financial supports received from Ontario Centres of Excellence (OCE), RioTinto Alcan and Air Products & Chemicals Inc., are gratefully acknowledged.

NOMENCLATURE

Symbol	Description	Unit
a_i	Coefficients for Equation (6)	mmol/g/atm
b_i	Coefficients for Equation (7)	mmol/g/atm
B	Adsorption affinity constant	atm^{-1}
B_i	Adsorption affinity constant for component 'i'	atm^{-1}
c	Sorbate concentration in bulk phase	mol/cm^3
G_i	Coefficients for Equation (5)	mmol/g/atm
K	Dimensionless Henry's law constant	dimensionless
K_P	Dimensional Henry's law constant	$mmole.g^{-1}.atm^{-1}$
L	Length of the chromatographic column	cm
P	(Total) Pressure	atm
P_1	Partial pressure of Component *1*	atm
P_2	Partial pressure of Component *2*	atm
q_i^0	Amount adsorbed of single component gas	$mmol.g^{-1}$

	(component 'i')	
q	Amount adsorbed	$mmol.g^{-1}$
q_1	Amount adsorbed of Component *1*	$mmol.g^{-1}$
q_2	Amount adsorbed of Component *2*	$mmol.g^{-1}$
q_m	Adsorption saturation capacity or maximum amount adsorbed	$mmol.g^{-1}$
q_{m1}	Adsorption saturation capacity or maximum amount adsorbed for component 1	$mmol.g^{-1}$
R	Gas constant	$8.314\ JK^{-1}.mol^{-1}$
t	Time	seconds
T	Temperature	K
x	Mole fraction in adsorbed phase at equilibrium	dimensionless
x_1	Mole fraction of component 1 in adsorbed phase at equilibrium	dimensionless
x_2	Mole fraction of Component 2 in adsorbed phase at equilibrium	dimensionless
y	Mole fraction in fluid phase at equilibrium	dimensionless
y_1	Mole fraction of Component 1 in fluid phase at equilibrium	dimensionless
y_2	Mole fraction of Component 2 in fluid phase at equilibrium	dimensionless

Greek Letters

Symbol	Description	Unit
$\alpha_{1/2}$	Separation factor (the ratio of Component 1 over Component 2)	dimensionless
ε	Porosity of the bed	dimensionless
θ	Fraction of monolayer coverage	dimensionless
μ	First moment (Average retention time)	seconds
μ_D	System dead time	seconds
v	Interstitial fluid velocity	cm/s
ρ	Density of adsorbent (without pores)	g/ cm^3

Abbreviations

Abbreviation	Description
CH_4	Methane
CPM	Concentration pulse method
GC	Gas chromatograph
He	Helium
HT	Harlick-Tezel
LFG	Landfill gas
MFC	Mass flow controller
N_2	Nitrogen
NI	National instruments
PSA	Pressure swing adsorption
TCD	Thermal conductivity detector
TSA	Temperature swing adsorption
VV	Van der Vlist and Van der Meijden

REFERENCES

1. A. Regnier, Oil and energy price volatility Energy economics, **29**,(3), 405-427 (2007).
2. A. Jayaraman, A. J. Hernandez-Maldonado, R. T. Yang, D. Chinn, C. L. Munson, and D. H. Mohr, Clinoptilolites for Nitrogen/Methane separation, Chemical engineering science, **59,** 2407-2417 (2004).
3. S. Cavenati, C. A. Grande, and A. E. Rodrigues, Upgrade of Methane from Landfill Gas by pressure swing adsorption, Energy and Fuels, **19**, 2545-2555 (2005).
4. K. Knaebel, S.Reinhold, and E.Herbert, Landfill Gas: From Rubbish to Resource, Adsorption **9**, (1), 87-94 (2003).
5. The Science and Environment Bulletin, (Environment Canada, 1999**),** http://www.ec.gc.ca/science/sandemay99/article1_e.html, Accessed 20 June 2007.
6. A. Jayaraman, R .T .Yang, D. Chinn, and C. L. Munson, Tailored Clinoptilolites for Nitrogen/Methane Separation, Ind. Eng. Chem. Res, **44**(14); 5184-5192 (2005).
7. X. Dai, X. Liu, L. Qian, Z. Yan, and J. Zhang, A novel method to synthesize super-activated carbon for natural gas adsorptive storage, Journal of Porous Materials **13**, 399–405 (2006).
8. R. Kumar, M. Huggahalli, and S. Deng, Trace Impurity Removal from Air, Adsorption **9**, (3), 243-250 (2003).
9. R. Kumar, and S. Deng, Trace carbon monoxide and hydrogen conversion prior to cryogenic distillation of air, Adsorption **12**, (5), 361 – 373 (2006).

10. B. G. Keefer, J. A. Sawada, E. P. Johannes, S. Roy, and M. J. Brown, Systems and Processes for Providing Hydrogen to Fuel Cells, World Intellectual Property Organization 02/35632 (2002).

11. P. Li, and F. H. Tezel, Pure and Binary Adsorption Equilibria of Methane and Carbon Dioxide on Silicalite, Separation Science and Technology, **42**, 3131-3153 (2007).

12. D. Do, and D. Duong, Adsorption Analysis: Equilibria and Kinetics, (Imperial College Press, London, UK, 1998), pp.1-148.

13. IPCC/TEAP, 2005: Special Report on Safeguarding the Ozone Layer and the Global Climate System: Issues Related to Hydrofluorocarbons and Perfluorocarbons, Cambridge University Press, Cambridge, United Kingdom and New York, NY, USA, 488 pp.

14. CRC Handbook of Chemistry and Physics, 85th edition, (CRC Press, Ohio, USA 2004-2005).

15. S. Cavenati, C. A. Grande, and A. E. Rodrigues, Adsorption Equilibrium of Methane, Carbon Dioxide, and Nitrogen on zeolite 13X at High Pressures, Journal of Chemical and engineering data, **49**, 1095-1101 (2004).

16. J. De Wall, R.M. Dimeo and P.E. Sokol, Slow diffusion of molecular hydrogen in zeolite 13 X, Journal of Low Temperature Physics, **129**, 171-184 (2002).

17. S. Cavenati, C. A. Grande, and A. E. Rodrigues, Layered Pressure swing adsorption for methane recovery from $CH_4/CO_2/N_2$ streams, Adsorption, **11**, 549-554 (2005).

18. P.Li and F.H.Tezel, Pure and Binary adsorption of methane and nitrogen by Silicalite, accepted to be published in Journal of Chemical and Engineering Data.

19. J. Karger, and D. M. Ruthven, Diffusion in Zeolites and Other Microporous Solids, (John Wiley and Sons Inc, New York, 1992).

20. D.B. Shah, and D. M. Ruthven, Measurement of zeolite Diffusivities by Chromatography, AIChE Journal **23**, 804-810 (1977).

21. R.W. Triebe, and F. H. Tezel, Adsorption of Nitrogen and Carbon Monoxide on Clinoptilolite: Determination and Prediction of Pure and Binary Isotherms, The Canadian Journal of Chemical Engineering **73**, 717-724 (1995).

22. P. Li, and F. H. Tezel, Pure and Binary adsorption equilibria of CO_2 and N_2 on Silicalite, Journal of Chemical and Engineering Data (in print).

23. P.J.E. Harlick, and F.H. Tezel, A Novel Solution Method for Interpreting Binary Adsorption Isotherms from Concentration Pulse Chromatography Data, Adsorption **6**, 293-309, (2000).

24. P. J. E. Harlick, and F. H. Tezel, CO_2-N_2 and CO_2-CH_4 Binary Adsorption Isotherms with H-ZSM-5: The Importance of Experimental Data Regression with the Concentration Pulse Method, The Canadian Journal of Chemical Engineering **79**, 236-245 (2001).

25. E. Van der Vlist, and J. Van der Meijden, Determination of the Adsorption Isotherms of the Components of Binary Gas Mixtures by Gas Chromatography, Journal of Chromatography **79**, 1-13 (1973).

26. P. J. E. Harlick, and F. H. Tezel, Use of Concentration Pulse Chromatography for Determining Binary Isotherms: Comparison with Statically Determined Binary Isotherms, Adsorption **9**: 275–286 (2003).

27. I. Langmuir, The Adsorption of Gases on Plane Surfaces of Glass, Mica and Platinum, Journal of the American Chemical Society **40**, 1361-1403 (1918).

28. P. J. E. Harlick, and F.H. Tezel, Adsorption of Carbon Dioxide, Methane and Nitrogen: Pure and Binary Mixture Adsorption for ZSM-5 with SiO_2/Al_2O_3 Ratio of 280. Separation and Purification Technology. **33**, 199-210(2003).

29. Choudhary, V. R.; Mayadevi, S. Adsorption of Methane, Ethane, Ethylene, and Carbon Dioxide on Silicalite-1. Zeolites. 1996, **17**, 501.

30. Rees, L. V. C.; Bruckner, P.; Hampson, J. Sorption of N_2, CH_4 and CO_2 in Silicalite-1. Gas Separation and Purification. 1991, **5**, 67-75.

31. T. C. Golden, and S. Sircar, Gas adsorption on Silicalite, Journal of Colloid and Interface science **162**, 182-188 (1994).

32. C.M.Yon, and J.D. Sherman, Adsorption, Kirk Othmer Encyclopaedia of Chemical Technology, (John Wiley and Sons, 2003).

33. Dunne, J. A.; Mariwala, R.; Rao, M.; Sircar, S. R.; Gorte, J. ; Myers, A. L. Calorimetric Heats of Adsorption and Adsorption Isotherms. 1. O_2, N_2, Ar, CO_2, CH_4, C_2H_6, and SF_6 on Silicalite. Langmuir. 1996, **12**, 5888-5895.

CHAPTER IV

ADSORPTION SEPARATION OF CO_2/N_2 AND CO_2/CH_4 BY 13X ZEOLITE

Mulgundmath, V.P [a], Tezel, F.H [a], Saatcioglu T [a], Golden, T.C [b]

[a] Department of Chemical and Biological Engineering, University of Ottawa, 161, Louis Pasteur, Ottawa. K1N 6N5. Canada

[b] Air Products and Chemicals, Inc., 7201, Hamilton Blvd., Allentown, PA USA 18195-1501, USA.

To be submitted to Canadian Journal of Chemical Engineering.

Presented at the Fundamentals of Adsorption (FOA9) conference, May 20-25, 2007, Sicily-Italy

ABSTRACT

Accumulation of greenhouse gases in the atmosphere is responsible for increased global warming of this planet. The increasing concentration of carbon dioxide mainly from flue gas, automobile and landfill gas (LFG) emissions is a major contributor to this problem.

In this work, adsorption separations of CO_2-CH_4 and CO_2 -N_2 were studied on Ceca 13X zeolite by determining single component and binary mixture behaviour using constant volume method and concentration pulse chromatographic technique at 40 °C and 100 °C, and compared to the predicted binary behaviour by extended Langmuir model.

Equilibrium phase diagrams were obtained from the experimental binary isotherms. For this system, the integral thermodynamic consistency tests were also conducted. It was found that Ceca 13X was a promising adsorbent that could be used in the flue gas separation of CO_2 from dry air and landfill gas applications.

INTRODUCTION

Adsorption based gas separations have found tremendous applications in upgrading both renewable and non renewable energy sources such as Landfill gas (LFG) and natural gas (NG). These gases have significant amounts of methane balanced by carbon dioxide, nitrogen and other contaminants. Natural gas is emerging as an alternative fuel with distinct advantages such as low cost and clean burning, but contains some contaminants like carbon dioxide and nitrogen that have to be removed in order to meet pipeline grade specifications [1]. LFG mainly constitutes methane and carbon dioxide which are GHG emissions responsible for global warming of this planet. Carbon dioxide accounts for nearly 83% of GHG emissions while methane accounts for about 10% of total GHG emissions in developed countries [2]. Methane (CH_4) has 25 times more greenhouse warming potential (GWP) than carbon dioxide [3]. Upgrading of CH_4 as a viable energy resource from LFG could be of commercial significance and meet Kyoto protocol standards at the same time. The LFG mixture varies from one site to another with the methane content ranging from 40-60% in the raw gas and the rest mainly carbon dioxide. About 4-6% of nitrogen is present along with trace impurities (<1%) in a typical LFG mixture. The heating value of natural gas which has around 85% methane is about 32.95 MJ/Nm^3 while a typical LFG mixture with 40-60% methane and the rest carbon dioxide has a heating value of 19.70 MJ/Nm^3 [4].

For the industrial flue gas applications, the removal of CO_2 from air is necessary to reduce GHG emissions. Hence the separation of methane from carbon dioxide and nitrogen has a huge commercial significance.

Depending on the specific requirements for this separation process, such as process scale and product purity, one of the techniques will economically be more attractive than others. Absorption preferably dissolves CO_2 but needs to be treated again for environmental considerations. Cryogenic distillation is highly energy intensive. Membrane applications are characterised by low selectivity for these gas separations, high cost and corrosion problems [5]. In general, a gas separation by membrane permeation is favourable at low process capacity and cryogenic separation at high process capacity. At intermediate to high process capacity, adsorption is an attractive process.

Cavenati et al. [1] measured the adsorption capacities of CO_2 and CH_4 on zeolite 13X and found that it exhibited higher working capacities when compared to hydrophobic and homogeneous adsorbents like activated carbon and silicalite. The measured CO_2 isotherm by Cavenati et al. [1] had a rectangular isotherm shape which indicated a higher interaction between CO_2 and the hydrophilic heterogeneous adsorbent, zeolite 13X. Zeolite 13X is characterised by a lower Si/Al ratio(1-1.5) [2] while silicalite and activated carbon exhibit a higher Si/Al ratio (in thousands) [4]. The presence of more Aluminium ions (Al^{3+}) within the zeolite framework results in the availability of more cationic adsorption sites, thus favouring the adsorption of CO_2 due to its higher quadrupole moment. This is preferred since CO_2 is the component that has to be adsorbed in the CO_2-CH_4 and CO_2-N_2 gas mixtures for landfill gas purification and flue gas application, respectively.

In this work, adsorption separation of CO_2-CH_4 and CO_2 -N_2 were studied on Ceca 13X adsorbent by determining single component and binary mixture behaviour using constant volume method and concentration pulse chromatographic technique at 40°C and 100°C respectively, and compared to the predicted ones, as well as other experimental data in the literature. The objective was to study the adsorption of CO_2 by hydrophilic 13X and compare its characteristics to hydrophobic silicalite adsorbent that exhibited Si/Al ratio in the thousands.

THEORY

Several theoretical adsorption models are used for interpreting single component and binary gas isotherms. The simplest and still the most useful single component gas isotherm model is the Langmuir isotherm [6]:

$$\theta = \frac{q}{q_m} = \frac{BP}{1 + BP} \quad \text{.....(1)}$$

where B is the affinity constant, θ is the fractional coverage, q is the amount adsorbed, q_m is the saturation adsorption capacity or maximum amount adsorbed, and P is the pressure. The parameters of single component isotherm fits to Langmuir model are determined by non linear regression in MS-Excel.

Binary models for mixture gas adsorption provide valuable information for the design of adsorptive gas separation processes by predicting the equilibrium amount adsorbed from single component gas adsorption isotherms. The simplest and the widely used model for a binary system is the extended Langmuir model:

$$q_1 = \frac{q_{m1} B_1 P_1}{1 + B_1 P_1 + B_2 P_2} \quad \text{.....(2)}$$

where subscripts 1 and 2 refer to gases 1 and 2, respectively.

Concentration Pulse Chromatographic (CPC) technique has been used for the determination of binary isotherms in this study. In this technique, a pulse of the sample gas is injected into the mixed carrier gas stream and the response is measured at the column exit as concentration vs. time. When the injected pulse is small, the concentration change is low enough so that the equilibrium relationships can be assumed to be in the linear range. The mean retention time, μ which is directly related to Henry constant, was determined from the corrected first moment of the response peak [7, 8].

$$\mu = \frac{\int_0^\infty c(t-\mu_D)dt}{\int_0^\infty cdt} = \frac{L}{v}\left[1 + \frac{(1-\varepsilon)K}{\varepsilon}\right] \quad \text{.....(3)}$$

Where t represents time, c is the outlet adsorbate concentration, L is the adsorption column length, ε is the porosity of the column, v is the interstitial fluid velocity, K is the dimensionless Henry's law constant and μ_D is the dead time. The dimensionless Henry's law constant, K can be converted to a dimensional constant, K_p using Equation (4):

$$K_p(Dimensional) = \frac{K(Dimensionless)}{RT\rho} \quad \text{.....(4)}$$

Where T is the absolute temperature, ρ is the density of adsorbent (without pores) and K_p is the dimensional Henry's law constant.

For a binary gas system, the K_p value is a function of the slopes of the binary isotherms of the individual components in the mixture and the relationship is given by Equation (5) [7]:

$$K_p = (1 - y_1)\frac{dq_1}{dP_1} + y_1\frac{dq_2}{dP_2} \quad \text{.....(5)}$$

where $\frac{dq_1}{dP_1}$ and $\frac{dq_2}{dP_2}$ are the slopes of the binary adsorption isotherms for components 1 and 2, respectively. K_p values are determined for various concentrations of the carrier gas from 0-100 %. The method of K_p-functions has been extensively used in literature for determining binary isotherms from concentration pulse chromatographic data and has been proven to interpret highly selective binary systems [4, 5, 9-15]. The interpretation of the non-ideal binary K_p data for CO_2-N_2 and CO_2-CH_4 can be best explained by Harlick Tezel concentration pulse method (HT-CPM) which is a second degree, polynomial function combined with a logarithmic term [9]:

$$K_p = A_1 + A_2 y_1 + A_3 y_1^2 + A_4 \ln|y_1 + \lambda| \quad \text{..... (6)}$$

where $\lambda \neq 0$. The corresponding isotherm slope functions are:

$$\frac{dq_1}{dP_1} = B_1 + 2B_2 y_1 + \frac{B_3}{|y_1 + \lambda|} \quad \text{.....(7)}$$

$$\frac{dq_2}{dP_2} = C_1 + 2C_2 y_1 + \frac{C_3}{|y_1 + \lambda|} \quad \text{.....(8)}$$

Integration of Equations (7) and (8) results in the following binary isotherm equations:

$$q_1 = \left(B_1 y_1 + B_2 y_1^2 + B_3 \ln\left|\frac{y_1 + \lambda}{\lambda}\right| \right) P \quad \text{.....(9)}$$

$$q_2 = \left[C_1(1-y_1) + C_2(1-y_1^2) - C_3 \ln\left|\frac{y_1+\lambda}{1+\lambda}\right| \right] P \quad \text{.....(10)}$$

By substituting Equations (7) and (8) into Equation (5), the following K_p function is obtained:

$$K_p = (1-y_1)\left[B_1 + 2B_2 y_1 + \frac{B_3}{(|y_1+\lambda|)} \right] + y_1\left[C_1 + 2C_2 y_1 + \frac{C_3}{(|y_1+\lambda|)} \right] \quad \text{.....(11)}$$

From this equation, the following objective function is defined to minimize the sum of square residuals (SSR) with respect to experimental K_p values to determine coefficients B and C's after the experimental determination of K_p values for different carrier gas compositions, y_1.

$$SSR = \sum_{y=y\min}^{y=y\max} \left\{ K_P[Experimental] - \left((1-y_1)\left[B_1 + 2B_2 y_1 + \frac{B_3}{(|y_1+\lambda|)} \right] + y_1\left[C_1 + 2C_2 y_1 + \frac{C_3}{(|y_1+\lambda|)} \right] \right) \right\}^2$$

.....(12)

Following boundary conditions are also applied for the determination of B and C coefficients:

1. $$q_1(Binary)| = q_1(\sin glecompone\ nt)|\ at \cdot\cdot y = 1.0 \text{.....(13)}$$

$$q_2(Binary)| = q_2(\sin glecompone\ nt)|\ at \cdot\cdot y = 0 \text{ .....(14)}$$

where the values of q_1(single component) and q_2 (single component) are taken from the end points (at P=1 atm) of the single component gas isotherms.

2. $$\frac{dq_1}{dP_1} > 0 \quad \ldots\ldots(15)$$

$$\frac{dq_2}{dP_2} > 0 \quad \ldots\ldots(16)$$

i.e., the isotherm slopes should be greater than zero across the entire range of y_1 if the adsorbates have similar properties and adsorption occurs at low fractional loading. No maximum should be observed in the isotherms.

After the determination of K_p values for different y_1, a constrained nonlinear regression is performed to determine the B and C parameters in equation (12) to minimise SSR. The binary isotherms are then calculated by Equations (9) and (10). Thus, by fitting the experimental binary adsorption K_p values to a non linear model, the coefficients of the binary gas mixture isotherm equations can be calculated and the isotherms are plotted.

THERMODYNAMIC CONSISTENCY TESTS

The measurement of binary gas adsorption equilibria by conventional methods can be complex, tedious, and time-consuming, and the accuracy of the data may not always be satisfactory [4, 5]. This is the reason for the lack of adsorption mixture experimental data in literature. However, the prediction of binary adsorption models using single component gas adsorption data is less accurate [16] and requires that a selective amount of mixture data too must be measured to verify the quality of prediction of the models. This consistency test can be used to validate the internal thermodynamic consistency of the experimental binary gas adsorption data and the predicted binary adsorption models

using single component gas adsorption data. The integral test equation (17) is shown below [17, 18]:

$$\int_0^P \frac{q_1^0}{P} dP - \int_0^P \frac{q_2^0}{P} dP = \int_0^1 \frac{q_1(1-y_1) - q_2 y_1}{y_1(1-y_1)} dy_1 \qquad \text{.....(17)}$$

where q^0 is the amount adsorbed of components 1 or 2, indicated by the subscript, in the single component gas system, P is the total pressure, q_1 and q_2 are the amount adsorbed of component 1 and 2 in the binary system, y_1 is the mole fraction of component 1 in the binary system. The two terms on the left side are determined as a function of pressure (at constant temperature) using the single component gas adsorption isotherm data for the components of the binary mixture while the term on the right side are evaluated using the binary gas adsorption isotherm at constant pressure and temperature.

EXPERIMENTAL SECTION

The properties of the adsorbate gases are listed in Table IV-1.

Table IV- 1. Properties of Adsorbate Gases [19]

Adsorbate gas	Molecular weight	Kinetic diameter (Å)	Polarizability (x 10^{-25} cm^3)	Dipole moment (x10^{18} esu.cm)	Quadrupole moment (x10^{-26} esu.cm^2)
CO_2	44	3.30	26.5	0.00	4.30
CH_4	16	3.80	26.0	0.00	0.00
N_2	28	3.64	17.6	0.00	1.52

CONSTANT VOLUME METHOD

A schematic diagram of the constant volume method apparatus is given in Figure IV-1 for the determination of single component gas isotherms. Ultra high pure methane, carbon dioxide, nitrogen and helium gases supplied by Prax Air Inc., Ottawa, Canada were used in this study. Zeolite, Ceca 13X was obtained from CECA, in Honfleur, France.

This method involves measuring the pressure change in a known volume of sample gas exposed to an adsorbent sample. As the gas is adsorbed and allowed to come to equilibrium with the adsorbent, the measured decrease of pressure in the closed system indicates the amount of gas adsorbed under the given isothermal conditions. Prior to each run, the adsorbent was regenerated at 300 ^{o}C for 12 hours. The experiment was initiated by admitting the adsorbate in the manifold and recording the pressure followed by releasing the adsorbate into the sample flask and recording the subsequent equilibrium pressure.

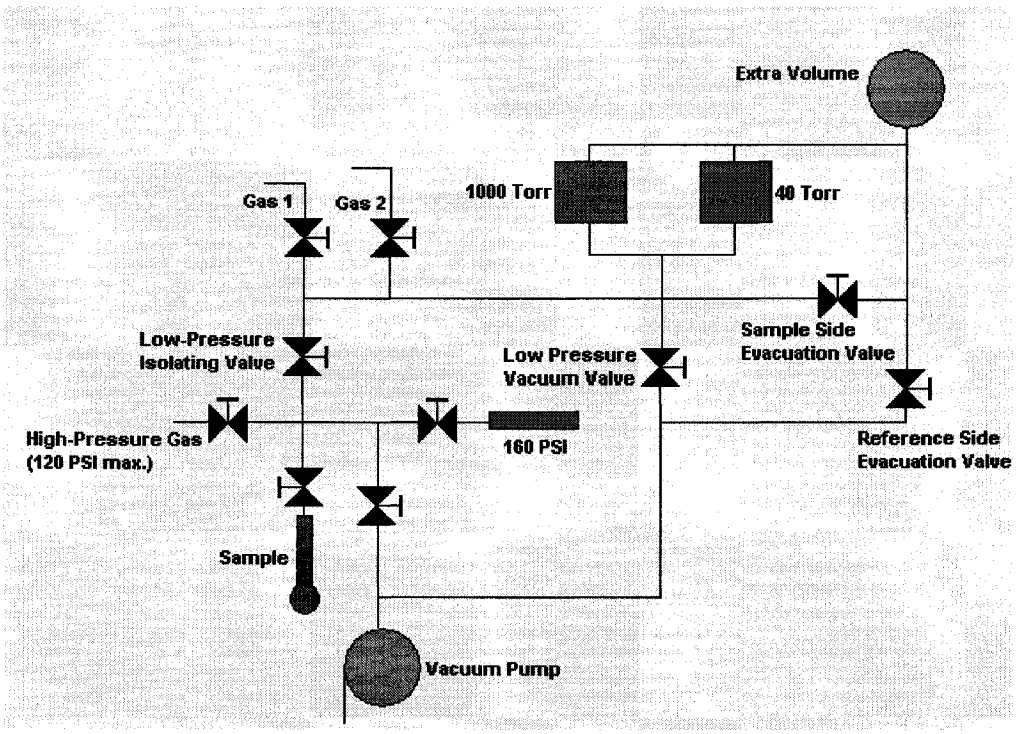

Figure IV- 1. Schematic Diagram of the Constant volume method apparatus used in this study for the determination of single component gas isotherms

An AccuSorb 2100E Physical adsorption analyser provided by Micromeritics Instrument Corporation and equipped with highly precise pressure transducers and thermocouples was used for this study. Data collection was done using a National Instruments (NI) based data acquisition card and Labview 6.1 on a computer.

CONCENTRATION PULSE CHROMATOGRAPHIC (CPC) TECHNIQUE

A schematic diagram of the experimental set up is shown in Figure IV-2. The experimental conditions and column specifications are given in Table IV-2. The packed adsorbent column was regenerated at 1 atm and 300 °C under a 15 mL (STP)/min helium purge, for 12 hours to ensure that all impurities adsorbed on the adsorbent were removed before the start of each experimental run. Data acquisition was done using a National Instruments (NI) data acquisition card and Labview software version 6.1 on a Pentium 4 computer. Details of operation regarding the concentration pulse chromatographic experimental technique have been outlined in the earlier paper (Mulgundmath et al., [25]).

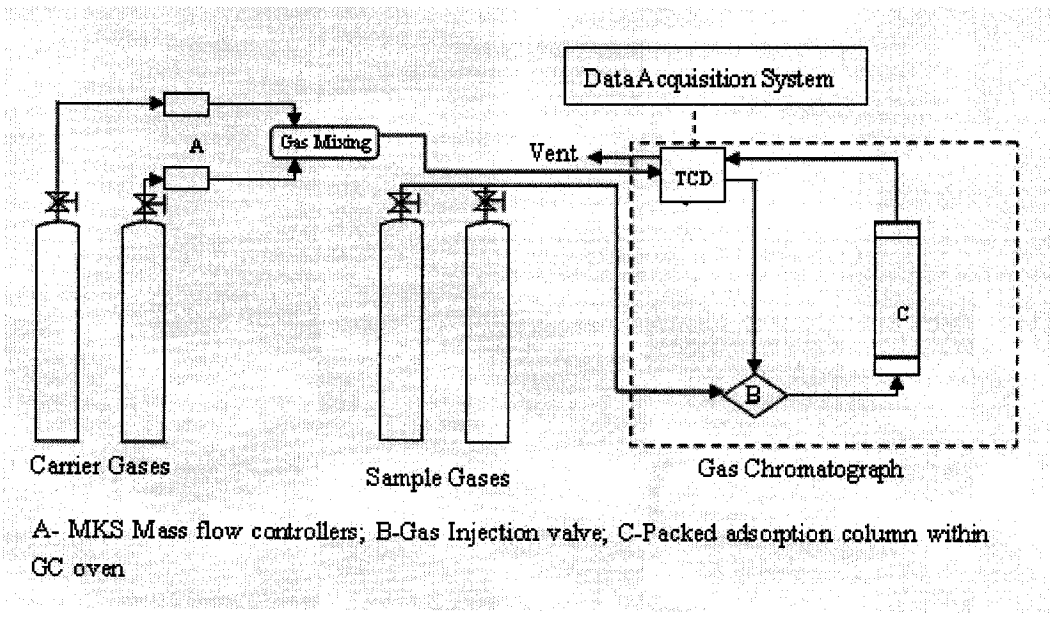

Figure IV-2. Schematic Diagram of the Concentration pulse chromatographic technique apparatus used in this study for the determination of binary adsorption isotherms

Table IV- 2. Experimental and column specifications

Ceca 13 X particle size	20 - 60 mesh
Bed porosity	0.35
Column length	10 cm
Column inner diameter	0.451 cm
Total pressure	1 atm
Regeneration temperature	300 °C
Regeneration pressure (He purge)	1 atm
Regeneration time	12 h

RESULTS AND DISCUSSIONS

SINGLE COMPONENT GAS ISOTHERMS

Single component gas equilibrium isotherms were determined using constant volume method at two different temperatures (40 °C and 100 °C) for Ceca 13X and pressures up to 5 atm. These isotherms are given in Figures IV-3 and IV-4 for CO_2-CH_4 and CO_2-N_2, respectively and are compared with the literature. Points are experimental data and curves through the data points represent Langmuir isotherm model at the corresponding temperature. CO_2 data for Ceca 13X are repeated in Figures IV-3 and IV-4 for comparison. Results indicated that CO_2 was the strongly adsorbed gas followed by CH_4 and N_2 by Ceca 13X. Higher adsorption capacities were always observed at the low temperature of 40 °C than 100 °C which is consistent with exothermic physical adsorption. Carbon dioxide possesses a large quadrupole moment which results in a strong interaction with the adsorbent surfaces of Ceca 13X [20]. While CH_4 has no dipole or quadrupole moment, its stronger adsorption in comparison to N_2 is due to its high

degree of polarizability. N_2 has a weak quadrupole moment and its polarizability is lower than that of CO_2 and CH_4. These properties contribute to the low adsorption capacity of N_2.

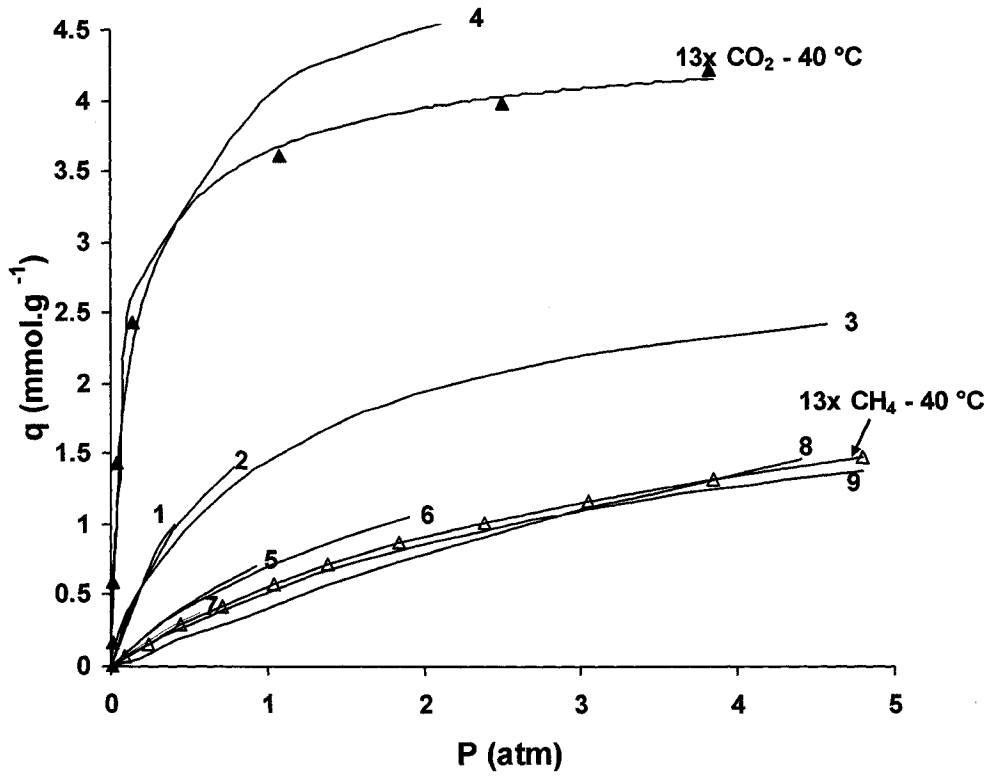

Figure IV-3a. Comparison of single component gas isotherms for CO_2 and CH_4 gases at 40 °C. Points represent experimental data for Ceca 13X from this study. Numbered curves are literature comparisons indicated as follows:

1: CO_2 – Silicalite at 25°C [21]
2: CO_2 - Silicalite at 31°C [22]
3: CO_2 - Silicalite at 40°C [4]
4: CO_2 – 13X at 35°C [1]
5: CH_4 - Silicalite at 23°C [22]
6: CH_4 - Silicalite at 31°C [23]
7: CH_4 - Silicalite at 25°C [21]
8: CH_4 – 13X at 35°C [1]
9: CH_4 - Silicalite at 40°C [4]

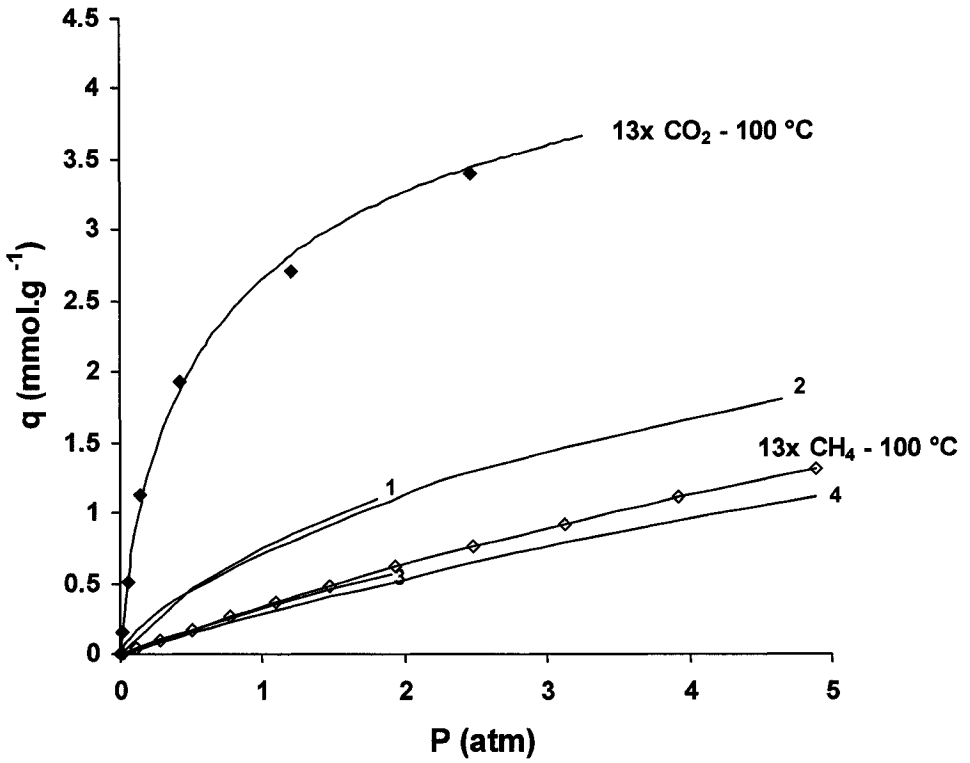

Figure IV- 3b. Comparison of single component gas isotherms for CO_2 and CH_4 gases at 100 °C. Points represent experimental data for Ceca 13X from this study. Numbered curves are literature comparisons indicated as follows:

1: CO_2 - Silicalite at 80°C [23]
2: CO_2 - Silicalite at 100°C [4]
3: CH_4 - Silicalite at 81°C [23]
4: CH_4 - Silicalite at 100°C [4]

Much lower adsorption capacities for UOP silicalite were observed for CO_2 by Rees et al. [21], (curve 1 in Figure IV-3a at 25°C), Dunne et al. [22], (curve 2 in Figure IV-3a at 31°C), and Li and Tezel, (2007a, [4])-(curve IV-3 in Figure 3a at 40 °C) than Ceca 13X at 40 °C. The higher interaction of Ceca 13X with CO_2 is due to its lower Si/Al ratio (1.17) and the presence of cations in its structure when compared to the hydrophobic silicalite which is practically pure silica with Si/Al ratio in thousands with no cations in its

structure. Different silicalite isotherms for CO_2 were consistent with each other having higher capacities as temperature decreases. Cavenati et al., (2005a, [1]) observed higher capacities for CO_2 at 35 °C for zeolite 13X (curve 4 in Figure IV-3a) at high pressures compared to Ceca 13X at 40 °C from this study. Although this behaviour is consistent with physical adsorption behaviour where high capacities are observed at low temperatures, the effect of temperature does not explain the relatively large difference in CO_2 capacity at high pressures. Different samples of the 13X adsorbent used for isotherm determination and different measurement techniques employed (Gravimetric method used by Cavenati et al., (2005a, [1]) against constant volume method employed in this study) add to this variation in the adsorption behaviours observed.

When CH_4 isotherm in Figure IV-3a is compared with the literature, it was observed that slightly higher CH_4 adsorption capacities for silicalite were observed in the literature at temperatures lower than 40 °C (Dunne et al., (1996, [22]) in curve 5 at 23°C, Choudhary and Mayadevi (1996, [23]) in curve 6 at 31°C and Rees et al., (1991, [21]) in curve 7 at 25°C of Figure IV-3a) which is consistent with physical adsorption behaviour (as temperature increases, adsorption capacity decreases). Methane adsorption isotherm curves for Ceca 13X at 40 °C from the present study, silicalite at 40 °C from Li and Tezel, (2007a, [4])-(curve 9 in Figure IV-3a) and zeolite 13X at 35 °C from Cavenati et al., (2005a, [1])-(curve 8 in Figure IV-3a) were observed to be very similar. This is a result of CH_4 not having any dipole or quadrupole moment. It has a similar affinity for both heterogeneous adsorbents like 13X (Si/Al=1.17) and homogeneous adsorbents like silicalite (Si/Al in thousands).

The larger adsorption capacity difference between CO_2 and CH_4 makes Ceca 13X and zeolite 13X (Cavenati et al., 2005a, [1]) desirable for landfill gas applications requiring the removal of CO_2.

Data given in Figure IV-3b at higher temperatures showed that Choudhary and Mayadevi (1996, [23]) (curve 1 at 80 °C) as well as Li and Tezel (2007a, [4]) (curve 2 at 100 °C) obtained a lower capacity for silicalite for CO_2 than Ceca 13X at 100 °C from the present study which was similar to the observations at 40 °C in Figure IV-3a. The trends of CO_2 isotherms were rectangular and more favourable for Ceca 13X indicating a higher interaction between the quadrupole moment of CO_2 and the heterogeneous surface of the 13X adsorbent at both temperatures. For the homogeneous silicalite adsorbents, the CO_2 isotherm trends at both temperatures (40 °C and 100 °C) were similar and more linear than Ceca 13X, which indicated a lower interaction of this adsorbate with silicalite.

From Figure IV-3b, it was observed that Ceca 13X had a slightly higher CH_4 adsorption capacity at 100°C than silicalites (curve 3 at 81°C of Choudhary and Mayadevi, 1996, [23]) and curve 4 at 100°C of Li and Tezel, 2007a, [4]).

A higher difference in adsorption capacities (working capacities) of CO_2 and CH_4 would be desirable to achieve a better separation between these gases. Although the observed capacities of silicalite for CH_4 (curve 3 at 80 °C and curve 4 at 100 °C in Figure IV-3b) were lower than that of Ceca 13X at 100 °C, their working capacities for CO_2 and CH_4

separation were lower than that of Ceca 13X, since silicate exhibited lower adsorption capacities for CO_2 (curve 1 for Choudhary and Mayadevi [23] at 80 °C in Figure IV-3b and curve 2 for Li and Tezel [4] at 100 °C in Figure IV-3b) than Ceca 13 X. Higher working capacities are preferable for a better separation between CO_2 and CH_4. In a landfill gas application, CO_2 and CH_4 are present in bulk quantities (40-60% and 45-60% by volume, respectively) and a higher working capacity is desirable for the Pressure Swing Adsorption (PSA) system.

Ceca 13X exhibited a larger capacity difference between CO_2 and CH_4 both at 40 °C and 100 °C than all the silicalites as can be seen in Figures IV-3a and IV-3b. It favours its application in landfill gas purification with a Pressure Swing Adsorption (PSA) system. In this application, CO_2 can be adsorbed and the product CH_4 can be removed efficiently at the same feed pressure. Adsorbing CO_2 prevents the need for re-pressurising the upgraded product methane. The bulk CO_2 that is adsorbed must be recompressed after the regeneration step in a Pressure Swing Adsorption (PSA)/Vacuum Swing Adsorption (VSA) application if it is to be marketed. Regardless, pressurisation will be required for the adsorbed component if it is to be sold.

Figure IV-4 shows the comparison of single component CO_2 and N_2 isotherms for Ceca 13X, together with their comparisons with the literature. CO_2 isotherm data for Ceca 13X given in Figure IV-3 are repeated in Figure IV-4 for comparison. The N_2 capacity on silicalite as reported by Dunne et al. (1996, [22]) – (curve 6 in Figure IV-4a at 61 °C), zeolite 13X by Cavenati et al. (2005a, [1]) – (curve 7 in Figure IV-4a at 35 °C) and

silicalite by Li and Tezel (2007a, [4]) – (curve 8 in Figure IV-4a at 40 °C), similar isotherms to Ceca 13X adsorbent at 40 °C from the present study.

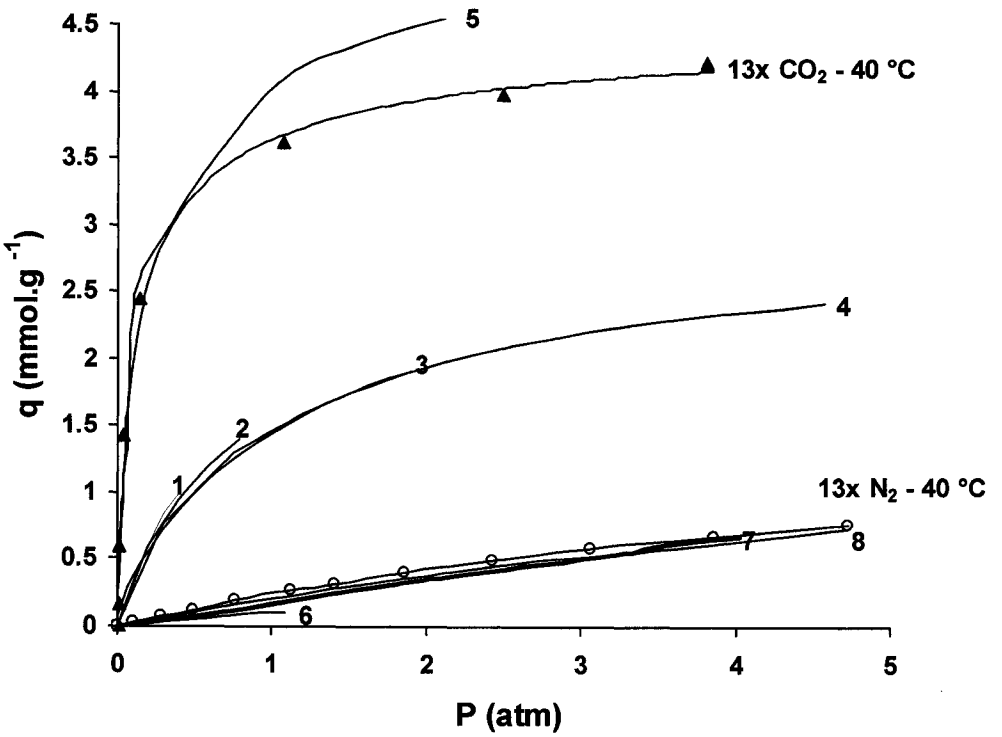

Figure IV-4a. Comparison of single component gas isotherms for CO_2 and N_2 gases at 40 °C. Points represent experimental data for Ceca 13X from this study. Numbered curves are literature comparisons indicated as follows:

1: CO_2 - Silicalite at 25°C [21]
2: CO_2 - Silicalite at 31°C [22]
3: CO_2 - Silicalite at 32°C [23]
4: CO_2 - Silicalite at 40°C [4]
5: CO_2 - 13X at 35°C [1]
6: N_2 - Silicalite at 61°C [22]
7: N_2 – 13X at 35°C [1]
8: N_2 - Silicalite at 40°C [4]

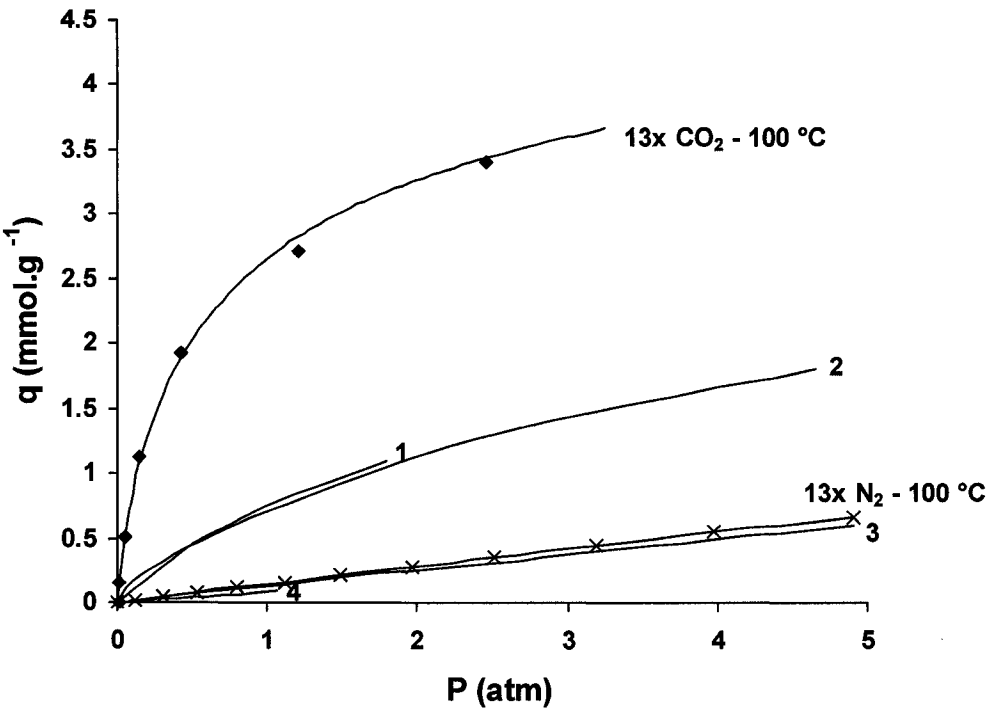

Figure IV-4b. Comparison of single component gas isotherms for CO_2 and N_2 gases at 100 °C. Points represent experimental data for Ceca 13X from this study. Numbered curves are literature comparisons indicated as follows:

1: CO_2 - Silicalite at 80°C [23]
2: CO_2 - Silicalite at 100°C [4]
3: N_2 - Silicalite at 100°C [4]
4: N_2 - Silicalite at 72°C [22]

Slightly lower capacities for silicalite were observed by Dunne et al. [22] (curve 4 in Figure IV-4b at 72 °C), but silicalite of Li and Tezel [4] (curve 3 in Figure IV-4b at 100 °C) showed better agreement with Ceca 13X at 100 °C, considering the effect of temperature on adsorption capacity. N_2 has a weaker quadrupole moment than CO_2 which is the reason for the lower capacities observed on these adsorbents. Higher CO_2 and lower N_2 capacities which are always desirable to achieve a better CO_2 separation from N_2 were observed for Ceca 13X. Hence, Ceca 13X had a higher working capacity (the

difference between adsorption capacities) for CO_2 and N_2 separation than silicalites given in the literature. A larger capacity difference between CO_2 and N_2 was observed even at a higher temperature of 100 °C for Ceca 13X than silicalites. This favourable property makes Ceca 13X a suitable adsorbent for industrial flue gas applications where CO_2 removal is required at higher temperatures.

BINARY GAS ISOTHERMS

Binary K_p values have been determined by injecting samples in a known composition of the mixed carrier gas, CO_2-CH_4. The mole fraction of CO_2 in the carrier gas was increased from 0% to 100% and samples were injected. Sample injection was done only when equilibrium was attained after each concentration change of the carrier gas mixture by observing that the baseline of the response would be steady. The binary K_p data for CO_2-CH_4 with Ceca 13X at 40 °C and 100 °C are shown in Figure IV-5. The regression curves were generated using the B_i and C_i parameters by using equation 11. These parameters were determined from the minimization of objective function for HT-CPM in Equation (12) by using constraints from equations (13-16). HT-CPM was chosen as it was a more versatile method that represented non-ideal adsorption systems with larger differences in individual adsorption capacities of components like CO_2 and CH_4 [12].

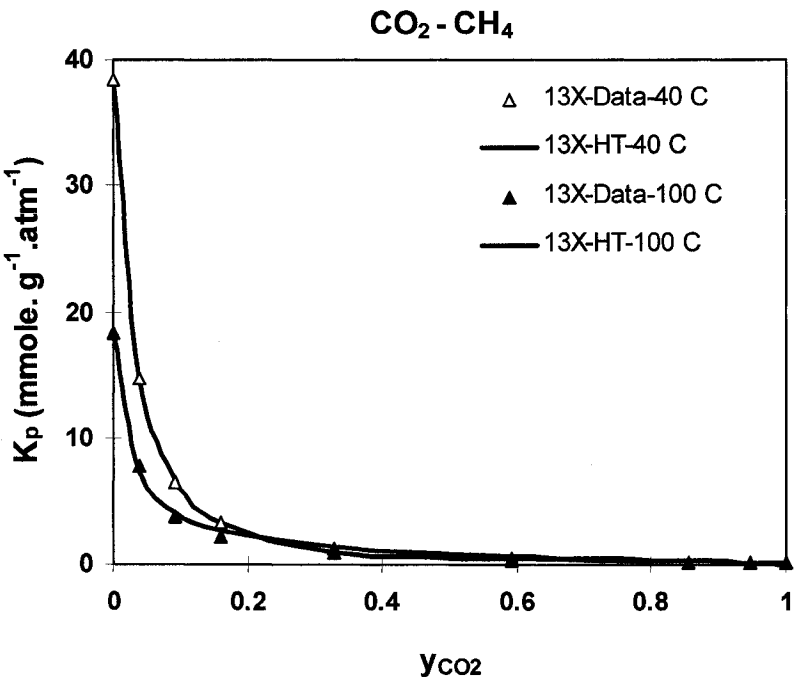

Figure IV-5. Regressions for CO_2-CH_4, binary K_p with Ceca 13X by HT-CPM at 40 °C, 100 °C and 1 atm total pressure.

The rapid drop of K_p data in the range of $0<y_1<10\%$ of CO_2 in the gas phase (see Figure IV-5) for Ceca 13X implied that adsorption was more competitive for the available adsorption sites. Higher K_p values were observed at the low temperature of 40 °C than 100 °C, which is consistent with single component gas adsorption behaviour. From this K_p data, the binary isotherms for CO_2-CH_4 with Ceca 13X were determined at 1 atm total pressure with HT-CPM at 40 °C and 100 °C and compared to silicalite from the literature [4] under the same experimental conditions. The results are given in Figures IV-6a and IV-6b, respectively.

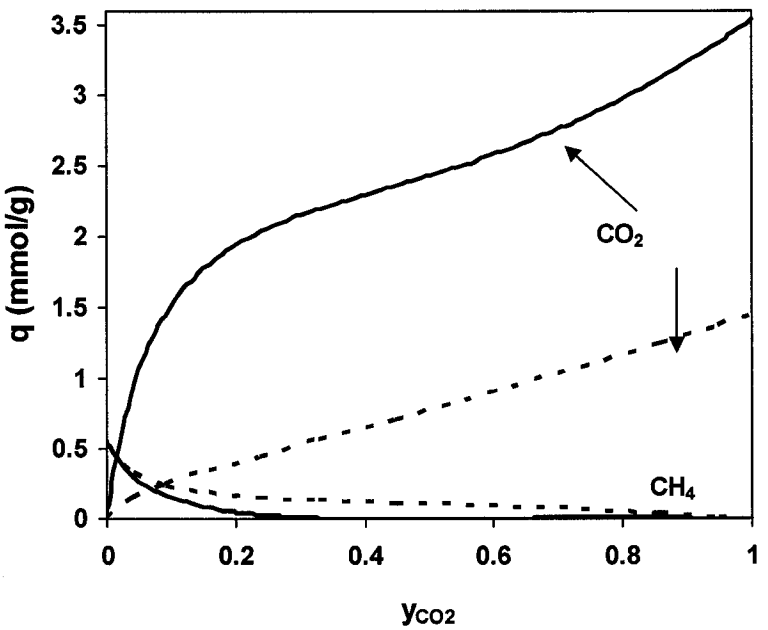

Figure IV-6a. CO_2 - CH_4 binary isotherms with Ceca 13X (—) from this study and silicalite (- - - -) from Li and Tezel (2007a, [4]) at 40 °C and 1 atm total pressure.

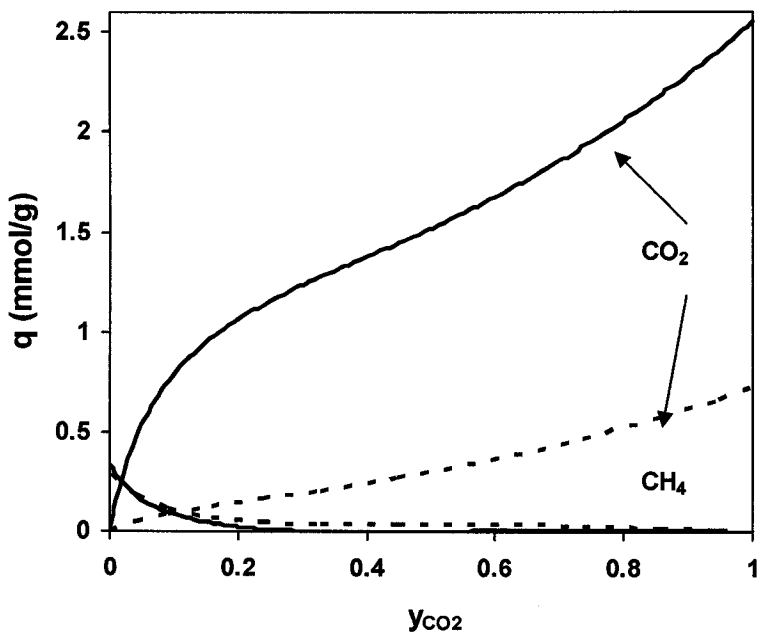

Figure IV-6b. CO_2 - CH_4 binary isotherms with Ceca 13X (—) from this study and silicalite (- - - -) from Li and Tezel (2007a, [4]) at 100 °C and 1 atm total pressure.

From these binary isotherms, it was observed that the adsorption capacity difference between CO_2 and CH_4 for Ceca 13X was higher than silicalite of Li and Tezel (2007a, [4]). This property exhibited by Ceca 13X is due to the presence of cations which renders its surface heterogeneous and makes more adsorption sites available, thus promoting a stronger interaction of CO_2 which has a higher quadrupole moment. For LFG, which has y_{CO2} around 0.4-0.6, CO_2 can be more easily separated from CH_4 on Ceca 13X than silicalite, thus making it a suitable adsorbent for the upgrading of CH_4. Also, temperature had a significant effect on the adsorption capacity of Ceca 13X and silicalite. It was observed that both higher capacities and higher capacity differences for CO_2 and CH_4 separation were obtained at low temperature of 40 °C compared to 100 °C which was consistent with single component gas adsorption behaviour.

Similar experiments were carried out for CO_2-N_2 mixture with Ceca 13X for the determination of K_p data using HT-CPM at 40 °C and 100 °C.

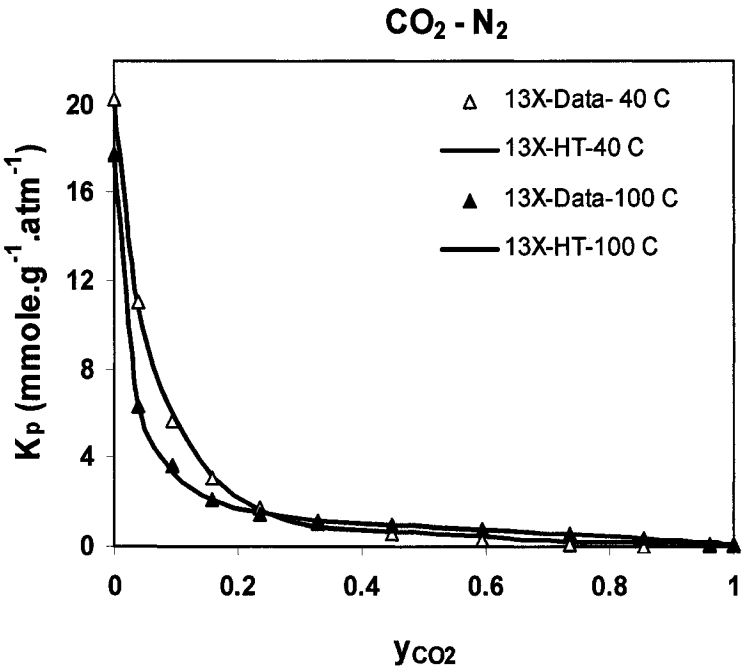

Figure IV-7. Regressions for CO_2-N_2 binary K_p with Ceca 13X by HT-CPM at 40 °C, 100 °C and 1 atm total pressure.

A sudden drop in K_p data for Ceca 13X at 40 °C & 100 °C indicated that adsorption was slightly competitive for the available adsorption sites. Due to its more interactive nature, Ceca 13X had higher K_p values at both temperatures of 40 °C and 100 °C. Higher K_p values were obtained at 40 °C than 100 °C, which is again consistent with single component gas adsorption behaviour.

From this K_p data, the binary isotherms for CO_2- N_2 with Ceca 13X were determined at 1 atm total pressure with HT-CPM at 40 °C and 100 °C and compared with silicalite from Li and Tezel [24] under the same experimental conditions in Figures IV-8a and IV-8b, respectively. A similar qualitative trend was observed when compared to CO_2-CH_4 binary isotherms in Figures IV-6a and IV-6b. Ceca 13X with a higher surface heterogeneity adsorbs more CO_2 than N_2 in the available active adsorption sites because of the

quadrupole moment of CO_2. Also, it was observed that higher capacities were obtained at 40 °C than 100 °C which is again consistent with the single component gas adsorption behaviour. The degree of curvature of the CO_2 isotherm with Ceca 13X reflects the stronger intensity of the sorbate-sorbent interactions. Ceca 13X could be a more suitable adsorbent candidate for CO_2 separation applications from industrial flue gas (y_{CO2} between 0.1-0.15) since it exhibits a higher adsorption capacity difference between CO_2 and N_2 than silicalite (Li and Tezel, in print).

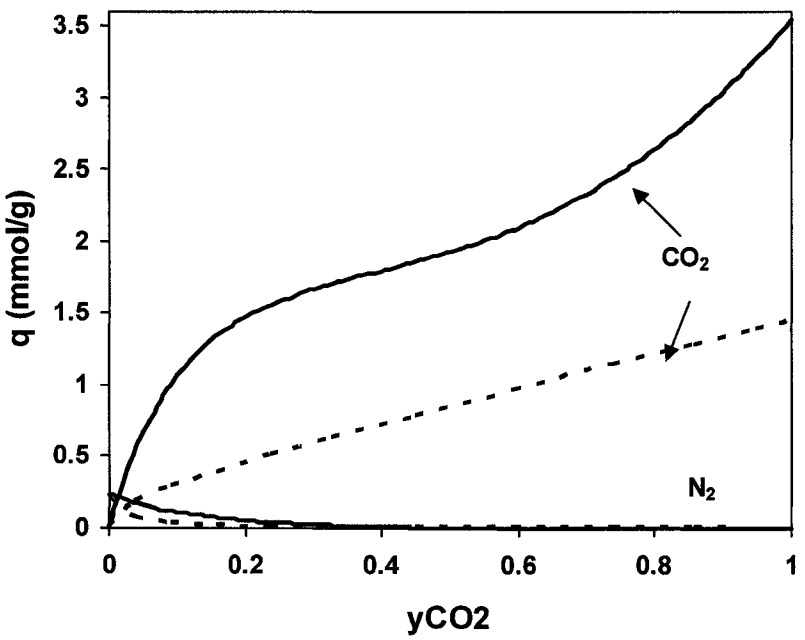

Figure IV- 8a. CO_2 – N_2 binary isotherms with Ceca 13X (—) from present study and silicalite (- - - -) from Li and Tezel [24] at 40 °C and 1 atm total pressure.

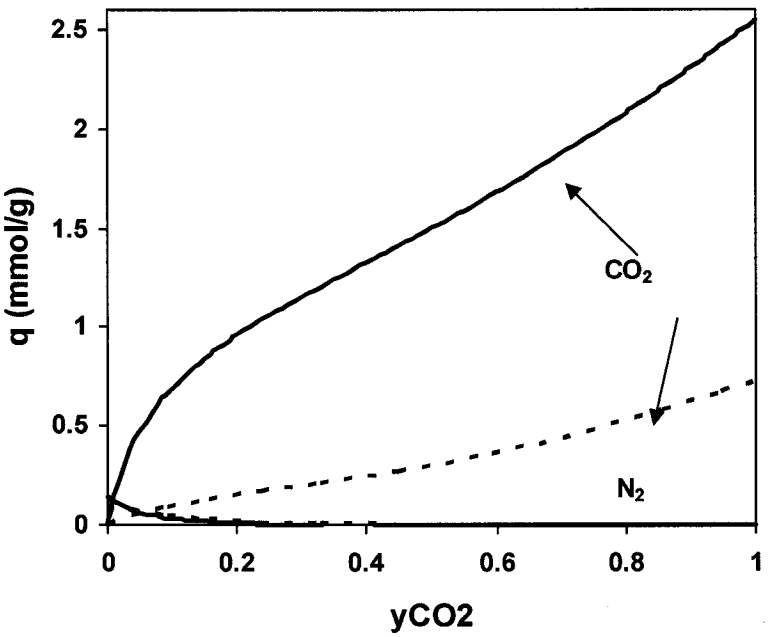

Figure IV-8b. CO_2 – N_2 binary isotherms with Ceca 13X (—) from present study and silicalite (- - - -) from Li and Tezel [24] at 100 °C and 1 atm total pressure.

The predictions given by extended Langmuir model were compared with the experimental binary isotherms determined for CO_2 - CH_4 at 40 °C and CO_2- N_2 at 100 °C. For CO_2- CH_4 binary mixture, a temperature of 40 °C was chosen since it represented the approximate temperature of landfill gas exiting a landfill. Similarly, 100 °C was selected as a more realistic temperature for flue gas applications involving the removal of CO_2 from dry air. These plots are shown in Figures IV-9a and IV-9b respectively.

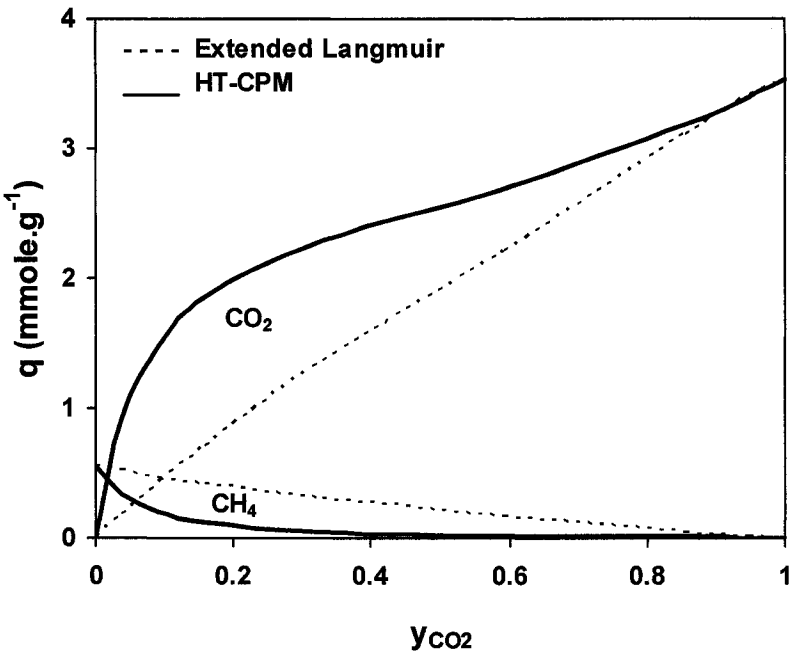

Figure IV-9a. Experimental CO_2-CH_4 binary isotherms for Ceca 13X compared with extended Langmuir model predictions at 40 °C and 1 atm total pressure.

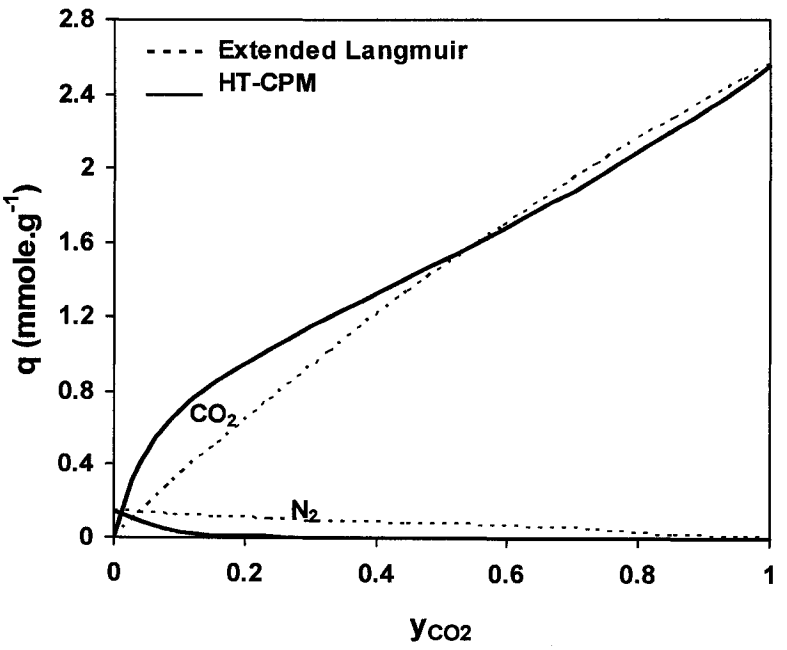

Figure IV-9b. Experimental CO_2- N_2 binary isotherms for Ceca 13X compared with extended Langmuir model predictions at 100 °C and 1 atm total pressure.

For the binary mixture of CO_2-CH_4 at 40 °C, it was observed from Figure IV-9a that extended Langmuir model under predicted the experimental data for CO_2 at all CO_2 gas phase concentrations less than 0.85 ($y_{CO2}<0.85$)

From the plot of IV-9b for the CO_2 - N_2 binary mixture at 100 °C, extended Langmuir model underpredicted the experimental data for CO_2 at low concentration of CO_2 (below 50%) for Ceca 13X and slightly overpredicted at higher compositions of y_{CO2}. This model slightly overpredicted the experimental data for N_2 at all CO_2 gas phase concentrations in the binary mixture of CO_2- N_2.

CO_2-CH_4 and CO_2-N_2 binary mixtures behave like non ideal systems and there is a large adsorption capacity difference between components. This would be the reason for the discrepancy between predictions by the ideal Extended Langmuir model and the experimental data.

THERMODYNAMIC CONSISTENCY TESTS

The data obtained from the equilibrium isotherms of single component gas and binary gas mixtures have been used to evaluate the integral thermodynamic consistency test using Equation 17 and the results are displayed in Table IV-3. The last row of the table indicates the amount of deviation between the single component gas and binary gas equilibrium adsorption data.

Table IV-3. The integral thermodynamic consistency test between single component gases and binary CO_2 -CH_4 and CO_2-N_2 equilibrium adsorption data for Ceca 13X at 40 °C and 100 °C.

(mmol/g)	**40 °C CO_2-CH_4**	**100 °C CO_2-CH_4**	**40 °C CO_2-N_2**	**100 °C CO_2-N_2**
$\int_0^1 \frac{q_1(1-y_1)-q_2 y_1}{y_1(1-y_1)} dy_1$ (RHS)	7.295	4.458	5.349	3.994
$\int_0^1 \frac{q_1^0}{P} dP$	7.833	4.598	5.528	4.176
$\int_0^1 \frac{q_2^0}{P} dP$	0.539	0.142	0.177	0.179
$\int_0^1 \frac{q_1^0}{P} dP - \int_0^1 \frac{q_2^0}{P} dP$ (LHS)	7.294	4.456	5.351	3.997
Difference (%) $\left\|\frac{LHS-RHS}{RHS}\right\|$	0.013	0.044	0.037	0.075

From Table IV-3, it can be observed that Ceca 13X agrees well with the integral thermodynamic consistency test for the binary CO_2-CH_4 and CO_2-N_2 adsorption data at both temperatures of 40 °C and 100 °C.

COMPARISON OF ADSORBENTS

From the binary isotherms plotted in Figures IV-6 and IV-8, it was observed that the adsorption capacity of CO_2 was much higher than that of CH_4 and N_2 in both Ceca 13X and UOP silicalite [4, 24] respectively. Both adsorbents are potential candidates for landfill gas application and the separation of CO_2 from dry air.

The corresponding equilibrium x-y diagrams for CO_2 - N_2 and CO_2 - CH_4 are shown in Figures IV-10a and IV-10b for Ceca 13X and silicalite [4, 24] at 40 °C and 100 °C. The diagrams provide valuable information on the selectivity of the solid adsorbent used to separate the binary gas mixtures.

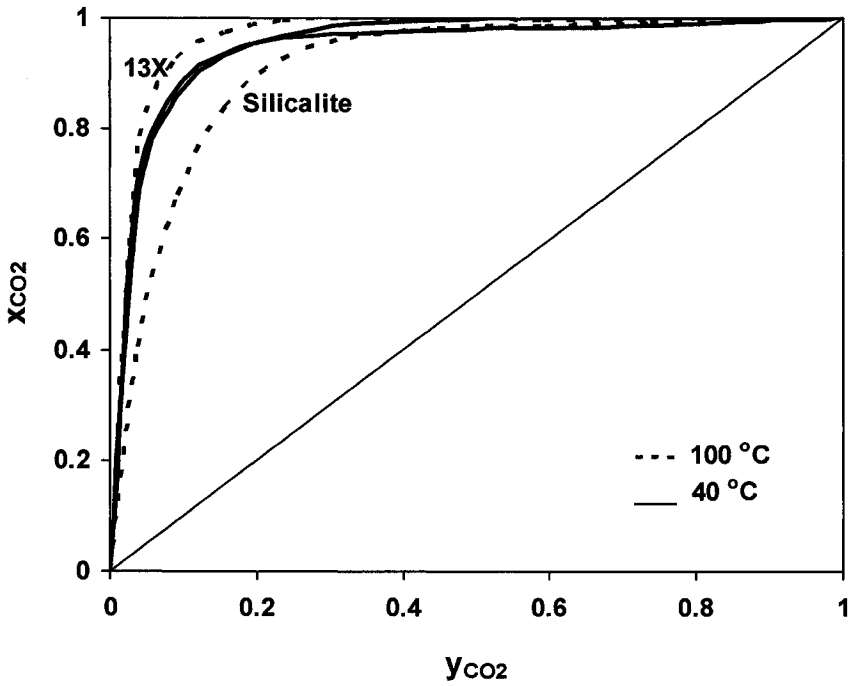

Figure IV- 10a. The x-y diagram for CO_2/N_2 Binary System with Ceca 13X from present study and UOP Silicalite from Li and Tezel [24] at 40 °C, 100°C and 1 atm total pressure.

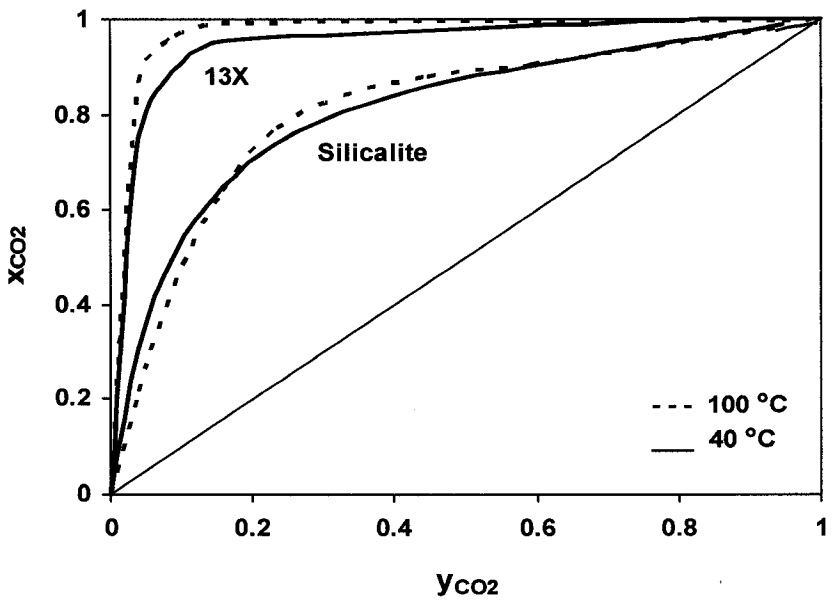

Figure IV- 10b. The x-y diagram for CO_2/CH_4 Binary System with Ceca 13X from present study and UOP Silicalite from Li and Tezel [24] at 40 °C, 100°C and 1 atm total pressure.

Both of the equilibrium curves at 40 °C and 100 °C for CO_2 - N_2 show that high purity CO_2 can be obtained and used as a product at low CO_2 feed gas concentrations. This property makes both Ceca 13X and silicalite [24] suitable for industrial flue gas separation which has y_{CO2} between 0.1 and 0.15. Ceca 13X could also be suitable for trace impurity removal applications from air (~400ppm) because of its high capacity for CO_2 at very low concentrations. The data at 100°C for Ceca 13X gave the best separation, since it was the furthest from the 45° line thus validating its use in the flue gas applications where temperatures are always higher. For landfill gas and natural gas applications, Ceca 13X proved to be a better adsorbent than UOP silicalite [4, 24] to adsorb CO_2 and a maximum separation was achieved at a higher temperature of 100 °C.

CONCLUSIONS

1. Single component gas adsorption data on Ceca 13X indicated that carbon dioxide is strongly adsorbed followed by methane and nitrogen. The heterogeneous Ceca 13X with a low Si/Al ratio (1.17) performed better than the hydrophobic and higher Si/Al ratio (thousands) of UOP silicalite. Adsorption capacity of single component gases increases as temperature decreases as expected.
2. The more versatile HT-CPM model fits the experimental data very well for the non ideal CO_2-CH_4 and CO_2- N_2 systems.
3. Extended Langmuir theoretical adsorption model can only be applied as an approximation to predict the experimental binary behaviour for the systems studied.
4. Ceca 13X appears to be a promising adsorbent for trace removal of CO_2, flue gas separation of CO_2 from dry air, natural gas and landfill gas purification applications.
5. Ceca 13X data showed excellent thermodynamic consistency at both temperatures studied.

ACKNOWLEDGEMENTS

Financial supports received from Ontario Centres of Excellence (OCE), RioTinto Alcan and Air Products & Chemicals Inc., are gratefully acknowledged.

NOMENCLATURE

A = parameter, mmol/g/atm

c = sorbate concentration in bulk phase, mol/cm^3

B = adsorption affinity constant, atm^{-1}

K = Henry's law constant, dimensionless

B_i = adsorption affinity constant for component 'i', atm^{-1}

K_P = Henry's law constant, mmol/g/atm

L = length of the chromatographic column, cm

P = (total) pressure, atm

P_1 = partial pressure of Component *1*, atm

P_2 = partial pressure of Component *2*, atm

q = amount adsorbed, $mmol.g^{-1}$

q_1 = amount adsorbed of Component *1*, $mmol.g^{-1}$

q^0_1 = amount adsorbed of Component *1* in single component system, $mmol.g^{-1}$

q_2 = amount adsorbed of Component *2*, $mmol.g^{-1}$

q^0_2 = amount adsorbed of Component *2* in single component system, $mmol.g^{-1}$

q_m = adsorption saturation capacity or maximum amount adsorbed, $mmol.g^{-1}$

q_{m1} = maximum amount adsorbed in site '1', $mmol.g^{-1}$

R = gas constant, 8.314J/K/mol

T = Temperature, K

x = mole fraction in adsorbed phase at equilibrium, dimensionless

y = mole fraction in fluid phase at equilibrium, dimensionless

y_1 = mole fraction of Component 1 in fluid phase at equilibrium, dimensionless

Greek letters

θ = fraction of monolayer coverage, dimensionless

ε = porosity of the bed, dimensionless

λ = adsorption parameter, dimensionless

μ = first moment (Average retention time), s

μ_D = system dead time, s

v = interstitial fluid velocity (cm/s)

ρ = density of adsorbent (without pores), g/ cm^3

Abbreviations

Abbreviation	Description
Al	Aluminium
CH_4	Methane
CO_2	carbon dioxide
CPC	concentration pulse chromatography
CPM	concentration pulse method
GHG	greenhouse gas
GWP	greenhouse warming potential
HT	Harlick-Tezel
LFG	landfill gas
LHS	left hand side
N_2	Nitrogen
NI	national instruments
ppm	parts per million
RHS	right hand side
Si	Silica
SSR	sum of the square residuals

REFERENCES

1. Cavenati, S., C.A. Grande, and A.E Rodrigues, "Layered Pressure Swing adsorption for methane recovery from $CH_4/CO_2/N_2$ streams", Adsorption **11**, 549-554, (2005a).
2. Cavenati, S., C.A. Grande, and A.E Rodrigues, "Upgrade of methane from landfill gas by pressure swing adsorption", Energy and Fuels **19**, 2545-2555, (2005b).
3. IPCC/TEAP, 2005: Special Report on Safeguarding the Ozone Layer and the Global Climate System: Issues Related to Hydrofluorocarbons and Perfluorocarbons, Cambridge University Press, Cambridge, United Kingdom and New York, NY, USA, 488 pp.
4. Li, P. and F. H. Tezel, "Pure and binary adsorption equilibria of methane and carbon dioxide on Silicalite", Separation Science of Technology, **42**, 3131-3153 (2007a)
5. Li, P. and F.H. Tezel, "Adsorption Separation of N_2, O_2, CO_2 and CH_4 Gases by β-Zeolite", Microporous & Mesoporous Materials, **98**, 94-101 (2007b).
6. Langmuir, I., "The Adsorption of Gases on Plane Surfaces of Glass, Mica and Platinum, Journal of the American Chemical Society", **40**, 1361-1403 (1918).
7. Shah, D. B. and D.M. Ruthven, "Measurement of Zeolite Diffusivities by Chromatography", AIChE Journal, **23**, 804-810 (1977).
8. Ruthven, D.M. and R. Kumar, "An experimental study of single component and binary adsorption Equilibria by a Chromatographic method", Ind. Eng. Chem. Fundam., **19**, 27-32 (1980).
9. Harlick, P.J.E. and F. H. Tezel, "A Novel solution method for interpreting binary adsorption isotherms from Concentration pulse chromatographic data" Adsorption **6**, 293-309 (2000).

10. Harlick, P. J. E. and F.H. Tezel, "CO_2-N_2 and CO_2-CH_4 Binary Adsorption Isotherms with H-ZSM-5: the Importance of Experimental Data Regression with the Concentration Pulse Method", The Canadian Journal of Chemical Engineering, **79**, 236-245 (2001).

11. Harlick, P. J. E. and F.H. Tezel, "Adsorption of Carbon Dioxide, Methane and Nitrogen: Pure and Binary Mixture Adsorption by H-ZSM-5 with SiO_2/Al_2O_3 Ratio of 30", Separation Science and Technology, **37**, 33-60 (2002).

12. Harlick, P. J. E. and F. H. Tezel, "Use of Concentration Pulse Chromatography for Determining Binary Isotherms: Comparison with Statically Determined Binary Isotherms", Adsorption, **9**, 275-286 (2003a).

13. Harlick, P. J. E. and F.H. Tezel, "Adsorption of Carbon Dioxide, Methane and Nitrogen: Pure and Binary Mixture Adsorption for ZSM-5 with SiO_2/Al_2O_3 Ratio of 280", Separation and Purification Technology, **33**, 199-210 (2003b).

14. Triebe, R. W., Tezel, F. H, "Adsorption of Nitrogen and Carbon Monoxide on Clinoptilolite: Determination and Prediction of Pure and Binary Isotherms", The Canadian Journal of Chemical Engineering,**73**, 717-724 (1995)

15. Tezel, F.H., H.O. Tezel, and D.M. Ruthven, "Determination of Pure and Binary Isotherms for Nitrogen and Krypton", Journal of Colloid and Interface Science, **149**, 197-207 (1992).

16. Rao, M. B. and S. Sircar, "Thermodynamic Consistency for Binary Gas Adsorption Equilibria", Langmuir, **15**, 7258-7267 (1999).

17. S. Sircar, "Excess Properties and Thermodynamics of multicomponent Gas Adsorption", J. Chem. SOC., Faraday Trans, **81**, 1527-1532 (1985).

18. S. Sircar, "R&D Note: Data Representation for Binary and multicomponent Gas Adsorption Equilibria", Adsorption, **2**, 327-331 (1996).

19. Golden, T.C. and S. Sircar, "Gas adsorption on Silicalite", Journal of Colloid and Interface Science, **162**, 182-188 (1994).

20. Huang, Y.Y., "Quadrupole interaction of carbon dioxide on silica-alumina surface", J. Phys.Chem., **77(1)**, 103-106 (1973).

21. Rees, L. V. C., P. Bruckner and J. Hampson, "Sorption of N_2, CH_4 and CO_2 in Silicalite-1", Gas Separation and Purification, **5**, 67-75 (1991).

22. Dunne, J. A., M. Rao, S. Sircar, R. J. Gorte and A. L. Myers, "Calorimetric Heats of Adsorption and Adsorption Isotherms. 1. O_2, N_2, Ar, CO_2, CH_4, C_2H_6, and SF_6 on NaX, H-ZSM-5 and Na-ZSM-5 zeolites", Langmuir, **12**, 5896-5904 (1996).

23. Choudhary, V. R. and S. Mayadevi, "Adsorption of Methane, Ethane, Ethylene, and Carbon Dioxide on Silicalite-1", Zeolites, **17**, 501-507 (1996).

24. P. Li, and F. H. Tezel, Pure and Binary adsorption equilibria of CO_2 and N_2 on Silicalite, Journal of Chemical and Engineering Data (in print).

25. Mulgundmath, V.P., Tezel, F.H, Feifei, H and Golden, T.C., "Binary adsorption behaviour of methane and nitrogen gases", Journal of Porous Materials (submitted).

CHAPTER V

FIXED BED ADSORPTION FOR THE REMOVAL OF CARBON DIOXIDE: BREAKTHROUGH BEHAVIOUR AND MODELLING FOR HEAT AND MASS TRANSFER

Mulgundmath, V.P., Jones, R.A., Tezel, F.H and Thibault, J

Department of Chemical & Biological Engineering, University of Ottawa,

161 Louis Pasteur, Ottawa. K1N 6N5. Canada

Submitted to Separation and Purification Technology journal.

Presented at the Fundamentals of Adsorption (FOA9) conference, May 20-25, 2007, Sicily-Italy

ABSTRACT

Concentration and temperature profiles for CO_2 adsorption from a CO_2-N_2 gas mixture (10 % CO_2 by vol in N_2) have been studied in a dynamic adsorption pilot plant unit to better understand the breakthrough behaviour. The scope of the present work is to study the adsorption characteristics and heat effects of this CO_2-N_2 gas mixture and to develop a simple model for the dynamic simulation of non-isothermal adsorption in a fixed bed.

Results indicated that adsorption heat effects were significant for this mixture while the breakthrough time obtained with Ceca 13X adsorbent was independent of the initial bed temperature. The cooling step that follows the thermal regeneration of the adsorption bed could be omitted entirely without affecting the adsorption performance. An earlier breakthrough time was observed for a higher feed flow rate of 6.6 SL/min compared to 4 SL/min. Cooling during the adsorption cycle decreased the width of the mass transfer zone and led to a longer breakthrough time. The study also indicated that online measurements of temperature at different locations along the column bed could be used to predict the concentration breakthrough for this CO_2-N_2 gas mixture. The novel two-population model used in this study provided an adequate representation of the temperature and concentration breakthrough profiles within the adsorption column.

INTRODUCTION

Carbon dioxide is an omnipresent species that has generated enormous attention since the turn of the century because of its contribution to the greenhouse gas effect. Combustion of fossil fuels is a major source of these harmful emissions which is the result of ever increasing world wide population and an increased per capita demand for energy. According to the International Energy Agency Working Party on Fossil Fuels [1], more than 85% of the world's energy needs are met by fossil fuels which account for the annual emission of 25 billion tons of CO_2 into the atmosphere. Fossil fuel-fired power generation facilities account for one-third of the global CO_2 emission to the atmosphere [2]. This has resulted in a global research effort to mitigate the emissions of CO_2 and examine ways to capture CO_2 directly from power plant flue gases [3].

For the purpose of reducing CO_2 emissions to the atmosphere, IEA WPFF [1] outlines the utilisation of Zero Emission Technologies (ZET) which virtually eliminate emissions from the conversion of fossil fuels and their consequences on health and environment. ZET promote the increase of the overall plant efficiency, the use of lower-carbon or carbon free energy sources, oxy-fuel combustion, CO_2 fixation using algae and the development of new power cycles. However, these are innovative technologies that cannot be easily used to retrofit existing power plants. Carbon sequestration involving the carbon dioxide capture and storage (CCS) has become a major focus of reducing point-source emissions. For CO_2 to be sequestered, it must be relatively pure (>95%) to find useful applications in the food refrigeration industry, fire extinguishers, enhanced oil recovery, beverage carbonation, metals fabrication, urea production and to reduce the

volume of stored CO_2 in deep saline aquifers, depleted oil and gas reservoirs and unminable coal/mineral beds [4].

Cryogenic distillation, liquid phase absorption and gas separation membranes compete with adsorption processes for CO_2 removal applications [5, 6]. The flue gas concentration ranges from 8-15 vol% for typical coal fired plants. Absorption using amines is the currently widely employed commercial technology but there is a significant energy penalty required to regenerate the solvent. Cryogenic distillation is only feasible for CO_2 concentrations greater than 90 vol% whereas membranes exhibit low fluxes, degradation, high cost and fouling [7]. Adsorption processes are increasing being used as they tend to utilise less resources and energy and are highly efficient [8-17].

The scope of the present work is to study the adsorption breakthrough characteristics and heat effects of a gas mixture (10 % CO_2 in 90% N_2 by vol) that resembles the concentration of CO_2 found in typical dry flue gases and to develop a simple model for the simulation of a non-isothermal adsorption in a fixed bed.

Selection of a suitable adsorbent is one of the important issues in an adsorption process. This adsorbent must possess a high selectivity for CO_2 over N_2 along with faster uptake rates in order to achieve a higher throughput. The most widely used adsorbents for CO_2 removal are zeolites, with 4A, 5A, and 13X being the most popular from this class [18, 19], although activated carbon and activated alumina are also used for Pressure Swing Adsorption (PSA) applications [20, 21]. Reynolds et al. [7] used a high temperature PSA

with potassium promoted hydrotalcite (HTlc) as adsorbent which exhibited higher capacity at elevated temperatures and good water insensitivity. Attempts have been made to develop and commercialise novel MCM-41 polymer modified molecular basket adsorbents for CO_2 removal [22] and amine impregnated pore expanded (PE) MCM-41 adsorbents [4]. Most recently activated Alumina composites are being developed in combination with zeolite 13X. The alkaline treated Alumina has better resistance against moisture and 13X with a narrow pore size distribution provides a selective adsorptive separation. The adsorbent candidates chosen for this study included Ceca 13X zeolite, Alcan activated alumina AA320-AP and a composite of activated alumina/13X adsorbent, Alcan 650 PC.

Single component gas adsorption isotherms for CO_2 and N_2 were measured at 40°C and 100°C for each adsorbent in a constant volume system (Accusorb 2100 Physical adsorption analyser supplied by Micromeritics Instrument Corporation) for Ceca 13X, Alcan AA320-AP and Alcan 650 PC (a third isotherm experiment for CO_2 was performed at 70°C on Ceca 13X). This method involves measuring pressure changes in a known volume of gas exposed to an adsorbent sample. As the gas is adsorbed and allowed to reach equilibrium, the measured decrease in the closed system pressure yields the amount of gas adsorbed under given operating conditions. The single component gas isotherms of CO_2 and N_2 are displayed in Figure V-1a for 13X and AA 320-AP and Figure V-1b for 13X and 650 PC. Isotherm data for 13X are repeated in these figures for comparison with other tested adsorbents. The experimentally determined single component gas isotherms have been fitted with the Langmuir model.

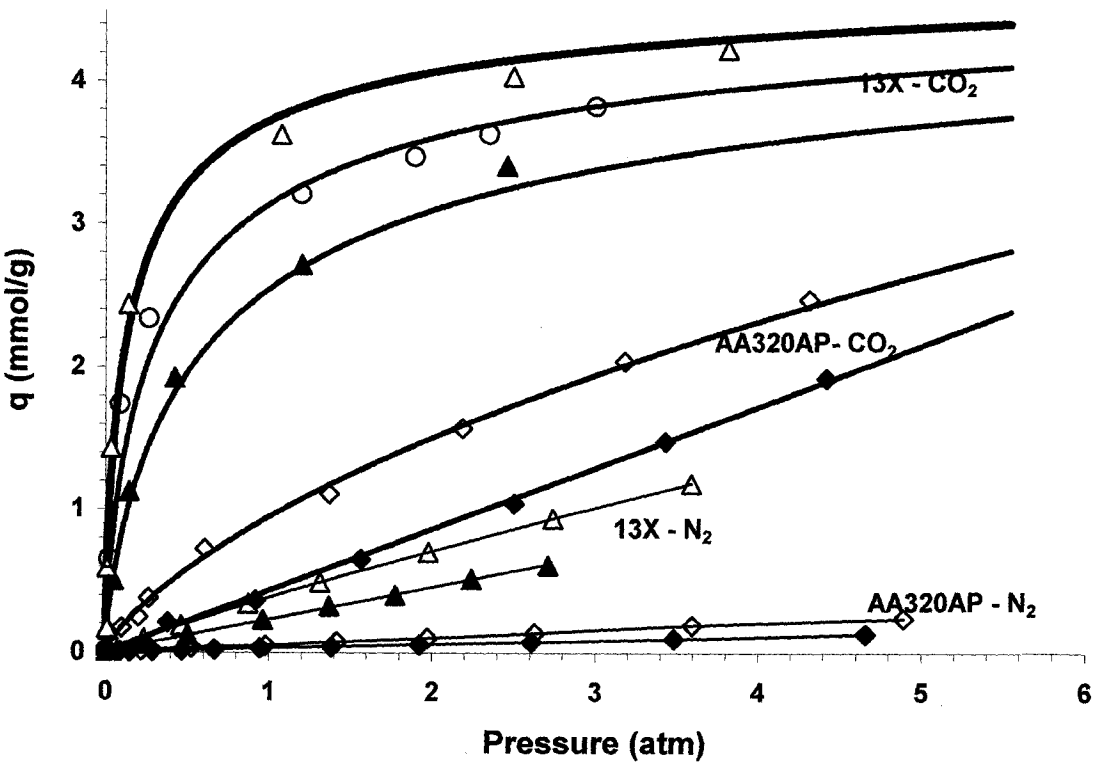

Figure V-1a. Single component isotherms of CO_2 on 13X and AA 320-AP at 40°C (hollow symbols) and 100°C (filled symbols). Hollow circles represent CO_2 data for 13X at 70°C. Lines represent the Langmuir fit.

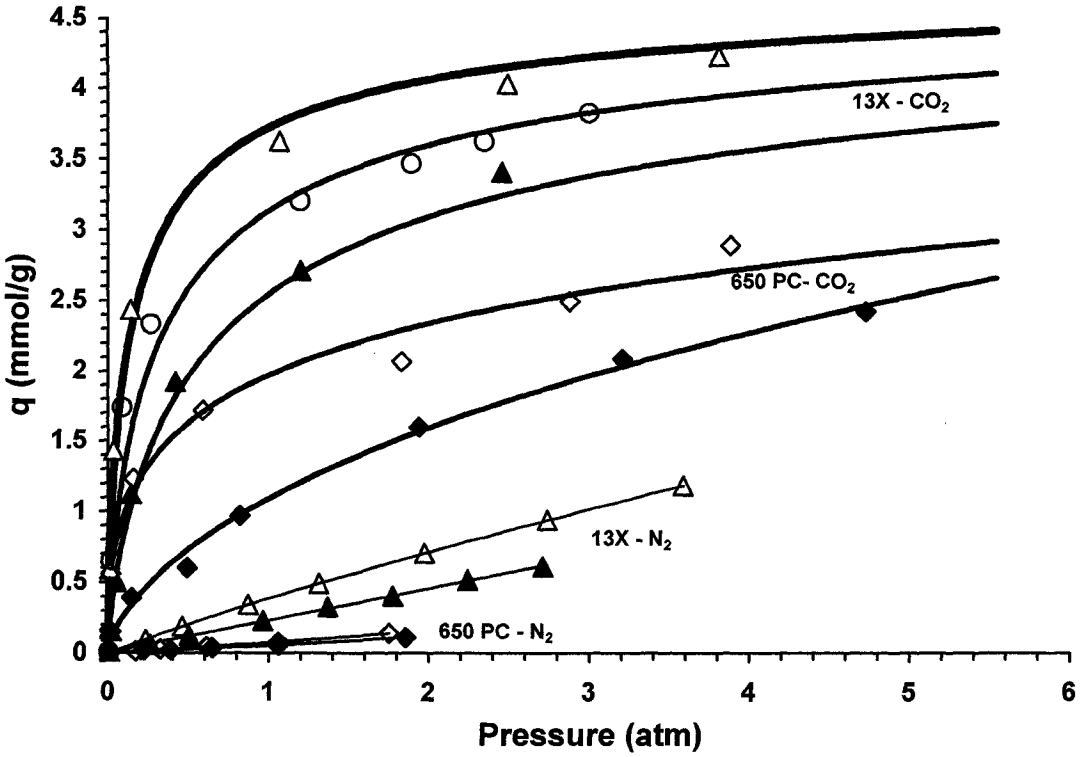

Figure V-1b. Single component isotherms of CO_2 on 13X and 650 PC composite at 40°C (hollow symbols) and 100°C (filled symbols). Hollow circles represent CO_2 data for 13X at 70°C. Lines represent the Langmuir fit.

From Figures V-1a and V-1b, it was observed that the shape of the CO_2 isotherms on 13X was very rectangular whereas the N_2 adsorption isotherms were linear. The initial slope of the CO_2 isotherm is very high. This indicates more interactions between CO_2 molecules and the heterogeneous surface of 13X adsorbent. CO_2 favours a more heterogeneous surface due to its higher quadrupole moment compared to N_2. At a lower temperature of 40°C, the capacities of all tested adsorbents were greater than at 100°C, as expected, and consistent with always exothermic physical adsorption behaviour.

13X had a large working capacity for CO_2 when compared to 650PC composite and AA320-AP. For the 10% CO_2 (by vol) gas composition used in this investigation and 6.44 atm total column pressure, the partial pressure for CO_2 was 0.644 atm. At this partial pressure for 40°C, the amount of CO_2 adsorbed was 3.444 mmol/g for 13X followed by 1.746 mmol/g for Alcan 650 PC and 0.694 mmol/g for Alcan AA320-AP. This observation indicates higher interactions between CO_2 and the more heterogeneous Ceca 13X structure which is highly desirable for the removal of CO_2 from flue gas.

Nitrogen capacities observed were slightly higher for Ceca 13X followed by Alcan 650 PC and Alcan 320-AP. Higher N_2 capacities are not desirable for this gas separation since it will be recovered as a product when CO_2 is adsorbed on the adsorbent. When all the above tested adsorbents were compared, Ceca 13X exhibited the larger differences in the adsorption capacities between CO_2 and N_2 at the operating pressure (6.44 atm) and feed concentration (10% CO_2 by vol) at 40°C. These single component gas isotherm observations suggest that 13X is a suitable adsorbent for the separation of CO_2 in a flue gas application followed by 650 PC composite and AA320-AP.

From the literature binary isotherm data, it was observed that 13X adsorbent is a promising adsorbent for CO_2 flue gas separations [23]. Also, the equilibrium phase diagrams obtained for this binary mixture on 13X adsorbent indicated that better separation of CO_2 and N_2 was achieved at high temperatures when compared to 40°C. This observation also indicates that Ceca 13X is suitable for flue gas separation applications. This finding is similar to the observation made on commercial 13X zeolite

by Zhang et al. [3]. 13X was chosen in this investigation as the adsorbent for the lab scale dynamic adsorption unit to study the breakthrough behaviour.

EXPERIMENTAL SECTION

A two column dynamic adsorption analysis unit has been designed and built to separate CO_2-N_2 mixtures using zeolite Ceca 13X as the adsorbent supplied by CECA, Honfleur, France. The properties of the adsorbent and the fixed bed are given in Table V-1 while Figure V-2 shows a simplified schematic diagram of the apparatus built in-house.

Table V- 1. Properties of the adsorbent and fixed bed

Bed length (m)	0.61
Column internal diameter (m)	0.044
Column wall thickness (m)	0.0029
Port 1 position[1] (m)	0.102
Port 2 position[1] (m)	0.305
Port 3 position[1] (m)	0.507
Ceca 13X pellet radius (m)	0.00103
Ceca 13 X bulk density ($kg.m^{-3}$)	705

[1] Tap location from the column inlet

This experimental system was designed to allow easy in-situ regeneration of the saturated adsorbent. It primarily consists of the following components: two identical adsorption columns, feed and purge gas , heating tape, an in-line gas heater, copper heating/cooling

tubes wrapped around the column, solenoid three-way and two-way valves, 1/4" and 1/8" outside diameter stainless steel tubing, a data acquisition system, customised control software, thermocouples, a multiposition valve, pressure transducers, mass flow controllers, a mass flow meter, a gas mixing chamber (MC), a gas chromatograph (GC), a non dispersive infrared analyser (NDIR) and an Edwards high vacuum pump.

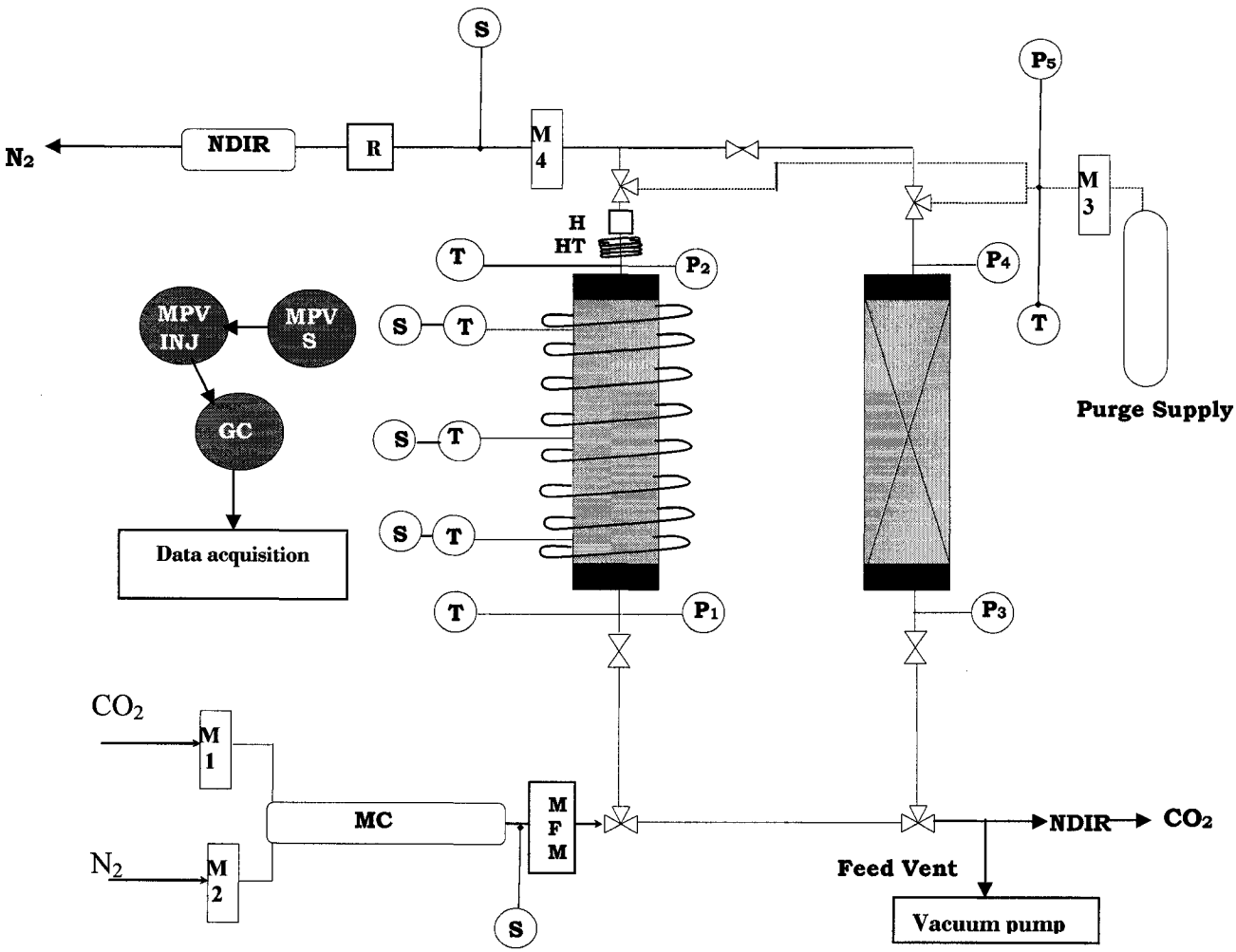

GC- Gas Chromatograph ; H- Heater ; HT- Electrical heating tape ; INJ - Injection valve ; NDIR- Non Dispersive Infrared analyser ;M- Mass flow controller ; MC- Mixing chamber ; MFM- Mass flow meter ; MPV- Multiposition valve ; P - Pressure transducer ; R- Rotameter ; S- Sample port ; T- Thermocouple

Figure V-2. Schematic diagram of the two bed Thermal Pressure Swing Adsorption (TPSA) system.

The two adsorption columns are made of 316 stainless steel which is known for its corrosion resistance, toughness even at elevated temperatures and for fast heat dissipation. The inside diameter of the column is 4.4 cm, and the length available for the adsorption bed is 61.0 cm. The columns are fitted to inlet and outlet stainless steel conical flow distributors in order to favour plug flow conditions. VCR® fittings and Teflon O-rings formed the seals between the column and the flow distributors. One of the columns has three ports that were simultaneously used for temperature and concentration measurements from column centre axis location. These sample ports were connected to a VALCO model SD 32-port micro-electric actuated multiposition valve. This multiposition valve had 32 ports (16 inlet and 16 outlet ports) and had the capability of connecting 16 different sample ports at any time A 6-port micro-electric actuated injector valve housed the sample gas cell (500 μL) and connected the 32-port micro-electric actuated multiposition valve to a Varian 3400 Series Gas Chromatograph (GC) for concentration measurements through 0.32 cm (1/8") outside diameter stainless steel tubing. The sample gas cell within the 6-port micro-electric actuated injector valve was purged with UHP helium for 5 seconds followed by injecting the CO_2-N_2 gas mixture sample from the desired sample port for a period of 3s. Each gas sample took 1 min to be analysed in the GC to obtain the CO_2 composition. Therefore, experimental composition data points from the GC were obtained every minute. Since there were three sample location ports along the column, the data point at each sample location was obtained every 3 minutes. Using a GC provided the flexibility of experimenting with various gases. Disadvantages with the GC included the difficulty in obtaining continuous gas detection at each sample port immediately, as there is a time lag involved with the GC detector. Along with the GC, a non dispersive infrared analyser (NDIR) was used for continuous CO_2 gas

detection (0-20% by vol) at the adsorber column exit. The zero and span drifts were less than ± 1% of the full scale. Accurate temperature measurements were obtained by using Omega type-K exposed tip thermocouples.

The two adsorption columns were each equipped with two 590 Barocel pressure transducers at the entrance and the exit of the columns for measuring pressures up to 10 atm with an accuracy of 1% of the reading. The average of the inlet and outlet column pressures was taken as the average column pressure. Due to the low pressure drops (0.26 - 0.44 kPa) in the range of flow rates studied (4 - 6.6 SL/min), it represented the true column pressure. A Proportional-Integral-Derivative (PID) controller was built into LABVIEW software (from National Instruments) that was used to control this average column pressure by manipulating column exit mass flow rate via the mass flow controller (MFC) M4. The feed, purge and sample flow rates were controlled by MKS type M100B mass flow controllers (0-10 SL/min) which had an accuracy of 1.5% of the full scale.

The column was fitted with flexible copper coils and a thermostat controlled 50:50 (vol/vol) ethylene glycol water mixture circulated inside the coils in order to achieve near isothermal conditions for the process. Various components of this system were connected by 0.64 cm (1/4") outside diameter stainless steel tubing. A data acquisition system in conjunction with LABVIEW software from National Instruments was used to collect and record the pressure, temperature, concentration and flow rate data. For the adsorption of carbon dioxide from nitrogen, nitrogen was used both as a feed component and as a purge gas.

At the beginning of the set of experiments used in this study, the adsorption column was isolated from the set up and packed with the Ceca 13X adsorbent. Uniform distribution of the adsorbent pellets inside the column was ensured by continuous tapping of the sides of column. The adsorbent was regenerated in an electric oven at 200°C under nitrogen flow in order to remove any impurities present in its structure followed by cooling it overnight. Then the two ends of the column (inlet and outlet) were plugged to prevent any leaks and it was connected back to the rest of the experimental set up.

Prior to each run, the NDIR analyser was calibrated with span gas, UHP N_2 and a standard calibrated gas mixture of 10% (by vol) CO_2 and 90% (by vol) N_2. During pressurisation and after NDIR calibration, the feed gas mixture was prepared in the mixing chamber (MC) filled with glass beads using two pre-calibrated mass flow controllers (MFC) M1 and M2. This gas mixture was sampled through NDIR and GC to establish the variability in concentration.

Before each run, the column was pressurised using UHP N_2 to the desired column pressure and maintained at the same pressure using the PID controller. During this cycle, N_2 is adsorbed by the adsorbent and heat is liberated which raises the temperature within the column to about 55 °C -60 °C. The column was cooled to ambient temperatures (30-33 °C) using ethylene glycol-water mixture that circulated in the copper coils that surrounded the column. When ambient column temperatures (30-33 °C) were attained, the flow of ethylene glycol-water mixture was stopped and adsorption cycle was started by introducing the feed gas mixture (10% CO_2 bal. N_2) into the column. For each run, the CO_2

concentration, flow rates, pressures and temperatures were continuously monitored and the data were recorded in an MS-Excel worksheet.

When the gas concentration at the last sample port reached the feed concentration (10 % CO_2 bal. N_2), the feed flow was stopped. A complete regeneration of the saturated adsorbent was performed by combining high temperature (120 ^{o}C) and vacuum in-situ, between different experimental runs. During the regeneration cycle, UHP N_2 gas was allowed to flow through the column. The completion of this step was verified by stopping the vacuum and analysing the desorbed gas coming out from the column for CO_2 concentration using the NDIR analyser. Complete regeneration of the adsorbent was achieved when the desorbed gas contained no traces of CO_2. The column was then allowed to cool under UHP N_2 purge. It was then isolated from the rest of the setup by closing the column inlet and the outlet valves.

Prior to the start of the next run, the column was re-pressurised to the desired column pressure and the adsorption cycle was repeated. Adsorption column breakthrough experiments were conducted at a constant adsorption column pressure of 6.44 atm (absolute).

MATHEMATICAL MODELLING OF THE PROCESS

The objective of this study was to accurately describe the mass and heat transfer taking place within a packed bed adsorber. The model outlined here describes both the mass and heat transfer in the bulk fluid flowing within the bed, as well as the transport phenomena occurring within the porous solid adsorbent pellets. The model is intended to simultaneously fit three concentration profiles and three temperature profiles at different locations within the packed column. Therefore, the principal assumptions made in the development of the model are as follows:

- Bulk concentration and temperature in the column does not change in radial direction.
- Mass transfer between the surface of the pellet and the fluid is described by a linear driving force model, while the intra-particle mass transfer is described by pore diffusion.
- Within the adsorbent pellets, instantaneous equilibrium is assumed between the mobile fluid phase and the solid surface.
- The adsorption process is non-isothermal. The energy balance accounts for heat generation due to adsorption, heat exchanged with ambient air surrounding the packed adsorber, heat accumulation in the column walls, and the heat accumulation within the pellet and fluid phases.
- Adsorption equilibrium is described by the Langmuir isotherm model.
- The velocity in the bed changes due to adsorption and heat effects.

- Within the pellet particles, the mobile fluid phase in the pellet void and the solid portion of the pellet are assumed to be locally in thermal equilibrium.
- The adsorbent pellets are assumed to be spheres of homogenous size, and the adsorption sites are energetically homogeneous.
- Ideal gas law applies.
- The model accounts for two separate populations of pores, each with their respective mass transfer resistances. The two populations of pores represent respectively pores that are easily accessed and those that are accessed with greater difficulty.

MASS BALANCE EQUATIONS

Figure V-3 displays the schematic diagram of the fixed bed column and the spherical pellet used for modelling in this study. Assuming that the bulk concentration of CO_2 in the column radial direction is constant, the rate of change in concentration of the flowing gas at any axial position along the column is given by Equation (1) [24]:

$$\varepsilon_c \frac{\partial C_B}{\partial t} = \varepsilon_c D_z \frac{\partial^2 C_B}{\partial z^2} - (1 - \varepsilon_c) k_f \frac{3}{r_p}\left(C_B - C_p\Big|_{r=r_p}\right) - \varepsilon_c u_G \frac{\partial C_B}{\partial z} \quad \text{.....(1)}$$

The term on the left hand side indicates the accumulation term, while the terms on the right hand side of the equation account for the axial dispersion within column, the CO_2 transferred from the bulk fluid phase to the adsorbent particles (predicted by the linear driving force model), and the CO_2 transferred by convection, respectively.

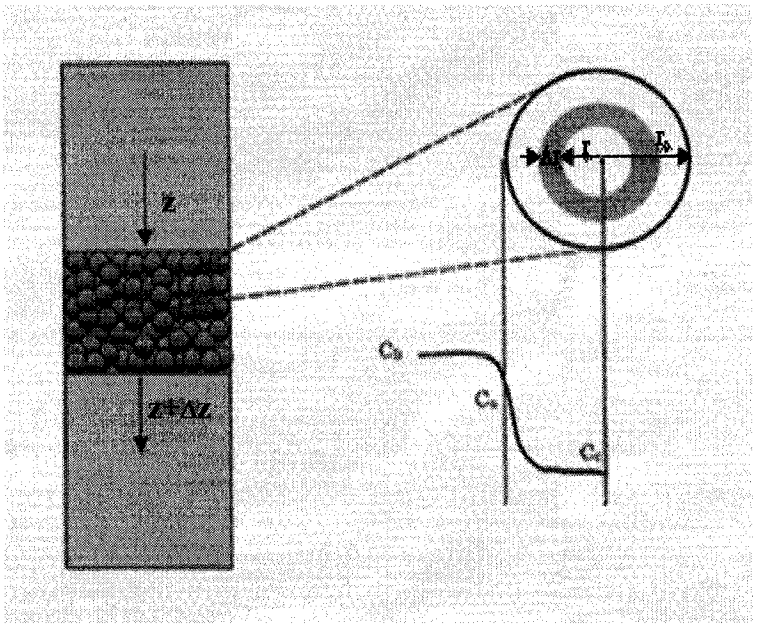

Figure V-3. Schematic diagram of the fixed bed column and the pellet.

The mass transfer within the pellet is predicted with a pore diffusion model. CO_2 reaching the surface of the solid from the bulk fluid diffuses, according to Equation (2), along the pores of the pellet due to a concentration gradient. Meanwhile, the concentration of the mobile gas phase within the pores is depleted due to adsorption of CO_2 onto the solid surface of the adsorbent pores. It is assumed that the adsorption of CO_2 onto the surface of the 13X adsorbent pellet can be considered instantaneous in comparison to the other mass transfer mechanisms [25].

$$\varepsilon_p \frac{\partial C_p}{\partial t} = D_x \left(\frac{1}{r^2} \frac{\partial}{\partial r} \left(r^2 \frac{\partial C_p}{\partial r} \right) \right) - (1 - \varepsilon_p) \rho_s \frac{\partial q}{\partial t} \qquad \text{.....(2a)}$$

$$\varepsilon_p \frac{\partial C_p}{\partial t} = D_r \left(\frac{1}{r^2} \frac{\partial}{\partial r} \left(r^2 \frac{\partial C_p}{\partial r} \right) \right) - (1 - \varepsilon_p) \rho_s \frac{\partial q}{\partial t} \qquad \text{.....(2b)}$$

An adsorbent particle normally possesses a wide distribution of pore sizes which for simplicity can be grouped into micro-pores and macro-pores having distinct mass transfer resistances. Equation (2a) represents those sites that are "easily accessed" while equation (2b) takes into account "difficultly accessed" sites only as displayed in Figure V-4.

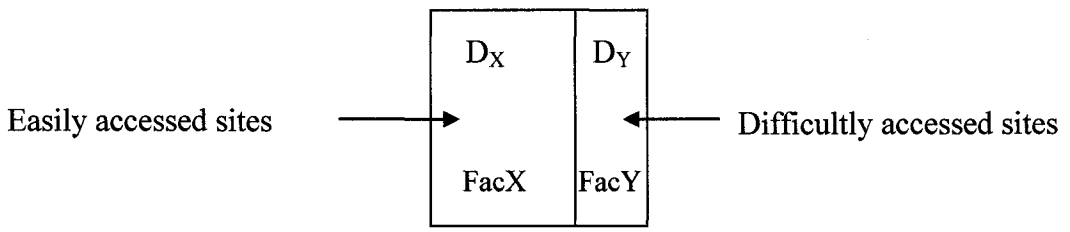

Figure V-4. Schematic diagram of the pellet showing easily accessed and difficulty accessed sites within the adsorbent pellet.

Equation (2) was solved twice simultaneously for the two "populations" of pellets (X, Y) that represented "easily accessed" (X) and "difficultly accessed"(Y) sites as represented in Equation (3).

$$C_p = FacX\ [C_{pX}] + FacY\ [C_{pY}] \qquad \text{.....(3)}$$

The "easily accessed" sites had the diffusion coefficient, D_x, which was calculated using Equation (6). D_Y represented the "difficultly accessed" sites and was optimised at the end of the simulation by fitting the model to the experimental data for temperature and concentration breakthrough curves at 3 different locations along the packed column. Each pellet population was given a weight representing the fraction of sites which were deemed to be "easily accessed" (FacX) and "difficultly accessed" (FacY). These population weighting factors (FacX and FacY) were also optimised by fitting the model to the experimental data for temperature and concentration breakthrough curves at 3

different locations along the packed column. The Langmuir isotherm model equation is used to describe the equilibrium that exists between the solid and the gas at a particular temperature.

Mass Transfer Correlations

The average external mass transfer coefficient between the flowing gas bulk and the pellet, k_f was calculated using the equation of Wakao and Funazkri [26]:

$$\mathrm{Sh} = 2.0 + 1.1(\mathrm{Re})^{0.6}(Sc)^{0.33} \qquad \text{.....(4)}$$

$$\text{i.e.,} \quad \frac{k_f D_p}{D_M} = 2.0 + 1.1\left(\frac{D_p \rho_G u_G}{\mu_G}\right)^{0.6}\left(\frac{\mu_G}{\rho_G D_M}\right)^{0.33} \qquad \text{.....(5)}$$

For the calculation of D_X, molecular and Knudsen diffusion coefficients were considered. The molecular diffusion of CO_2 in N_2 was estimated using the Chapman-Enskog equation [17] as follows:

$$D_M = \frac{0.0018583\sqrt{T^3\left(\frac{1}{M_A}+\frac{1}{M_B}\right)}}{P\sigma_{AB}^2\Omega_{AB}} \qquad \text{.....(6)}$$

For Knudsen diffusion, the collisions between the solute and the walls of the adsorbent are more frequent than collisions between the adsorbate molecules. It can be estimated using Equation (7) [17]:

$$D_K = 9700(r')\left(\frac{T}{M}\right)^{1/2} \qquad \text{.....(7)}$$

When D_K and D_M were both considered for the calculation of D_X, it was found that the effect of Knudsen diffusion was negligible for this system and molecular diffusion was found to be dominant.

The axial dispersion coefficient was estimated using the following correlation [27].

$$\frac{\varepsilon_c D_Z}{D_M} = 20 + 0.5 \mathrm{Re} Sc \qquad \text{..... (8)}$$

Initial and boundary conditions for mass transfer equations

Initially, the packed column adsorber has been regenerated and carbon dioxide is not present such that the fluid and the solid concentrations are zero everywhere within the column:

$$C_B = 0,\ C_p = 0,\ q = 0; \quad t = 0,\ \forall (z, r) \qquad \text{.....(9)}$$

This initial condition applies for the bulk fluid concentration as well as the concentration in the pellet. Two boundary conditions are required to solve Equation (1). At the entrance to the column, the feed concentration is known and remains constant throughout the experiment.

$$C_B = C_{Feed}\,(\text{i.e., } 25\ \text{mol/m}^3); \quad z = 0,\ t \geq 0 \qquad \text{.....(10)}$$

At the exit of the packed bed, it is assumed that the diffusive flux is equal to zero:

$$\frac{\partial C_B}{\partial z} = 0;\ z = L,\ t \geq 0 \qquad \text{.....(11)}$$

To solve Equation (2), two boundary conditions are required along with the initial condition given by Equation (9). At the center of the pellet, symmetry prevails whereas at

its surface, the rate of diffusion within the pellet must equal the convective mass flux from the bulk fluid.

$$\frac{\partial C_p}{\partial r} = 0 \;\; ; \; r = 0, t \geq 0 \qquad \text{.....(12)}$$

$$-D_i \frac{\partial C_p}{\partial r} = k_f \left(C_B - C_p \Big|_{r=r_p} \right) ; \; r = r_p, t \geq 0 \qquad \text{.....(13)}$$

where (D_i, i = X or Y).

ENERGY BALANCE EQUATIONS

The energy balance on the system consists of a balance on the bulk gas phase, a balance on the pellet which is comprised of the solid and the void portions of the pellet, and finally, a balance on the walls of the adsorption column. The energy balance for the bulk gas phase is given by Equation (14) [24]:

$$\varepsilon_c \rho_G C_{pG} \frac{\partial T_{bg}}{\partial t} = k_g \frac{\partial^2 T_{bg}}{\partial z^2} \varepsilon_c - (1-\varepsilon_c) h_f \frac{3}{r_p} (T_{bg} - T_P|_{r=r_p}) - u_G \frac{\partial T_{bg}}{\partial z} \varepsilon_c \rho_G C_{pG} - \frac{4}{r_b} h_f (T_{bg} - T_W)$$

.....(14)

This balance accounts for the transfer of energy by axial heat diffusion through the bed, energy transfer between the flowing fluid and the surface of the solid adsorbent due to temperature differences, the energy transfer by convection through the bed due to the bulk movement of gas, and finally, the energy transferred to the wall of the column.

Equation (15) accounts for the energy balance on the pellet [24]:

$$\left[\varepsilon_p \rho_G C_{pG} + (1-\varepsilon_p)\rho_s C_{pS}\right]\frac{\partial T_p}{\partial t} = k_{gs}\left(\frac{1}{r^2}\frac{\partial}{\partial r}\left(r^2\frac{\partial T_p}{\partial r}\right)\right) + \Delta H_{ads}\rho_B\frac{\partial q}{dt} \quad \text{.....(15)}$$

Equation (15) accounts for both the void and solid portions of the pellet. As was stated previously, the solid and mobile phases within the pellet are assumed to be in thermal equilibrium at a given radial position. The energy balance states that the local rate of change of temperature within the pellets is caused by energy transfer by thermal diffusion within the pellet and the energy generated within the system due to the exothermic heat of adsorption released when a molecule of CO_2 binds to the surface of the adsorbent. Equation (16) represents the energy balance on the column wall [24]. The balance accounts for the heat transfer to the wall from the bulk gas and the heat transfer from the wall to the outside surroundings.

$$\left[\left(\frac{d_2}{d_1}\right)^2 - 1\right]C_{pw}\rho_w\frac{\partial T_w}{\partial t} = \frac{4}{d_1}h_f\left(T_{bg} - T_w\right) - \frac{4}{d_1}\left(\frac{d_2}{d_1}\right)h_o\left(T_w - T_a\right)$$

.....(16)

Heat Transfer correlations

Chilton-Colburn analogy [30] was used to estimate the convective heat transfer coefficient for forced convection inside the packed bed:

$$j_D = j_H \Rightarrow Nu = 2.0 + 1.1(\mathrm{Re})^{0.6}(\mathrm{Pr})^{0.33}$$

.....(17)

As the experimental conditions represented a laminar flow of the bulk feed gas through the column, Churchill and Chu correlation [31] was used to deduce the average Nusselt number for laminar flow by Equation (18):

$$Nu = \frac{h_o L}{k_g} = 0.68 + 0.67(Ra \times \psi)^{1/4} \quad \text{.....(18)}$$

$$Ra = \frac{\beta \Delta T g L^3}{\nu^2} \mathrm{Pr} \quad \text{.....(19)}$$

$$\psi = \left[1 + \left(\frac{0.492}{\mathrm{Pr}}\right)^{9/16}\right]^{-16/9} \quad \text{.....(20)}$$

Initial and boundary conditions for heat transfer equations

Initially, the entire column and its contents are at ambient temperature (306 K).

$$T_{bg} = T_p = T_w = 306 \text{ K}; \quad z = 0, t \geq 0 \quad \text{.....(21)}$$

Insulation boundary condition is assumed to be valid at the column entrance and exit:

$$\frac{\partial T_{bg}}{\partial z} = 0; \quad z = 0, L; t \geq 0 \quad \text{.....(22)}$$

To solve Equation (15), two boundary conditions are required in the pellet, along with the initial condition given by Equation (21). At the center of the pellet, symmetry prevails whereas at its surface, the rate of conduction within the pellet must equal the convective heat flux from the bulk fluid.

$$\frac{\partial T_p}{\partial r} = 0 \quad r = 0, t \geq 0 \quad \text{.....(23)}$$

$$-k_{gs} \frac{\partial T_p}{\partial r} = h_f \left(T_{bg} - T_p\big|_{r=r_p}\right); \quad r = r_p, t \geq 0 \quad \text{..... (24)}$$

A two-population adsorbent particle model, representing easily accessible adsorbent sites and those sites which are more difficult to access, was solved. When simulating the temperature and concentration breakthrough curves, the only parameter that was optimised from the energy balance equations was the bulk thermal conductivity of the pellet (k_{gs}). All other parameters in the energy balance were determined either experimentally or calculated using the empirical correlations given in this paper.

Table V-2 lists all the parameters inputted into the simulation (as estimated or calculated), as well as the 3 parameters that were optimised by fitting the model to the experimental data for temperature and concentration breakthrough curves at 3 different locations along the packed column.

The equations for mass and energy balances are solved by the method of finite differences. Equations (1), (14) and (16) for the column have been solved using the Explicit method while Equations (2) and (15) for the pellets have been solved using the Implicit method. The Levenberg-Marquardt multivariable optimisation technique has been employed to minimise the SSR to the set of non linear differential equations and obtain the numerical solution. This model is intended to provide a simplified approach to representing these two types of adsorption sites within the pellet without having to accurately estimate the radius of the zeolite crystals and the intra-crystalline diffusion resistance within the crystal. Similar systems have been modeled in the literature by including these experimentally determined parameters [32, 33].

Table V-2. Input and optimised parameters used in the simulation model for concentration and temperature breakthrough curves for 3 positions in the column.

Model data	Method	Source
C_{ps} (J.kg^{-1}.K^{-1}) = 920	estimated	Cavenati et al., [28]
C_{pG} (J.kmol^{-1}.K^{-1}) = 1023	estimated	A.F. Mills, [29]
C_{pw} (J.kg^{-1}.K^{-1}) = 500	estimated	A.F. Mills, [29]
$D_X = D_M$ (m^2 s^{-1}) = 6.7 x 10^{-5}	calculated	Equation# 6
D_z (m^2 s^{-1}) = 1.2 x 10^{-4}	calculated	Equation # 8
h_o (W m^{-2}K^{-1}) = 2.1	calculated	Equation# 18
h_f (W m^{-2}K^{-1}) =95	calculated	Equation# 17
k_f (W m^{-1}K^{-1}) = 0.0059	calculated	Equation # 5
k_g (W m^{-1}K^{-1})= 0.027	calculated	A.F. Mills, [29]
ε_c = 0.35	estimated	Cavenati et al., [28]
ε_p = 0.54	calculated[1]	-
ρ_p (kg .m^{-3})= 1085	calculated[1]	-
ρ_s (kg adsorbent.m^{-3} bed)= 2359	estimated	Cavenati et al., [28]
D_Y (m^2 s^{-1}) = 5.6 x 10^{-8}	optimised[2]	--
FacX = 0.73	optimised[2]	-
FacY = 0.27	(1-FacX)	-
k_{gs} (W m^{-1}K^{-1})= 0.045	optimised[2]	-

[1] - Calculated by estimating the column void and the bulk density of the adsorbent.
[2] - Since the exact proportion of the easily accessed sites was unknown and the diffusion coefficient in the difficult sites could not be determined, this parameter was optimised by fitting the model to the experimental data such that to minimize the sum of squares of residuals.

RESULTS AND DISCUSSIONS

The scope of this study was the experimental determination of adsorption breakthrough behaviour and heat effects for CO_2-N_2 gas mixture (10 % CO_2 by vol. in N_2) using the Ceca 13X adsorbent in the laboratory scale set-up. Concentration and temperature breakthrough profiles were determined to understand the adsorbent behaviour. The effects of parameters like the omission of the initial cooling step, feed flow rate, and external cooling during the adsorption step were investigated. A novel approach describing two different populations of the adsorbent pellets was used to develop a simple model for the simulation of non-isothermal adsorption in a fixed bed.

OMISSION OF THE INITIAL COOLING STEP

When the thermal regeneration of the adsorption bed is completed, generally a cooling step follows with a purge gas before adsorption step is implemented. This cooling step generally comprises 10-25% of the total cycle time [34]. There is a significant economic advantage if this step could be omitted entirely without affecting the adsorption performance. Basmadjian [34] derived the following two criteria under which the breakthrough time would be independent of the initial bed temperature using equilibrium theory. The first criterion is that the ratio of the equilibrium loading to the feed concentration must be larger than the ratio of adsorbent to gas heat capacity and is given by the following inequality:

$$(q_F / y_F) > C_{ps} / C_{pG} \qquad \text{.....(25)}$$

where q_F is the solid phase adsorbate concentration at the feed conditions, y_F is the component molar fraction at the feed conditions, C_{ps} is the solid adsorbent heat capacity

and C_{pG} is the gas phase heat capacity. The second and more important criterion based on adiabatic conditions is given by:

$$F = (q_{pl} / y_F)/(C_{ps} / C_{pG}) > 1.5 \qquad \text{.....(26)}$$

where q_{pl} is the solid phase adsorbate concentration at the plateau temperature. This temperature, T_{pl}, is obtained from Equation (27):

$$T_{pl} = T_F - (q_F \Delta H)/(C_{ps}(q_F / y_F) - C_{ps}) \qquad \text{.....(27)}$$

where T_F is the inlet feed temperature and ΔH is the heat of adsorption. At the beginning of each experimental run, the bed is still hot due to N_2 adsorption during the pressurisation step. However, these criteria were easily fulfilled in this investigation and confirmed by observations during the concentration and temperature breakthrough experiments. The breakthrough times were similar for the experimental runs that were performed while the bed was hot (55-60 ^{o}C) and while the bed was at ambient temperature (30-33 ^{o}C). The effect of parameters like low feed concentration (10% CO_2 bal. N_2), high equilibrium loading of the 13X adsorbent (at 0.644 atm. partial pressure, q=3.444 mmol/g), high total system pressure (6.44 atm), and a moderate heat of adsorption (25 kJ/mol) contributed to satisfy these criteria. Therefore, for all the rest of the runs, the initial cooling step was omitted at the beginning of the adsorption cycle.

It was observed that these criteria contributed to the slow movement of the adsorbate concentration front thus allowing the temperature wave to pass ahead. An interesting observation to note was the viable option of using thermocouples only to detect breakthrough behaviour under similar conditions, without the use of sample gas

concentration detectors. This is possible for bulk gas separations that exhibit a higher heat of adsorption.

EFFECT OF FEED FLOW RATE

Figure V-5 gives the concentration breakthrough curves obtained for CO_2 adsorption from a CO_2/N_2 mixture (10 % CO_2 bal. N_2) on a packed bed of 13X for two different flow rates to see the effect of the feed flow rate at a constant adsorption pressure of 6.44 atm (absolute). The plot gives the concentration of CO_2 in the gas phase as a function of time at the column outlet. A Non-Dispersive Infrared (NDIR) analyser was used at the column exit to obtain continuous gas concentration measurements. It was observed that a higher feed flow rate of 6.6 SL/min contributed to an early breakthrough since the bed got saturated faster with more CO_2 going through the column compared to a lower feed flow rate of 4 SL/min. For 6.6 SL/min, the mass transfer zone moved quicker and mass transfer coefficient was higher because of the higher Reynolds number.

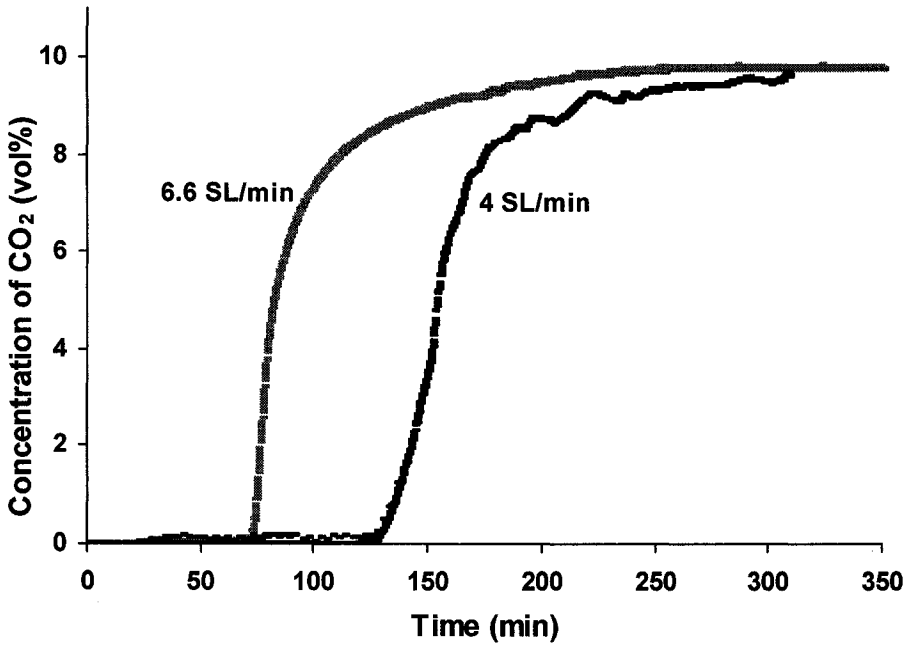

Figure V-5. Effect of flowrate on concentration breakthrough profile for CO_2 adsorption (10% CO_2 bal. N_2) with 13X adsorbent at 6.44 atm column pressure.

Tailing was seen towards the bed exit for both flow rates. This is an indication of the slow intra-particle diffusion within micro-pores of the adsorbent, presence of non homogeneous particles and varying flow patterns.

EFFECT OF EXTERNAL COOLING

Figure V-6 gives the concentration breakthrough curves obtained with and without cooling for CO_2 adsorption from a CO_2/N_2 mixture (10 % CO_2 bal. N_2) on a packed bed of 13X at two different flow rates to see the effect of external cooling at a constant adsorption pressure of 6.44 atm (absolute). The plot gives the concentration of CO_2 in the gas phase as a function of time at the column outlet. During the adsorption step, a mixture of 50:50 (by vol) ethylene glycol and water was circulated as a coolant (at 0 °C) in the copper coils that surround the column. The objective of these runs was to study the

breakthrough behaviour of this adsorption column which reached a relatively low temperature (2-3 °C) using a coolant circulating around the column at 0°C and a constant column pressure of 6.44 atm (absolute). For identical feed flow rates, it was observed that the cooling effect made the breakthrough curves steeper, decreasing the mass transfer zone. Since physical adsorption is exothermic, lower column temperatures contributed to an increase in the capacity of Ceca 13X adsorbent and, as a result, led to a delayed concentration breakthrough when compared to ambient non-isothermal operations.

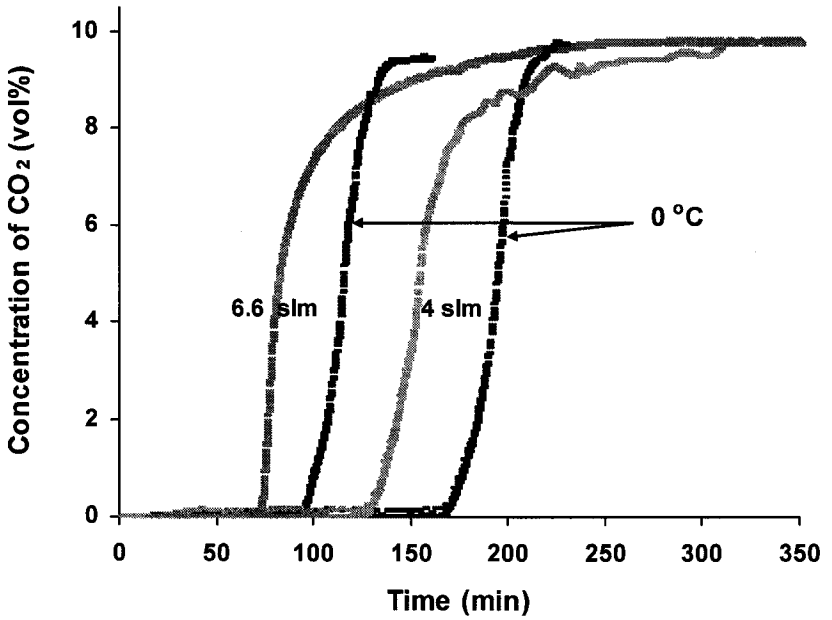

Figure V-6. Effect of cooling during the adsorption cycle on concentration breakthrough profile for CO_2 adsorption (10% CO_2 bal. N_2) with 13X adsorbent at 6.44 atm column pressure. Dark lines indicate the presence of a coolant at 0°C while grey lines represent experimental runs in the absence of the coolant.

Apart from studying the concentration breakthrough behaviour using an NDIR analyser, thermocouples were located at different sample ports (at positions 10.2 cm, 30.5 cm and 50.7 cm from column inlet)) to study the temperature breakthrough behaviour. Heat is liberated during the adsorption cycle when CO_2 is physically adsorbed on 13X. The

amount of heat liberated depends on the strength of the interaction between the adsorbent and CO_2, the concentration of CO_2 in the feed gas and the temperature of the column. The heat of adsorption basically dictates the type of adsorbent regeneration conditions that have to be employed. A higher heat of adsorption requires high temperature and/or lower pressures during regeneration.

Figure V-7a gives the temperature breakthrough curves obtained for CO_2 adsorption from a CO_2/N_2 mixture (10 % CO_2 bal. N_2) on a packed bed of Ceca 13X at 4 SL/min to see the effect of external cooling during adsorption step at a constant adsorption pressure of 6.44 atm (absolute). The plot gives the temperatures of the column at different positions as a function of time. The higher heat of adsorption observed for CO_2 on Ceca 13X (25 kJ/mol) contributed to reach a temperature of about 117°C when the column was at room temperature, as observed in Figure V-7a. Although more heat was released during the experiments with cooling due to higher capacities at low temperatures, the presence of the coolant resulted in a lower peak temperature (around 98°C). The temperature rise in port #1 (at 10.2 cm from column inlet) was smaller when compared to the ports (#2, #3) closer to the column exit. When the feed gas is introduced, adsorption begins to take place within a narrow mass transfer zone at the entrance of the column. The energy that is released due to adsorption, heats the adsorbent particles as well as the gas within the bed and the column walls near the entrance of the column. Some of the energy that is released will be transferred through convection and axial heat diffusion which begins to warm the downstream column contents. By the time the mass transfer zone has moved down the bed to the downstream

sampling ports, the adsorbent particles have already been heated partially due to the energy carried from the upstream sections of the bed. When energy is released due to adsorption in this section of the bed, a higher peak is attained. This release of energy that is carried along the length of the column also explains the presence of tailing particularly for the experiments in which no cooling is present. When cooling is conducted, less tailing is evident. The coolant provides a higher driving force for energy transfer through the walls of the column due to a larger temperature gradient as opposed to along the length of the column.

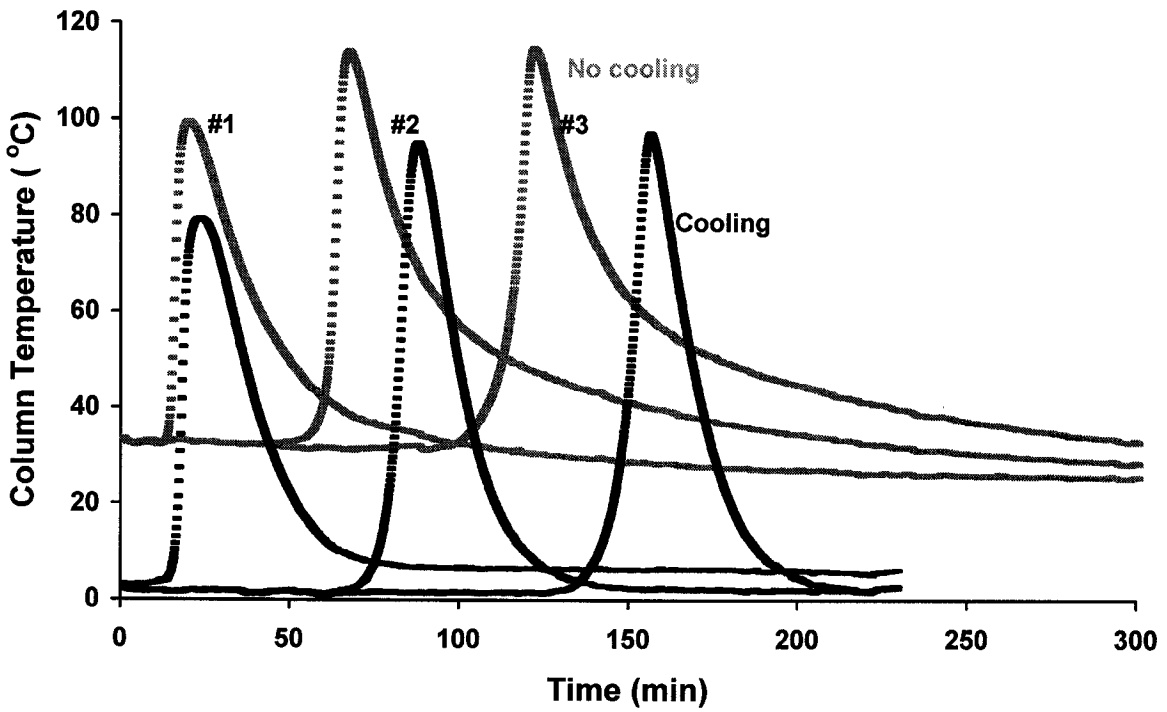

Figure V-7a. Effect of cooling/no cooling during adsorption cycle on temperature fronts in column (4 SL/min) for CO_2 adsorption (10% CO_2 bal. N_2) with 13X adsorbent at 6.44 atm column pressure. Dark lines indicate the presence of a coolant at 0°C while grey lines represent experimental runs in the absence of the coolant.

Similar results were obtained for a higher feed flow rate of 6.6 SL/min as observed in Figure V-7b. Temperatures obtained were higher for 6.6 SL/min run, since the quantity of CO_2 being fed into the column was greater than at 4 SL/min (Figure V-7a). A higher feed flow also signified a larger Reynolds number and thus a higher mass transfer coefficient which resulted in faster adsorption and thus a higher temperature.

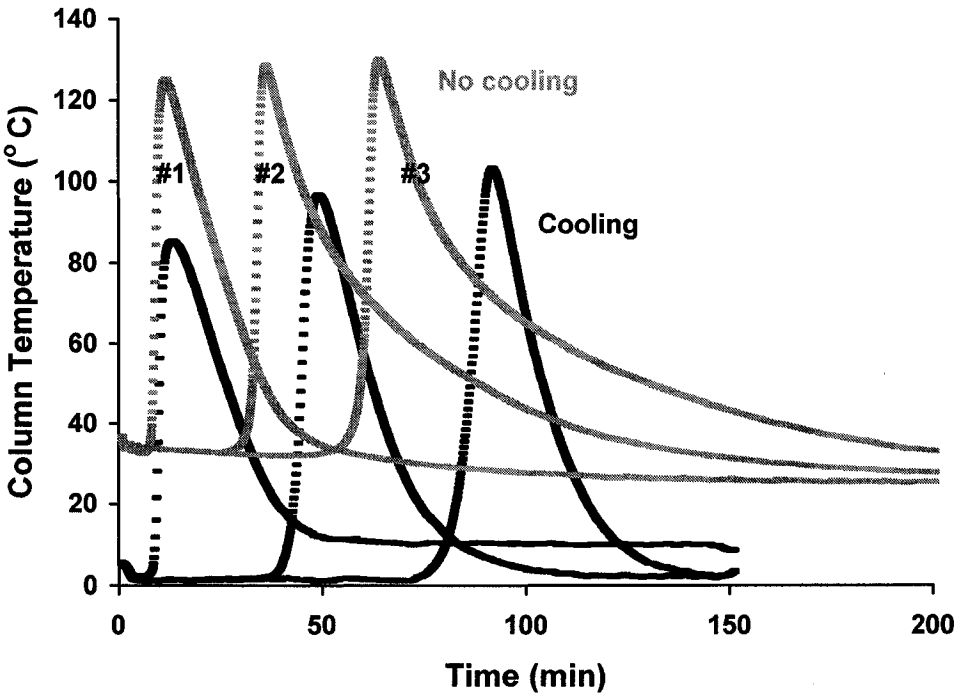

Figure V-7b. Effect of cooling during adsorption cycle on temperature fronts in the column for CO_2 adsorption (10% CO_2 bal. N_2) with 13X adsorbent at 6.44 atm column pressure and 6.6 SL/min feed flow-rate. Dark lines indicate the presence of a coolant at 0°C while grey lines represent experimental runs in the absence of the coolant.

MODELLING

For an experimental feed flow rate of 6.6 SL/min, a constant column pressure of 6.44 atm (absolute) and a feed composition of 10% CO_2 and 90% N_2, samples were obtained at three different positions along the length of the packed column and analysed for their composition by a gas chromatograph (GC) through the multiposition valve. The experimental concentration vs. time plots obtained for different positions in the column are given in Figure V-8 and compared to the same plots from modelling. This figure clearly shows that the experimental data are very well represented by the two-population model at all three

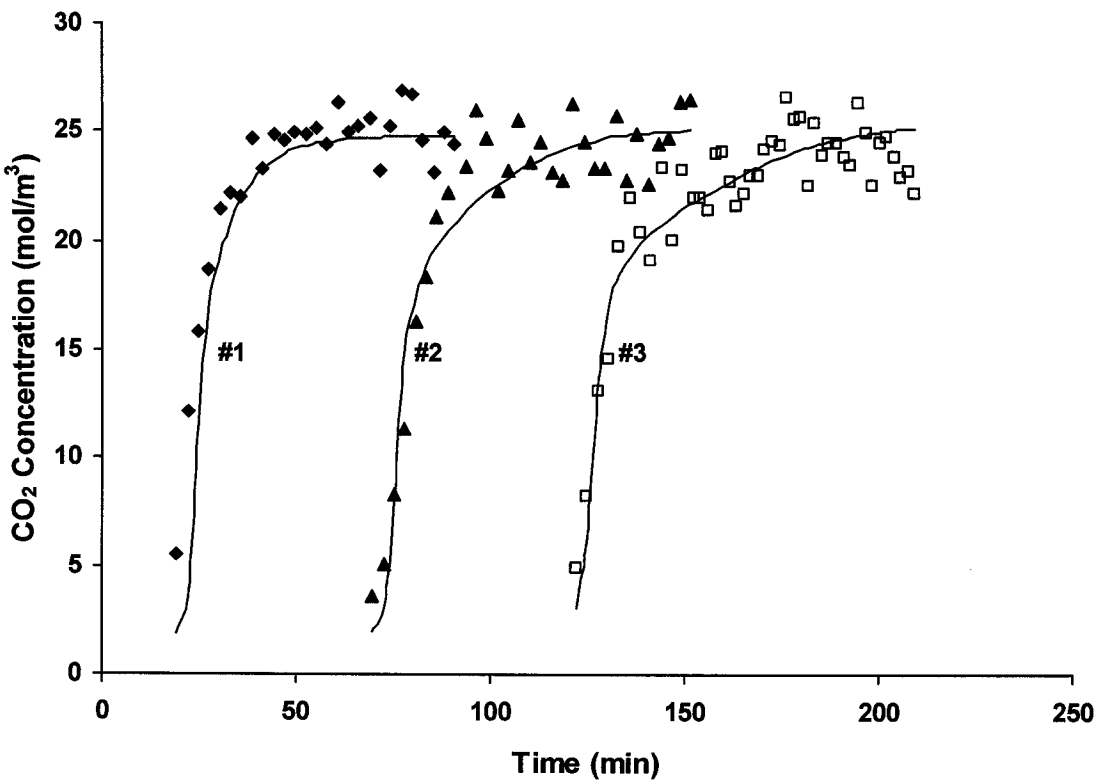

Figure V-8. Concentration profiles at three different locations along the packed adsorption column for CO_2 adsorption from 10% CO_2 bal. N_2 mixture with 13X adsorbent at 6.44 atm column pressure and 6.6 SL/min flow-rate. Points represent experimental data while solid lines represent model fits.

ports for the duration of the experiment. The experimental data display a significant amount of "tailing" when the feed concentration is approached. Tailing is a common observation in breakthrough experiment in liquid and gas systems [35]. Within the porous adsorbent pellets, there exists a distribution of pores ranging from micro-pores to macro-pores. Typically, the macro-pores which are larger in size are the first to fill with the adsorbate feed gas. The micro-pores which are smaller in diameter tend to fill at slower rates. This difference in the rate of diffusion causes a proportion of the adsorbent sites to remain unsaturated while the other proportion of easily accessed sites saturates quicker. Due to the slower rate at which the pores get saturated, also, since most of adsorption uptake happens in the smaller pores, the width of the mass transfer zone is extended causing the "tailing" characteristics observed in many adsorption systems.

The two-population adsorbent pellet model appears to adequately describe the tailing that is present in the experimental data. The proposed model is considerably less complex in terms of computational resources required to solve the system of differential equations and the type of experiments which are required to determine the intra-crystalline diffusivity.

The temperature changes in the column were also obtained by taking temperature measurements using thermocouples at the same three positions along the length of the packed bed as the concentration measurements. For the experimental conditions of 6.6 SL/min feed flow rate, a constant column pressure of 6.44 atm (absolute) and a feed

composition of 10% CO_2 and 90% N_2, the temperature changes measured at three ports in the column along with the predicted model fits are displayed in Figure V-9.

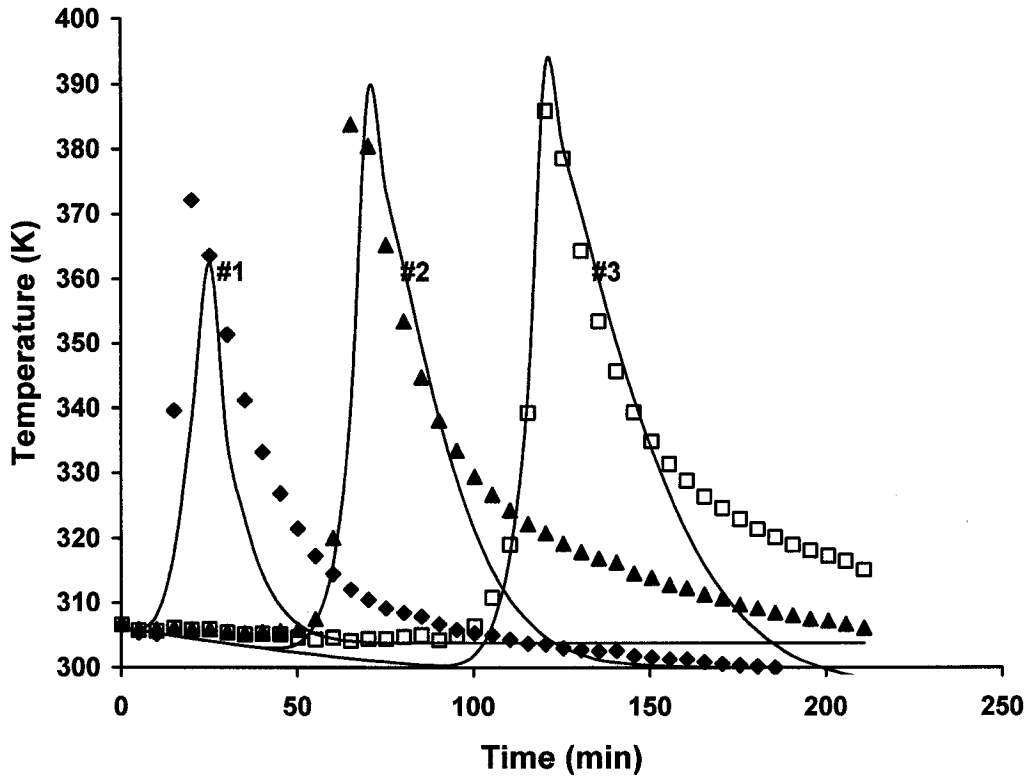

Figure V-9. Temperature profiles at three different locations along the packed adsorption column for CO_2 adsorption (10% CO_2 bal. N_2) with Ceca 13X adsorbent at 6.44 atm column pressure and 6.6 SL/min flow-rate. Points represent experimental data while solid lines represent model fits.

The model predicts the breakthrough time associated with the sharp temperature rise at each port very well. However, the amplitude and the curvature of the temperature changes were not matched exactly. This observed deviation may be caused by use of a constant heat of adsorption for CO_2 in the model and common with gas adsorption systems [9, 15, 28 and 36].

Figure V-10 combines the plots of concentration breakthrough (from Figure V-8) and temperature breakthrough profiles (from Figure V-9) along the length of the column. Temperature and concentration measurements were performed at the same location in the column. Since there were three different ports, measurements were done at three different positions along the length of the column. This figure clearly shows that the temperature front moves slightly ahead of the concentration front, while concentration breakthrough is observed approximately at the peak of the temperature as the feed gas moves from the column inlet to the outlet.

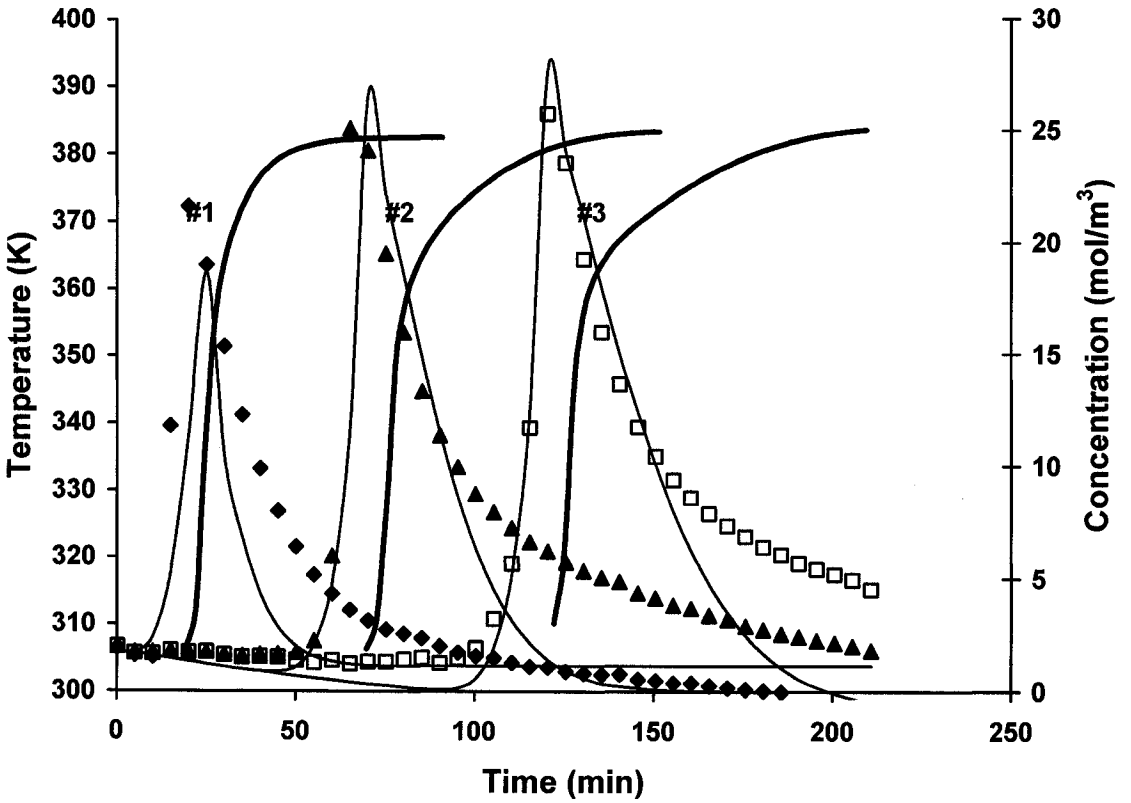

Figure V-10. Temperature and concentration breakthrough at three different locations along the packed adsorption column for CO_2 adsorption from a 10% CO_2 bal. N_2 mixture with 13X adsorbent at 6.44 atm column pressure and 6.6 SL/min flow-rate. Points represent experimental data while solid lines represent model fits.

This observation is very significant since it suggests that concentration breakthrough in a column could be easily detected by using thermocouples only. In the case of gas mixtures that exhibit significant heat effects, thermocouples can be used as an indirect method of predicting the concentration breakthrough. An expensive concentration measurement device would not be needed. Similar behaviour was observed for the experimental run with the feed flow rate of 4 SL/min.

By establishing a model which can predict the mass and heat transfer within the fixed bed, it has been shown that one can depend on the movement of heat transfer zone in this application and use this to infer about the state of the composition within the packed bed adsorber.

CONCLUSIONS

1. Heat effects are significant for a bulk carbon dioxide separation from a gas mixture of 10 % CO_2 (by vol) in N_2 using Ceca 13X adsorbent.
2. The breakthrough time of Ceca 13X adsorbent is independent of the initial bed temperature resulting in a significant economic advantage without affecting the adsorption performance.
3. An earlier breakthrough time was observed for a higher feed flow rate of 6.6 SL/min compared to 4 SL/min.
4. Cooling during the adsorption cycle decreases the mass transfer zone and leads to a longer breakthrough time.

5. By using the two population model, the curvature of the concentration breakthrough curve including the noted tailing was predicted with good accuracy.
6. The prediction of the energy profile was less accurate by the model. However, the point at which the temperature breakthrough occurs is estimated with good accuracy which is the most important factor for industrial applications.
7. Using online measurements of temperature in the column bed, can predict the concentration breakthrough for mixtures and adsorbents exhibiting high heat effects.

ACKNOWLEDGEMENTS

Financial supports received from Ontario Centres of Excellence (OCE), RioTinto Alcan and Air Products & Chemicals Inc., are gratefully acknowledged.

NOMENCLATURE

Symbols

C_B Concentration of gas in the bulk phase ($mol.m^{-3}$)

C_c Concentration of gas at the center of the pellet ($mol.m^{-3}$)

C_{FEED} Concentration of the feed ($mol.m^{-3}$)

C_p Concentration in the mobile phase of the pellet ($mol.m^{-3}$)

C_{pG} Heat capacity of the gas ($J.kmol^{-1}.K^{-1}$)

C_{ps} Heat capacity of the adsorbent ($J.kg^{-1}.K^{-1}$)

C_{pw} Heat capacity of the column wall ($J.kg^{-1}.K^{-1}$)

C_{pX} Concentration in the mobile phase of easily accessed sites of the pellet ($mol.m^{-3}$)

C_{pY} Concentration in the mobile phase of difficulty accessed sites of the pellet ($mol.m^{-3}$)

C_s Concentration of gas on the surface of the pellet ($mol.m^{-3}$)

d_1 Internal diameter of the column (m)

d_2 External diameter of the column (m)

D_i Effective diffusion coefficient of CO_2 in N_2 [i=X (or) Y] ($m^2.s^{-1}$)

D_K Knudsen diffusion coefficient of CO_2 in N_2 ($m^2.s^{-1}$)

D_M Molecular diffusion coefficient of CO_2 in N_2 ($m^2.s^{-1}$)

D_p Particle diameter (m)

D_X Effective diffusion coefficient of the easily accessed sites of the adsorbent ($m^2.s^{-1}$)

D_Y Effective diffusion coefficient of the difficultly accessed sites of adsorbent ($m^2.s^{-1}$)

D_z Axial diffusion coefficient ($m^2.s^{-1}$)

F Function (dimensionless)

g Acceleration due to gravity (9.81 $m.s^{-2}$)

h_f Heat transfer coefficient between gas and wall ($W.m^{-2}.K^{-1}$)

h_o Heat transfer coefficient between wall and surroundings ($W.m^{-2}.K^{-1}$)

j_D Chilton-Colburn j-factor for mass transfer

j_h Chilton-Colburn j-factor for heat transfer

k_f External film mass transfer coefficient ($m.s^{-1}$)

k_g thermal conductivity of gas ($W.m^{-1}.K^{-1}$)

k_{gs} Bulk thermal conductivity of pellet (including pores) ($W.m^{-1}.K^{-1}$)

L Column length (m)

M Molecular weight ($g.mol^{-1}$)

Nu Nusselt number (dimensionless)

P Total pressure (atm)

Pr Prandtl number (dimensionless)

q Adsorbed phase concentration on the solid (adsorbent) ($mol.kg^{-1}$)

q_F Solid phase adsorbate concentration at the feed conditions ($mol.kg^{-1}$)

q_{pl} Solid phase adsorbate concentration at plateau temperature ($mol.kg^{-1}$)

q Equilibrium loading (or) the amount adsorbed (mmol/g)

r Distance in the radial position of the pellet (m)

r^1 Adsorbent pore radius (Å)

r_b Bed radius (m)

r_p Pellet radius (m)

Ra Rayleigh number (dimensionless)

Re Reynolds number (dimensionless)

Sc Schmidt number (dimensionless)

Sh Sherwood number (dimensionless)

t Time (s)

T Temperature (K)

T_a Ambient temperature (K)

T_{bg} Temperature of the bulk gas (K)

T_F Inlet feed temperature (^oC)

T_p Pellet temperature (K)

T_{pl} Plateau temperature (^oC)

T_w Wall temperature (K)

u_G Superficial velocity ($m.s^{-1}$)

y_F Component molar fraction at the feed conditions

z Distance in the axial direction of the column (m)

Greek Letters

β Volumetric thermal expansion coefficient (equal to T^{-1}) (K^{-1})

ΔH Heat of adsorption ($J.mol^{-1}$)

ε_c Bed void (m^3 void.m^{-3} bed)

ε_p Pellet void fraction (m^3 void.m^{-3} pellet)

ν Kinematic viscosity ($m^2\ s^{-1}$)

ρ_B Bulk density of the adsorbent (kg adsorbent.m^{-3} bed)

ρ_G Gas mixture density ($kg.m^{-3}$)

ρ_S Solid density (kg solid.m^{-3} solid)

ρ_w Column wall density (kg .m^{-3})

μ_G Viscosity of gas mixture(Pa.s)

σ Collision diameter of Lennard Jones (Å)

Ω Collision integral (dimensionless)

ψ Prandtl number function (dimensionless)

Abbreviations

CCS Carbon dioxide capture and storage

CPC Concentration pulse Chromatography

CO_2 Carbon dioxide

FacX Weighting factor for the easily accessed sites of the adsorbent

FacY Weighting factor for the difficultly accessed sites of the adsorbent (FacY= 1-FacX)

GC Gas Chromatograph

IEA International Energy Agency

MC Mixing chamber

min Minute

MFC Mass flow controller

NDIR Non dispersive infrared analyser

N_2 Nitrogen

PID Proportional-Integral-Derivative

SL Standard Litres

SSR Sum of square residuals

UHP Ultra high purity

vol Volume

WPFF Working Party on Fossil Fuels

ZET Zero emission technologies

Subscripts

ads Adsorption

g Gas

A Component A

B Component B

AB Binary component AB

REFERENCES

1. International Energy Agency Working Party on Fossil Fuels, "Solutions for the 21st century: Zero emissions technologies for fossil fuels", OECD/IEA, Paris, FR, 1-50, (2002).

2. International Energy Agency Working Party on Fossil Fuels, " CO_2 capture at power stations and other major point sources", OECD/IEA, Paris, FR ,1-12, (2003).

3. Zhang, J., Webley, P.A., and Xiao, P., "Effect of process parameters on power requirements of vacuum swing adsorption technology for CO_2 capture from flue gas", Energy conversion and management, 49, 346-356 (2008).

4. Franchi, R.S., Harlick, P.J.E., and Sayari, A., "Applications of Pore-Expanded Mesoporous Silica. 2. Development of a High-Capacity, Water-Tolerant Adsorbent for CO_2" Ind. Eng. Chem. Res., 44, 8007-8013 (2005).

5. Reynolds, S.P., Mehrotra, A., Ebner, A.D., and Ritter, J.A., "Heavy reflux PSA cycles for CO2 recovery from flue gas: Part I. Performance evaluation", Adsorption, 14, 399-413 (2008)

6. De Witt, J.J., "Recovery of pure CO_2 from flue gases", World Intellectual Property Organization PCT Application WO 02/09849 A2 (2002)

7. Reynolds, S.P., Ebner, A.D., and Ritter, J.A., "New pressure swing adsorption cycles for carbon dioxide sequestration", Adsorption., 11, 531-536 (2005)

8. Li, P and Tezel, F.H., "Adsorption Separation of N_2, O_2, CO_2 and CH_4 Gases by β-Zeolite", Microporous & Mesoporous Materials, **98**, 94-101 (2007).

9. Kim, M.B., Bae. Y.S., Choi, D.K., and Lee, C.H., "Kinetic separation of landfill gas by a two-bed pressure swing adsorption process packed with carbon molecular sieve: Non isothermal operation, Ind.Eng. Chem. Res., 45, 5050-5058, (2006).

10. Park J.H. and R. T. Yang, "A Simple Criterion for Adsorbent Selection for Gas Separation by PSA Processes," Ind. Eng. Chem. Res., 44, 1914 (2005)

11. Cavenati, S., Grande, C.A., and Rodrigues, A.E., "Adsorption Equilibrium of Methane, Carbon Dioxide, and Nitrogen on Zeolite 13X at High Pressures", Journal of Chemical and Engineering Data, vol. 49, p. 1095-1101 (2004).

12. Clausse, M., Bonjour, J., and Meunier, F., "Adsorption of gas mixtures in TSA adsorbers under various heat removal conditions", Chemical Engineering Science, 59, 3657-3670 (2004).

13. Keefer, B. G., J. A. Sawada, E. P. Johannes, S. Roy and M. J. Brown, "Systems and Processes for Providing Hydrogen to Fuel Cells", World Intellectual Property Organization 02/35632 (2002).

14. Ma, X., L. Sun and C. Song, "A New Approach to Deep Desulfurization of Gasoline, Diesel Fuel and Jet Fuel by Selective Adsorption for Ultra-Clean Fuels and for Fuel Cell Applications", Catalysis Today 77, 107-116 (2002)

15. Chue, K. T., J. N. Kim, Y. J. Yoo, S. H. Cho and R. T. Yang, "Comparison of Activated Carbon and Zeolite 13X for CO_2 recovery from flue gas by Pressure Swing Adsorption", Industrial and Engineering Chemistry Research 34, 591-598 (1995).

16. Ruthven, M., Farooq, S., Knaebel, K., "Pressure swing adsorption", John Wiley and Sons Inc., pp.5-93, (1994).

17. Ruthven, D. M., "Principles of Adsorption and Adsorption Processes", John Wiley and Sons, Inc., New York, NY, pp. 1-433, (1984).

18. Harlick, P.J.E and F.H. Tezel, "An experimental adsorbent screening study for carbon dioxide removal from nitrogen" Microporous Mesoporous Mater. 76, 71-79 (2004).

19. Yon, C.M., and Sherman, J. D., "Adsorption", Kirk Othmer Encyclopaedia of Chemical Technology, John Wiley and Sons (2003)

20. Birbara, P.J., Filburn, T.P., H. Michels and T.A. Nalette, "Sorbent system and method for adsorbing carbon dioxide from the atmosphere of a closed habitable environment", U.S. Patent 6364938 (2002).

21. Kanazirev, V.I., and D.J. Latus, "Composite adsorbents for Air Purifiction", U.S. Patent 6638340 (2003).

22. Xu, X., Song, C., Andressen, J.M., B.G. Miller and A. W. Scaroni, "Preparation and characterization of novel CO_2 molecular basket adsorbents based on polymer modified Mesoporous molecular sieve MCM-41", Microporous Mesoporous Mater. 62, 29-45 (2003).

23. Mulgundmath, V.P., Tezel, F.H, Saatcioglu, T and Golden, T.C., "Adsorption separation of CO_2/N_2 and CO_2/CH_4 by 13X zeolite", Canadian Journal of Chemical engineering (to be submitted).

24. Warmuzinski, K and Tanczyk, M., "Multi component pressure swing adsorption. Part I. Modelling of large scale PSA installations", Chemical Engineering and Processing, 36, 89-99 (1997).

25. Chou, C.T., and Chen, C.Y., "Carbon dioxide recovery by vacuum swing adsorption", Separation and Purification Technology, 39, 51-65 (2004).

26. Wakao, N., Funazkri, T., "Effect of Fluid Dispersion Coefficients on Particle-to-Fluid Mass Transfer Coefficients in Packed Beds." Chem. Eng. Sci. 33, 1375-1384 (1978).

27. Welty, J.R., Wicks, C.E., Wilson, R.E., and Rorrer, G., "Fundamentals of Momentum, Heat and Mass Transfer", John Wiley and Sons, New York, (2000).

28. Cavenati, S., Grande, C.A., and Rodrigues, A.E., "Layered Pressure Swing Adsorption for Methane Recovery from $CH_4/CO_2/N_2$ Streams", Adsorption, vol. 11, p. 549-554 (2005).

29. A.F. Mills, Heat Transfer, Second edition, Prentice Hall, Inc., NJ, USA.

30. Chilton, T. H. and Colburn, A. P., "Mass Transfer (Absorption) Coefficients Prediction from Data on Heat Transfer and Fluid Friction", Ind. Eng. Chem., 26, 1183-1187 (1934).

31. Churchill, S. W., and Chu, H.H.S., "Correlating equations for laminar and turbulent free convection from a vertical plate" Int. J. Heat Mass Transfer, 18, 1323-1329 (1975).

32. Grande, C.A., and Rodrigues, A.E., "Electric Swing Adsorption for CO_2 removal from flue gases", International Journal of Greenhouse gas control, 2, 194-202 (2008).

33. Delgado.J.A., Uguina, M.A., Sotela, J.L., and Ruiz, B., "Fixed Bed adsorption of carbon dioxide-helium, nitrogen-helium and carbon dioxide-nitrogen mixtures onto silicalite pellets", Separation and Purification Technology, 49, 91-100 (2006).

34. Basmadjian, D., "On the possibility of omitting the cooling step in thermal gas adsorption cycles", The Canadian Journal of Chemical Engineering, 53, 234-238 (1975).

35. Jones, R.A, Tezel, F.H. and Thibault, J., "Simulation and validation of ethanol removal from water in an adsorption packed bed: Isotherm and mass transfer parameter determination in batch studies", Canadian Journal of Chemical Engineering (submitted).

36. Kim, J., Chue, K., Kim, K., Cho, S., Kim, J., "Non-isothermal adsorption of nitrogen-carbon dioxide mixture in a fixed bed of zeolite-X, J. Chem. Eng. Jpn., 27 (1), 45-51 (1994).

CHAPTER VI

PARAMETRIC STUDY OF CARBON DIOXIDE RECOVERY FROM FLUE GAS IN A TPSA SYSTEM

Mulgundmath, V.P and Tezel, F.H

Department of Chemical & Biological Engineering, University of Ottawa, 161, Louis Pasteur, Ottawa. K1N 6N5. Canada

Submitted to Adsorption Journal.

Presented at the Fundamentals of Adsorption (FOA9) conference, May 20-25, 2007, Sicily-Italy

ABSTRACT

Power stations and industrial processes burning fossil fuels account for the largest percentage of carbon dioxide emissions. Carbon capture and sequestration has received enormous global attention to reduce the carbon footprint and combat global warming. Adsorption has become an alternative technique to the conventional absorption process for capturing carbon dioxide due to its low operating and capital costs.

In this study, Pressure Swing Adsorption (PSA) process has been compared with Thermal Pressure Swing Adsorption (TPSA) process for CO_2 recovery from a flue gas composition of 10 % CO_2 (by vol) in N_2 using Ceca 13X adsorbent. A factorial design set of experiments was performed to optimise the carbon dioxide recovery and study the effects and interaction of four control parameters namely, purge/feed flow ratio, purge time, purge gas temperature and adsorption column pressure.

Results indicated that better regeneration conditions used in a TPSA cycle was essential over a PSA cycle for regaining maximum adsorption capacity of the used Ceca 13X adsorbent. It was found that Purge time had a significant effect on the CO_2 recovery followed by Column pressure, purge/feed flow ratio and purge temperature. A Minitab® statistical software was used to analyse the data. It was found that the test of significance for lack of fit showed the fitted model to be an adequate representation of the experimental data. The results showed that to maximise the CO_2 recovery, highest values of the control parameters have to be used.

INTRODUCTION

Accumulation of greenhouse gases (GHG's) in the atmosphere due to carbon dioxide (CO_2) emissions is a global environmental issue. The most important sources of CO_2 emissions are fossil fuel fired plants for electricity generation [1]. The solution prevails in point source reduction and recovery in order to meet the present and future constraints on the allowable emissions of CO_2. Several technologies are being developed to capture CO_2 in post combustion, pre-combustion or oxyfuel combustion processes [2]. However, these novel technologies come with economic penalties which require retrofits for existing power plants.

The most common approach appears to be with liquid phase absorption. However, this process has been more widely adopted by large scale CO_2 emitters which are economically feasible leaving the small scale CO_2 emitters with little economic viable options. Recently, adsorption processes have become an alternative to the conventional absorption process for low to medium CO_2 emitters. Most of the research in adsorption is focussed on pressure/vacuum swing adsorption for separating CO_2 (15 % by vol) from flue gas in power stations that use coal as fuel [3-17]. Kim et al. [18] reported that PSA process was uneconomical for the removal of CO_2 in a low concentration range (5-15 vol %) from power stations that use oil or natural gas as fuels. For this CO_2 concentration range, higher economic penalties may be needed to attain lower adsorbent regeneration pressures as in a Vacuum Pressure Swing Adsorption (VPSA) system. Thermal Swing Adsorption (TSA) process too is energy intensive because of the need to supply heat to the regenerating gas. Thermal Pressure Swing Adsorption (TPSA) system could be a

promising option if waste heat which is readily available in power stations could be used to regenerate the adsorbents to offset the large amount of regenerative purge gas needed and thus reduce the power consumption for vacuum pumps [15]. TPSA set up works very closely to TSA, by supplying external heat through inline gas heaters or heating tapes to the purge gas under a low pressure. However, the amount of external heat required will be less since the warmer gas from the column product end can be used as a purge gas to desorb all the impurities from the column bed. By suitable adjustment of the operating conditions, it is possible to utilise only a fraction of the heat of desorption being supplied to the purge gas [19]. The addition of a temperature swing increases the regenerative capacity and reduces the power consumption for the vacuum pump. Another interesting alternative could be to compress the feed equivalent to the power consumed by the vacuum pump, perform adsorption at higher pressures and regenerate the adsorbent with waste heat and atmospheric pressure. Wright et al. [19] reports that a significant saving of thermal energy in the order of 20-60% could be realised without requiring a significant decrease in cycle time.

The most widely used adsorbents for CO_2 removal in flue gas applications are zeolite13X and activated carbon [20-23]. Kikkinides and Yang [17] reported that CO_2 adsorption on zeolites is too strong, leading to a higher heat of adsorption which makes desorption difficult under VSA cycles. Chue et al. [3] reported that zeolite 13X performed better than activated carbon in a PSA/VSA CO_2 capture process.

Previously, single component gas isotherms of CO_2 and N_2 on different adsorbents indicated that Ceca 13X was the preferred adsorbent for CO_2 removal [24]. Therefore, in this study, this zeolite was chosen as the suitable adsorbent for the lab scale TPSA system.

EXPERIMENTAL SECTION

A schematic diagram of the Thermal Pressure Swing Adsorption (TPSA) system designed and built in-house is shown in Fig. VI-1. For the experiments in this study, one column was used to analyse the breakthrough concentration and temperature profiles. Zeolite Ceca 13X supplied by CECA, from France was used to pack the adsorbent column (Length: 61 cm, Diameter: 4.4 cm). Uniform distribution of the Ceca 13X pellets inside the column was ensured by continuous tapping of the sides of the column. The adsorbent was regenerated in Fisher Scientific electric oven at 200 ^{o}C with UHP N_2 purge gas in order to remove any impurities present followed by cooling it overnight. The flue gas composition (10% CO_2 by vol. in N_2) was prepared in the gas mixing chamber using two pre-calibrated CO_2 and N_2 mass flow controllers (M1 and M2) which were connected to CO_2 and N_2 gas cylinders. A combined flow rate of 7 SL/min was prepared and used for all the experimental runs.

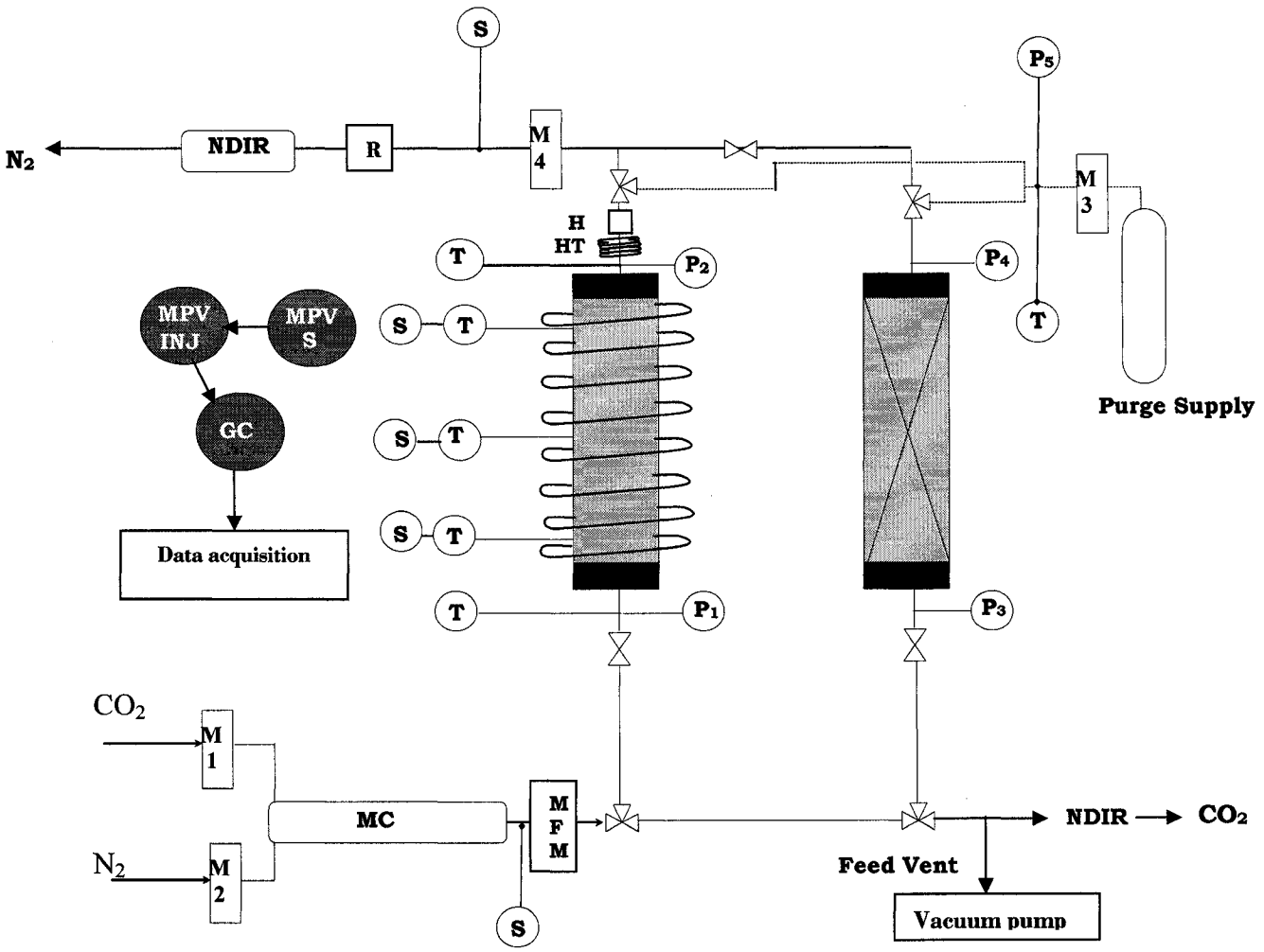

GC- Gas Chromatograph ; H- Heater ; HT- Electrical heating tape ; INJ - Injection valve ; NDIR- Non Dispersive Infrared analyser ;M- Mass flow controller ; MC- Mixing chamber ; MFM- Mass flow meter ; MPV- Multiposition valve ; P - Pressure transducer ; R- Rotameter ; S- Sample port ; T- Thermocouple.

Figure VI- 1.Schematic diagram of the two bed TPSA system

Analysis of the breakthrough concentration and temperature profiles were obtained at three sample ports (at positions 10.2 cm, 30.5 cm and 50.7 cm from column inlet) at column centre axis. These sample ports were connected to a VALCO model SD 32-port micro-electric actuated multiposition valve. This multiposition valve had 32 ports (16 inlet and

16 outlet ports) and had the capability of connecting to 16 different sample ports. A 6-port micro-electric actuated injector valve housed the sample gas cell (500 μL) that connected the 32-port micro-electric actuated multiposition valve to a Varian 3400 Series Gas Chromatograph (GC). Temperature measurements were done using Omega type-K exposed tip thermocouples while CO_2 concentration measurements at the sample ports were obtained by using a Varian 3400 Series Gas Chromatograph (GC). A Non Dispersive Infrared Analyser (NDIR) was also used for continuous CO_2 gas detection at the adsorber column exit. A data acquisition system in conjunction with LABVIEW software obtained from National Instruments Inc. was used to monitor and record the pressure, temperature, CO_2 concentration and flow rate data continuously in an MS-Excel worksheet. The detailed experimental procedure has been explained in the earlier paper [24].

The cycle steps used in the Thermal Pressure Swing Adsorption (TPSA) process were: pressurisation, adsorption at a constant high pressure, depressurisation and heated purge gas flow under low pressure as shown in Figure VI-2. Before the beginning of each experimental run, the regenerated column was pressurised to the desired adsorption pressure using UHP N_2. When the desired pressure was attained, the flue gas composition (10% CO_2 by vol. in N_2) was prepared in the gas mixing chamber and introduced at the column entrance. Temperature and CO_2 concentrations were analysed as a function of time at three different ports along the length of the column.

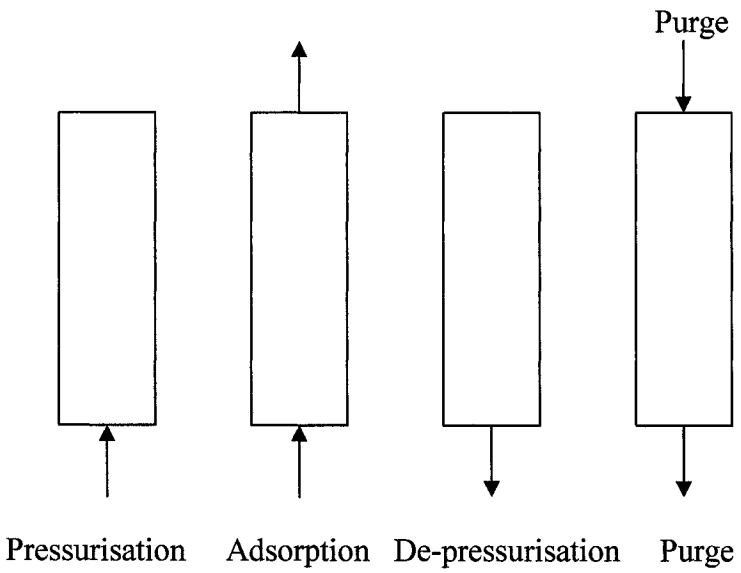

Figure VI- 2. Schematic diagram of the step cycles in the TPSA system

When the gas concentration at the column exit reached the breakthrough CO_2 concentration in air (400 ppm –[25]), the feed flow was stopped. At that point, the column was switched from the adsorption mode to counter current depressurisation mode to recover pure CO_2. The gas in the column was allowed to bleed at constant flow-rate to atmospheric pressure slowly through a calibrated Rotameter (R) while the exit gas concentration was measured by a Non Dispersive Infrared (NDIR) analyser. These measured flow rate and concentration data were used in Equation (1) to calculate the CO_2 recovery. When the flow neared zero, the cycle was switched to counter-current purge mode. A constant purge pressure of 2 atm (absolute) was maintained to obtain the GC readings. Regeneration was carried out by a heated purge gas inside the insulated column. An inline gas heater, a thermostat controlled heating tape at the purge entrance of the column contributed to attaining higher regeneration temperatures (80- 105°C) within a short interval of time. When the desired cycle time was

reached, the flow of heated purge gas was stopped. The recorded Thermal Pressure Swing Adsorption (TPSA) cycle data of flow rate, column pressure, temperatures and CO_2 concentration data were used to calculate the amount of carbon dioxide recovered during this cycle.

Complete regeneration of the adsorbent between different experimental runs was achieved on-site by a combination of high temperature (by using a thermostat controlled 50:50 (vol/vol) ethylene glycol water mixture at 95 ^{o}C circulating inside copper coils around the column and a heated purge gas to achieve a temperature of 120 ^{o}C in the column) and high vacuum (using Edwards dual stage high vacuum pump). During the regeneration cycle, UHP N_2 gas flowed through the column. The completion of this step was checked by stopping the vacuum and analysing the desorbed gas from the column for CO_2 concentration using the NDIR analyser. Complete regeneration of the adsorbent was achieved when the desorbed gas contained no traces of CO_2. The column was then allowed to cool under UHP N_2 purge followed by isolating it from the rest of the setup by closing the column inlet and the outlet valves. Prior to the next experimental run, the column was re-pressurised to the desired pressure and the TPSA cycle steps were repeated.

For each experimental run, the recorded data was analysed to determine the amount of CO_2 recovered in a TPSA cycle, which is given by Equation (1):

$$CO_2 RECOVERY = \frac{(Q_{depress} \times X_{CO2\,depress} \times Time_{depress}) + (Q_{purge} \times X_{CO2\,purge} \times Time_{purge})}{(Q_{ads} \times X_{CO2\,ads} \times Time_{ads})} \quad .....(1)$$

where Q is the flow rate of gas in a cycle step (L/min) and assumed to be constant, X_{CO2ads} is the composition of CO_2 during the adsorption step (vol %) which is equal to the feed concentration. $X_{CO2\ depress}$ and $X_{CO2\ purge}$ are the time averaged compositions of CO_2 during the depressurisation and purge steps (vol %), respectively. Time is the time required to complete a cycle step (min) whereas the subscripts depress, purge and ads refer to depressurisation step, purge step and adsorption step, respectively.

FACTORIAL DESIGN

A 2^k factorial design experiment was conducted to optimise the recovery for carbon dioxide from flue gas composition (10 % CO_2 by vol. in N_2) in a TPSA cycle. The four control parameters as operating variables chosen for this study were purge/feed flow ratio, purge time, purge gas temperature and adsorption column pressure. A two level factorial (high and low) were considered for these control parameters in the experiments. Table VI-1 shows all the sixteen experimental runs that correspond to the chosen control parameters.

Table VI- 1. The 2^4 design for the TPSA experiment.

Run	Purge/Feed	Purge time	Purge gas temperature	Column pressure
1	-1	-1	-1	-1
2	1	-1	-1	-1
3	-1	1	-1	-1
4	1	1	-1	-1
5	-1	-1	1	-1
6	1	-1	1	-1
7	-1	1	1	-1
8	1	1	1	-1
9	-1	-1	-1	1
10	1	-1	-1	1
11	-1	1	-1	1
12	1	1	-1	1
13	-1	-1	1	1
14	1	-1	1	1
15	-1	1	1	1
16	1	1	1	1

This factorial design has four main effect interactions, six two-factor interactions, four three-factor interactions and one four-factor interaction. The CO_2 recovery determined by these runs was analysed for process optimisation. Table VI-2 details the two level factorial (high and low) range used for the control parameters.

Table VI- 2. The 2-level factorial range for the control parameters.

	Purge/Feed	Purge time (hr)	Purge gas temperature (^oC)	Column pressure (atm)
Low level	0.75	1	80	5.08
Centre point	0.875	1.25	92.5	5.76
High level	1	1.5	105	6.44

Along with the above sixteen experimental runs, four random runs corresponding to centre point replicates (purge/feed = 0.875, purge time = 1.25 hr, purge gas temperature=92.5 ^oC and column pressure = 5.76 atm) were performed to fit the data for statistical analysis.

RESULTS AND DISCUSSIONS

PSA CYCLE

Initial concentration breakthrough experiments at 7 SL/min feed flow rate were performed for CO_2 (10% by vol.) and N_2 (90% by vol.) feed gas mixture to see if high temperature was necessary for complete regeneration of the adsorbent. This Pressure Swing Adsorption (PSA) cycle was followed without the addition of heat during the purge and it consisted of pressurising the column with UHP N_2 and carrying out the adsorption by introducing the feed mixture at desired column pressure (6.44 atm). When the breakthrough CO_2 concentration of 400 ppm was reached, the column was switched to counter current depressurisation mode in order to recover pure CO_2. The quantity and concentration of CO_2 recovered in the depressurisation mode was determined using a Rotameter at the column exit and a Non Dispersive Infrared (NDIR) analyser between the

operating pressures of 6.44 atm to 1 atm (absolute), respectively. When the flow rate of the depressurised gas neared zero, the column was re-pressurised to the adsorption pressure using UHP N_2 and the cycle was repeated. However, the adsorbent capacity recovered during this cycle amounted to only 15% of the total capacity of Ceca 13X adsorbent. This indicated that lowering the pressure alone during regeneration was not sufficient to completely regenerate the Ceca 13X adsorbent. This observation suggested that a combination of high temperature and lower pressure during the regeneration could be a viable option to recover maximum capacity of the adsorbent. Hence, a TPSA cycle which also exhibits a larger working capacity when compared to a PSA cycle alone was chosen to optimise the CO_2 recovery in this study.

TPSA CYCLE

Breakthrough experiments were performed according to the procedure described in the experimental section and CO_2 recovery was determined for each of the 16 TPSA cycle runs shown in Table VI-1, plus the 4 random runs corresponding to center point replicates. A feed flow rate of 7 SL/min (10% CO_2 by vol in N_2) was maintained for all the experimental runs. Table VI-3 shows results obtained for % CO_2 recovery for each run along with the values of the control parameters while Figures VI-3 to VI-6 explain the effect of control parameters on the CO_2 recovery in the form of 3D-Surface plots.

Table VI- 3. CO_2 recovery for the TPSA factorial design experiments (Highlighted numbers indicate center point replicates)

Purge/Feed	Purge Time (hr)	Purge gas Temperature (°C)	Column pressure (atm)	% CO_2 recovery
0.75	1.5	105	5.08	56.66
0.75	1.5	80	5.08	55.42
1	1.5	105	5.08	57.27
0.75	1.5	80	6.44	55.83
1	1.5	80	6.44	59.79
0.75	1.5	105	6.44	57.05
1	1.5	105	6.44	60.04
0.75	1	80	5.08	47.47
1	1	80	5.08	52.78
1	1.5	80	5.08	55.55
1	1	105	5.08	52.92
0.75	1	80	6.44	49.72
1	1	80	6.44	57.89
0.875	**1.25**	**92.5**	**5.76**	**55.18**
0.75	1	105	6.44	56.44
0.875	**1.25**	**92.5**	**5.76**	**55.45**
1	1	105	6.44	58.84
0.875	**1.25**	**92.5**	**5.76**	**55.95**
0.75	1	105	5.08	51.4
0.875	**1.25**	**92.5**	**5.76**	**55.81**

It was observed that CO_2 recovery ranged from 47.47% to 60.04%, for the chosen range of control parameters. The lowest recovery (47.47%) was obtained for the lowest range of control parameters (purge/feed = 0.75, purge time = 1hr, purge temperature = 80 °C and column pressure = 5.08 atm) while the highest recovery (60.04%) was obtained for

the highest range of the control parameters (purge/feed = 1, purge time = 1.5 hr, purge temperature = 105°C and column pressure = 6.44 atm). The control parameters at the highest range contributed to better regeneration conditions and higher capacity, and therefore more CO_2 recovery. Higher CO_2 recoveries were observed at higher adsorption column pressures. The remaining factorial design experimental runs were performed to study the effect of interactions between the control parameters. The four random center-point replicate runs indicated a similar CO_2 recovery (55.18% to 55.95%) which was within acceptable experimental error.

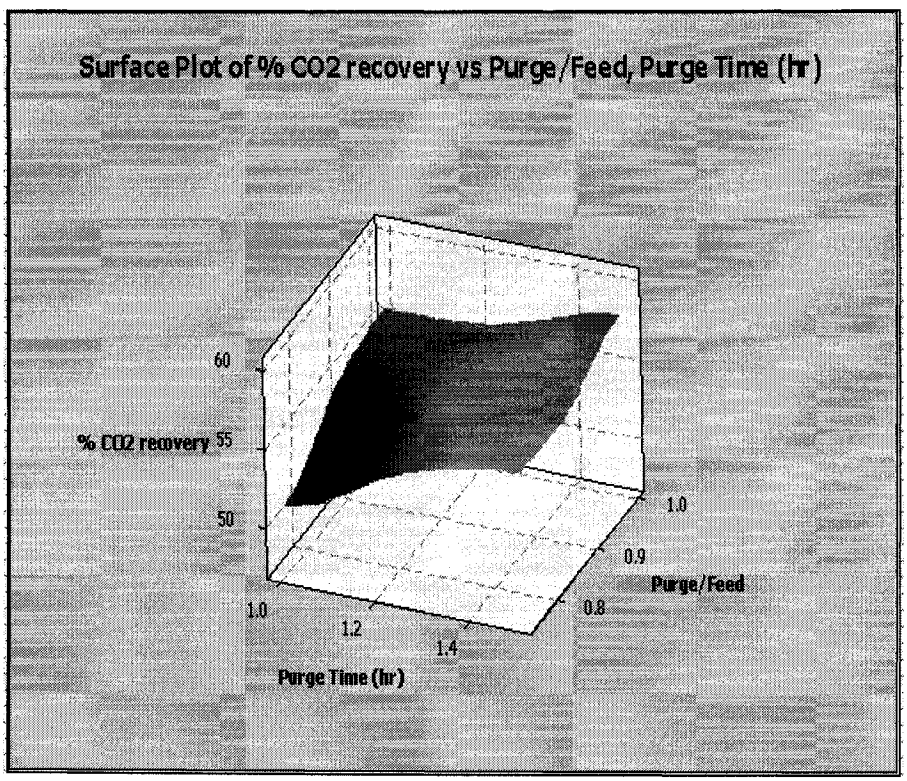

Figure VI- 3. Effect of Purge time and Purge/Feed on the CO_2 recovery.

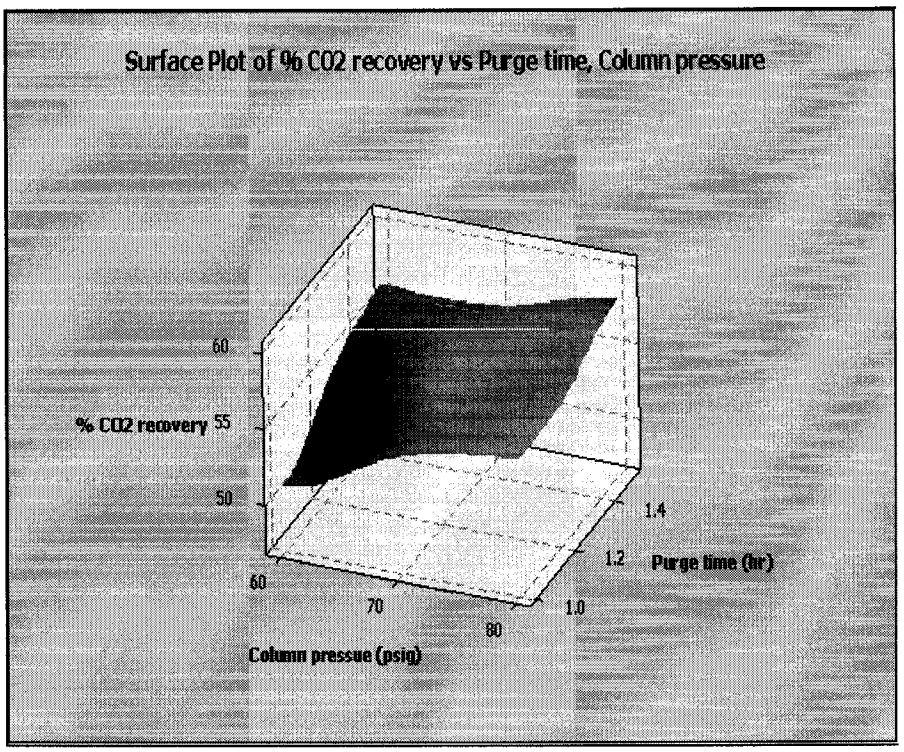

Figure VI- 4. Effect of Purge time and Column pressure on the CO_2 recovery.

Figure VI- 5.

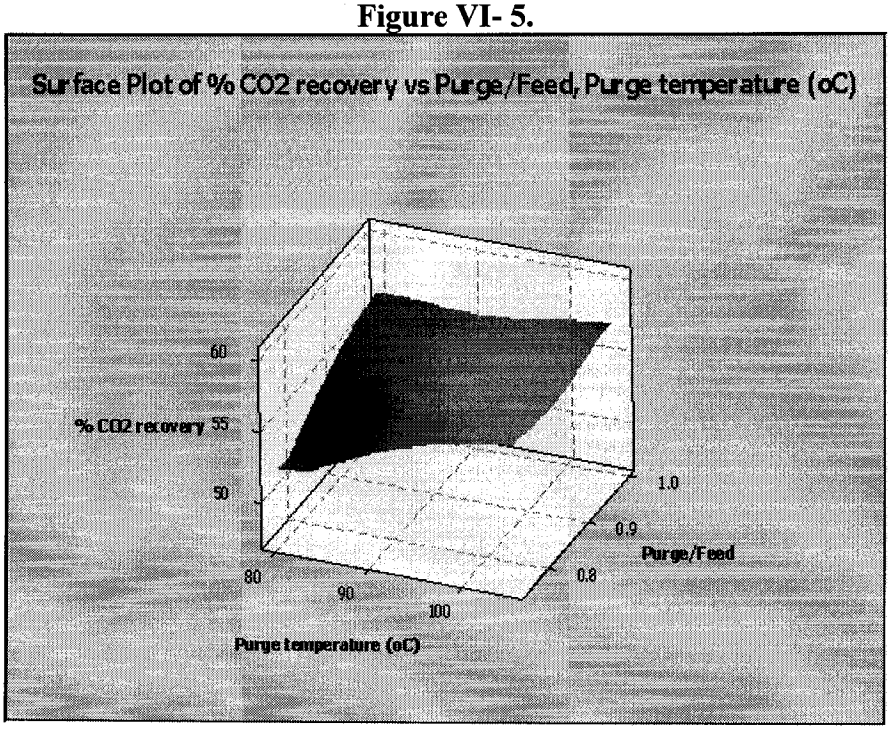

Figure VI- 5. Effect of Purge temperature and Purge/Feed on the CO_2 recovery.

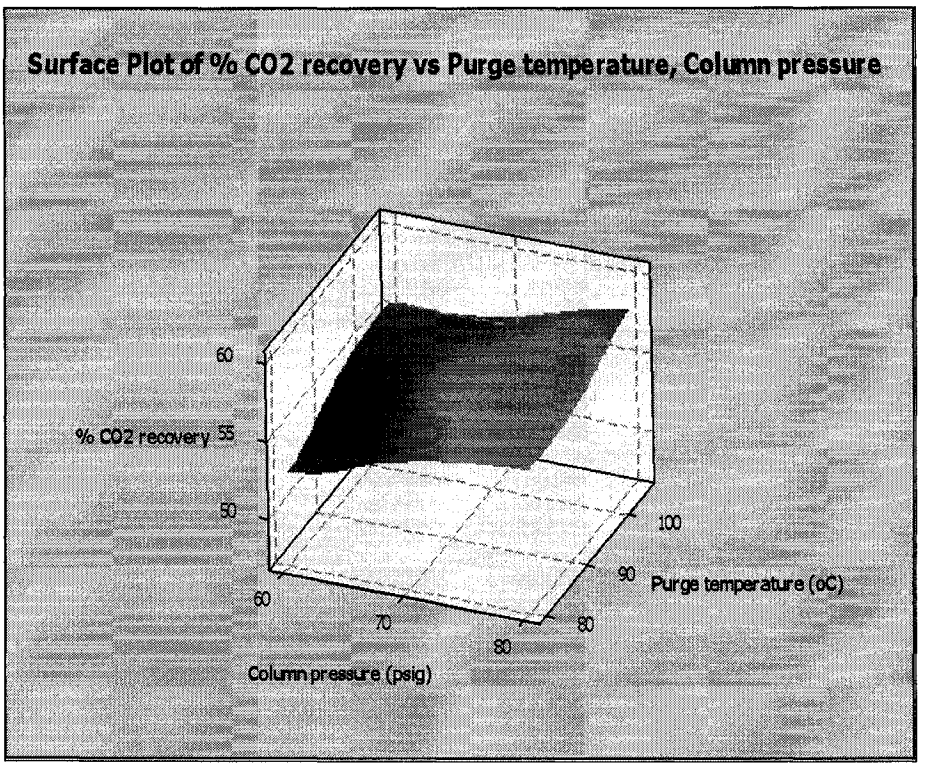

Figure VI- 6. Effect of Purge temperature and Column pressure on the CO_2 recovery.

OPTIMISATION

Minitab® statistical software was used to analyse the factorial design experimental data. This software provides tools to build a factorial design set of experiments, interpret and analyse the experimental data. Based on the experimental results, this software has the ability to analyse and estimate the main effects, as well as the interactions between parameters affecting the CO_2 recovery. From these estimated effects, the software determines the parameter coefficients as well as the analysis of variance for CO_2 recovery. These results help to build a model that is representative of the experimental results. Figure VI-7 (Main Effects Plot for Recovery) shows the statistically significant contributors "main effects" to the response mean. These plots compare the relative

magnitude of the main effect parameters. Analysis shows that all four factors (purge time, column pressure, purge/feed flow ratio and purge temperature) have a significant effect on the "control" (CO_2 recovery in this case) since the lines are not parallel to the reference line (which represents the overall mean). The plots indicate that the CO_2 recovery increases when these control parameters move from the low level to the high level. "Purge time" control factor has the highest magnitude of the main effect (CO_2 recovery), since it had the highest slope, followed by column pressure, purge/feed flow ratio and purge temperature.

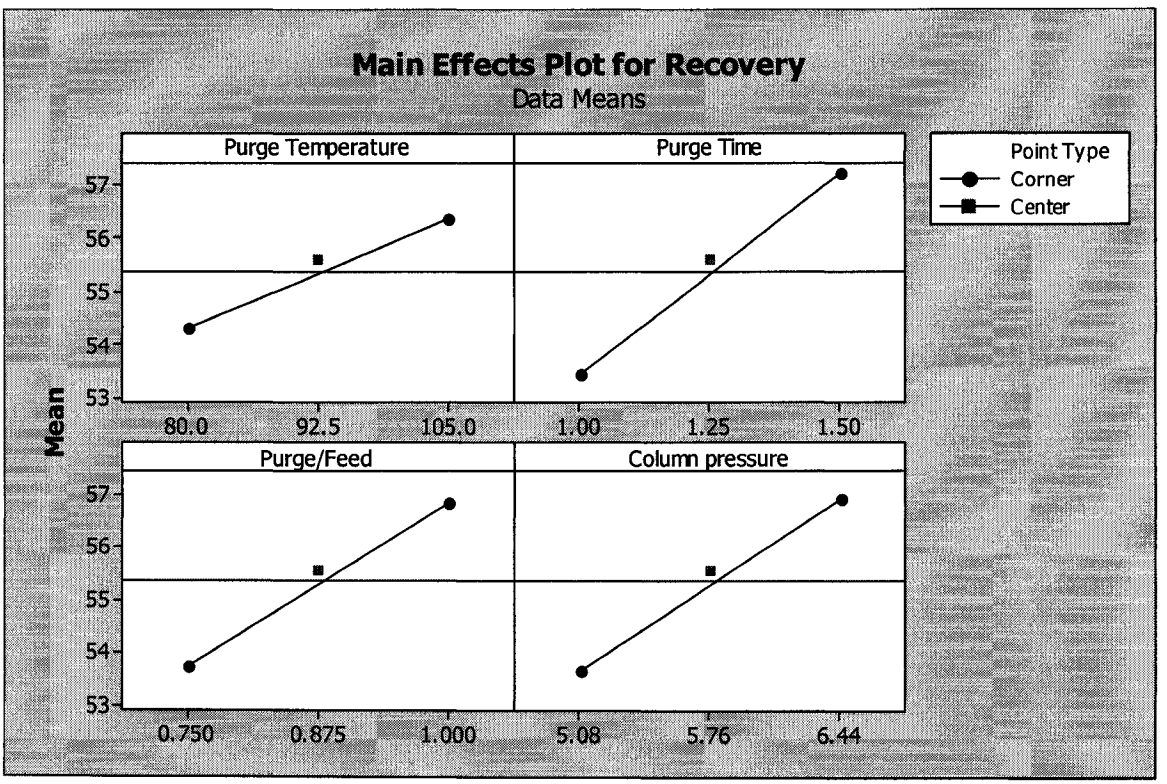

Figure VI- 7. Main effects plot for CO_2 recovery.

One common objective in a process investigation is the development of an adequate mathematical model for the behaviour of a process within a defined operating region. Another common objective is the improvement of process performance, perhaps leading to the location of optimum operating conditions. In this study, four control factors

(purge/feed ratio, purge time, purge gas temperature and adsorption column pressure) were selected to study their effects on the amount of CO_2 recovery in the defined operating region.

Figure VI-8 represents the interaction plots for CO_2 recovery based on the effects of each control factor studied. Perfect parallel lines in these plots indicate no interaction between parameters considered. A greater departure from parallel lines indicates a higher degree of interaction between the control factors. From the plot in Figure VI-8, it was observed that purge temperature and column pressure plots were close to parallel indicating a smaller degree of interaction between these parameters when compared to the remaining parameters considered.

Figure VI-9 gives the normal plot of the standardised effects. In this plot, points that are further from the line indicate important effects. It can be seen from this figure that the most significant factor effects in descending order are the purge time (B), column pressure (D), purge/feed ratio (C), and purge temperature (A) for a maximum acceptable level of risk for rejecting a true null hypothesis, α=0.05 or 95% confidence interval. The insignificant effects tend to be smaller and are centred on zero. In addition, there are two-factor and three-factor interaction effects that are also significant to note. Of most significance is the two-factor purge/feed - column pressure (denoted as CD) followed by the three-factor purge temperature - purge time - purge/feed (denoted ABC).

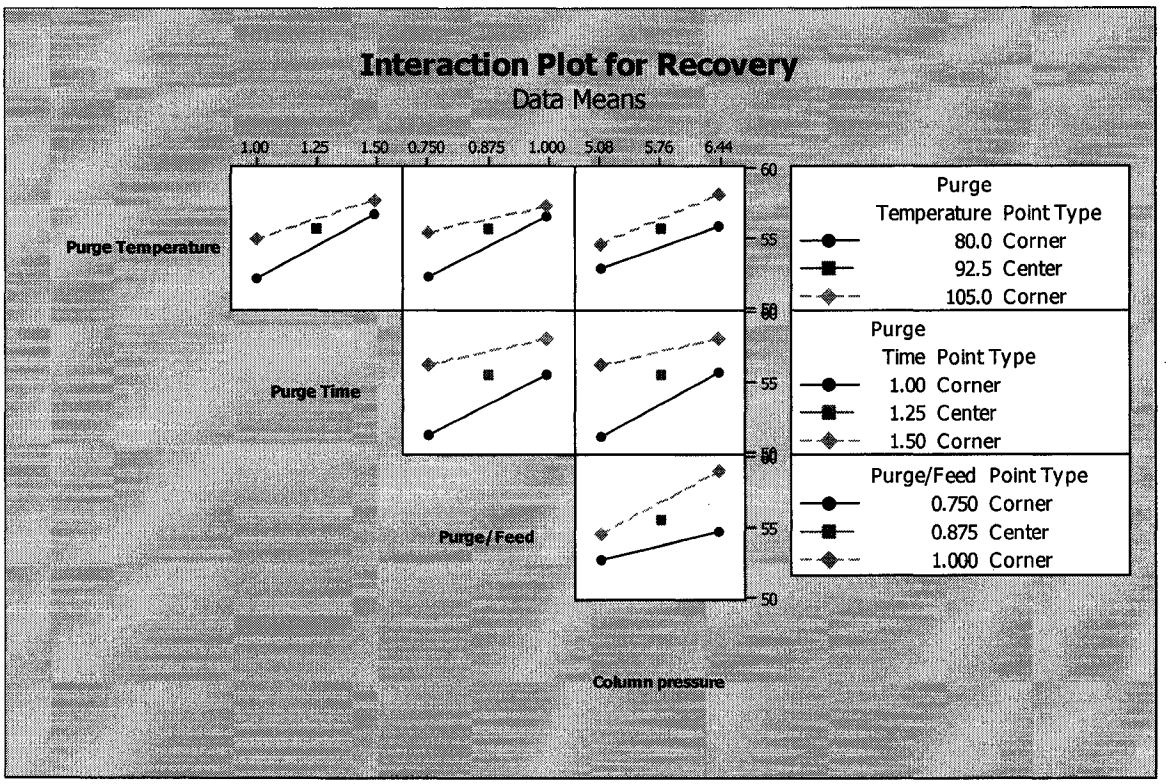

Figure VI- 8. Interactions plot for CO_2 recovery.

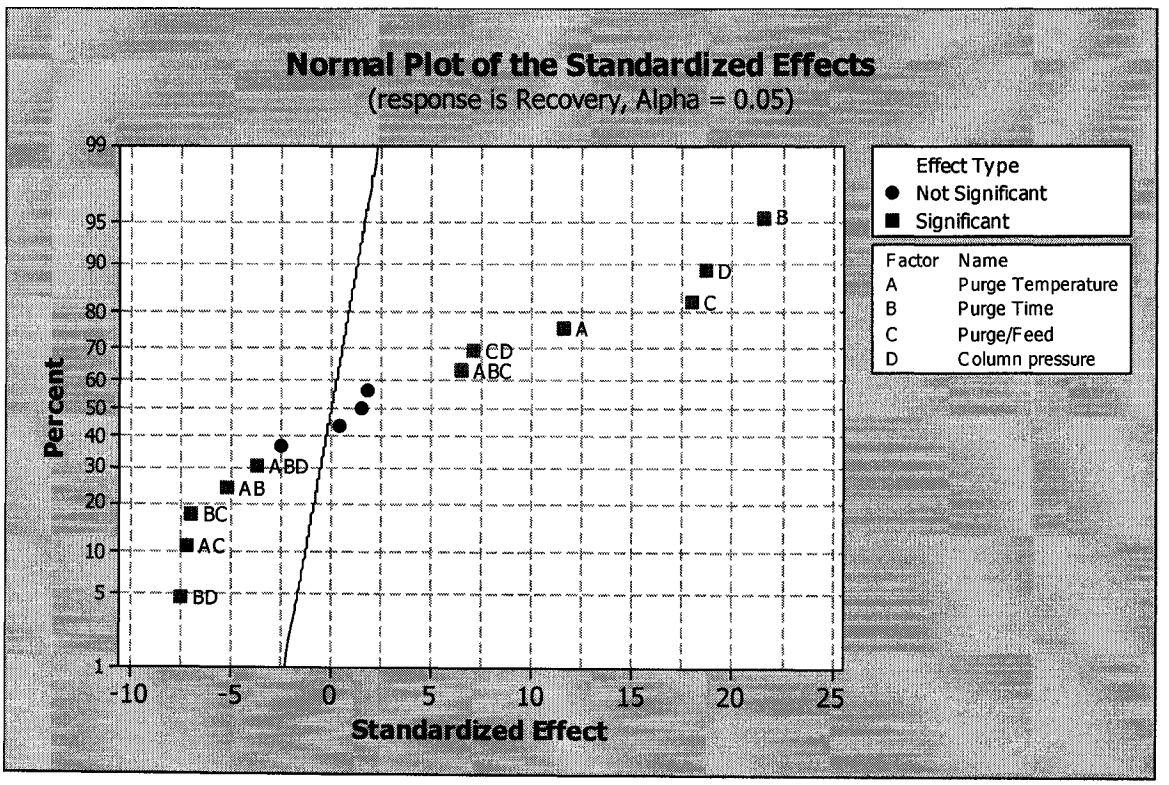

Figure VI- 9. Normal plot of the standardised effects

Figure VI-10 shows the Pareto chart of the standardised control factor effects. These effects determine the magnitude and importance of an effect. The plot displays the absolute value of the effects and draws a reference line on the chart which represents the "T" distribution value (for 95% confidence interval). All control factors that extend beyond the reference line are considered to be potentially important. From Figure VI-10, the most significant factors contributing to the increase in CO_2 recovery in descending order are the purge time, column pressure, purge/feed ratio, and purge temperature. These observed results are consistent with results obtained from Figure VI-9.

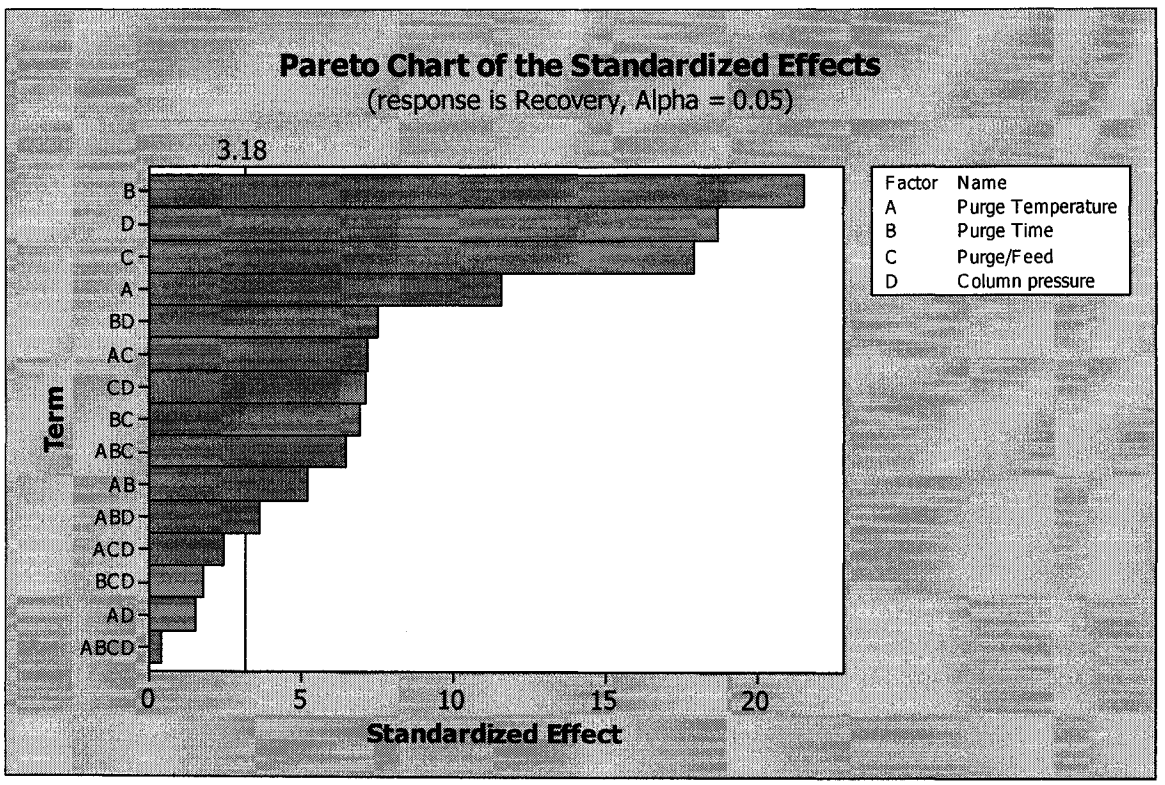

Figure VI- 10. Pareto chart of the standardised effects.

TESTING THE ADEQUACY OF A FITTED MODEL

Based on the Factorial fit, the model was fitted to the data from the 20 runs of this central composite design using the same coded values of the four control factors (denoted by the variables A, B, C and D) as denoted in the general equation (2).

$$R = \beta_o + \beta_A A + \beta_B B + \beta_C C + \beta_D D + \beta_{AB} AB + \beta_{AC} AC + \beta_{AD} AD + \beta_{BC} BC + \beta_{BD} BD + \beta_{CD} CD + \beta_{ABC} ABC + \beta_{BCD} BCD + \beta_{ACD} ACD + \beta_{ABD} ABD + \beta_{ABCD} ABCD$$

.....(2)

where A, B, C and D represent purge temperature, purge time, purge/feed flow ratio and column pressure control parameters, respectively. Based on the estimated parameter coefficients by Minitab® software for a 95% confidence interval, the following fitted model was obtained as denoted by Equation (3):

$$R = 55.3169 + 1.0106A + 1.8844B + 1.5681C + 1.6331D - 0.4569AB - 0.6281AC - 0.6069BC - 0.6569BD + 0.6219CD + 0.5669ABC - 0.3181ABD$$

.....(3)

Coefficients from Equation (3) indicate that main effects contribute to a higher CO_2 recovery when compared to 2-way and 3-way interaction parameters, with higher coefficients in this equation. Purge time (B) had a significant effect on the CO_2 recovery followed by column pressure (D), purge/feed flow ratio (C) and purge temperature (A) control parameters, respectively, with coefficients decreasing in this order. Analysis of variance for recovery (P-values < α=0.05 or 95% confidence interval for main effects, 2-way interactions and 3-way interactions) showed this model to be an adequate

representation of this data set. A test of significance of lack of fit can be determined by comparing the values obtained for:

$$L = \frac{MS_{LF}}{MS_{PE}} \quad \text{to} \quad F_{vLF,vPE,\alpha} \qquad \text{.....(4)}$$

where MS refers to the mean of squares and subscripts LF, and PE refer to lack of fit error (or residual error) and pure error, respectively while ν_{LF} and ν_{PE} refer to the degree of freedom with respect to lack of fit error (LF) and pure error (PE), respectively. So, if $L > F_{\nu LF,\ \nu PE,\alpha}$ there is no bias due to model inadequacy and the null hypothesis could be rejected. This condition concludes that there is a significant lack of fit in the fitted model. Since $L = \frac{MS_{LF}}{MS_{PE}} = \frac{0.33}{0.33} = 1$ which is less than $F_{3,\,3,\,0.05} = 9.28$, there is no significant lack of fit in the fitted model and the null hypothesis is not rejected, thus signifying that the model is a good fit. Therefore, by using such a model, one can deduce the main interaction effects to be concentrated upon and minimise the usage of less prominent interaction effects. The next step would be to increase the range of the main interaction effects in order to achieve a higher CO_2 recovery.

CONCLUSIONS

For the recovery of CO_2 from flue gas composition (10 % CO_2 by vol. in N_2) by Ceca 13X adsorbent, it was found that better regeneration conditions used in a TPSA cycle was essential over a PSA cycle. The stronger interaction between CO_2 and Ceca 13X leading to a high heat of adsorption was the reason to substantiate the choice of the TPSA cycle. A 2^k factorial design set of experiments was conducted to optimise the recovery of carbon dioxide with respect to the effects of four control parameters (purge/feed ratio, purge

time, purge gas temperature and adsorption column pressure) within a desired range in order to understand the interaction effects. It was found that each control parameter had a significant effect. Purge time had the most significant effect, followed by column pressure, purge/feed flow ratio and purge temperature on the CO_2 recovery, followed by 2-way and 3-way interactions. A Minitab® statistical software was used to analyse the data. It was found that the test of significance for lack of fit showed the fitted model to be an adequate representation of the experimental data. The results showed that to maximise the CO_2 recovery, highest values of the control parameters have to be used.

ACKNOWLEDGEMENTS

Financial supports received from Ontario Graduate Scholarship in Science and Technology (OGSST), Rio Tinto Alcan and Air Products& Chemicals Inc., are gratefully acknowledged.

NOMENCLATURE

Symbols

A Purge temperature control parameter

B Purge time control parameter

C Purge/Feed flow ratio control parameter

D Column pressure control parameter

F "F" distribution

k Control parameter

L	Parameter (dimensionless)
LF	Lack of fit
MS	Mean of squares
PE	Pure error
Q	Flow rate of gas in a cycle step (L/min)
R	Carbon dioxide recovery function
X	Composition of carbon dioxide in a cycle step (vol %)
Time	Time required to complete a cycle step (min)

Abbreviations

CO_2	Carbon dioxide
GC	Gas Chromatograph
GHG	Greenhouse gas
min	Minute
N_2	Nitrogen
NDIR	Non Dispersive Infrared analyser
PSA	Pressure Swing Adsorption
SL	Standard Litre
TPSA	Thermal Pressure Swing Adsorption
TSA	Temperature Swing Adsorption
UHP	Ultra high pure
vol	Volume
VPSA	Vacuum Pressure Swing Adsorption

Greek letters

α Level of significance (0-1)

β Coefficient of model fit equation (dimensionless)

REFERENCES

1. Grande, C.A., and Rodrigues, A.," Electrical Swing Adsorption for CO_2 removal from flue gases" International Journal of Greenhouse gas Control, 2, 194-202, (2008).
2. International Energy Agency Working Party on Fossil Fuels, "Solutions for the 21st century: Zero emissions technologies for fossil fuels", OECD/IEA, Paris, FR, 1-50, (2002).
3. Chue, K. T., J. N. Kim, Y. J. Yoo, S. H. Cho and R. T. Yang, "Comparison of Activated Carbon and Zeolite 13X for CO_2 recovery from flue gas by Pressure Swing Adsorption", Industrial and Engineering Chemistry Research 34, 591-598 (1995).
4. Zhang, J., Webley, P.A., and Xiao, P., "Effect of process parameters on power requirements of vacuum swing adsorption technology for CO_2 capture from flue gas", Energy conversion and management, 49, 346-356 (2008).
5. Reynolds, S.P., Ebner, A.D., and Ritter, J.A., "New pressure swing adsorption cycles for carbon dioxide sequestration", Adsorption., 11, 531-536 (2005).
6. Reynolds, S.P., Ebner, A.D., and Ritter, J.A., "Stripping PSA cycles for CO_2 recovery from flue gas at high temperature using a hydrotalcite-like adsorbent", Ind. Eng. Chem. Res., 45, 4278-4294 (2006).

7. Reynolds, S.P., Mehrotra, A., Ebner, A.D., and Ritter, J.A., "Heavy reflux PSA cycles for CO_2 recovery from flue gas: Part I. Performance evaluation", Adsorption, 14, 399-413 (2008).
8. Franchi, R.S.,Harlick, P.J.E., and Sayari, A., "Applications of Pore-Expanded Mesoporous Silica. 2. Developmentof a High-Capacity, Water-Tolerant Adsorbent for CO_2" Ind. Eng. Chem. Res., 44, 8007-8013 (2005).
9. Golden, T.C., Taylor, W.T., Malik, N.H., C.J.Raiswell and E.H. Salter, "Process for reducing the level of carbon dioxide in a gaseous mixture", U.S. Patent 6506236 (2003).
10. Ko, D., Siriwardane, R., Biegler, L.T., "Optimization of a Pressure swing adsorption process using Zeolite 13X for CO2 sequestration, Ind. Eng. Chem. Res., 42, 339-348 (2003).
11. Gomes, V. G. and K. W. K. Yee, "Pressure Swing Adsorption for Carbon Dioxide Sequestration from Exhaust Gases", Separation and Purification Technology 28, 161-171 (2002).
12. Takamura, Y., S. Narita, J. Aoki and S. Uchida, "Application of High-Pressure Swing Adsorption Process for Improvemant of CO_2 Recovery System from Flue Gas", The Canadian Journal of Chemical Engineering79, 812-816 (2001a).
13. Takamura, Y., S. Narita, J. Aoki, S. Hironakaand S. Uchida, "Evaluation of Dual-Bed Pressure Swing Adsorption for CO_2 Recovery from Boiler Exhaust Gas", Separation and Purification Technology 24, 519-528 (2001b).
14. Zhang, Z., J. Guan and Z. Ye, "Separation of a Nitrogen-Carbon Dioxide Mixture by Rapid Pressure Swing Adsorption", Adsorption 4, 173-177 (1998).

15. Ishibashi, M., H. Ota, N. Akutsu, S. Umeda, M. Tajika, J. Izumi, A. Yasutake, T. Kabata and Y. Kageyama, "Technology for removing Carbon Dioxide from Power Plant Flue Gas by the Physical Adsorption Method", Energy Conversion and Management, 37, 929-933 (1996).

16. Ruthven, M., Farooq, S.,Knaebel, K., "Pressure swing adsorption", John Wiley and Sons Inc., pp.5-93, (1994).

17. Kikkinides, E. S. and R. T. Yang, "Concentration and Recovery of CO_2 from Flue Gas by Pressure Swing Adsorption", Industrial and Engineering Chemistry Research 32, 2714-2720 (1993).

18. Kim, J., Chue, K., Kim, K., Cho, S., Kim, J., "Non-isothermal adsorption of nitrogen-carbon dioxide mixture in a fixed bed of zeolite-X, J. Chem. Eng. Jpn., 27 (1), 45-51 (1994).

19. Wright A., Kalbassi M., and Golden C., "Prepurification of Air using an advanced Thermal Pressure Swing adsorption cycle", Proceedings of AIChE conference, Cincinatti, U S A, October 30 – Nov 4, (2005)

20. Harlick, P.J.E and F.H. Tezel, "An experimental adsorbent screening study for carbon dioxide removal from nitrogen" Microporous Mesoporous Mater. 76, 71-79 (2004).

21. Yon, C.M., and Sherman, J. D., "Adsorption", Kirk Othmer Encyclopaedia of Chemical Technology, John Wiley and Sons (2003).

22. Birbara, P.J., Filburn, T.P., H. Michels and T.A. Nalette, "Sorbent system and method for adsorbing carbon dioxide from the atmosphere of a closed habitable environment", U.S. Patent 6364938 (2002).

23. Kanazirev, V.I., and D.J. Latus, "Composite adsorbents for Air Purification", U.S. Patent 6638340 (2003).

24. Mulgundmath, V.P., Jones, R., Tezel, F.H and Thibault, J., "Fixed bed adsorption for the removal of carbon dioxide: breakthrough behaviour and modelling for heat and mass transfer", Separation and Purification technology (submitted).

25. Kumar, R., Huggahalli, M., Deng, S., and Andrecovich, M., " Trace impurity removal from air", Adsorption, 9 (3), 243-250 (2003).

Appendix

Factorial Fit using Minitab® software: Recovery versus Purge Temperature, Purge Time, Purge/Feed and Column pressure

Estimated Effects and Coefficients for Recovery (coded units)

Term	Effect	Coef	SE Coef	T	P
Constant		55.3169	0.08726	633.94	0.000
Purge Temperature (A)	2.0212	1.0106	0.08726	11.58	0.001
Purge Time (B)	3.7687	1.8844	0.08726	21.60	0.000
Purge/Feed (C)	3.1362	1.5681	0.08726	17.97	0.000
Column pressure (D)	3.2662	1.6331	0.08726	18.72	0.000
Purge Temperature*Purge Time(AB)	-0.9137	-0.4569	0.08726	-5.24	0.014
Purge Temperature*Purge/Feed(AC)	-1.2562	-0.6281	0.08726	-7.20	0.006
Purge Temperature*Column pressure(AD)	0.2637	0.1319	0.08726	1.51	**0.228**
Purge Time*Purge/Feed (BC)	-1.2138	-0.6069	0.08726	-6.95	0.006
Purge Time*Column pressure(BD)	-1.3137	-0.6569	0.08726	-7.53	0.005
Purge/Feed*Column pressure(CD)	1.2438	0.6219	0.08726	7.13	0.006
Purge Temperature*Purge Time* Purge/Feed (ABC)	1.1338	0.5669	0.08726	6.50	0.007
Purge Temperature*Purge Time* Column pressure (ABD)	-0.6363	-0.3181	0.08726	-3.65	0.036
Purge Temperature*Purge/Feed* Column pressure (ACD)	-0.4288	-0.2144	0.08726	-2.46	**0.091**
Purge Time*Purge/Feed* Column pressure (BCD)	0.3087	0.1544	0.08726	1.77	**0.175**
Purge Temperature*Purge Time* Purge/Feed*Column pressure (ABCD)	0.0662	0.0331	0.08726	0.38	**0.730**
Ct Pt		0.2806	0.19512	1.44	0.246

S = 0.349034 PRESS = *
R-Sq = **99.81**% R-Sq(pred) = *% R-Sq(adj) = 98.80%

Analysis of Variance for Recovery (coded units)

Source	DF	Seq SS	Adj SS	Adj MS	F	P
Main Effects	4	155.174	155.174	38.7934	318.44	0.000
2-Way Interactions	6	28.915	28.915	4.8191	39.56	0.006
3-Way Interactions	4	7.877	7.877	1.9694	16.17	0.023
4-Way Interactions	1	0.018	0.018	0.0176	0.14	0.730
Curvature	1	0.252	0.252	0.2520	2.07	0.246
Residual Error	3	0.365	0.365	0.1218		
Pure Error	3	0.365	0.365	0.1218		
Total	19	192.601				

CHAPTER VII

CONCLUSIONS

CONTRIBUTIONS

RECOMMENDATIONS

CONCLUSIONS

Several conclusions were reached by considering the results of the studies that are incorporated in this thesis. These conclusions are summarised as follows:

1. Carbon dioxide capture by adsorption processes is a promising technology to reduce the carbon footprint and combat global warming due to its low operating and capital costs. The present study incorporated the determination of adsorption equilibrium parameters on pure and composite adsorbents by both static and dynamic approaches. The objectives met included the determination of Henry's law constants for various trace impurities present in air like CO_2, C_2H_2, C_2H_4, N_2O etc., pure and binary isotherms for CO_2, CH_4 and N_2, actual breakthrough experiments for the flue gas separation of CO_2 from dry air on my designed labscale setup and model the system by a novel two population model. The scale up experiments and the modelling approach took CO_2 capture to the application level thereby demonstrating that my lab scale unit could function as a viable CO_2 capture system. This unit could be used for both trace and bulk CO_2 removal in industrial applications such as trace removal of CO_2 in air separation plants, flue gas separation of CO_2 from dry air and natural gas, coal bed gas and landfill gas purification.
2. The adsorbents (Alcan AA-300 activated alumina), activated alumina/13X zeolite composites (Alcan Actiguard 600 PC and Alcan Actiguard 650 PC), CABSORB Chabazite, 13X zeolite (CECA G5-13X) and Ash Meadows Clinoptilolite find applications in trace impurity removal from air.

3. A higher composition of 13X zeolite in the composite 13X/AA adsorbent exhibited higher Henry's Law constants for ethylene, compared to both pure 13X zeolite and pure activated alumina (AA) adsorbents. This observation can be tied to the compositions of the hybrid adsorbents and suitable for trace impurity removal applications.

4. According to the single component gas isotherm data for the gases studied in this thesis, the order of single component gas adsorption capacity is CO_2 > CH_4 > N_2 for adsorbates and Ceca 13X > Alcan 650 PC composite >Alcan pure activated alumina for adsorbents. The single component gas adsorption capacity increases with decreasing temperature in the systems studied which is consistent with physical adsorption behaviour.

5. Among the various concentration pulse methods, VV-CPM fits the CH_4-N_2 binary experimental data well while the more versatile HT-CPM fits the experimental data very well for the non ideal CO_2-CH_4 and CO_2-N_2 systems.

6. For predicting the experimental binary system behaviour from the single component data, extended Langmuir theoretical adsorption model can only be applied as an approximation when there is no experimental data available

7. Ceca 13X is a promising adsorbent for trace removal of CO_2, flue gas separation of CO_2 from dry air, as well as natural gas and landfill gas purification applications. This adsorbent showed excellent thermodynamic consistency at both temperatures of 40°C and 100°C.

8. Heat effects are significant for carbon dioxide separation from air (10 % CO_2 by vol in N_2) using Ceca 13X adsorbent. It was found that better regeneration conditions used in a TPSA cycle were essential over a PSA cycle.

9. The breakthrough time of Ceca 13X adsorbent is independent of the initial bed temperature while an earlier breakthrough time is observed for a higher feed flow rate of 6.6 SL/min compared to 4 SL/min for 10 % CO_2 (by vol) in N_2 mixture adsorption. Also, cooling during the adsorption cycle decreases the mass transfer zone and leads to a longer breakthrough time, since adsorption capacity is higher at low temperatures.

10. By using the novel two-population model, the curvature of the concentration breakthrough curve including the noted tailing was predicted with good accuracy. Also, the point at which the temperature breakthrough occurs is estimated with good accuracy with the model prediction.

11. Using continuous measurements of temperature in the column bed along with this model, concentration breakthrough can be easily predicted for gas mixtures and adsorbents exhibiting higher heat effects. For practical applications, this model can be used to eliminate the need for online composition measurements during operation.

12. Temperature measurements on operating columns can be used as a simple and cost effective method of validating the model during operation.

13. TPSA optimisation runs showed that the four control parameters studied had a significant effect on the CO_2 recovery. Purge time had the most significant

effect followed by column pressure, purge/feed flow ratio and purge temperature on the CO_2 recovery, followed by 2-way and 3-way interactions.

CONTRIBUTIONS

The following is a list of the contributions resulting from this study:

1. New adsorbents including pure materials and composites were tested. A composite adsorbent material was proven to perform better than a pure adsorbent material for the ethylene trace impurity removal applications which validated our hypothesis.
2. Designed and built a novel and a mobile two-bed lab scale dynamic adsorption analysis unit for the separation of gas mixtures. This unit has been modified to perform different types of adsorption cycle runs, viz. Thermal Swing Adsorption (TSA), Pressure Swing Adsorption (PSA), Thermal Pressure Swing Adsorption (TPSA) and Vacuum Swing Adsorption (VSA). This unit has the flexibility of on-site regeneration of the adsorbent and the ability to maintain isothermal conditions within the column.
3. Single component and binary gas experiments were done by volumetric and concentration pulse methods, respectively while the fixed bed breakthrough experiments were done by the dynamic adsorption analysis system that was built in-house. Pilot scale experiments were performed to evaluate the performance of the selected adsorbent (Ceca 13X) for dry flue gas separation of carbon dioxide from air.

4. Heat effects were significant for the flue gas separation of carbon dioxide from N_2 (representing air) using Ceca 13X adsorbent. The temperature front moved slightly ahead of the concentration front while moving from the column inlet to the outlet. This behaviour suggested that concentration breakthrough in a column could be detected by the temperature breakthrough using thermocouples only. For similar mixtures exhibiting higher heat effects, an expensive concentration measurement device would not be needed to detect the concentration breakthrough of the feed gas mixture.
5. A simple and yet a novel two-population model was developed to describe the mass and heat transfer taking place within the packed bed adsorber. The predicted concentration and temperature breakthrough behaviours agreed very well with the experimental data, thus validating the model.
6. The detailed results, discussions and conclusions of these studies have been submitted in the form of five scientific journal papers.

RECOMMENDATIONS

The following are a few recommendations for future research directions resulting from this study:

Single component gas isotherms on adsorbents were determined by the constant volume method only. This method has to be compared with other adsorption techniques, namely, the Gravimetric method and the Chromatographic method for consistency.

Binary gas mixture experiments were performed at 1 atm total pressure only. These experiments have to be performed at higher pressures to evaluate the performance of adsorbents for PSA applications usually held at high pressures.

For the flue gas separation, moisture is a bulk component which was not included in this study. Ternary mixture separations including moisture have to be incorporated in the experiments. The possibility of using layered adsorbent beds to target specific gas components should be investigated.

A wider range of interaction control parameters should be employed for the TPSA optimisation runs. A comprehensive list of adsorbents including both pure and composite adsorbents should be tested. Different adsorption cycles have to be performed and a detailed economic analysis should be done to compare the probable adsorption cycle options.

APPENDICES

APPENDIX I

STRUCTURE OF 13X ADSORBENT

The crystal structure is based upon repeating units consisting of a silicon atom (+4 valence) surrounded by four oxygen atoms (-2 valence) in a tetrahedral configuration. Each oxygen atom is shared by two silicon atoms, giving the tetrahedral structure, a net valence of zero. When aluminium (with a valence of +3) is substituted in the tetrahedral structure, a net charge defect of -1 occurs. This gives rise to the cation exchange properties of zeolites. Another interesting property of zeolites is their very uniform pore sizes (10 °A in case of Ceca 13X) which occur as a consequence of their unique crystal structures.

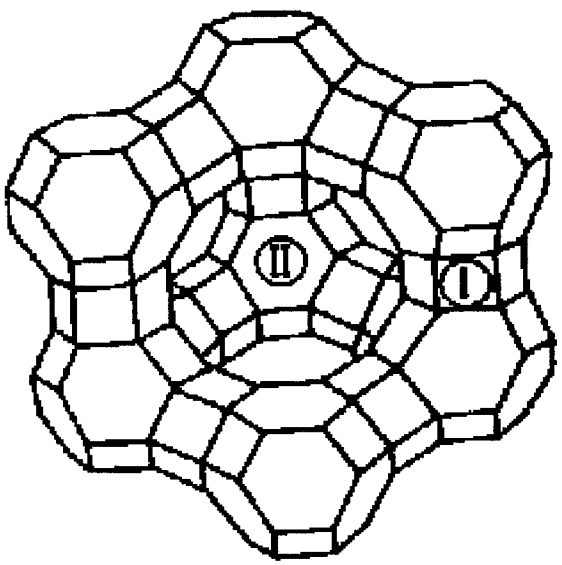

Figure 1. Structure of 13X adsorbent

APPENDIX II

DETERMINATION OF SYSTEM DEAD TIME

In concentration pulse chromatography, a pulse of the sample gas is injected into the carrier gas stream which passes through a packed adsorbent column. From this response peak, a mean retention time, μ is determined experimentally to estimate the Henry's Law constant. However, this is not the real retention time and the system dead time has to be incorporated into the calculations.

The system dead time was determined experimentally. In our case, non-adsorbing glass-beads that have the same size as the adsorbents used (20-60 mesh) were packed in the column, and then dead time was measured at different flow rates and temperatures with different sample and carrier gases. The retention time for glass-beads i.e., the system dead time (μ_D) decreased as superficial fluid velocity (v_S) increased and shown in Figure 1. Three different conditions, viz. column temperature, type of sample gas, and type of carrier gas, were analysed to study their effects on the system dead time. Results indicated that these factors were independent of the system dead time, as expected. From the experimental data, a linear relation of μ_D vs. v_S^{-1} is obtained and shown in Figure 1. A proportional constant is introduced as shown in Equation [1]:

$$\mu_D = \frac{k_C}{v_S} \qquad [1]$$

where μ_D is the dead time, v_S is the superficial fluid velocity, and k_C is the proportionality constant.

Regression calculations indicated the proportionality constant (k_C) to be 22.6 for the three different conditions used. From Equation [1], the system dead time was determined for our experimental runs and incorporated into the real retention time calculations to evaluate the Henry's law constant. For all our experimental runs, the same column was used.

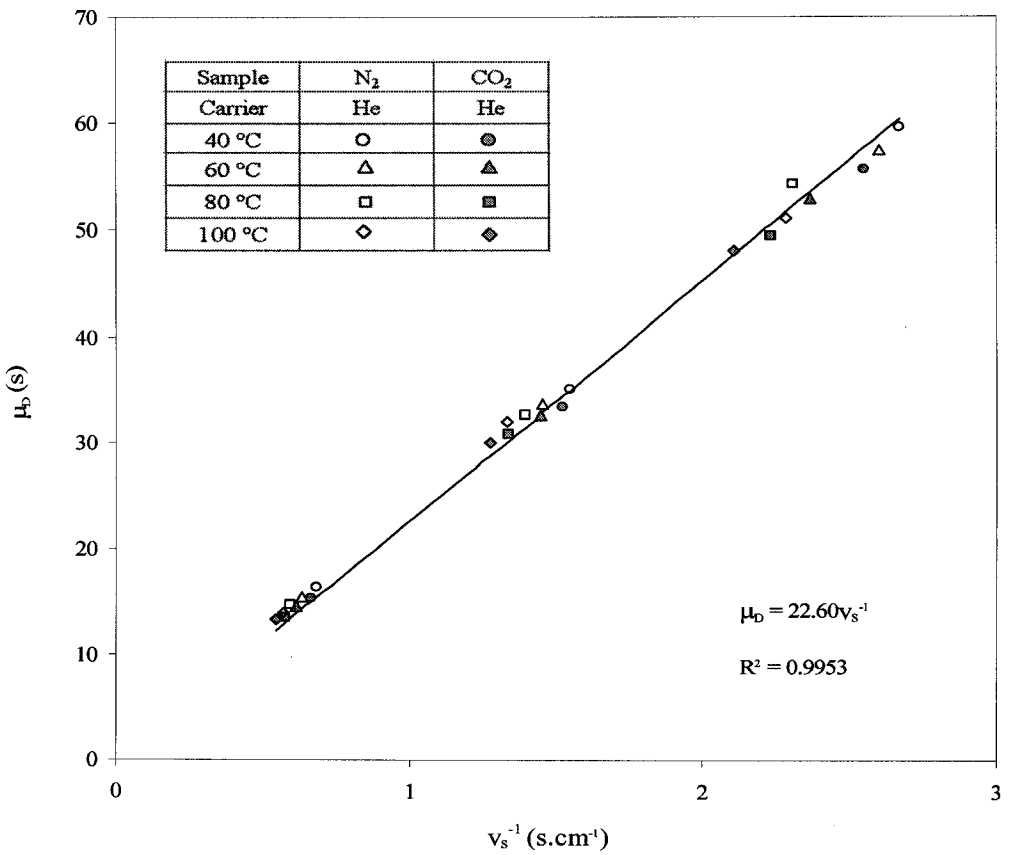

Figure 1. Linear regression of the relation between dead times (μ_D) and superficial fluid velocities (v_S) on the adsorption column packed with glass beads (20–60 mesh).

APPENDIX III

CONCENTRATION PULSE CHROMATOGRAPHY FOR THE DETERMINATION OF BINARY ISOTHERMS

INTRODUCTION

The purpose of this report is to provide a user friendly guide for those who wish to use the Gas Chromatograph, (GC) Varian 3300. It is also important to note that this document is written based on the assumption that the user is familiar with the concept of gas chromatography and adsorbent packing for the GC column. Hence, this manual will only provide the user with the basic procedures for operating the equipment including calibrating, regenerating and running the system. An illustration is shown below of the Varian GC 3300 in Figure 1.

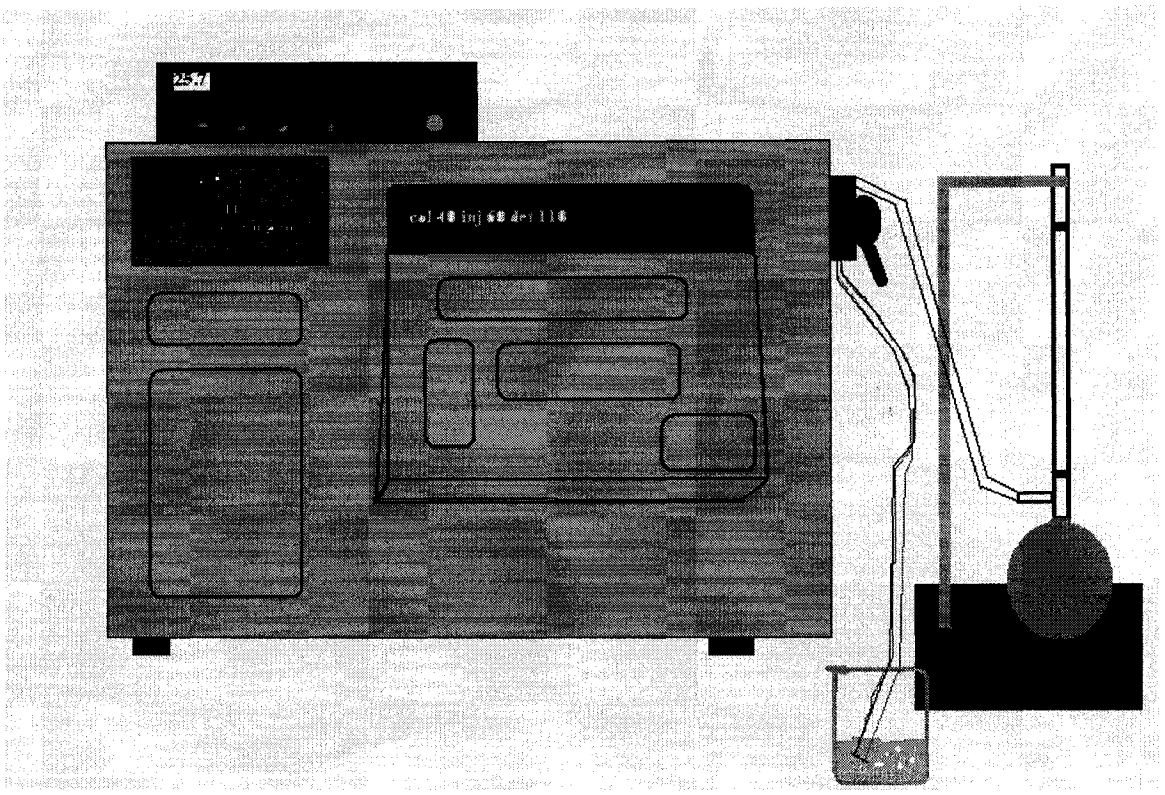

Figure 1. Schematic diagram of the Varian 3300 Gas Chromatograph.

CALIBRATION

Before commencing any GC experiment, it is essential to calibrate the system for each individual carrier gas. In a binary system we have two carrier gases, Carrier A and Carrier B. These are labelled on the mass flow controllers (MCF's) accordingly. The Channel Controller (the black box on top of the GC) has 4 channels which are connected to four different MFCS. The one's we are interested in are channels number TWO and number FOUR. By using the switch on the right of the Channel Controller we can adjust which MFC we would like to control.

When calibrating it is important to remember that we calibrate each Carrier Gas individually. Thus, if we are calibrating Carrier A then we must make sure that Carrier B is set to ZERO on channel 2 or the valve is closed on our Carrier B gas cylinder. Once the user has made sure that Carrier B is set to a flow rate of ZERO, then they are ready to calibrate Carrier Gas A. For our calibration processes, we will be using a Bubble Meter illustrated in Figure 2.

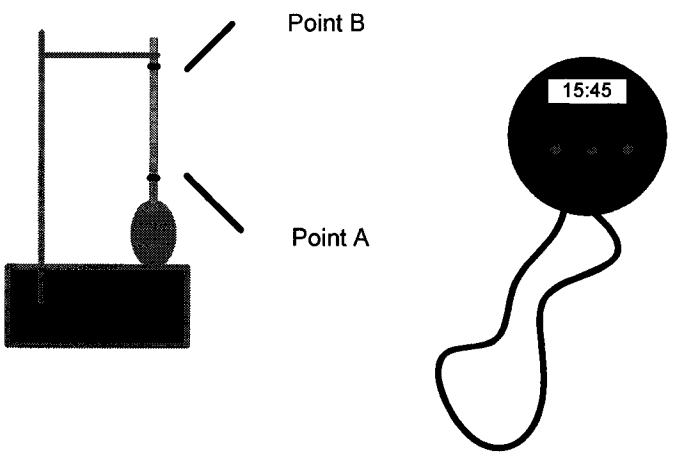

Figure 2. Schematic diagram of the Bubble flow meter and a stopwatch.

When calibrating we would like to have our highest indicator value set to a value that will give a 15 cc/min flow rate on the bubble meter. What this means, is that the time required for a bubble to travel from point A to point B (15 mL or 15 cubic centimetres) should take approximately 15 seconds on our stop watch. It is also important to note that when the user is doing this process, the choice of bubbles should be ones that are NOT foamy and ones that are clear. Bubbles can be obtained by squeezing the rubber band at the bottom of the 25 mL cylinder shown in the illustration.

The only way to set the indicator to a specific value is through trial and error. First set the indicator to an arbitrary value, say 50.0, then proceed to take some time measurements using the bubble meter with the stop watch.

* If the time taken for a bubble to travel 15 mL is higher than 15 seconds, set a higher flow rate until you get your time to be approximately 15 seconds.
* If the time taken for a bubble to travel is less than 15 seconds, set a lower flow rate until you get your time to be approximately 16 seconds.

Once you have an indicator value which gives you a 15 cc/min flow rate on the bubble meter, divide the indicator value by 10 so as to obtain 10 additional indicator values.

Then take time trials with the indicator value that was set to obtain 15cc/min as your highest value. In other words if an indicator value of 50.0 was needed to record a 16 cc/min flow rate, then you should have 10 additional points decreasing by 5, so your next

value would be 45.0 and then 40.0 and etc. until you reach 5.0 as your last value. It is recommended that the user takes several time trials for each indicator value (e.g. 4). Also, when setting an indicator value, the user must wait for the process to be steady.

In order to know when the process is steady, we use the computer software LABVIEW. This can be done by running the program (press the white arrow on the top left corner), Scaling the X-axis (time) to about 600-1000 times greater than the start of the line and the y-axis (voltage) to about 3.0 higher and lower then the line and wait until the line straightens out. This is shown in Figure 3.

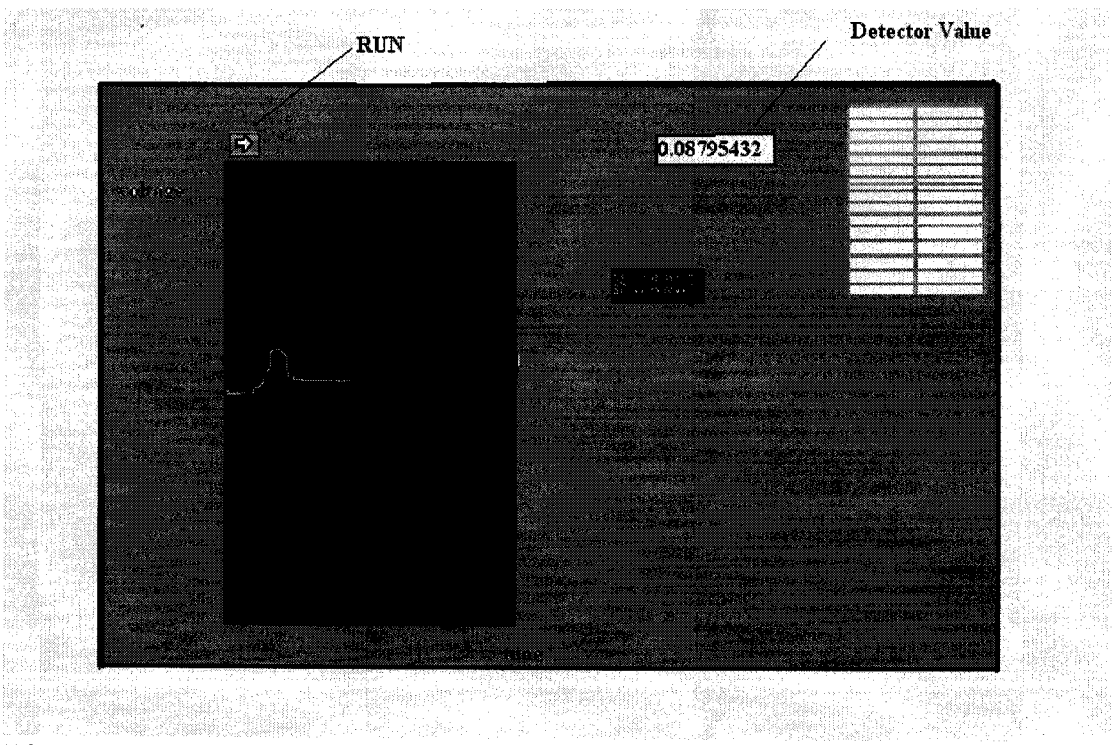

Figure 3. Steady state indicator of the process.

Once the calibration is done for Carrier Gas A, set the channel reading to 0.0 and then proceed to repeat all of the steps for calibrating Carrier Gas B. The regeneration of the adsorbent column is done using helium and the GC column set to 300 ^{o}C.

In order to switch the carrier gas to helium without fear of damaging the detector, the user can have one carrier gas running, let's say carbon dioxide as our Carrier B Gas set to any arbitrary flow rate and switch the Carrier Gas A with the Helium. Then the user can open the valve for the helium gas cylinder and set a fairly high flow rate (ex. 65.0) then turn off the Carrier Gas B and using the build/modify key on the machine raise the column temperature to 300 degrees. Make sure that helium is the only carrier gas running before raising the temperature and also make sure that if any other carriers are connected they are set to 0.0 or have their valve closed. The system should be allowed to regenerate for 24 hours. After 24 hours, the user can bring down the column temperature to the desired value and then switch the helium to the desired Carrier Gas using the same method that was used to connect the helium before regenerating. Once the regeneration has been completed and the temperature has been set to the desired value, the user is now ready to commence the experiments.

The first experiment that is usually run is the pure carrier gas (ex. Pure CARRIER GAS A) with an injection of the Sample Gas (ex. Sample Gas B). The sample gases are the same as the carriers but only used for a short sample injection. For instance if the binary experiment one is doing is nitrogen and carbon dioxide, they will have four gas cylinders to work with, one nitrogen cylinder as the carrier gas and one as the sample gas, as well

as one carbon dioxide cylinder as the other carrier gas and one as other the sample gas. For each different gas compositions/indicator values one must do two sample injections, one with sample gas A and another with sample gas B.

STEP BY STEP PROCEDURE TO FOLLOW

1. Use the bubble meter to make sure there is gas running through the GC machine. This can be done by squeezing the rubber band and if there are liquid lines flowing up the cylinder then everything is ok.
2. Check the carrier gas cylinders, make sure the valves are completely open, the regulators are set to 40 PSI and use soap water to spray on the connection tubing at the valve to make sure there are no leaks.
3. Make sure the indicator values are set accordingly to the desired compositions. Remember: Channel 2 is for carrier B and Channel 4 is for Carrier A.
4. Open LABVIEW and run the program at the desired scan rate (ex. 1 point per second or 10 points per second). Use the stopwatch to make sure that the scan rate is correct (computers are not always reliable!!).
5. Make sure the set indicator values/flow rates are in steady-state using the method discussed in the calibration section. In other words, make sure that the voltage readings are not fluctuating significantly.
6. If the Voltage Readings are fluctuating significantly, push metal lining on the connection holding the injector a few times until it improves.

7. Connect the desired sample gas and just like the Carrier Gases, check for leaks and so on.
8. Turn on the sample gas and use the side tubing from the GC and submerge it in a beaker of water to see that there is gas flowing from the sample.
9. Adjust the flow rate using only the valve of the sample gas cylinder (open the valve very little) so that there is a low flow rate coming from the sample gas.
10. Before injecting check that the column, injector and detector temperatures are correct.
11. Using your left hand grip the injector so that your hand is in a "thumbs down" position (not too tightly) and using the stop watch in your right hand. Turn the injector switch up (counter clockwise) in one swift motion and time your injection, usually about 6 seconds. Once this is done turn the injector switch back down (clockwise) again in one swift motion.
12. Wait for your CURVE and make sure the base line on the LABVIEW program comes back to the initial range as displayed in Figure 4.

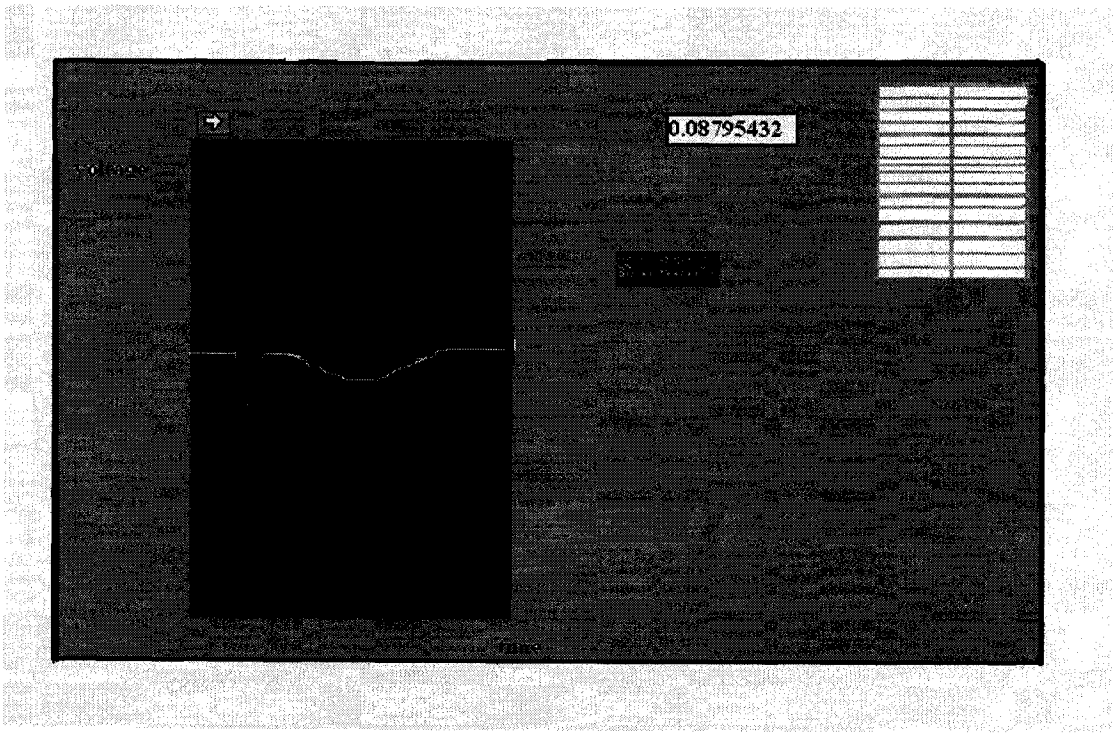

Figure 4. Baseline steady state indicator.

COMMON ERRORS AND PROBLEMS ENCOUNTERED

This section is strictly intended to aid the user with general information on problems that arise quite frequently.

1. The first and foremost hardship the user will encounter is when switching the GC system on using the switch on the left hand side on the back of the machine. When turning the system on, immediately there will a FAULT MESSAGE saying either POWER FAILURE/WARM START or LOST CARRIER GAS or TCD FILAMENT TEMP LIMITED.

Solution: *Press the RESET button on the machine.

2. Often the connection to the detector will not be excellent. Hence sometimes the voltage values on the computer screen seem to fluctuate even though you know for a fact that the system is at steady-state.

Solution: * Push on the metal piece on the small black compartment holding the injector about 20 times.

3. Often when changing a carrier gas for example when we would like to regenerate and switch one carrier to helium, the machine sometimes displays a fault message indicating a LOST CARRIER GAS even though by checking with the bubble meter we know that there is a carrier running through the system.

Solution: * Again, press the RESET button on the machine.

4. Often when doing the first injection using a pure carrier gas with the other set to 0, so for example 100% Nitrogen carrier and Carbon Dioxide sample the curve takes about 2 days to be completed and over 70 000 second readings on the computer. However excel only allows a maximum of 65000 points.

Solution: * Set the scan rate on the computer software to 1 point per 10 s.

5. Almost always when we start approaching the high CO_2 concentrations, so towards the final few curves the data readings or data processing values may not be completely on par with the data one would expect to see. These injections are more difficult and must be done very carefully if the user would like accurate results.

Solution: * These curves do not take very long and several injections can be made and the best results can be used. Also, the user should decrease the injection time of their sample gas to approximately 2-3 s or maybe even less depending on their curves.

6. When dealing with CO_2-N_2 binary experiments the user will find that towards the higher CO_2 concentrations mentioned in problem 5 that the N_2 sample injections from approximately 85%-100% CO_2 concentrations reach a maximum voltage value and instead of observing a curve the user observes what appears to be a rectangular curve with the peak turning into a straight line and then decreasing to the baseline value. This is illustrated on the next page in Figure 5.

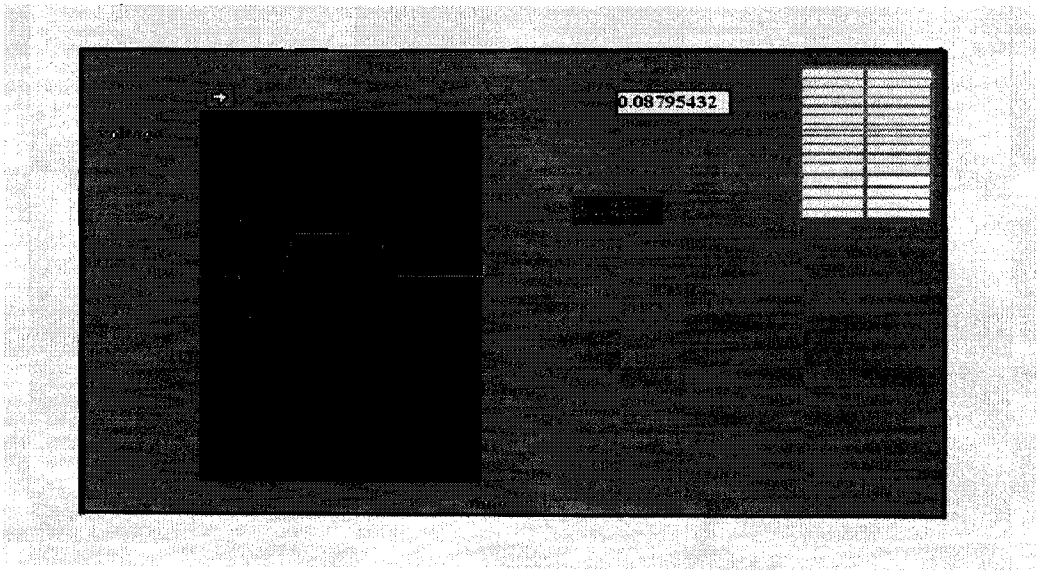

Figure 5. Rectangular curve observation during gas injection.

Solution: * When doing the N_2 injection, keep the injector UP (Opened) and push on the metal connection piece about 20 times. Then turn it back down. Do this until the baseline values after the curve are very close to the baseline values before the curve.

7. FINAL PROBLEM

The user may find a lack of information or perhaps an overwhelming amount of information at first. This may result in slower progress and many mistakes to be made.

Solution: * Ask for help and proper training. You are dealing with an expensive piece of equipment and it is your right to be supervised and trained.

SAMPLE BINARY DATA CALCULATIONS

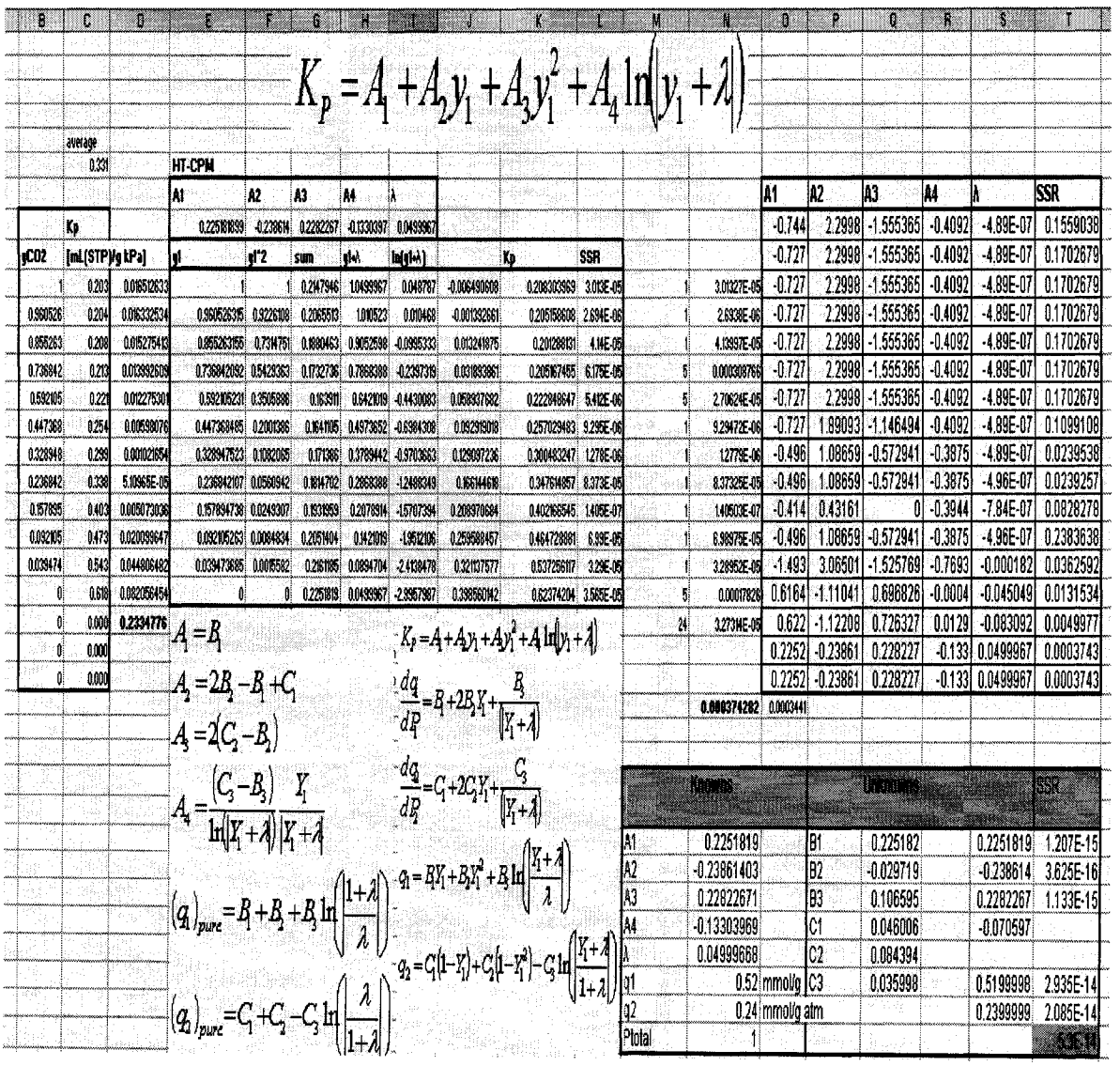

$$K_p = A_1 + A_2 y_1 + A_3 y_1^2 + A_4 \ln(y_1 + \lambda)$$

average	
	0.331

HT-CPM

A1	A2	A3	A4	λ
0.22518839	-0.23861	0.2282267	-0.1330397	0.0499967

	Kp	
yCO2	mL(STP)/g	kPa
1	0.203	0.016512633
0.960526	0.204	0.016332534
0.855263	0.208	0.016275413
0.736842	0.213	0.013982609
0.592105	0.221	0.012275301
0.447368	0.254	0.00598076
0.328948	0.299	0.001021854
0.236842	0.338	5.10965E-05
0.157895	0.403	0.005073036
0.092105	0.473	0.020099647
0.039474	0.543	0.044906482
0	0.618	0.082056454
0	0.000	0.2334776
0	0.000	
0	0.000	

g1	g1^2	sum	g1+λ	ln(g1+λ)		Kp	SSR
1	1	0.2247946	1.0499967	0.048787	-0.006490869	0.206303969	3.03E-05
0.960526395	0.9226018	0.2065513	1.009523	0.009468	-0.00132661	0.205158608	2.69E-06
0.855263155	0.7314751	0.8880463	0.9052598	-0.0995333	0.013241875	0.20028831	4.16E-05
0.736842092	0.5429363	0.1732736	0.7868388	-0.2397319	0.031883961	0.205167455	6.17E-05
0.592105231	0.3506886	0.163911	0.642019	-0.4430083	0.058937932	0.222948647	5.41E-06
0.447368485	0.2000386	0.1641105	0.4973652	-0.6984308	0.092916018	0.257029483	9.29E-06
0.328947523	0.1082065	0.171386	0.3789442	-0.9703683	0.129097236	0.300483247	1.27E-06
0.236842107	0.0560942	0.1814702	0.2868388	-1.2498349	0.16644618	0.347594857	8.37E-05
0.157894738	0.0249307	0.1533959	0.2078914	-1.5707394	0.208970684	0.402166545	1.40E-07
0.092105263	0.0084934	0.2051404	0.1421019	-1.9562106	0.259588457	0.464728891	6.99E-05
0.039473685	0.0015582	0.2261895	0.0894704	-2.4138478	0.321137577	0.537256017	3.29E-05
0	0	0.2251819	0.0499967	-2.9957987	0.398560142	0.623724204	3.66E-05

$$A_1 = B_1$$

$$A_2 = 2B_2 - B_1 + C_1$$

$$A_3 = 2(C_2 - B_2)$$

$$A_4 = \frac{(C_3 - B_3)\ Y_1}{\ln(Y_1 + \lambda)(Y_1 + \lambda)}$$

$$(q_1)_{pure} = B_1 + B_2 + B_3 \ln\left(\frac{1+\lambda}{\lambda}\right)$$

$$(q_2)_{pure} = C_1 + C_2 - C_3 \ln\left(\frac{\lambda}{1+\lambda}\right)$$

$$K_p = A_1 + A_2 y_1 + A_3 y_1^2 + A_4 \ln(y_1 + \lambda)$$

$$\frac{dq}{dP} = B_1 + 2B_2 Y_1 + \frac{B_3}{(Y_1 + \lambda)}$$

$$\frac{dq}{dP} = C_1 + 2C_2 Y_1 + \frac{C_3}{(Y_1 + \lambda)}$$

$$q_1 = B_1 Y_1 + B_2 Y_1^2 + B_3 \ln\left(\frac{Y_1 + \lambda}{\lambda}\right)$$

$$q_2 = C_1(1 - Y_1) + C_2(1 - Y_1^2) - C_3 \ln\left(\frac{Y_1 + \lambda}{1+\lambda}\right)$$

A1	A2	A3	A4	λ	SSR
-0.744	2.2998	-1.555365	-0.4092	-4.89E-07	0.1559038
-0.727	2.2998	-1.555365	-0.4092	-4.89E-07	0.1702679
-0.727	2.2998	-1.555365	-0.4092	-4.89E-07	0.1702679
-0.727	2.2998	-1.555365	-0.4092	-4.89E-07	0.1702679
-0.727	2.2998	-1.555365	-0.4092	-4.89E-07	0.1702679
-0.727	2.2998	-1.555365	-0.4092	-4.89E-07	0.1702679
-0.727	2.2998	-1.555365	-0.4092	-4.89E-07	0.1702679
-0.727	1.89093	-1.146494	-0.4092	-4.89E-07	0.1099108
-0.496	1.08659	-0.572941	-0.3875	-4.89E-07	0.0239538
-0.496	1.08659	-0.572941	-0.3875	-4.96E-07	0.0239257
-0.414	0.43161	0	-0.3944	-7.84E-07	0.0826278
-0.496	1.08659	-0.572941	-0.3875	-4.96E-07	0.2383638
-1.493	3.06601	-1.525769	-0.7693	-0.000182	0.0362592
0.6164	-1.11041	0.696826	-0.0004	-0.045049	0.0131534
0.622	-1.12208	0.726327	0.0129	-0.083092	0.0049977
0.2252	-0.23861	0.228227	-0.133	0.0499967	0.0003743
0.2252	-0.23861	0.228227	-0.133	0.0499967	0.0003743
					0.0003441

	Knowns		Unknowns		SSR
A1	0.2251819		B1	0.225182	
A2	-0.23861403		B2	-0.029719	
A3	0.22822671		B3	0.106595	
A4	-0.13303969		C1	0.046006	
λ	0.04999668		C2	0.084394	
q1	0.52	mmol/g	C3	0.035998	
q2	0.24	mmol/g	atm		
Ptotal	1				

A1	0.2251819		B1	0.225182	1.207E-15
A2	-0.23861403		B2	-0.029719	3.625E-16
A3	0.22822671		B3	0.106595	1.133E-15
A4	-0.13303969		C1	0.046006	-0.070597
λ	0.04999668		C2	0.084394	
q1	0.52	mmol/g	C3	0.035998	0.5198998 2.935E-14
q2	0.24	mmol/g	atm		0.2399999 2.086E-14
Ptotal	1				5.5E-14

g1	Kp	q1	q2	qT	X1
1	0	0.62374204	0	0.2399999	0.2399999	0
0.999	0.001	0.620868946	0.002336148	0.2392409	0.241577	0.0096704
0.995	0.005	0.609673935	0.011295379	0.2363365	0.2476219	0.045575
0.99	0.01	0.597121245	0.021694556	0.2329677	0.2546523	0.0851536
0.98	0.02	0.574294362	0.040359963	0.2269329	0.2672929	0.1509953
0.965	0.035	0.545071967	0.064410086	0.219836	0.2835937	0.227121
0.95	0.05	0.520161398	0.08507422	0.2125353	0.2976096	0.2856985
0.93	0.07	0.4916802	0.10894651	0.2048492	0.3137909	0.3471792
0.92	0.08	0.4788716	0.11968254	0.203811	0.3220823	0.3727664
0.91	0.09	0.46712948	0.129782283	0.198097	0.327892	0.395808
0.9	0.1	0.455997369	0.139332071	0.1950057	0.3343377	0.4167406
0.89	0.11	0.445504736	0.14840098	0.192045	0.3404461	0.4359018
0.88	0.12	0.435577874	0.157046852	0.1892085	0.3462554	0.4535581
0.87	0.13	0.426157818	0.165307389	0.1864798	0.3517572	0.4699226
0.86	0.14	0.417194674	0.173252364	0.1838455	0.3570978	0.4851677
0.85	0.15	0.40864523	0.180895679	0.1812942	0.3621799	0.499436
0.84	0.16	0.400476459	0.18824623	0.178961	0.3670624	0.5129454
0.83	0.17	0.392654363	0.195359844	0.1764029	0.3717617	0.5254948
0.82	0.18	0.38515308	0.202245043	0.1740473	0.3762923	0.5374679
0.81	0.19	0.37794918	0.208923589	0.1717428	0.3806664	0.5488364
0.8	0.2	0.37102105	0.215410985	0.1694841	0.3848951	0.5596618
0.79	0.21	0.364353714	0.221721734	0.1672661	0.3889879	0.5699965
0.78	0.22	0.357927924	0.227868733	0.1650846	0.3929533	0.5798875
0.77	0.23	0.351730405	0.233863465	0.1629356	0.396799	0.5893751
0.76	0.24	0.345748338	0.2397152	0.160856	0.4005316	0.5984948
0.75	0.25	0.339970206	0.245436165	0.1587726	0.4041578	0.6072761
0.74	0.26	0.334385626	0.251031679	0.1566508	0.4076824	0.615753
0.73	0.27	0.328985205	0.256510269	0.1545805	0.4111109	0.6239444
0.72	0.28	0.323760418	0.261876765	0.1525585	0.4144473	0.6318747
0.71	0.29	0.318703502	0.267143387	0.1505829	0.4176961	0.6395639
0.7	0.3	0.313807369	0.272309814	0.148651	0.4208611	0.6470302
0.69	0.31	0.309065531	0.277383243	0.1467623	0.4239455	0.6542898
0.68	0.32	0.304472035	0.282368447	0.1449042	0.4269527	0.661357
0.67	0.33	0.300021401	0.287269813	0.1430755	0.4298854	0.6682474
0.66	0.34	0.29570958	0.29209109	0.140655	0.4327464	0.6749713
0.65	0.35	0.291528902	0.29683697	0.1387012	0.4355381	0.6815408
0.64	0.36	0.287478047	0.301508656	0.1367531	0.4382629	0.6879657
0.63	0.37	0.283552005	0.30613342	0.1348035	0.4409223	0.6942562
0.62	0.38	0.27974705	0.310650594	0.1328694	0.44352	0.7004206
0.61	0.39	0.276059714	0.31524158	0.1309319	0.4460661	0.7064676
0.6	0.4	0.27249676	0.319536703	0.1289961	0.4485528	0.7124043
0.59	0.41	0.269025168	0.323890652	0.1270613	0.4509819	0.7182377
0.58	0.42	0.26567211	0.328168269	0.1251265	0.4533548	0.7239743
0.57	0.43	0.262424938	0.332393675	0.123192	0.4556229	0.7296202
0.46	0.55	0.230943581	0.37974463	0.0937123	0.4734578	0.7920297
0.44	0.56	0.228691692	0.383428514	0.0977211	0.4811496	0.7969006
0.43	0.57	0.226921207	0.387077804	0.095722	0.4827998	0.8017356
0.42	0.58	0.225030982	0.390693416	0.0937154	0.4844089	0.8065365
0.41	0.59	0.223219927	0.394276224	0.091701	0.4859773	0.8113059
0.4	0.6	0.221487001	0.39782705	0.0896796	0.4875056	0.8160461
0.39	0.61	0.219831214	0.40134672	0.0876477	0.4889945	0.8207592
0.38	0.62	0.218251618	0.404835962	0.0856063	0.4904442	0.8254475
0.37	0.63	0.216747307	0.408295512	0.08356	0.4918555	0.8301127
0.36	0.64	0.215317417	0.411726062	0.0815026	0.4932288	0.834757
0.35	0.65	0.213961119	0.415128277	0.0794359	0.4945641	0.8393823
0.34	0.66	0.21267762	0.418502792	0.0773596	0.4958624	0.8439898
0.33	0.67	0.21146161	0.421850215	0.0752736	0.4971238	0.8485817
0.32	0.68	0.210326013	0.42517113	0.0731777	0.4983488	0.8531597
0.31	0.69	0.209256479	0.428466096	0.0710717	0.4995378	0.8577251
0.3	0.7	0.208256998	0.431735651	0.0689553	0.500691	0.8622797
0.29	0.71	0.207326595	0.434980309	0.0668285	0.5018088	0.8668249
0.28	0.72	0.206464984	0.438200568	0.064691	0.5028916	0.8713619
0.27	0.73	0.205671456	0.441396902	0.0625427	0.5039396	0.8758924
0.26	0.74	0.204945447	0.444568771	0.0603835	0.5049533	0.8804176
0.25	0.75	0.204286401	0.447719614	0.0582132	0.5059328	0.8849389
0.24	0.76	0.203693789	0.450846857	0.056031	0.5068784	0.8894575
0.23	0.77	0.203167101	0.453951908	0.0538386	0.5077905	0.8939749
0.22	0.78	0.202705846	0.457035161	0.051634	0.5086692	0.8984919
0.21	0.79	0.20230955	0.460096395	0.0494179	0.5095149	0.90301
0.2	0.8	0.201977756	0.463137778	0.0471899	0.5103277	0.9075302
0.19	0.81	0.201710022	0.466157562	0.0449501	0.5110079	0.9120537
0.18	0.82	0.201505923	0.469157588	0.0426982	0.5116559	0.9165816
0.17	0.83	0.20136504?	0.472137287	0.0404342	0.5122715	0.921143
0.16	0.84	0.201286998	0.475097276	0.038158	0.5128553	0.9256549
0.15	0.85	0.201271391	0.478037864	0.0358695	0.5139073	0.9302024
0.14	0.86	0.201317855	0.480959346	0.0335685	0.5145278	0.9347596
0.13	0.87	0.201426031	0.483862012	0.031255	0.515117	0.9393245
0.12	0.88	0.201595572	0.486746139	0.0289289	0.5156675	0.943901
0.11	0.89	0.20182614?	0.489611997	0.02659	0.516202	0.9484891
0.1	0.9	0.202117414	0.492459847	0.0242383	0.5166982	0.9530899
0.09	0.91	0.202469074	0.495289941	0.0218739	0.5171637	0.9577043
0.08	0.92	0.202880915	0.498102524	0.0194963	0.5175988	0.9623332
0.07	0.93	0.203352243	0.500897834	0.0171057	0.5180035	0.9669776
0.06	0.94	0.203883369	0.5036761	0.014702	0.5183781	0.9716384
0.05	0.95	0.204473616	0.506437546	0.0122851	0.5187227	0.9763166
0.04	0.96	0.205122812	0.509182389	0.0098549	0.5190373	0.9810131
0.03	0.97	0.205830697	0.511910837	0.0074114	0.5193222	0.9857287
0.02	0.98	0.206597014	0.514623095	0.0049544	0.5195775	0.9904645
0.01	0.99	0.207421519	0.517319362	0.002484	0.5198034	0.9952213
0	1	0.208303969	0.519999829	0	0.5199998	1

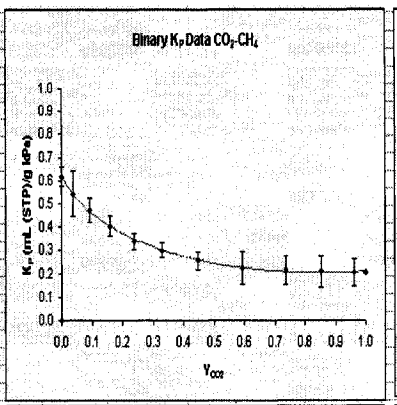

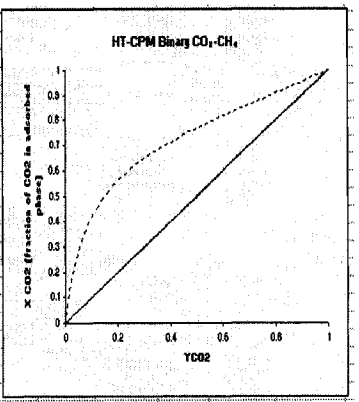

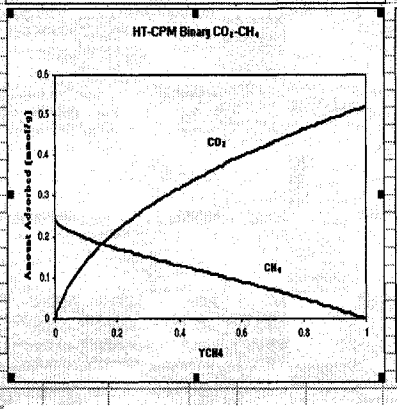

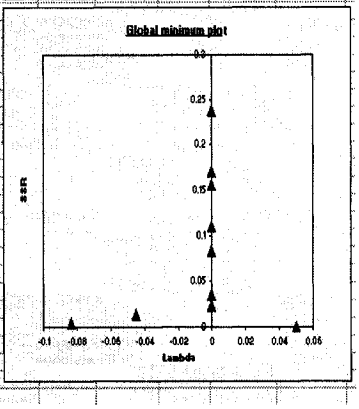

APPENDIX IV

DETERMINATION OF SINGLE COMPONENT ISOTHERMS BY CONSTANT VOLUME METHOD

Single Component gas Isotherms

The technique utilised to obtain this equilibrium data is the volumetric method. This method is based on measuring the change in pressure for a fixed volume of gas at constant temperature that is in contact with the adsorbent.

In this system a known quantity of single component gas contained in the manifold volume is admitted into the interconnecting tubing and sample cell volume that contains the adsorbent at a constant temperature. As adsorption takes place the sample cell pressure decreases. Once the system has reached equilibrium, the volume of adsorbed gas can be calculated from the difference between the initial and final pressure. This calculation is possible because the amount of gas required to fill the free space in the sample cell is known from the dead volume estimate.

This system is equipped with Swagelok® valves and two MKS *Baratron®* pressure transducers that were employed for their respective low and high pressure ranges. The first pressure transducer, a *1000 Torr MKS Baratron® Capacitance Manometer*, is

applied to the lower pressure range of up to 120 kPa with an uncertainty of ± 0.001 kPa. The second pressure transducer, a *250 psia MKS Baratron® Pressure Transducer*, is applied in the range of pressures above 120 kPa with an uncertainty of ± 0.08 kPa. The volume of the interconnecting tubing (V_i) and manifold (V_d) are displayed in Table 2 for the volumetric system used in the following experiments.

The free space (V_s) or "dead volume" is the volume of the sample cell that is not occupied by the adsorbent. The dead volume is estimated after initial adsorbent regeneration and before the isotherm measurements are taken. The dead space is measured by the expansion of Helium (He) gas into the sample cell (with adsorbent) at the same temperature as the isotherm. It is assumed that the volume available to the He atoms is the same as that for the N_2O and CO_2 gas molecules. Also, He adsorption and swelling of the adsorbent is considered negligible. The dead volume is calculated for each isotherm and is estimated with an uncertainty of ± 0.3 mL.

Table 2: Volume of manifold with both pressure transducers open (V_{d1}), with only 250 psia pressure transducer open (V_{d2}), and interconnecting tubing (V_i).

V_{d1} (mL)	V_{d2} (mL)	V_i (mL)
53.97	39.42	6.70

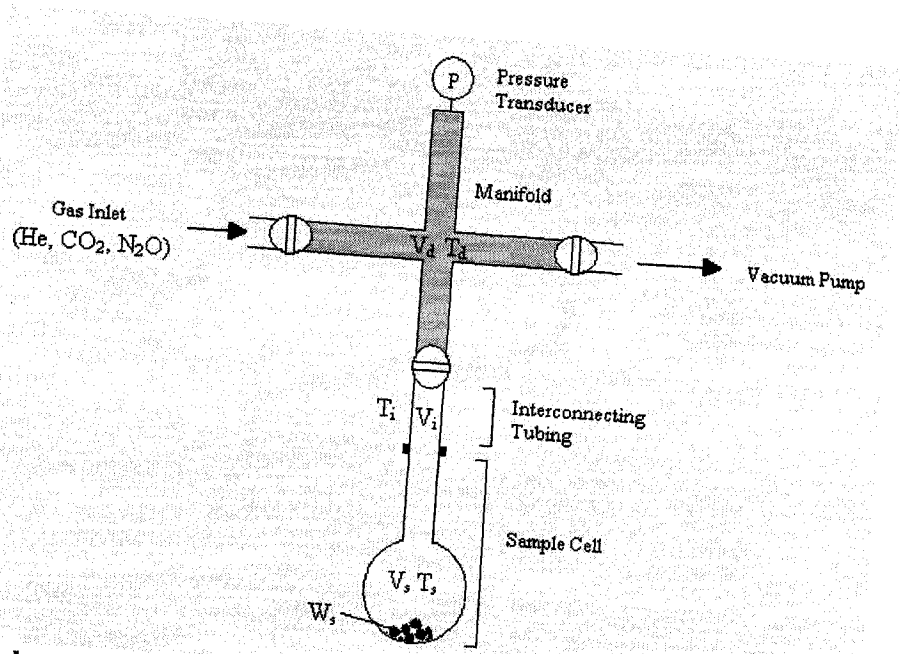

Figure 1: Schematic of volumetric system with manifold, interconnecting tubing, and free space in sample cell.

The operation of the volumetric apparatus is based upon the gas laws. In the pressure range for the experiments presented in this report, the ideal gas law is considered applicable (below critical pressures of CO_2 and N_2O). In this system a known quantity of single component gas is admitted into a sample cell volume that contains the adsorbent at a constant temperature. As adsorption takes place the sample cell pressure decreases as shown in Figure 2. Once the system has reached equilibrium, the volume adsorbed can be calculated from the difference between the pressure and the amount of gas required to fill the free space in the sample cell.

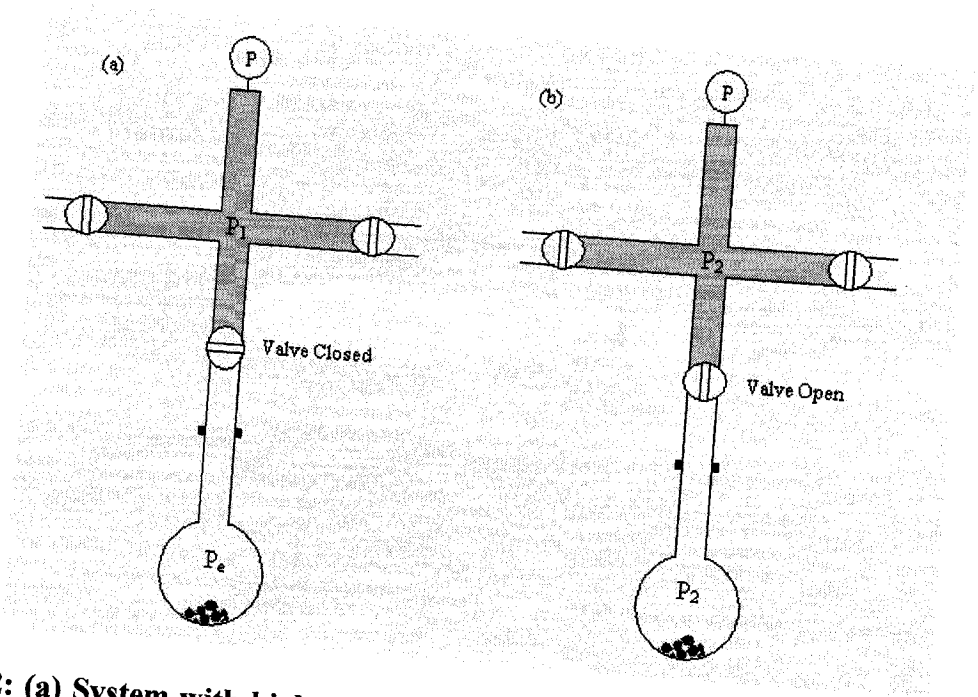

Figure 2: (a) System with high pressure single component gas in manifold (P_1) and sample cell at previous equilibrium pressure (P_e). (b) System at final equilibrium pressure (P_2) after expansion.

The operation of the volumetric system follows an isotherm construction based upon a point-by-point measurement of the pressure change in the gas. The pressure of the gas is increased incrementally for each measurement of the equilibrium.

The following equations illustrate the determination of the number of moles of adsorbed gas (n_a) per adsorbent weight by estimation of the volume of gas adsorbed (V_a).

$$\frac{n_a}{W_s} = \frac{V_a P_R}{W_s T_R} = \frac{1}{W_s}\left[\frac{P_1 V_d}{T_{d1}} - \frac{P_2 V_d}{T_{d2}} - P_2\left(\frac{V_s}{T_{s2}} + \frac{V_i}{T_{i2}}\right) + P_e\left(\frac{V_s}{T_{se}} + \frac{V_i}{T_{ie}}\right)\right] \qquad (1)$$

Where n_a is the number of moles of gas adsorbed (m-mol)

V_a is the volume of gas adsorbed (mL)

W_s is the weight of the outgassed sample (g)

P_R is the pressure of the adsorbed gas at standard conditions (760 mmHg)

P_1 is the pressure in the manifold before introduction into the sample cell (mmHg)

P_2 is the pressure of the expanded gas into the sample cell and manifold (mmHg)

P_e is the equilibrium pressure in the sample cell (previous equilibrium pressure in mmHg)

V_d is the volume of the manifold (mL)

V_s is the volume of the free space in the sample cell (mL)

V_i is the volume of the interconnecting tubing (mL)

T_R is the temperature of the adsorbed gas at standard conditions (273.15 K)

T_d is the temperature of the manifold (K)

T_s is the temperature of the adsorbent sample (K)

APPENDIX V

DYNAMIC ADSORPTION ANALYSIS UNIT

EXPERIMENTAL SET UP

A two column dynamic adsorption analysis unit has been designed and built in-house. Table 1 details the characteristics of the column while Figure 1 shows a simplified schematic diagram of the apparatus.

Table 3. Characteristics of the fixed bed column

Bed length (m)	0.61
Column internal diameter (m)	0.044
Column wall thickness (m)	0.0029
Port 1 position[1] (m)	0.102
Port 2 position[1] (m)	0.305
Port 3 position[1] (m)	0.507

[1] Tap location from the column inlet

This experimental system is designed to allow easy in-situ regeneration of the saturated adsorbent. It primarily consists of the following components: two identical adsorption columns, feed and purge gas , heating tape, an in-line gas heater, a vacuum pump, copper heating/cooling tubes wrapped around the column, solenoid three-way and two-way valves, 1/4" and 1/8" outside diameter stainless steel tubing, a data acquisition system, customised control software, thermocouples, a multiposition valve, pressure transducers, mass flow controllers, a mass flow meter, a gas mixing chamber (MC), a gas chromatograph (GC), a non dispersive infrared analyser (NDIR) and an Edwards high vacuum pump.

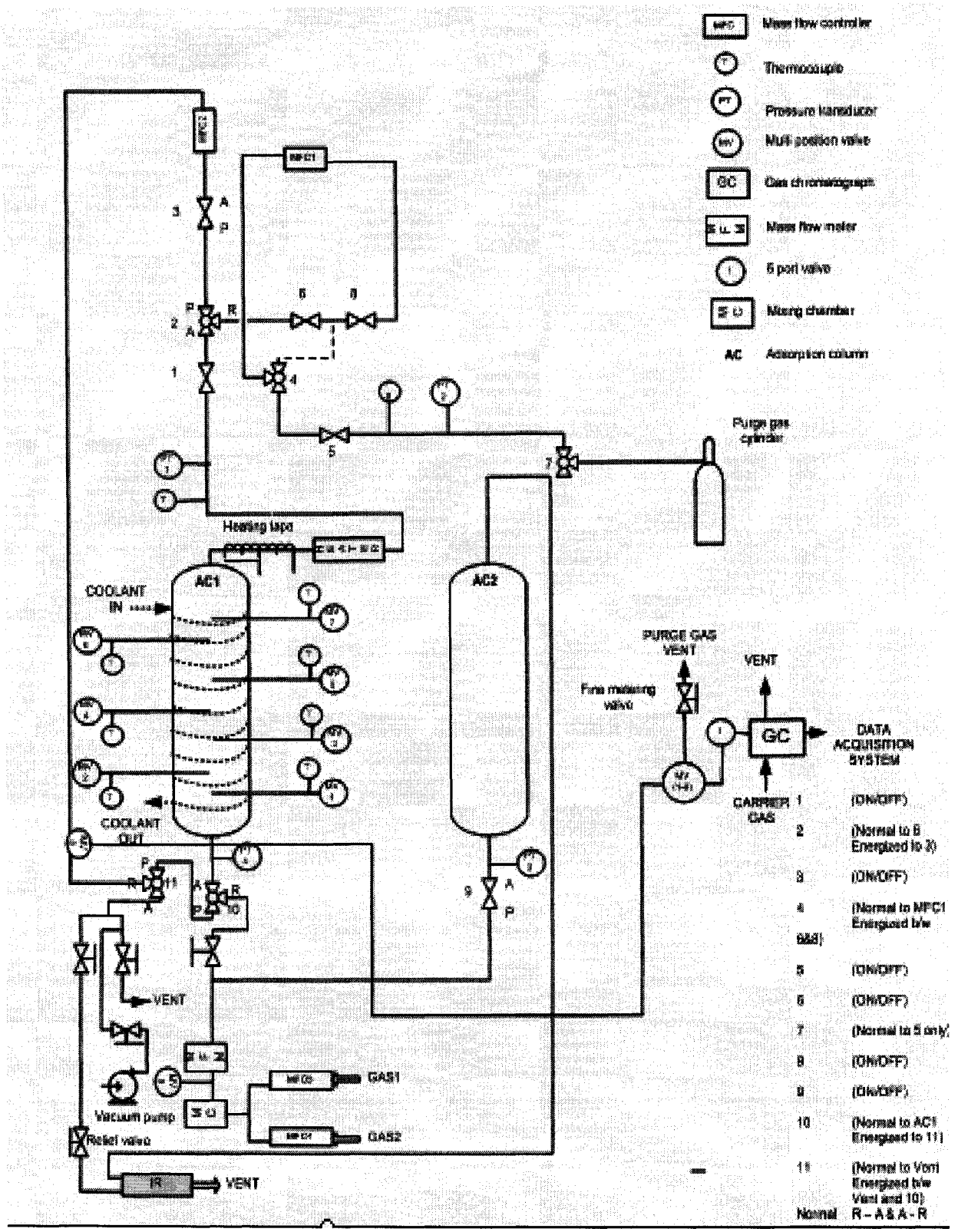

Figure 1. Schematic diagram of the two bed Dynamic Adsorption Analysis Unit.

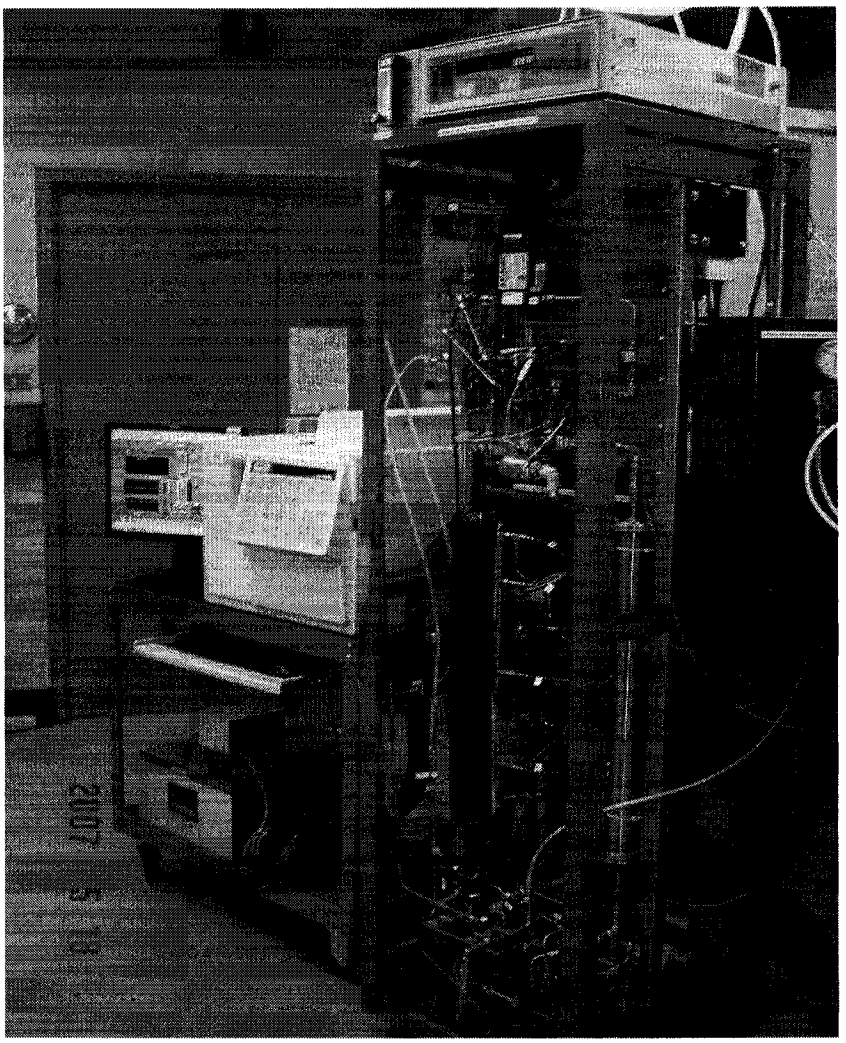

Figure 2. Dynamic Adsorption Analysis Unit.

The two adsorption columns are made of 316 stainless steel which is known for its corrosion resistance, toughness even at elevated temperatures and for fast heat dissipation. The inside diameter of the column is 4.4 cm, and the length available for the adsorption bed is 61.0 cm. The columns are fitted to inlet and outlet stainless steel conical flow distributors in order to favour plug flow conditions. VCR® fittings and Teflon O-rings formed the seals between the column and the flow distributors. One of the columns has seven ports that are simultaneously used for temperature and concentration measurements from column centre

axis location. These sample ports are connected to a VALCO model SD 32-port micro-electric actuated multiposition valve. This multiposition valve has 32 ports (16 inlet and 16 outlet ports) and has the capability of connecting 16 different sample ports at any time A 6-port micro-electric actuated injector valve houses the sample gas cell (500 μL) and connects the 32-port micro-electric actuated multiposition valve to a Varian 3400 Series Gas Chromatograph (GC) for concentration measurements through 0.32 cm (1/8") outside diameter stainless steel tubing. The sample gas cell within the 6-port micro-electric actuated injector valve is purged with UHP helium for 5 seconds followed by injecting the desired gas mixture sample from the desired sample port for a period of 3s. Each gas sample takes about 1 min to be analysed in the GC to obtain the gas composition. Therefore, experimental composition data points from the GC are obtained every minute. Since there are seven sample location ports along the column, the data point at each sample location was obtained every 7 minutes. Using a GC provides the flexibility of experimenting with various gases. Disadvantages with the GC include the difficulty in obtaining continuous gas detection at each sample port immediately, as there is a time lag involved with the GC detector. Along with the GC, a non dispersive infrared analyser (NDIR) is used for continuous gas detection (0-20% CO_2 by vol) at the adsorber column exit. Accurate temperature measurements are obtained by using Omega type-K exposed tip thermocouples.

The two adsorption columns are each equipped with two 590 Barocel pressure transducers at the entrance and the exit of the columns for measuring pressures up to 10 atm with an accuracy of 1% of the reading. The average of the inlet and outlet column pressures is taken as the average column pressure. Due to the low pressure drops (0.26 - 0.44 kPa) in the range

of flow rates studied (4 - 6.6 SL/min), it represents the true column pressure. A Proportional-Integral-Derivative (PID) controller is built into LABVIEW software (from National Instruments) that is used to control this average column pressure by manipulating column exit mass flow rate via the mass flow controller (MFC) M4. The feed, purge and sample flow rates are controlled by MKS type M100B mass flow controllers (0-10 SL/min) which has an accuracy of 1.5% of the full scale.

The column is fitted with flexible copper coils and a thermostat controlled 50:50 (vol/vol) ethylene glycol water mixture circulated inside the coils in order to achieve near isothermal conditions for the process. Various components of this system are connected by 0.64 cm (1/4") outside diameter stainless steel tubing. A data acquisition system in conjunction with LABVIEW software from National Instruments is used to collect and record the pressure, temperature, concentration and flow rate data.

At the beginning of the set of experiments used in this study, the adsorption column is isolated from the set up and packed with the desired adsorbent. Uniform distribution of the adsorbent pellets inside the column is ensured by continuous tapping of the sides of column. The adsorbent is regenerated in an electric oven at 200°C under purge flow in order to remove any impurities present in its structure followed by cooling it overnight. Then the two ends of the column (inlet and outlet) are plugged to prevent any leaks and it is connected back to the rest of the experimental set up.

Prior to each run, the NDIR analyser is calibrated with span gas, purge gas and a standard calibrated gas mixture. During pressurisation and after NDIR calibration, the feed gas mixture is prepared in the mixing chamber (MC) filled with glass beads using two pre-calibrated mass flow controllers (MFC) M1 and M2. This gas mixture is sampled through NDIR and GC to establish the variability in concentration.

Before each run, the column is pressurised using purge gas to the desired column pressure and maintained at the same pressure using the PID controller. During this cycle, purge gas is adsorbed by the adsorbent and heat is liberated which raises the temperature within the column to about 55 ^{o}C -60 ^{o}C. The column is cooled to ambient temperatures (30-33 ^{o}C) using ethylene glycol-water mixture that circulates in the copper coils that surround the column. When ambient column temperatures (30-33 ^{o}C) are attained, the flow of ethylene glycol-water mixture is stopped and adsorption cycle is started by introducing the feed gas mixture into the column. For each run, the gas concentration, flow rates, pressures and temperatures are continuously monitored and the data are recorded in an MS-Excel worksheet.

When the gas concentration at the last sample port reached the feed concentration, the feed flow is stopped. A complete regeneration of the saturated adsorbent is performed by combining high temperature (120 ^{o}C) and vacuum in-situ, between different experimental runs. During the regeneration cycle, purge gas is allowed to flow through the column. The completion of this step is verified by stopping the vacuum and analysing the desorbed gas coming out from the column using the NDIR analyser. Complete regeneration of the adsorbent

is achieved when the desorbed gas contains no traces of adsorbed gas. The column is then allowed to cool under purge. It is then isolated from the rest of the setup by closing the column inlet and the outlet valves. Prior to the start of the next run, the column is re-pressurised to the desired column pressure and the adsorption cycle is repeated.

The cycle steps followed for the continuous operation of experimental set up are:

1. Pressurisation of the feed
2. Adsorption at feed pressure
3. Depressurisation
4. Purge
5. Re-pressurisation

DETAILED OPERATION PROCEDURE

I. COLUMN PACKING AND REGENERATION

Detach the column from the setup and unscrew the top column head. Pack the column with the desired adsorbent. This is done by adding small quantities of the adsorbent into the column and continuously tapping the sides of the column using an electronic vibrator (available with the technicians- D302). Sufficient care and time should be taken to ensure a proper packing of the adsorbent column. The filled adsorbent column has to be regenerated under purge gas at 200 ^{o}C overnight using an electric oven (D-202). When the desired regeneration time is attained, the heater should be turned off and the column allowed to cool under purge gas to ambient temperature.

The column should be plugged at both ends during transportation to prevent leaks and fitted to the experimental setup.

II. START UP CHECKS

i. Check for column leaks. Ensure that the screws on the column heads (top and bottom) are tightened properly. Make sure that the inlet and the outlet column valves are shut to prevent any contamination.

ii. Check if feed and purge gas cylinders are properly installed and have enough gas for the experimental run.

iii. Calibrate the NDIR using the span gas (UHP N_2) and calibrated gas mixture separately.

iv. Set the outlet regulator on the feed gas cylinders to about 100 psig for all runs.

v. If an isothermal experimental run has to be carried out, make sure that a 50:50 ethylene glycol-water mixture is filled within the recirculating bath and set to the desired operating temperature. Check if its inlet and outlet screws are properly tuned in to the column coil screws.

vi. Start the Labview software on the computer. Click on "empty array" and "set records to zero" to erase previous data. Click the "Run" button to start the control software. Click "save process data" and "time v/s voltage" button. The process data is saved every second and time v/s voltage button saves the complete details of every peak (time and voltage) appearing in the GC. Click "Run" on the GC to measure the gas composition.

III. PRESSURISATION OF THE COLUMN & SAMPLE GAS MIXTURE PREPARATION

i. Pass the purge gas into the operating column until desired pressure (5 psig more than desired pressure) with the column exit closed.

ii. At the same time, prepare the desired gas mixture in the gas mixing chamber by operating feed gas mass flow controllers (MFC 3 and MFC 4). Click on port #9 on the labview software to analyse the gas mixture in the GC. Start "sampling and analysis" button on the GC. Use the second column and open valve, SV9 to analyse the gas mixture in the NDIR.

IV. ADSORPTION

i. Set the PID controlled mass flow controller (MFC 2) to the desired constant operating column pressure to be maintained during the experimental run, on the Labview software.

ii. Select the desired gas mixture analyzing ports (e.g., #2, #4, and #6). Make sure to de-select port #9 used for sample gas preparation at the beginning.

iii. When the desired feed gas mixture is prepared and the column pressure reaches the desired column pressure, close valve SV9 (inlet valve to second column).

iv. For isothermal operation, circulate the ethylene glycol-water (50/50) mixture from the circulating bath (set at the desired temperature) into the copper coils surrounding the column.

v. Open fixed valve, F1 which is the inlet valve to the operating column to allow the gas mixture to enter the operating column. Note down this time (start of adsorption).

V. COUNTER CURRENT DEPRESSURISATION

i. When complete breakthrough concentration behaviour is observed, close fixed valves F3 and F4. Close mass flow controller (MFC 2), solenoid valve SV1 and fixed valve F1 (isolate the column).

ii. Stop inlet gas flows at the feed mass flow controllers (MFC 3 and MFC 4)

iii. Open solenoid valves through labview, SV 10 and SV 11.

iv. Slightly open fixed valve (F3) which connects to NDIR and adjust the rate of flow (by turning the fixed valve F3).

v. Use a stopwatch to note down the flow rate of depressurization step.

vi. When the operating column pressure drops to the desired purge pressure (approx. 15-20 psig needed to see peaks in the GC), depressurization step is completed.

vii. Completely close fixed valves F3 and F4.

VI. PURGE

i. Verify if the inline heater and electrical tape are plugged to the circuit board if heat energy is being used to regenerate the column during purge step. Set the desired purge temperature on these instruments.

ii. If the column needs to be heated to regenerate the column, circulate the ethylene glycol-water (50/50) mixture from the circulating bath (set at the desired temperature) into the copper coils surrounding the column.

iii. Open solenoid valves SV2, SV4, SV6 and SV8 through labview. Open solenoid valves through labview, SV 10 and SV 11.

iv. Check if fixed valve F4 is completely closed and F3 very slightly open (as in depress step).

v. Circulate the purge gas through the column counter currently through MFC1 and purge gas cylinder. Maintain a constant pressure in the column by adjusting fixed valve F3.

vi. When the purge time is completed, stop the purge gas flow through the column.

vii. Stop labview. The entire file is saved according to the experimental run date.

viii. Close fixed valves F3 and F4.

ix. Stop the GC operation (stop sampling and analysis button).

VII. ON-SITE REGENERATION OF THE ADSORBENT COLUMN

i. Maintain a low purge gas flow rate of about 1 SLM through the column. Raise the temperature of the heating tape and circulating bath to about 90-100 deg C. Keep valves SV 10 and SV11 open. Close valves SV1, SV3, SV6 and SV8. Close F3.

ii. Start the vacuum pump and slightly open its inlet valve (F5) to let the gases enter the vacuum pump. Gradually increase the vacuum pump valve opening as the gas flow decreases until it is fully open.

iii. Every 25-30 mins, close the valve (F5) to the vacuum pump and check if the column adsorbent is free of the adsorbed gas by passing the fresh purge gas through NDIR and verifying the composition.

iv. For a complete adsorbent regeneration, start the vacuum pump again, pass the purge gas through the heated column and repeat steps i-iii. Do not turn off the vacuum pump during low flow rate of purge gas passing through it (or) oil may enter the tubing.

VIII. SHUT-OFF INSTRUCTIONS

i. Unplug inline heater, electrical tape, vacuum pump and turn off the circulating bath.

ii. Stop the purge gas flow.

iii. Close F1 and SV1.

iv. Turn off the NDIR.

v. It is a good practice to keep the operating column open to purge gas regulator pressure (about 15-20 psig) to prevent any leaks until the next experimental run.

TROUBLE SHOOTING

GAS CHROMATOGRAPH (No peaks observed)

a. Check whether gas is flowing through the column especially during injection step. Verify this using a bubble flow meter at the GC column exit.

b. Check for GC columns leaks using soap water. If bubbles start to grow, it is a sign of leak.

c. Change the amplitude and sensitivity settings

d. Check if the GC column is suitable for measuring your gas mixtures. Regenerate the GC column.

ADSORBENT COLUMN LEAKS

a. During pressurization, the pressure will not rise beyond 50 psig. Tighten the screws on the adsorbent column heads (top and bottom).

b. Check for any leaks at the points where the column is connected to the tubing.

c. Check for leaks at the column ports.

CALIBRATIONS

Make sure that all mass flow controllers, mass flow meters, pressure transducers, heating tape, circulating bath and thermocouples are calibrated every six months.

NDIR ANALYSER CALIBRATION

Flow N2 at a 0.5 SLM and let analyzer stabilize and then press the ZERO key. This should pull the display to zero. To calibrate the span you first need to input the span

gas value into the analyzers memory. We do this by pressing the DISP key which changes the display to the cal gas value display. You then enter the span gas value by pressing the DIGIT key to make the first digit of the display to blink which then can be changed with the SET key. Do this to all the digits until you have the cal gas value correct on the display and hit the DISP key to get back to the normal measure display. Flow the span gas at 0.5 LPM and let stabilize and then press the SPAN key. Calibration is complete. If you get a red SPAN and/or Zero alarm on the display we might have to do an initialization calibration. To do this, call Greg Anderson at 800-446-7422 ext. 240.